Universidad de Málaga
Facultad de Ciencias
Departamento de Bioquímica, Biología Molecular, Inmunología y
Química Orgánica

TRANSFERENCIA ELECTRÓNICA FOTOINDUCIDA BASADA EN ACEPTORES TIPO *N*-ÓXIDOS DE ISOQUINOLINAS: PROCESOS OXIDATIVOS RADICALARIOS Y OPERADORES LÓGICOS MOLECULARES

PHOTOINDUCED ELECTRON TRANSFER BASED ON ISOQUINOLINE *N*-OXIDES AS ELECTRON ACCEPTORS: RADICAL OXIDATIVE PROCESSES AND MOLECULAR LOGIC SWITCHES

Memoria que para optar al grado de
Doctor en Química (Doctorado Europeo)
por la Universidad de Málaga

Presenta:
José María Montenegro Martos

Málaga, diciembre de 2009

SPICUM servicio de publicaciones

UNIVERSIDAD DE MÁLAGA

SPICUM
servicio de publicaciones

AUTOR: José María Montenegro Martos

EDITA: Servicio de Publicaciones de la Universidad de Málaga

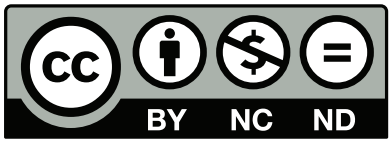

Esta obra está sujeta a una licencia Creative Commons:
Reconocimiento - No comercial - SinObraDerivada (cc-by-nc-nd):
Http://creativecommons.org/licences/by-nc-nd/3.0/es
Cualquier parte de esta obra se puede reproducir sin autorización
pero con el reconocimiento y atribución de los autores.
No se puede hacer uso comercial de la obra y no se puede alterar,
transformar o hacer obras derivadas.

Esta Tesis Doctoral está depositada en el Repositorio Institucional de
la Universidad de Málaga (RIUMA): riuma.uma.es

SPICUM
servicio de publicaciones

UNIVERSIDAD DE MÁLAGA

D. **Rafael Suau Suárez**, Catedrático de Química Orgánica y D. **Ezequiel Pérez-Inestrosa**, Profesor Titular de Química Orgánica de la Facultad de Ciencias de la Universidad de Málaga,

Certifican:

Que la memoria adjunta, titulada "TRANSFERENCIA ELECTRÓNICA FOTOINDUCIDA BASADA EN ACEPTORES TIPO *N*-ÓXIDOS DE ISOQUINOLINAS: PROCESOS OXIDATIVOS RADICALARIOS Y OPERADORES LÓGICOS MOLECULARES", que para optar al grado de Doctor (Doctorado Europeo) presenta José María Montenegro Martos, ha sido realizada bajo nuestra dirección en los laboratorios del Departamento de Bioquímica, Biología Molecular, Inmunología y Química Orgánica de la Universidad de Málaga.

Considerando que constituye un trabajo de Tesis Doctoral, autorizamos su presentación en la Facultad de Ciencias de la Universidad de Málaga.

Y para que conste, firmamos el presente certificado en Málaga a diciembre de 2009.

Fdo. Dr. Rafael Suau Suárez

Fdo. Dr. Ezequiel Pérez-Inestrosa

SPICUM servicio de publicaciones

SPICUM
servicio de publicaciones

Acknowledgements

I would like to express my sincere gratitude to all the people who helped and leant me during the execution of the Doctoral Thesis presented here, and especially,

To the professors Dr. Rafael Suau and Dr. Ezequiel Pérez-Inestrosa, both directors of my work, for all their efforts, their teachings, their help and their trust in me from the beginning of my Ph.D.

To the Organic Chemistry Department professors and lecturers, María Valpuesta, Rodrigo Rico, Rafael García, Gregorio Torres, Mª Soledad Pino, Francisco Sarabia, Juan Manuel López, Francisco Nájera and Amelia Díaz for their education during the degree and the Ph.D. years.

Specially, my gratitude to the lecturers, colleagues and friends Daniel Collado and Yolanda Vida for their help when I started in the laboratory and for these years full of nice moments shared in the laboratory.

To my laboratory colleagues, Antonio Jesús, Isabel and Elena for making easier the working hours, especially to Maribel for the time we shared and for her friendship.

To my colleagues of the plants laboratory, Mª Carmen, Manuela and Jesús.
To my colleagues of the sugars laboratory, Samy, Francisca, Miguel, Jose, Antonio, Carlos and Noe.
To our laboratory technician, José Beltrán and our secretary, Isabel Viola.

I also feel very grateful to Dr. Dario Bassani, Jean Pierre Desvergne and Nathan McClenaghan for their help, kindness and teaching during my stay in the *"Laboratoire de Chimie Organique et Organometallique"* (LCOO) of the *Université Bordeaux I*.

To the Dr. Juan Casado for its help with the electrochemistry measurements.
To the Professors Rafael Asenjo and Francisco R. Villatoro for the useful discussions about logic gates.

I would like to thank the Spanish Ministry of Education and Science for the Ph.D. fellowship awarded.

SPICUM servicio de publicaciones

To my degree colleagues and friends, Francisco Javier Jiménez, Antonio Lucio Mancebo, Juan Francisco Agüera and Marcos Antonio Guerrero.

To my colleagues of the Physical Chemistry department, and my friend Alejandro.

To all my friends, for the moments we have lived together, especially to Dr. Francisco Javier Fortes, because he knows how hard is the way to become Doctor.

I want to show gratitude to all my family for its help and leant, especially to my grandparents. Thanks for being there. You are always on my mind.

My gratitude to my in-laws for being a second family for me.

To my parents and brother for your help, love and because you have always encouraged me to follow my dreams. All I've got is for you.

To Rocío, for your understanding and patience, and because you have suffered this thesis with me trying always to make me smile and making it bearable. Thank you for your love and for your life. You are the sunshine of my life.

Finally I would like to thank all the people that I haven't mentioned but have helped me these years.

SPICUM servicio de publicaciones

SPICUM
servicio de publicaciones

SPICUM
servicio de publicaciones

To my parents

To my brother

SPICUM
servicio de publicaciones

SPICUM
servicio de publicaciones

To Rocío

SPICUM
servicio de publicaciones

SPICUM
servicio de publicaciones

Abbreviations / Abreviaturas

A	Acceptor / Aceptor
A-S-D	Acceptor-Spacer-Donor / Aceptor-Espaciador-Dador
MCPBA	*m*-Chloroperoxybenzoic acid / Ácido *m*-cloroperbenzoico
atm	Atmosphere / Atmósfera
bs	Broad singlet / Singlete ancho
CMOS	Complementary Metal Oxide Semiconductor /Semiconductor complementario de óxido metálico
CT	Charge transfer / Transferencia de carga
D	Donor / Dador
d	Doublet / Doblete
dd	Doble doblete / Double doublet
DMF	*N,N*-Dimethylformamide / *N,N*-Dimetilformamida
dt	Double triplet / Doble triplete
ε	Molar absorption coefficient / Coeficiente de absorción molar
EDTA	Ethylenediaminetetraacetic acid / Ácido etilendiaminotetraacético
ET	Electron transfer / Transferencia electrónica
ϕ_{Fluo}	Fluorescence quantum yield / Rendimiento cuántico de fluorescencia
FAB-HRMS	Fast atom bombardment - High Resolution Mass Spectrometry / Espectrometría de masas de alta resolución por bombardeo con átomo rápido.
FRET	Förster Resonance Energy Transfer / Transferencia de energía de resonancia de Förster
HOMO	Highest occupied molecular orbital / Orbital molecular ocupado más alto
Hz	Hertz / Hertzios
I_F	Fluorescence intensity / Intensidad de fluorescencia
ICT	Internal charge transfer / Transferencia interna de carga
In	Input
J	Coupling constant / Constante de acoplamiento
LE	Local emission / Emisión local
LUMO	Lowest unoccupied molecular orbital / Orbital molecular no ocupado más bajo
m	Multiplete / Multiplet
MS-EI	Mass spectrometry - Electronic impact / Espectrometría de masas por impacto electrónico

SPICUM servicio de publicaciones

NBS	*N*-bromosuccinimide / *N*-bromosuccinimida
NIH	NIH shift / Desplazamiento NIH
NMM	*N*-metilmorfolina / *N*-methylmorpholine
NMR	Nuclear magnetic resonance / Resonancia magnética nuclear
Out	Output
PET	Photoinduced electron transfer / Transferencia electrónica fotoinducida
ppm	Parts per million / Partes por millón
q	Quartet / Cuadruplete
qu	Quintet / Quintuplete
S	Spacer / Espaciador
s	Singlet / Singlete
t	Triplet / Triplete
TBAH	Tetrabutylammonium hydroxide / Hidróxido de tetrabutil amonio
TEBA	Triethylbenzylammonium chloride / Cloruro de bencil trietilamonio
TEGDT	Tetraethyleneglycol ditosylate / Tetraetilenglicol ditosilato
TFA	Trifluoroacetic acid / Ácido trifluoroacético
THF	Tetrahidrofurano / Tetrahydrofuran
TTF	Tetratiafulvaleno / Tetrathiafulvalene

SPICUM
servicio de publicaciones

SPICUM
servicio de publicaciones

SPICUM
servicio de publicaciones

INDEX

SPICUM
servicio de publicaciones

SPICUM
servicio de publicaciones

Index

SPICUM servicio de publicaciones

SPICUM servicio de publicaciones

SPICUM servicio de publicaciones

SPICUM
servicio de publicaciones

SUMMARY

SPICUM
servicio de publicaciones

SPICUM
servicio de publicaciones

In this doctoral thesis I present the results of the study of the photoinduced electron transfer in a serie of electron Donor (D) and Acceptor (A) moieties, linked by a Spacer (S). These systems are involved in a serie of photophysical and photochemical processes including fluorescence emission and quenching and bond cleavage and formation.

The A-S-D systems studied here are based on isoquinoline *N*-oxide as electron acceptor, 4-methoxy substituted aryl as electron Donor and an alkyl Spacer increased in length from an ethylene (compound **33**) to a propylene (compound **34**) chain. This way, the distance between A and D is increased to three and four $\sigma_{C\text{-}C}$ bonds respectively. The key step in the preparation of these compounds was the isoquinoline Reissert reaction pathway.

The photophysical studies of **(33)** and **(34)** were recorded in neutral and acidic media. The emission spectra of both compounds are very similar, showing a dual-channel fluorescence emission in acidic media. Upon excitation at $\lambda_{exc} \leq 330$ nm a band at $\lambda_{em} =$ 380 nm is observed, corresponding to the isoquinoline *N*-oxide chromophore local

SPICUM servicio de publicaciones

emission (LE). Upon excitation at λ_{exc} ≥ 360 nm a second band at λ_{em} = 500 nm is observed, corresponding to the emission of a charge transfer excited state (CT).

We studied the photochemical reactivity of **(33)** and **(34)** in acidic media. The photolysis of these systems leads to two main reaction products: photodeoxygenation to yield the starting isoquinoline derivative, and photohydroxilation.

For **(33)**, the hydroxylation process takes place in the spacer chain instead of the aryl Donor positions that, in the acidic reaction conditions, dehydrates to produce the conjugated styryl derivative **(50B)**.
After photolysys of **(34)**, two different hydroxilated products in Donor aryl ring, **(51)** and **(52)**, are obtained.

We prepared the homologous serie in which the spacer moiety introduces an amide bond with two main objectives: increasing the system rigidity and using the amide bond as a connection-disconnection system where the electron acceptor could be reused in consecutives reaction cycles.

We synthesized several systems increasing the S length, always based on the structure of 1-isoquinoline-carboxamide, to obtain derivatives where A and D are located at three (compounds **37** and **38**), four (compounds **35**, **39** and **40**) and five bonds (compounds **36**, **41** and **42**). The key step of the synthesis of these compounds is the amide bond formation between 1-isoquinoline carboxylic acid and the corresponding amine, followed by *N*-oxidation.

The photophysical studies of these compounds show a similar behaviour to the alkyl spacer derivatives. The emission spectra in acidic media show a dual-channel fluorescence emission. Upon excitation at λ_{exc} ≤ 330 nm a band at λ_{em} = 345 nm (**37** and **38**), λ_{em} = 365 nm (**35**, **39** and **40**) and λ_{em} = 350 nm (**36**, **41** and **42**) is observed, corresponding to the isoquinoline *N*-oxide chromophore local emission (LE). Upon excitation at λ_{exc} ≥ 360 nm a second band at λ_{em} = 415 nm is observed, corresponding to the emission of a charge transfer excited state (CT).

We studied the photochemical reactivity of **(33)**-**(42)** in acidic media. The photodeoxygenation product is always found. For the irradiation of compounds **(39)** and **(40)**, we also detect hydroxylation products in the Donor ring. This

SPICUM servicio de publicaciones

photohydroxylation is regioselective and the product obtained in both cases is the hydroylated in *ortho* position to the hydroxy or methoxy group.

The changes of the fluorescence emission profile of compounds **(89)**, **(97)** and **(98)** (called output) upon the addition of selected chemical species (called inputs) as can be acids for *N*-oxide function (**(89)**, **(97)** and **(98)**), bases for phenol (**(97)**) and alkaline and alkaline earth metallic cations for the benzocrown ether moiety (**(89)**) have been studied.

These interactions produce changes in its fluorescence emission that can be studied from the Boolean logic gates point of view in order to develop molecular logic gates and switches.

The changes in the fluorescence emission of **(89)** upon addition of acid (TFA) and metallic cations (K^+, Ba^{2+}, Zn^{2+}), leads us to define an INHIBIT (INH) logic gate when inputs are TFA (acting over *N*-oxide function) and K^+ (acting over crown ether moiety) and two more complex systems, one of them when TFA and Zn^{2+} are inputs acting over the isoquinoline *N*-oxide and the other one when K^+ and Ba^{2+} are acting over the benzocrown ether moiety.

The photophysical studies of **(97)** upon interaction with acid (TFA) and base (TBAH) produce four different fluorescent-emitting excited states. The Boolean interpretation of these properties leads us to define an INH and a XOR logic gate. The combination of INH and XOR, produce a Half-Subtractor logic gate. With this result, is possible to develop a reversible molecular logic system, restricted to the case where the fluorescence emission is on. This behaviour is good approach to get a totally reversible molecular system.

The photophysical properties of **(98)** can be defined as a demultiplexer (DEMUX). This molecular switch steers an input to one of many possible outputs. In this case, we define a molecular 1:2 DEMUX. This switch can direct the input data stream to two different output receptors, directed by a digit control "*c*".

SPICUM servicio de publicaciones

SPICUM
servicio de publicaciones

SPICUM
servicio de publicaciones

SPICUM
servicio de publicaciones

CHAPTER I.

GENERAL INTRODUCTION

SPICUM
servicio de publicaciones
uma

SPICUM
servicio de publicaciones

I.1. Electron Transfer

The electron transfer plays a central role in a great variety of processes in several science fields, as physics, chemistry and biology.[1] These processes are interesting, from gas phase to homogeneous and inhomogeneous condensed-phase media, and their description involve an important number of basic questions in chemical energetics, dynamics and electronic and geometric structure.

The electron transfer (ET), *the transfer of an electron from one molecular entity to another one, or between two localized sites in the same molecular entity*[2] needs the presence of two components, one molecule or one molecule part where the electron proceed, called donor (D), and another molecule or molecule part, which receives the electron, called acceptor (A). The real coupling between electron donor and electron acceptor is mediated by the electronic and energetic characteristics of the unit joining

[1] Newton, M.D.; *Electron transfer in Chemistry*, vol 1 (Ed. V. Balzani), Wiley-VCH, Weinheim (Federal Republic of Germany) **2001**, p. 3-63.
[2] Braslavsky, S.E.; *Glossary of terms used in photochemistry 3rd Edition*, *Pure Appl. Chem.* **2007**,*79*, 293-465.

SPICUM servicio de publicaciones

the donor and acceptor moiety, called spacer (S), and the immediate medium surrounding the molecules. An acceptor-spacer-donor system (A-S-D) is shown on Fig. 1 where are distinguished intramolecular coupling (when D and A are covalently linked *via* a molecular spacer S), or intermolecular coupling when there is not a molecular spacer S, and it is defined for the presence of the solvent.

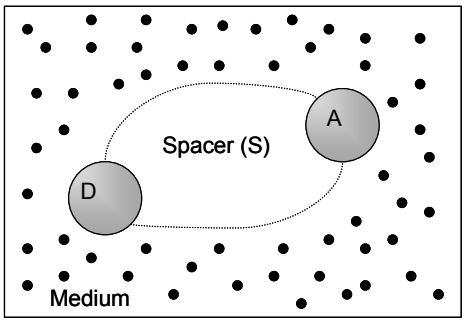

Fig. 1. General scheme of an Acceptor-Spacer-Donor (A-S-D) system.

When two molecules in solution exchange one electron, a redox process is produced where one molecule accept the electron (reduction) and the other one transfer the electron (oxidation). The electron transfer between the two molecules is given in a *encounter complex* formed by the molecular entities, in direct contact or separated by a small distance compared to the solvent molecules diameter. This encounter complex is surrounded by several shells of solvent molecules. The innermost shell is called the solvent "cage".[2]

Electron transfer in A-S-D systems leads to the formation of charge separation states $A^{-\cdot}SD^{+\cdot}$, which can have absorption bands and, sometimes, can be emissives. Traditionally, the ET reactions have been classified in *outer sphere* and *inner sphere* reactions.[3] The inner sphere electron transfer was defined by Taube, referring to the inorganic redox centres, connected by one bridge ligand in the transient state. This definition, is applied to any situation where the interaction between the electron donor and acceptor centres in the transition state is up to 20 $KJ \cdot mol^{-1}$. The outer sphere electron transfer is used for redox centres that don't share one atom or group. In this case, the electronic orbital interaction is weak, less to 20 $KJ \cdot mol^{-1}$.

[3] Nelsen, S.F.; *Electron transfer in Chemistry*, vol. 1 (Ed. V. Balzani), Wiley-VCH Weinheim (Federal Republic of Germany) **2001**, p. 342-392.

SPICUM servicio de publicaciones

Bimolecular electron transfer reactions in solution need the free diffusion of the acting molecules. Electron acceptor and donor must reach the right orientation in the *encounter complex* formed, which can promote one electron from the electron donor HOMO to the electron acceptor LUMO. The distance and the relative orientation of the molecules in this complex, control the orbital or electronic coupling ratio of the redox couple in the transition state. Depending on the energetic conditions, the electron transfer can occur *via* a thermal reaction (thermal ET) or may need an additional energy support in a photoinduced reaction (activated ET).[4] In this case, the irradiation of the complex in the Charge Transfer (CT) absorption band produces the direct transfer from the D to the A. One alternative procedure is the photoactivation of one of the encounter complex components (sensitized ET). In this case, the reactive in excited state can transfer the electron while the complex is generating (Fig. 2).

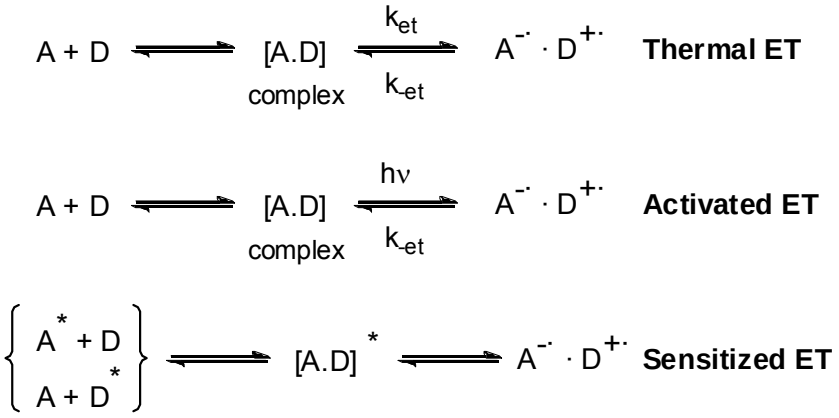

Fig. 2. Types of Electron Transfer.

Depending on the initial oxidation state, we can define four kinds of electron transfer if the participating molecules are charged or not. If D and A are neutral, ionic CT pairs are formed. If only electron Donor or electron Acceptor is charged, there is not an effective charge generation in the CT process. If both D and A are charged, the CT produces the disappearing of the neat charges (Fig. 3).

[4] Hubig, S.M.; Kochi, J.K.; *Electron transfer in Chemistry*, vol. 2 (Ed. V. Balzani), Wiley-VCH, Weinheim (Federal Republic of Germany) **2001**, p. 618-676.

SPICUM servicio de publicaciones

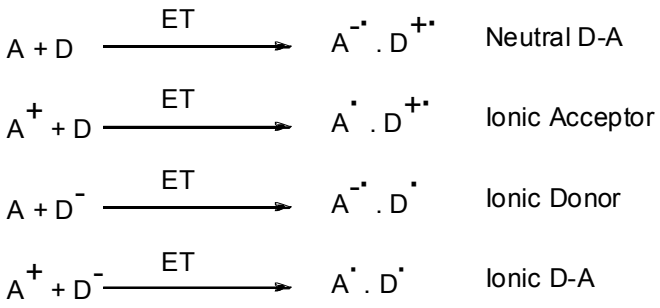

Fig. 3. Kind of ET depending of the initial oxidation state.

The charge arrangements of initial and final states involve solvation changes of reactants and products, one effect with influence in the total energy of the system. The charge separations in these systems are clearly observed when solvatochromic studies are carried out. The absorption maximum of the complexes and the ionic pairs are displaced with solvent polarity changes. The systems with charge separation are more stabilized in polar solvents (Fig. 4). When D, A or both are charged, the solvent effect is not high.

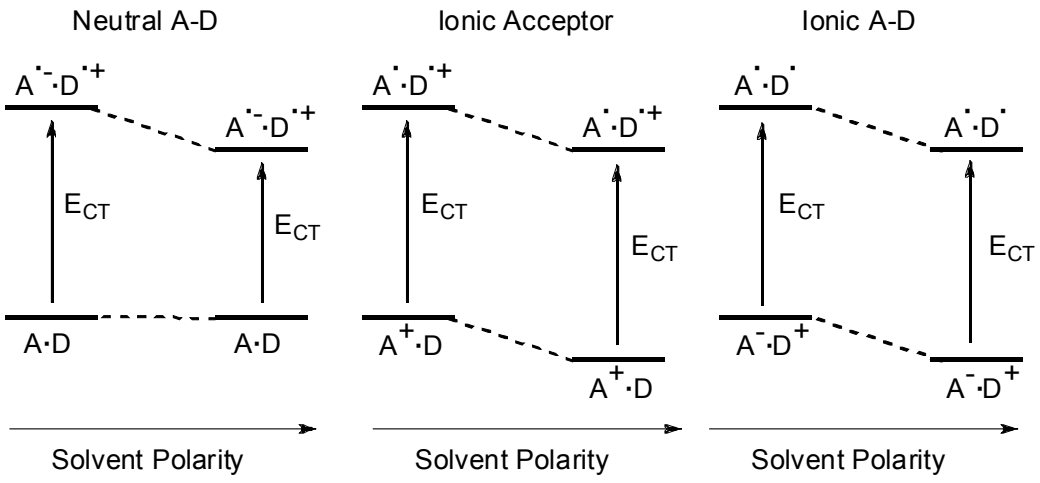

Fig. 4. Solvent effect in CT process.

SPICUM servicio de publicaciones

I.2. Marcus Theory

At the beginning of the 50's, it was possible to determine the reaction rate of several number of electron transfer reactions between inorganic ions. Some of these reactions were, apparently, too slow to be electron transfer reactions.

Between 1956 and 1965, Rudolph A. Marcus, published a set of articles studying the electron transfer reactions.[5] His work leads the scientist to solve the problem of the great variety of electron transfer ratio known. There is not bonds cleavage during the reaction but there are small changes in the structure when one electron is added or removed. The bond length is modified and the solvent molecules change their position and orientation. Obeying the Franck-Condon principle, the electron transfer can only take place between two isoenergetic states, and this premise can only be reached enhancing the components energy until reaching the crossing point of the two potential surfaces. These structural changes require an energetic support, called reorganizational energy, λ.[6]

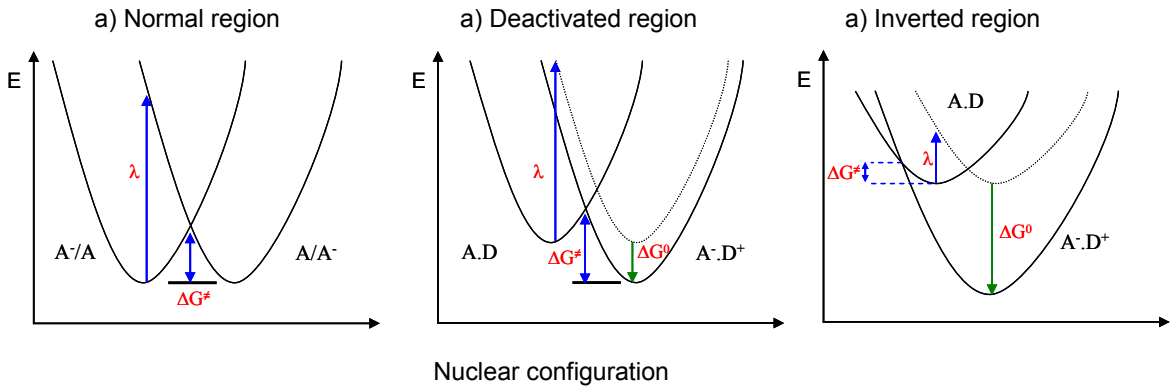

Fig. 5. Potential energy curves for reactants and products in a ET process.

The λ value can be explained with the energy curves shown on Fig. 5. These curves represent the potential energies of reactants and products as a function of a reaction coordinate. For 5a, λ corresponds to the vertical separation in the geometric balance between reactants and products for an isoergonic electron auto-exchange:

$$A + A^- \rightarrow A^- + A$$

[5] a) Marcus, R.A.; *J. Chem. Phys.* **1956**, *24*, 966. b) Marcus, R.A.; *J. Chem. Phys.* **1957**, *26*, 867. c) Marcus, R.A.; *J. Chem. Phys.* **1957**, *26*, 872.
[6] Balzani, V.; Scandola, F.; *Supramolecular Photochemistry*, Ellis Horwood Limited, Chichester (UK), **1991**, p. 51-75.

SPICUM servicio de publicaciones

In this case, the cross point between the parabolas enables the electron transfer, with a free energy of activation value of $\Delta G^{\neq} = \lambda/4$. Activation energy depends on the reorganizational energy of the system. Since electronic motions are much faster than nuclear motions (Franck-Condon principle), in a classical approach is required an adjustment of the nuclear configuration prior to electron (or energy) transfer.[6]

Marcus defined a simple mathematical equation which calculates this energy value and, consequently, the height of the energy barrier needed to the process occur.
The rate constant is defined by the Eyring equation (Equation 1):

$$k_{et} = \nu_N \kappa \exp\left(-\Delta G^{\neq} / kT\right) \qquad \text{(Equation 1)}$$

Where k is Boltzmann constant, T is the temperature, ν_N is the nuclear frequency factor of the atoms around their equilibrium position and κ represents the transmission coefficient, the probability for the reactants to products passing.

For a general ET reaction (Fig. 5b), the Marcus equation relates the activation energy with the free energy of the process (Equation 2).

$$\Delta G^{\neq} = \left(\lambda / 4\right)\left(1 + \Delta G^{0} / \lambda\right)^2 \qquad \text{(Equation 2)}$$

The λ parameter is formed by two values: the bond length and angles between A and D (λ_i inner) and the orientation of the solvent surrounding the reactants and products (λ_o outer) (Equation 3).[7]

$$\lambda = \lambda_i + \lambda_o \qquad \text{(Equation 3)}$$

The outer reorganizational energy can be easily calculated *via* some physical data like the dielectric constant of the solvent, the reactants radius and the distance between A and D. λ_o depends on the geometric distortion level of the redox pairs and the ET bonding character. The reorganizational energy λ and $\Delta G^{\neq}$ have different values depending on the reactions considered, explaining the different rate constants found. This equation establishes a relationship between the ET rate and the free energy of the process. This relation is quadratic, describing a parabola (Fig. 6).

[7] Marcus. R.A.; *Angew. Chem. Int. Ed.* **1993**, *32*, 1111.

SPICUM servicio de publicaciones

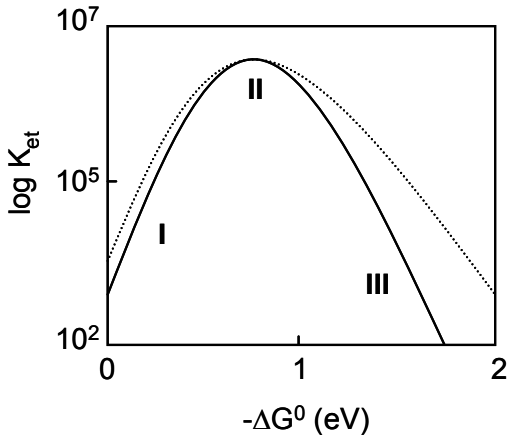

Fig. 6. Parabolic relation between ET rate and process free energy, showing normal **(I)** and inverted region **(III)** as well as the higher k_{el} point **(II)**.

As seen on Fig. 6, for moderately exoergonic reactions, the relation between the ET rate and the free energy increases while driving force is expected to help the reaction kinetics (from I to II on the parabola), but for strongly exoergonic reactions, oppositely behaviour is predicted, acting the driving force against the rate constant. This is called the *Marcus inverted region*.

On Fig. 5c, the *inverted region* is shown. When the system presents higher free energy (a more exoergonic system), the reaction rate is lower. When $\Delta G^0 = 0$, the activation energy is $\Delta G^{\neq} = \lambda/4$ is called the intrinsic barrier (I).[2] When the process become more exoergonic, ΔG^0 increases and when $\Delta G^0 = -\lambda$, $\Delta G^{\neq} = 0$ (II) and the ET is very fast. For higher values of ΔG^0, $\Delta G^{\neq}$ becomes lower and k_{et} is reduced (III)

The κ value on Equation 1, is related to the potential curve shape in the intersection zone. If there were no electronic interaction (electronic coupling H_{DA}) between the zero-order states, the transition from reactants to products would not be possible. For small H_{DA} values, the rate-determining step is the electron transfer at the transition state geometry. This is called the nonadiabatic limit.

When H_{DA} is high enough, the rate-determining step is the nuclear motion that leads to the transition state. The system stays in the same electronic surface in the reactants to products passing.

SPICUM servicio de publicaciones

The value of H_{DA} depends on the overlapping between the electronic wavefunctions of the donor and acceptor groups, decreasing while increasing D-A distance. When D and A are remote, the orbital overlapping is very small. In these conditions, the spacer plays a key role as a propagation of D-A coupling (bond interaction).

The super-exchange model[8] is a mechanism that explains the interaction through the bond considering that electron donor and acceptor orbitals don't overlap directly but they do with the spacer HOMO and LUMO, increasing H_{DA} in comparison with the same intermolecular D-A distance. This overlapping produces the direct orbital mixture of both compounds.

The stable intermediates are called *electron transfer intermediate* ($A\text{-}S^{-}\text{-}D^{+}$) and *hole transfer intermediate* ($A^{-}\text{-}S^{+}\text{-}D$). These intermediates are not real, and they are called *virtual states*.[9]

[8] Smith, T.A.; Lokan, N.; Cabral, N.; Davies, S.R.; Paddon-Row, M.N.; Ghiggino, K.P.; *J. Photochem. Photobiol. A: Chem.* **2002**, *149*, 55.
[9] Paddon-Row, M.N.; *Electron transfer in Chemistry*, vol. 3 (Ed. V. Balzani), Wiley-VCH, Weinheim (Federal Republic of Germany) **2001**, p. 179-271.

SPICUM servicio de publicaciones

I.3. Intermolecular Electron Transfer

The most important bimolecular processes (D-A) are energy and electron transfer. Electron transfer produces a redox process of excited state.[6]

$A + D^{*} \rightarrow A^{*}.D$ Energy transfer

$A^{*} + D \rightarrow A^{-}.D^{+}$ Reductive electron transfer

$A + D^{*} \rightarrow A^{-}.D^{+}$ Oxidative electron transfer

These processes can be applied to deactivate the excited states and can sensitize other chemical species to produce chemical changes, luminescence, etc. There are three kinds of processes: radiatives, thermal electron transfer and photoinduced electron transfer.

I.3.1. Radiative processes

The absorption spectra of D-A systems can be substantially different in comparison with the individual molecular spectra. The appearance of new bands is attributed to optical electron transfer processes that commonly appear in ionic pairs systems.

$$A\text{-}D \xrightarrow{h\nu} A^{-}\text{-}D^{+}$$ Optical electron transfer

The optical ET transition energy, ΔE_{op}, is related with the minimum of energy of A-D and A^{+}-D^{-} curves, ΔE, and the reorganizational energy in the Marcus-Hush relationship (Fig. 7).[10]

$$\Delta E_{op} = \Delta E + \lambda \qquad \text{(Equation 4)}$$

[10] Hush, N.S.; *Electrochim. Acta* **1968**, *13*, 1005.

SPICUM servicio de publicaciones

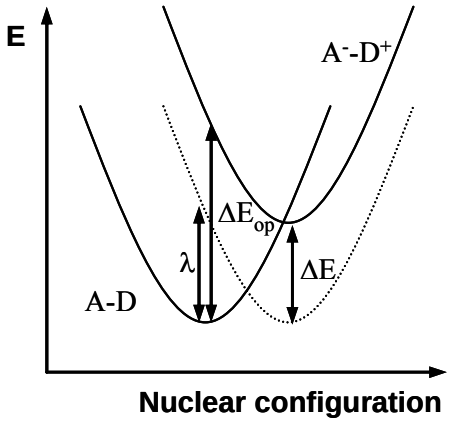

Fig. 7. Optical Electron Transfer.

ΔE values can be estimated from the standard redox potential of the reaction components. The absorption bands are Gaussian type curves and their intensity can be correlated with the electronic coupling H_{DA}. For values of $H_{DA,}$ around 100 cm^{-1}, the molar absorption coefficient values obtained are low, ε_{max} = 30 M^{-1} cm^{-1}. This absorption band is only visible if it's located in a region of the spectrum without influence of the absorption bands of donor and acceptor. It is usual to find this band in the visible or near infrared region.

I.3.2. Thermal electron transfer

For an A-D system as shown on Fig. 7, the thermal electron transfer to generate A^--D^+ would not be a thermodynamically favoured process. Nevertheless, the inverse process can spontaneously be given. This kind of process is usually called back electron-transfer or charge recombination.[2]

I.3.3. Photoinduced electron transfer (PET)

In this process, the electron transfer is produced from an excited state of one of the components in a radiationless process.

$$A\text{-}D \xrightarrow{h\nu} A\text{-}D^* \longrightarrow A^-\text{-}D^+$$ Photoinduced electron transfer

SPICUM servicio de publicaciones

These processes are characterized by a rate constant, k_{et} and the efficiency η_{et}. The rate constant can be calculated by flash photolysis experiments or by the lifetime of A-D^* (τ) and D^* (τ_0) ratio: $k_{et} = (1/\tau - 1/\tau_0)$.

The efficiency is calculated comparing the fluorescence quantum yields of A-D^* (Φ) and D^* (Φ_0), $\eta_{el} = \Phi_0 - \Phi$

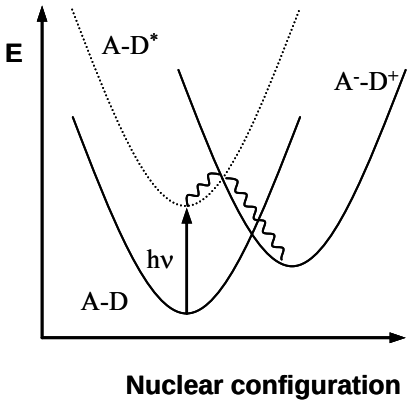

Fig. 8. Photoinduced Electron Transfer.

On PET process the electron Donor excited state can be deactivated by the presence of the electron Acceptor *via* electron exchange or dipole-dipole interaction (Fig. 8). The diffusion of the reactants in solution makes more complex the kinetic process.

SPICUM servicio de publicaciones

I.4. Intramolecular Electron Transfer

The systems using a Spacer (S) that covalently join D and A (A-S-D systems) have several advantages over bimolecular reactions because the problems associated to the bimolecular processes, as reactants diffusion or bimolecular complex formation, disappear. In A-S-D systems, the distance and orientation between D and A are limited by the molecular structure. These structural limitations have been very interesting to study specific parameters of the ET as the thermodynamic driving force, the distance, the orientation, the spacer and medium nature and physical parameters as temperature influence. As well, the study of these systems has proved the theoretical models of ET proposed.

There are several processes that A-S-D systems can undergo: optical electron transfer, photoinduced electron transfer, emissive processes and back electron-transfer.

$A\text{-}S\text{-}D + h\nu' \rightarrow A^{+}\text{-}E\text{-}D^{-}$ optical electron transfer

$A\text{-}S\text{-}D + h\nu'' \rightarrow A^{*}\text{-}S\text{-}D^{-}$

$A^{*}\text{-}S\text{-}D^{-} \rightarrow A^{+}\text{-}S\text{-}D$ photoinduced electron transfer

$A^{-}\text{-}S\text{-}D^{+} \rightarrow A\text{-}S\text{-}D + h\nu'''$ emissive back charge transfer

$A^{-}\text{-}S\text{-}D^{+} \rightarrow A\text{-}S\text{-}D$ back electron transfer

The non-radiative processes in electron transfer are called charge separation reactions, charge recombination and charge shift too.

SPICUM servicio de publicaciones

I.4.1. Saturated spacer systems

The work developed by Closs and Miller with covalently linked systems, permitted to demonstrate Marcus theory experimentally.[11]

The systems studied were connected with spacers based on cyclohexane, decaline or androstane **(1)**. This rigid spacer provides fixed distances and geometry, with the exception of the terminal C-C bonds.

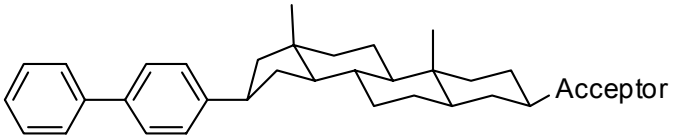

(1)

The ET process values are between 0 and -2.4 eV. If we assume that the electronic overlapping is quite small at 10 σ bonds distance, the rate constants were too high to measure ($k_{et} > 2 \cdot 10^9$ s^{-1}) when the electron acceptor used were a naphthalene unit. Nevertheless, it could be possible to measure lower k_{et} values when ΔE were higher than $-\lambda$, in the Marcus inverted region, where high exoergonic ET have lower rate constants.

These results show a clear decreasing in the ET rate for the highly exoergonic systems as classic and quantum mechanical models. This is the first evidence of the Marcus inverted region in ET processes in solution. It also shows that the solvent moves ΔG^0 to lower values at the beginning of the inverted region when the solvent polarity decreases, according with the theory.[6]

Studies in parallel made using known spacer distances of 10 and 17 Å show that the rate constant decreases with the distance, being this behaviour correlated with the theoretical predictions. Non-covalent linked systems located on rigid crystals show an enhanced decrease on the rate constant with the distance, and it is a proof of the important interaction across the bond in the covalently-linked systems.

[11] Closs, G.L.; Miller, J.R.; *Science* **1988**, *240*, 440.

SPICUM servicio de publicaciones

Paddon-Row and Verhoeven studied systems with dimethoxynaphthalenes as donors, dicyanovinylene as electron acceptor and bicyclic spacers as bicycle[2,2,1]heptane **(2)** and **(3)**.[12] D and A were bonded to the spacer without free orientation and the spacer lengths were between 7 and 15 Å.

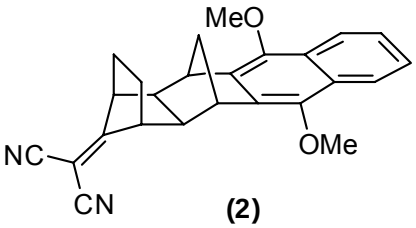

(2)

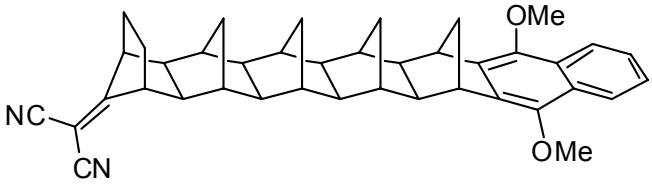

(3)

The fluorescence emission of dimethoxynaphthalene unit is deactivated *via* photoinduced electron transfer from the S_1 excited state of the dimethoxynaphthalene to the dicyanovinylene unit. By means of increasing the length of the spacer, the lifetime fluorescence emission is shorter being possible to calculate ET rate constants. This rate constants decreases with spacer length increase.

The charge separated states generated by ET are influenced by the media. Increasing the polarity of the solvent produces the stabilization of the charge transfer state and is possible to detect photoinduced electron transfer in systems where the use of less polar solvents didn't make it possible (Fig. 9).[13]

In polar solvents this reaction is more exothermic but, according with Marcus theory, the process rate decay at the same time.

The decay time of the charge shift intermediate also depends on the solvent polarity, showing fast back electron transfer in polar solvents.[14] This is due to the high influence of the solvent polarity in the value of k_{-et}.

[12] Paddon-Row, M.N.; Cotsaris, E., Patney, M.K.; *Tetrahedron* **1986**, *42*, 1789.
[13] Pasman, P.; Mes, G.F.; Koper, N. W.; Verhoeven, J.W.; *J. Am. Chem. Soc.* **1985**, *107*, 5839.
[14] Jones II, G.; Farahat, M.S.; Greenfield, S.R.; Gosztola, D.J.; Wasielewski, M.R.; *Chem. Phys. Lett.* **1994**, *229*, 40.

SPICUM servicio de publicaciones

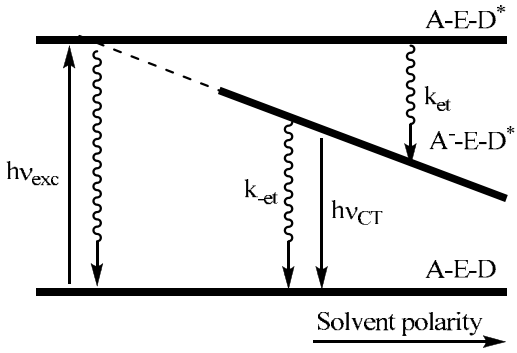

Fig. 9. Stabilization of excited state with the solvent polarity.

The back electron transfer process depends on the solvent and on the distance between D and A.[12,13] The value of k_{-et} depends on the solvent and decreases with the D-A distance, in contrast with k_{et}. For example, if we use cyclohexane, k_{-et} value is two orders of magnitude slower than the value when we use dioxane as solvent. For each covalently-linked system, the recombination processes have lower rate constants than charge separation processes. It is explained by the moderated exoergonic character of the charge separation rate, usually deactivated ($-\Delta G^0 \approx \lambda$) whereas reorganization is highly exoergonic and is located in the Marcus inverted region.

I.4.2. Unsaturated spacer organic systems

The systems studied by Heitele et al.[15a] are based on dimethylaniline electron donor, an electron acceptor based on pyrene and methylene or aromatic derivatives as spacers **(4)**. Interesting systems with porphyrins subunits **(5)** (Fig. 10), have also been studied because of its presence on photosynthetic reaction centres and other biological systems, as well as systems based on metal complexes **(6)**.[15b]

The studies carried out on fluorescence deactivation and absorption measurements show that the electronic coupling value, H_{DA}, slowly decreases while the distance increase as result of the aromatic rings presence in the spacer. This value, in comparison with saturated spacers and with approximated D-A distances is similar or lower.

[15] a) Heitele, H.; Michel-Beyerle, M.E.; *J. Am. Chem. Soc.* **1985**, *107*, 8286. b) Nakamura, A.; Okutsu, S.; Oda, Y.; Ueno, A.; Toda, F.; *Tetrahedron Lett.* **1994**, *35*, 7241.

SPICUM servicio de publicaciones

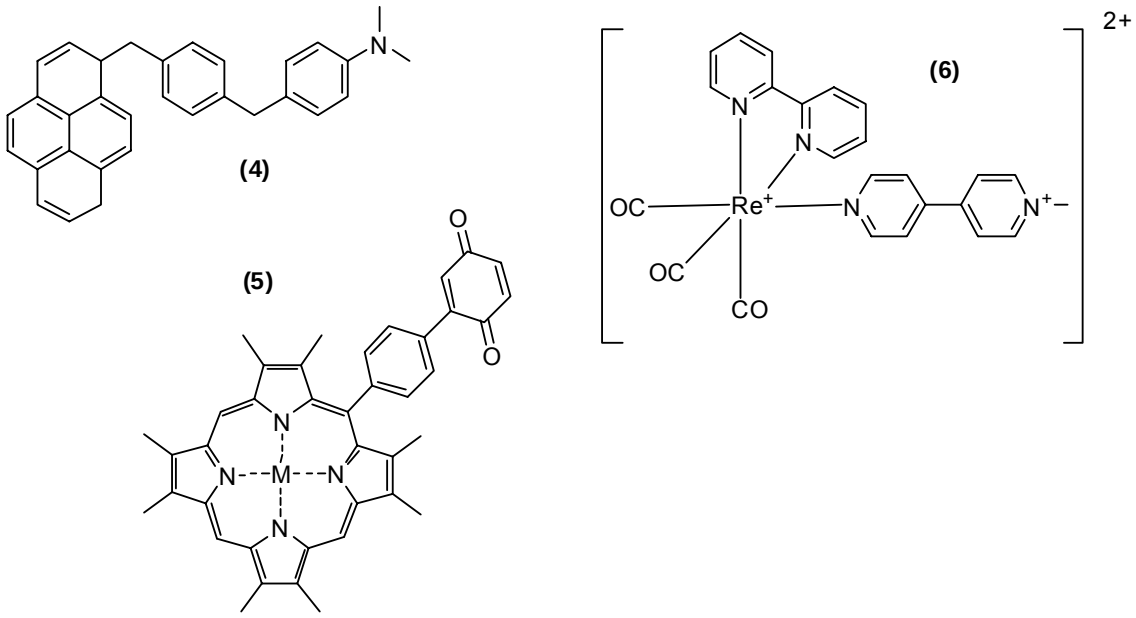

Fig. 10. Systems with unsaturated spacer.

If the spacer is conjugated with D and A, it takes part in ET process with two possible mechanisms:[16]

- In two steps, producing an ET first from the electron Donor to Spacer followed by a second ET from Spacer to the electron Acceptor.

- In one step, *via* the formation of "super-acceptors" or "super-donors" result of the delocalization of the electronic levels of the D and A in the spacer.

[16] Pourtois, F.; Beljonne, D.; Cornil, J.; Ratner, M.A.; Brédas, J.L.; *J. Am. Chem. Soc.* **2002**, *124*, 4436.

SPICUM servicio de publicaciones

I.5. Physical and Chemical PET Associated Processes

The Photoinduced Electron Transfer has been associated to a series of physical and chemical processes including:

A) Chemical reactivity.

The PET associated chemical processes usually lie in bond cleavage, including deprotonation at the α carbon in aminium radical additions,[17] retro-aldol cleavage reactions,[18] oxidations,[19] and reactions in dendrimers.[20]
Some PET process involve bond formation like the C-C bond formation in fullerenes,[21] benzyl sulfides[22] and addition to alkenes.[23]
One novel PET initiated bond formation process is the generation of C-O bonds *via* insertion of hydroxyl radicals, previously generated *via* PET induced bond cleavage in Donor moieties of A-S-D systems (see chapter IV).

B) Photophysical properties.

The most important process involving PET is the fluorescence quenching *via* the formation of a charge-transfer complex that is quenched returning to the ground state. Sometimes, the deactivation of this complex is *via* emission as an exciplex.[24]
Its applicability is in the field of sensors like pH indicators or cation sensors.[25] A recent application of PET effect in fluorescence is its use in the development of molecular logic gates where the photophysical properties are reinterpreted according to the Boolean logic.[26]

[17] a) Lewis, F.D.; Ho, T.-I.; Simpson, J.T.; *J. Org. Chem.* **1981**, *46*, 1077. b) Lewis, F.D.; Ho, T.-I.; *J. Am. Chem. Soc.* **1977**, *99*, 7991.
[18] Su, Z.; Mariano, P.S.; Falvey, D.E.; Yoon, U.C.; Oh, S.W.; *J. Am. Chem. Soc.* **1998**, 120, 10676.
[19] Berglund, J.; Pascher, T.; Winkler, J.R.; Gray, H.B.; *J. Am. Chem. Soc.* **1997**, *119*, 2464
[20] Juris, A.; Balzani, V.; Barigelletti, F.; Campagna, S.; Belser, P.; von Zelewsky, A.; *Coord. Chem. Rev.* **1988**, *84*, 85.
[21] Tokuyama, H.; Isobe, H.; Nakamura, E.; *J. Chem. Soc. Chem. Commun.* **1994**, 2753.
[22] Yusuke, K.; Yoshikazu, K.; Masahiro, T.; Kazuhiro, C.; *Nippon Kagakkai Koen Yokoshu* **2001**, *79*, 730
[23] a) Shigemitsu, Y.; Katsuhara, Y.; Odaira, Y.; *Tetrahedron Lett.* **1971**, *12*, 2887 b) Meggers, E.; Steckhan, E.; Blechert, S.; *Angew. Chem. Int. Ed.* **1995**, *34*, 2137. c) Majima, J.; Pac, C.; Nakasone, A.; Sakurai, H.; *J. Am. Chem. Soc.* **1977**, *99*, 5806.
[24] Lakowicz, J.R.; *"Principles of fluorescence spectroscopy. 3rd Ed"* Springer Science+Business Media, LLC, New York (USA) **2006**, p. 335.
[25] Valeur, B.; *"Molecular fluorescence: Principles and applications"* Wiley-VCH Verlag GMBH **2001**, p.286-292.
[26] Szaciłowski, K.; *Chem. Rev.* **2008**, *108*, 3481.

SPICUM servicio de publicaciones

SPICUM
servicio de publicaciones

CHAPTER II.

OBJECTIVES

SPICUM
servicio de publicaciones

SPICUM
servicio de publicaciones

The doctoral thesis presented here is structured in two main chapters (**III** and **IV**) related with the photochemical reactivity and the study of the photophysical properties of covalently linked electron Donor and Acceptor moieties. The structures object of research always comprises isoquinoline *N*-oxide as electron acceptor. The electron Donor moiety will be oxygen substituted electron rich aromatic rings.

Chapter III

The photochemical reactivity of A-S-D Systems based on isoquinoline *N*-oxide as electron Acceptor and electron rich substituent modified aryl groups as electron Donor is studied in this chapter together with a comprehensive study of their photophysical properties. The variability in the structures is given by changes in the Spacer length to distances larger to one methylene i.e., two bonds.

SPICUM servicio de publicaciones

Objective 1

The analysis of the photophysical properties of systems where the Spacer is increased in length from an ethyl to a propyl alkyl chain will be carried out. The increase of the distance between the electron Acceptor and Donor will be made *via* single bonds placing A and D to a distance of 3 or 4 flexible single bonds respectively. The study of the photochemical reactivity of these systems will lead us to determine the photohydroxylation processes in long-spacer systems.

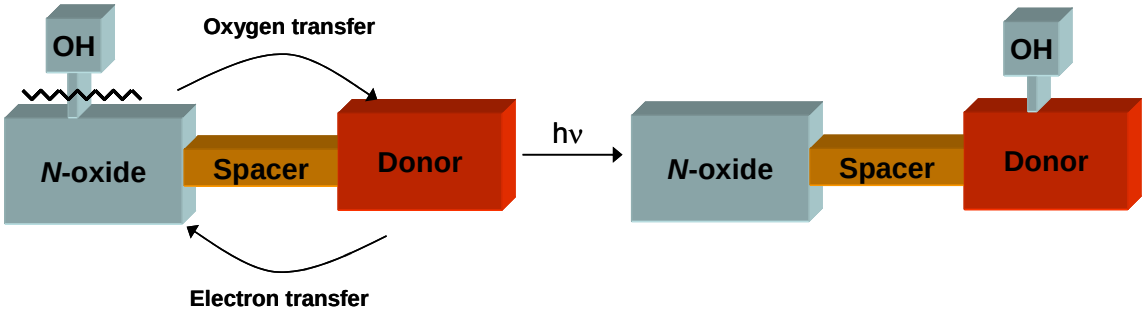

Objective 2

The study of long-spacer systems where the alkyl chains include an amide bond will be developed. The aim to introduce an amide bond in the spacer responds to two main aspects:

- Increase the rigidity of the spacer.
- Define a plug-unplug system with the photohydroxylation reaction as key step in order to:

a) Connect the electron Acceptor and the electron Donor.

b) Produce the photohydroxylation.

c) A final disconnection step to give the hydroxylated electron Donor moiety and the electron Acceptor, recycled to produce a new photohydroxylation process.

SPICUM servicio de publicaciones

Chapter IV

The luminescent properties of the A-S-D systems based on isoquinoline *N*-oxide, mainly the dual-channel fluorescence emission derived from the electron transfer processes observed in acidic media, will be the photophysical properties subjected to study. Based on these properties, it will be possible to develop systems which behaviour is reinterpreted from the Boolean logic.

Objective 3

Synthesis and photophysical study of A-S-D system based on isoquinoline *N*-oxide as electron acceptor and electron donor groups substituted aryl as electron Donor have been studied. The design of this system will be done according to the necessity to get structures capable to interact with chemical species present in the media, specially acids (*N*-oxide), bases (phenol groups) and metallic (alkaline and alkaline earth) cations (benzo-15crown-5 ether as Donor).

Objective 4

The reinterpretation of the A-S-D systems photophysical properties from the field of the Boolean logic will generate truth tables where the response (Output) to the different chemical species present in the media (Input) can connect the behaviour of these chemical structures to electronic logic gates.

SPICUM servicio de publicaciones

SPICUM
servicio de publicaciones

CHAPTER III.

ELECTRON ACCEPTOR-SPACER-DONOR SYSTEMS BASED ON ISOQUINOLINE N-OXIDE

SPICUM
servicio de publicaciones

SPICUM
servicio de publicaciones

III.1. Introduction

III.1.1. Organic reactivity derived from electron transfer processes

The studies of electron transfer reactions have had an increasing interest in the latest years with studies in outer sphere reactions and processes with bond cleavage or formation.

Radical ions are usually generated by one-electron reduction or oxidation process starting from neutral compounds. One electron loss leads to the formation of a radical-cation due to the HOMO electron transfer. At the same time a radical anion is produced *via* the gain of one electron, incorporating to the LUMO. These processes can generate big changes in the atoms bond strength, making the bond cleavage possible.[27]

[27] Schmittel, M.; Ghorai, M.K.; *Electron transfer in chemistry*, vol. 2 (Ed. V. Balzani), Wiley-VCH, Weinhemi (Federal Republic of Germany) **2001**, p. 5-54.

SPICUM servicio de publicaciones

III.1.1.1. Bond cleavage

The injection of one electron into an antibonding orbital or the electron removal from a bonding orbital produce the weakening of characteristics bonds. If we deal with a pure σ^* LUMO (or σ HOMO), electron injection (or removal) will entail the strongest bond weakening effect. ET activation of such systems will always lead to bond dissociation. In highly delocalized radical ions ($\sigma^* + \pi^*$ LUMO), ET will produce reduced bond weakening, but it will still undergo efficient bond cleavage. If LUMO is pure π^*, the cleavage will be efficient if there are σ^* orbitals energetically accessible.
The ionic radicals bond cleavage can be homolytic or heterolytic.[27]

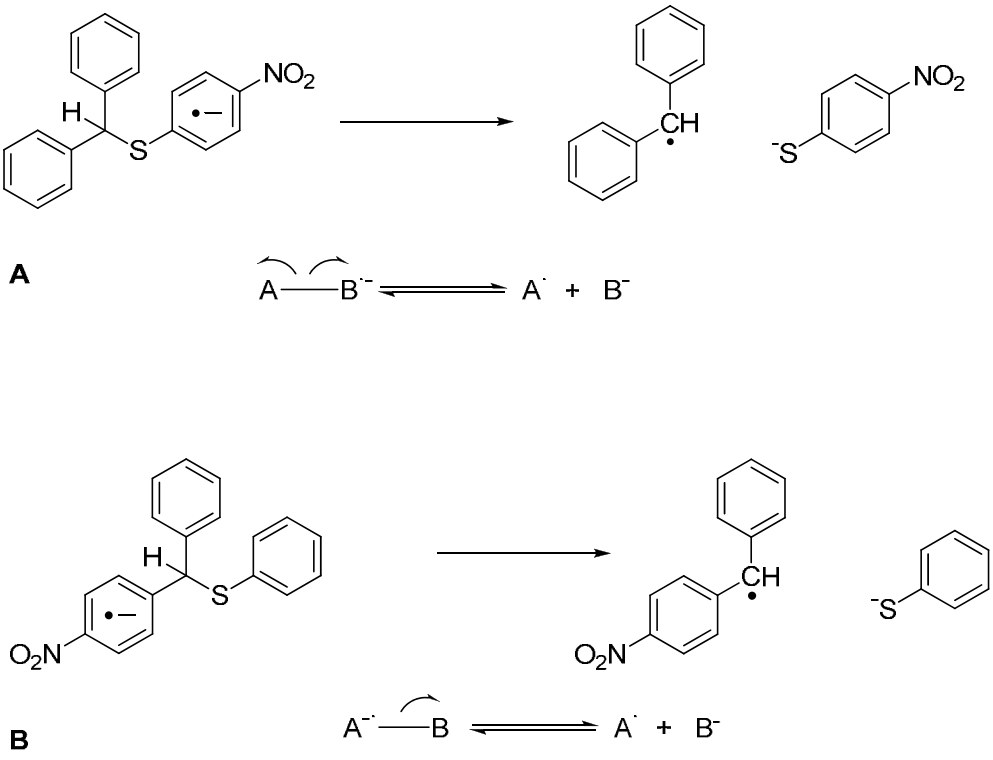

Fig. 11. Homolytic **(A)** *vs.* Heterolytic **(B)** bond cleavage.

In the homolytic cleavage (Fig. 11 **A**), the charge remains on the starting position, while in the heterolytic cleavage (Fig. 11 **B**) the electron pair moves to the initially neutral moiety, being the heterolytic cleavage energy 8 kcal/mol lower.

SPICUM servicio de publicaciones

III.1.1.2. Electron-transfer-initiated nucleophilic substitution

The mechanisms to achieve nucleophilic substitution vary depending on the substrate, the nucleophile and the reaction conditions. For a compound to be substituted by ET, its radical has to be formed by an initial ET, which can be performed by different means as electrochemical initiation, thermal ET from an adequate donor, and photoinitiated ET from the nucleophile. Thermal and photoinitiated ET are favored between nucleophiles that are very good electron donors and substrated that are very good electron acceptors. Once the radicals are formed, they can react through the $S_{RN}1$ chain mechanism with neutral radicals and radical anions as intermediates (Fig. 12).[28]

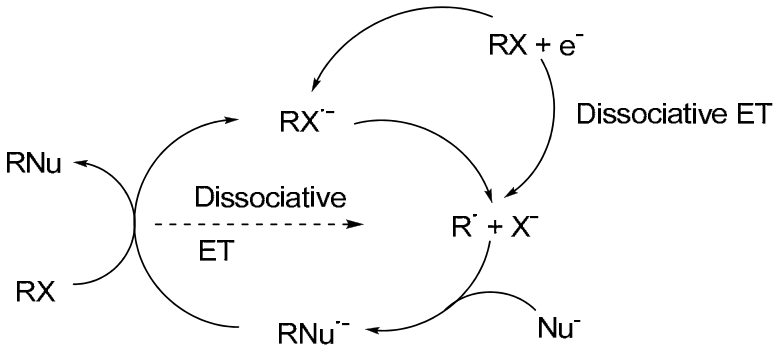

Fig. 12. $S_{RN}1$ mechanism.

It has been shown that excellent yields of substitution can be achieved by a nonchain $S_{RN}1$ reaction[29] albeit the cases known are more limited. In these systems, is possible a cage mechanism followed by coupling of the $R^{\cdot}$ radicals with $Nu^{\cdot}$ to give the substitution product by a geminate or cage collapse process.

$$R\text{-}X\ Nu^{-} \xrightarrow{ET} R^{\cdot}\ X^{-}\ Nu^{\cdot} \longrightarrow RNu + X^{-}$$

[28] Rossi, R.A.; Pierini, A.B.; Peñéñory, A.B.; *Chem. Rev.* **2003**, *103*, 71.
[29] Ahbala, M.; Hapiot, P.; Houmam, A.; Jouini, M.; Pinson, J.; Savéant, J.-M.; *J. Am. Chem. Soc.* **1995**, *117*, 11488.

SPICUM servicio de publicaciones

On aromatic sytems (ArX) is possible a $S_{RN}2$ instead of a $S_{RN}1$ reaction. In the $S_{RN}2$ process, a direct coupling between the Nu^- and $ArX^{\cdot-}$ is proposed.

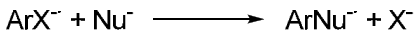

If the aryl group is an unsubstituted aryl halide, this mechanism is completely disregarded, mainly on the basis of the extremely short lifetimes of their radical anions.[30]

III.1.1.3. Rearrangements initiated by bond cleavage in radical cations

The removal of one electron from a σ bond generates a one-electron σ bond. If the cationic radical is delocalized in a π system, the σ bond cleavage can occur quickly. When the reaction is carried out with rings, the cleavage leads to transposition or external reactants addition reactions when the bond has been broken. If there are not nucleophiles present in the media, transpositions in insaturated and rigid structures as compound **(7)** (Fig. 13), produce bond displacement **(8)**, ring contraction **(9)** and spirofluorenebarbaralene **(10)**.[31]

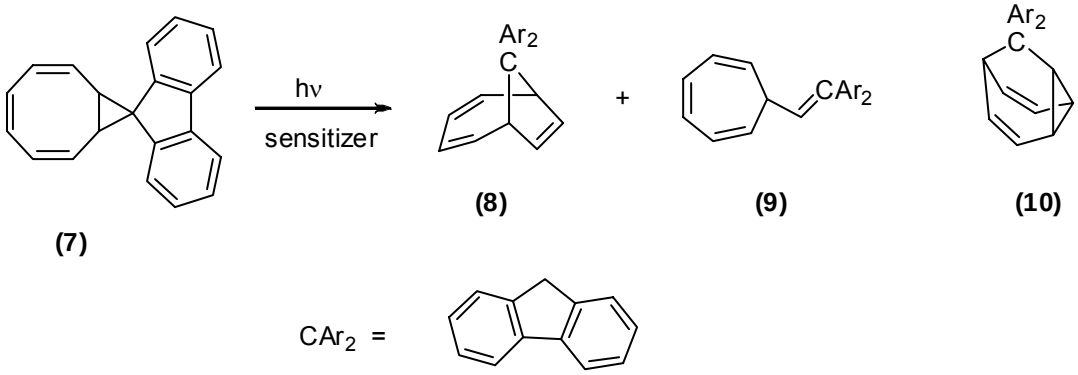

Fig. 13. Rearrangement initiated by bond cleavage in cationic radicals

[30] a) Bunnett, J.F.; *Tetrahedron* **1993**, *49*, 4477. b) Rossi, R.A.; Palacios, S.M.; *Tetrahedron* **1993**, *49*, 4485.
[31] Miyashi, T.; Takahashi, Y.; Konno, A.; Mukai, T.; Roth, H.D.; Schilling, M.L.; Abelt, C.J.; *J. Org. Chem.* **1989**, *54*, 1445.

SPICUM servicio de publicaciones

III.1.1.4. Nucleophile addition to radical cations σ-bonds

Substituted cyclopropanes undergo electron-transfer-induced nucleophilic addition of alcoholic solvents. For example, the electron transfer reaction of phenylcyclopropane **(11)** with *p*-dicyanobenzene in methanol, resulted in a ring-opened ether **(12)** (Fig. 14).[32]

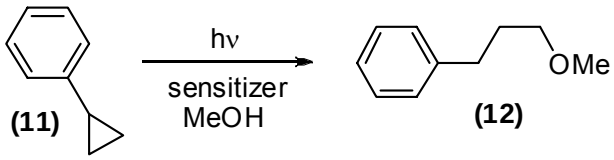

Fig. 14. Methanol addition to cyclopropane cation radical.

This ring opening can also be given on bicyclic systems as bicycle[3.1.0]hexane.[33]

III.1.1.5. Nucleophile addition to radical cations π-bonds

Addition reactions of nucleophiles to π radical cations include reactions at alkenes, alenes, aromatic and heteroaromatic systems amongst others.[27] Electron transfer photochemistry of norbornadiene **(13)** in methanol is shown on Fig. 15. Addition to π bond **(14)** and rearrangement followed by addition **(15)**, **(16)** is performed after irradiation using 1-cyanonaphthalene as sensitizer.[34]

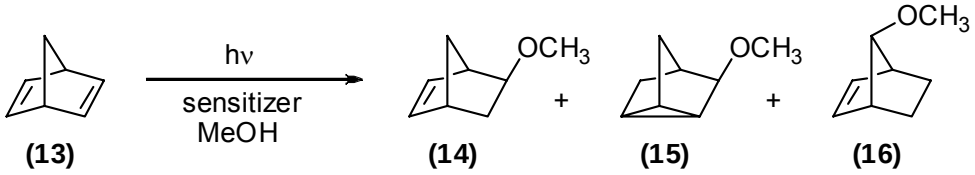

Fig. 15. Nucleophile π bond addition to norbornadiene.

[32] Mizuno, K.; Ogawa, J.; Otsuji, Y.; *Chem. Lett.* **1981**, 741.
[33] Arnold, D.R.; Du, X.; *Can. J. Chem.* **1994**, *72*, 403.
[34] Weng, H.; Roth, H.D.; *J. Org. Chem.* **1995**, *60*, 4136.

SPICUM servicio de publicaciones

III.1.2. Photochemical reactivity of heterocyclic *N*-oxides

N-Oxides form an important family of compounds used as pharmaceuticals, agrochemicals, intermediates in synthetic chemistry and as ligands in metal complexes. *N*-Oxides are common metabolites because they can be formed by oxidation of the N atom of many drugs and xenobiotics.[35] Pharmaceutical products[36] and their metabolites[37] have become of general public concern due to their potential impacts to the environment and *N*-oxides have generated particular interest due to their carcinogenic[38] and toxicological effects.[39]

N-oxides are characterized by the presence of a so-called "donative" bond between nitrogen and oxygen formed by the overlap of the nonbonding electron pair on the nitrogen with an empty orbital on the oxygen atom.[40] This is usually represented by an arrow or by formal charges, with a positive charge on the nitrogen atom and negative charge on the oxygen atom (Fig. 16).

The charge separation in the *N*-oxide function is the basis of its properties. Compounds containing *N*-oxides have been used in coordination chemistry as Lewis base due to their ability to coordinate with metals, protons, halides and organic electron pairs acceptors and have been also applied with macrocyclic compounds.[41]

Fig. 16. *N*-oxide function representation

The organic compounds containing *N*-oxide groups generally exhibit photochemical reactivity, often with moderate quantum yield. Photochemistry of imino *N*-oxides (sp^2 nitrogen hybridization) has been widely studied due to the stability of the final products

[35] Miao, X.-S.; March, R.E.; Metcalfe, C.D.; *Int. J. Mass Spectrom.* **2003**, *230*, 123.
[36] Budzikiewicz, H.; Schaller, U.; Korth, H.; Pulverer, G.; *Monatsh. Chem.* **1979**, *110*, 947.
[37] Gorrod, J.W.; Damani, L.A.; *J. Drug. Metab. Pharmacokinet.* **1980**, *5*, 53.
[38] Bosin, T.R.; Maickel, R.P.; *Res. Commun. Chem. Pathol. Pharmacol.* **1973**, *6*, 813.
[39] Antkowiak, W.Z.; Gessner, W.P.; *Tetrahedron Lett.* **1979**, *20*, 1931
[40] Albini, A.; Pietra, S.; *Heterocyclic N-oxides*, CRC Press, Florida (USA) **1991**, p. 1-5.
[41] a) Ulrich, G.; Hissler, M.; Ziessel, R.; *New J. Chem.* **1997**, *21*, 147. b) Lehn, J.-M.; Pietraszkiewicz, M.; Karpiuk, J.; *Helv. Chim. Acta* **1990**, *73*, 106. c) Collado, D.; Perez-Inestrosa, E.; Suau, R.; Desvergne, J.-P.; Bouas-Laurent, H.; *Org. Lett.* **2002**, *4*, 855.

SPICUM servicio de publicaciones

and the higher quantum yields compared to acyclic derivatives.[42] The photochemistry of the *N*-oxide group can be summarized in two kinds of reactions: oxygen atom rearrangement and *N*-deoxygenation.

For aromatic *N*-oxides, rearrangement reactions involve ring modification or ring expansion *via* insertion of the oxygen atom **(19)** or rearrangement to the ring α *N*-oxide position **(20)**.[40] The choice of the solvent may dramatically affect the course of the photochemical reactions (Fig. 17).[43]

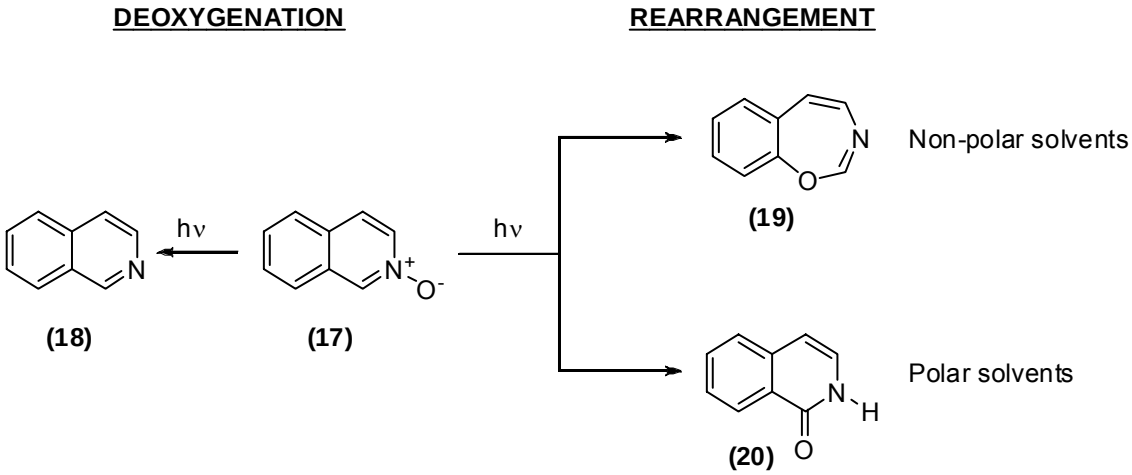

Fig. 17. Deoxygenation vs. Rearrangement in isoquinoline *N*-oxide photochemistry.

[42] Albini, A.; Alpegiani, M.; *Chem. Rev.* **1984**, *84*, 43.
[43] Albini, A.; Fasani, E.; Dacrema, L.M.; *J. Chem. Soc., Perkin Trans. 1*. **1980**, 2738.

SPICUM servicio de publicaciones

III.1.2.1. Oxygen rearrangement

Irradiation of imine *N*-oxides, leads to the formation of oxaziridines as the intermediate for the rearrangement of these molecules. The observed reactions can be discussed in terms of a series of concerted (sigmatropic and electrocyclic) rearrangements. The solvent effect lies in the N^{+}-O^{-} bond polarity. Molecules containing *N*-oxide function are highly polar and can easily make hydrogen bonds with protic solvents. In polar solvents, evolution to the lactam is favoured owing to the zwitterionic stabilized intermediate. In non-polar solvents, this form is not stabilized, evolving to the benzoxazepine.

III.1.2.2. Deoxygenation

Deoxygenation process has been widely studied due to the usefulness of *N*-oxide group as N atom protective groups in aromatic rings and its synthetic use as nitrogen containing aromatic rings substitution. Usually, deoxygenation is not the predominant process in the photochemistry of compounds containing the *N*-oxide function, being a very common byprocess.[42] The detailed mechanism of the photoreactions of *N*-oxides is not known. As far as the photo-deoxygenation is concerned, various models have been proposed:[44]

1.- Direct oxygen transfer from an excited state of the *N*-oxide, presumably *via* previous electron-transfer.

2.- Hydrogen abstraction by an excited state.

3.- Photoisomerization of the *N*-oxide to yield an unstable intermediate, with strong oxidizing properties.

4.- Photocleavage of the N-O bond to give the reactive oxygen "*oxene"*.

For the unimolecular photodeoxygenation processes, two interpretations of the rearrangement and deoxygenation mechanisms were usually accepted. Two different excited states were related with the process: singlet for rearrangement reactions and

[44] Fasani, E.; Amer, A.M.; Albini, A.; *Heterocycles* **1994**, *37*, 985.

SPICUM servicio de publicaciones

triplet for deoxygenation processes. It has been proposed that both reactions come from the same oxaziridine intermediate evolving in one or the other direction (Fig. 18).

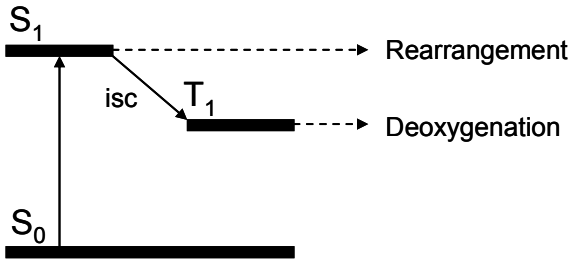

Fig. 18. Rearrangement *vs.* Deoxygenation.

The studies made with sensitized solutions increase the deoxygenation product, demonstrating that the triplet state is an intermediate of the reaction.[45] These results, lead to propose that the rearrangements come from S_1 and deoxygenation come from T_1. It is also shown the appearing of *oxene* in the deoxygenation process.[46]

III.1.2.3. Oxygen transfer

The oxygen transfer is the process that transfers the oxygen atom of the N^+-O^- bond from the *N*-oxide (donor) to the acceptor. It has been developed intermolecular and intramolecular oxygen transfer, but the intermolecular process has lower quantum yields. *N*-oxides have been used synthetically to obtain hydroxylated derivatives.

Mechanistically, the deoxygenation process can be defined as a stepwise or a concerted process. The concerted process needs to start from oxaziridine intermediate and the stepwise process can be radicalic or *via oxene* liberation.[40] Alternative ET mechanisms have been reported.[47]

[45] Tokumura, K.; Matsushita, Y.; *J. Photochem. Photobiol. A: Chem.* **2001**, *140*, 27.
[46] Bucher, G.; Saciano, J.C.; *J. Phys. Chem.* **1994**, *98*, 12471.
[47] Sako, H.; Shimada, K.; Hirota, K.; Maki, Y.; *J. Am. Chem. Soc.* **1986**, *108*, 6039.

SPICUM servicio de publicaciones

Several examples of oxygen transfer in aromatic compounds have been described, studied *via* NIH shift.[48] It is also known that the presence of a Lewis acid, enhance the hydroxylation quantum yield in benzene derivatives.[49] The proposed mechanism described is *via* an *oxenoid* intermediate (**(22)**, **(25)**), with an *oxygen walk* process to obtain the *para* isomer derivative **(29)** (Fig. 19).[50]

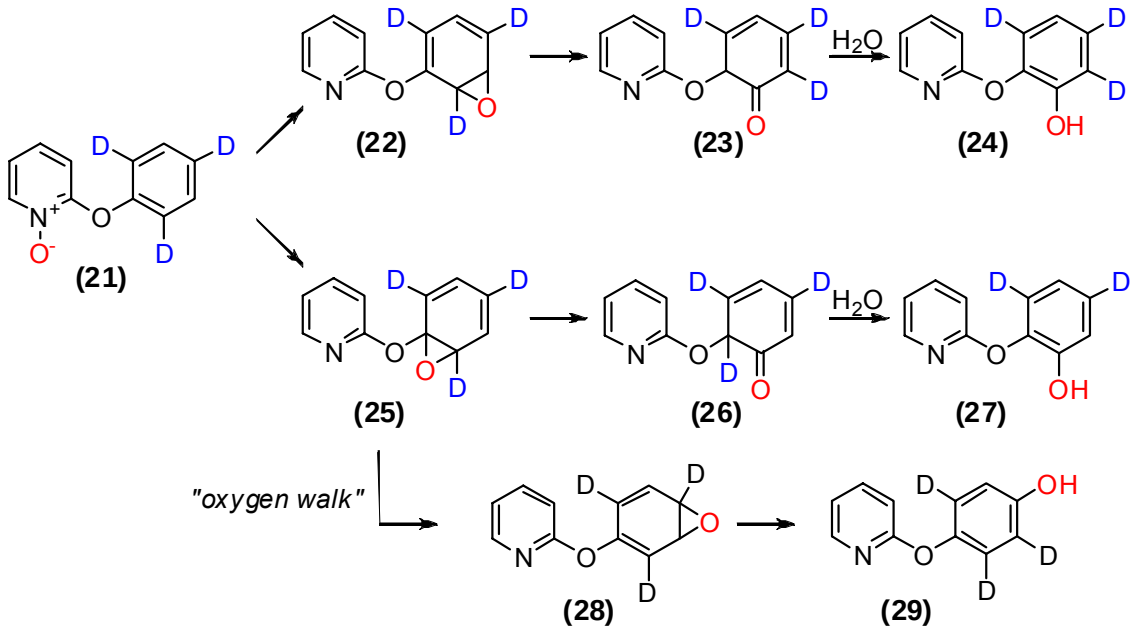

Fig. 19. Oxygen transfer mechanism

For this photoreaction, it is also possible to describe a radicalic mechanism with the generation of a triplet biradical leading to the phenol derivative formation.[50]

If we assume an oxaziridine as a reaction intermediate, the oxygen addition must be a concerted process *via* an intermediate like **(30)** (Fig. 20), leading to the compound **(31)** after addition of the oxygen atom.

[48] a) Mitchell, K.H.; Rogge, C.E.; Gierahn, T.; Fox, B.G.; *Proc. Natl. Acad. Sci. USA*, **2003**, *100*, 3784. b) Jerina, D.M.; Boyd, D.R.; Daly, J.W.; *Tetrahedron Lett.* **1970**, *11*, 457.
[49] Sammes, P.G.; Serra-Errante, G.; Tinker, A.C.; *J. Chem. Soc., Perkin Trans. 1* **1978**, 853.
[50] Zadok, E.; Rubinraut, S.; Frolow, F.; Mazur, Y.; *J. Am. Chem. Soc.* **1985**, *107*, 2489.

SPICUM servicio de publicaciones

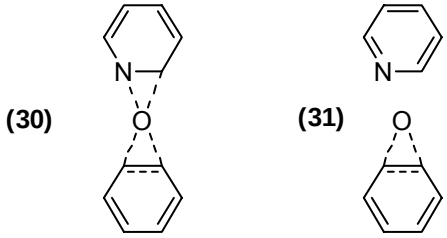

Fig. 20. Concerted process

In our research group, the reactivity of papaverine *N*-oxide **(32)** has been studied showing that the photochemical reactivity of this compound is due to a ET process. Papaverine *N*-oxide can be defined as an A-S-D system where the electron acceptor is the 6,7-dimethoxyisoquinoline *N*-oxide moiety, the electron donor is the dimethoxybenzene moiety and the spacer is a methylene group (Fig. 21).[51]

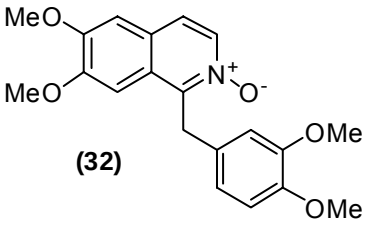

Fig. 21. Papaverine *N*-oxide

Photophysics of **(32)** shows a high influence of the medium, due to the *N*-oxide function capability to form hydrogen bonds, showing a hypsochromic shift while enhancing the polarity and the hydrogen bond formation possibility of the solvent. It is also fluorescent, due to the local emission (LE) of the isoquinoline *N*-oxide moiety.

As well, **(32)** shows that the *N*-oxide function can coordinate with electrophiles as H^+, Zn^{2+}, etc., increasing its electron-acceptor capacity. This union produces changes in its photophysical properties, observing an ET process from dimethoxybenzene moiety

[51] a) Suau, R.; Rico-Gómez, R.; Souto-Bachiller, F.A.; Rodríguez-Rodríguez, L.A.; Ruiz, M.L.; *Tetrahedron Lett.* **1995**, *36*, 2653. b) Souto-Bachiller, F.A.; Perez-Inestrosa, E.; Suau, R.; Rico-Gómez, R.; Rodríguez-Rodríguez, L.A.; Coronado-Pérez, M.E.; *Photochem. Photobiol.*, **1999**, *70*, 875.

SPICUM servicio de publicaciones

(donor) to the enhanced *N*-oxide electron-acceptor, and in the photochemical reactivity. Like this, after protonation with trifluoroacetic acid, a second fluorescence emission band is observed, centred at λ_{em} = 500 nm due to an emissive charge transfer (CT) excited state.

On the same way, there are changes on the photochemistry of the system in neutral media. The reactivity is the expected for isoquinoline *N*-oxide,[52] where deoxygenation competes with rearrangement reactions. Insertion of the oxygen atom in the heterocycle to obtain 1,3-benzoxazepine in non-protic solvents or isocarbostyril in protic solvents are the main rearrangement processes. When papaverine *N*-oxide is protonated, irradiation produces the deoxygenation product and a new photochemical process, leading to the hydroxylation of the Donor benzene ring.

Deoxygenation process occurs from a triplet excited state while hydroxylation and rearrangement processes are due to a singlet excited state. The intramolecular hydroxylation is due to a charge transfer (CT) state.

The *N*-oxide redox potentials are pH dependent. Protonation of *N*-oxide produces a net positive charge on isoquinoline ring and makes it a better electron acceptor.[53] The variation of the acid concentration has influence in the photochemistry of **(32)**. Higher acid concentrations displace the acid-basic balance to the protonated *N*-oxide increasing the hydroxylation yield while the deoxygenation process is hardly affected, showing the independence of both processes.

With these results, the hydroxylation mechanism proposed is based on the formation of a CT state. The ET process produces the generation of a radical in the isoquinoline moiety and a radical cation on the benzene ring. The homolytic N-OH bond cleavage rearomatizes the isoquinoline ring and produces the insertion of the hydroxyl radical generated on the electron poor benzene ring (Fig. 22).

[52] Bremmer, J.B.; Wiriyachitra, P.; *Aust. J. Chem.* **1973**, *26*, 437.
[53] Jaffé, H.H.; Doak, G.O.; *J. Am. Chem. Soc.* **1955**, *77*, 4441.

SPICUM servicio de publicaciones

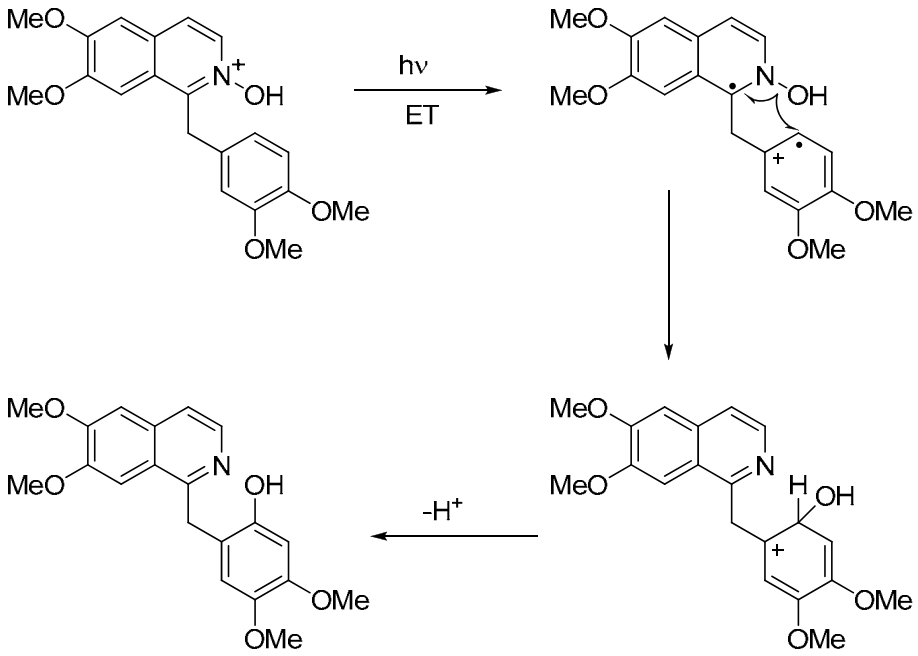

Fig. 22. Hydroxylation mechanism on papaverine *N*-oxide

The hydroxylation is a regioselective process where the -OH group is placed in *ortho* position to the methylene bridge.

The modification of the electron donor and acceptor leads to changes in the photophysical and photochemical properties. The studies carried out in our research laboratory, where the electron acceptor is an isoquinoline *N*-oxide moiety and the donor is a modified benzene ring, shows effective photohydroxylation processes after irradiation in acidic media regioselectively and with high yields (Fig. 23), detecting the CT fluorescent emissive state.[54,55]

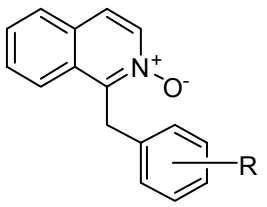

R= H, OMe, OH

Fig. 23. Isoquinoline *N*-oxides derivatives studied

[54] Collado, D.; Perez-Inestrosa, E.; Suau, R.; *J. Org. Chem.* **2003**, *68*, 3574.
[55] Collado, D.; Perez-Inestrosa, E.; Suau, R.; Lopez Navarrete, J.T.; *Tetrahedron* **2006**, *62*, 2927.

SPICUM servicio de publicaciones

III.2. Reactividad fotoquímica de sistemas A-S-D de electrones basados en *N*-óxido de isoquinolina

En nuestro grupo de investigación se han sintetizado previamente sistemas Aceptor-Espaciador-Dador (A-S-D) basados en un aceptor electrónico de *N*-óxido de isoquinolina, espaciador metileno y como dador una unidad de benceno modificada con grupos dadores de electrones, metoxilo e hidroxilo (Fig. 24).[54,55]

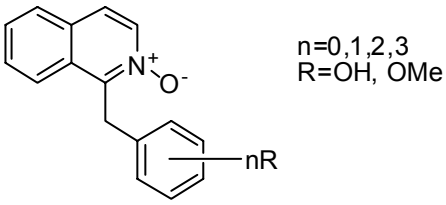

Fig. 24. Sistema modelo

SPICUM servicio de publicaciones

Los estudios de estos sistemas se han centrado en observar la modificación de sus propiedades fotofísicas y fotoquímicas en función del cambio de la sustitución del anillo dador mediante la introducción de sustituyentes metoxilo o hidroxilo, alterando así las propiedades redox del sistema.

Nuestro objetivo en este trabajo se centra en el estudio de cómo afecta a las propiedades de estos sistemas la modificación de la distancia entre el aceptor y dador de electrones, es decir, el cambio en la longitud del espaciador.

De esta forma, en primer lugar se plantea la síntesis de los sistemas **(33)** y **(34)** donde se aumenta la longitud de la cadena alquílica espaciadora siendo una unidad etileno para **33** y propileno para **34**. De esta forma la separación entre el Aceptor y el Dador de electrones será de 3 y 4 enlaces respectivamente. (Fig. 25).

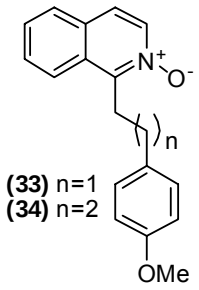

Fig. 25. Sistemas A-S-D con espaciador alquílico

En segundo lugar, planteamos que la longitud del espaciador aumente mediante la inserción de un enlace amida, basándonos en la estructura de 1-isoquinolina carboxamida modificando el residuo amino. De esta forma, abordamos la síntesis de los compuestos **(35)** - **(42)** (Fig. 26).

SPICUM servicio de publicaciones

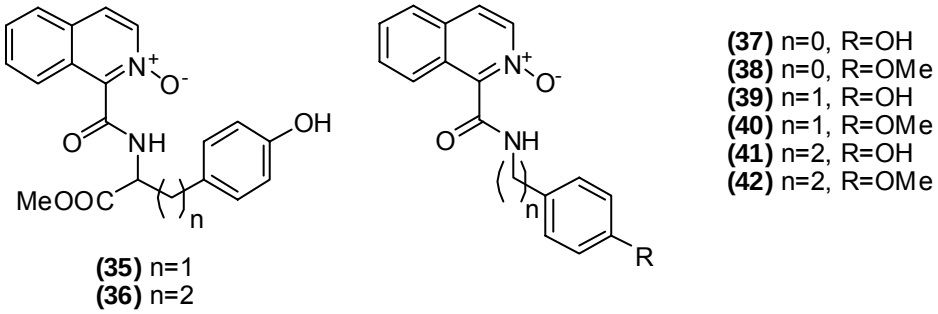

Fig. 26. Sistemas A-S-D con espaciador amida

La inserción de un enlace amida en el espaciador obedece a dos ideas principales:

a) Conferir cierta rigidez al sistema.
b) Posibilidad de ruptura del enlace amida con el objetivo de reciclado del aceptor electrónico en sucesivos ciclos de reacción.

III.2.1. Sistemas A-S-D con espaciador alquílico

III.2.1.1. Síntesis de sistemas de *N*-óxidos A-S-D con S de 2 y 3 átomos de carbono

La estructura básica de estos sistemas A-S-D está formada por la unión de un anillo de isoquinolina y un anillo bencénico sustituido a través de un puente etileno o propileno. Esta sustitución, situará al aceptor y al dador de electrones a una distancia de 3 y 4 enlaces simples para **(33)** y **(34)** respectivamente.

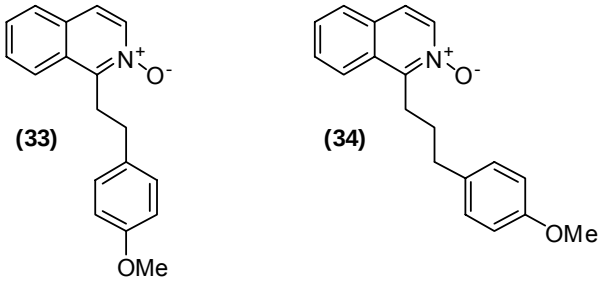

SPICUM servicio de publicaciones

Para la síntesis de estos compuestos, nos planteamos como paso clave la síntesis de una isoquinolina 1-sustituida. Existen varios métodos descritos para la síntesis de estos sistemas, siendo las más usuales la síntesis de Bischler-Napieralski o la reacción de condensación de Reissert (Fig. 27).[56]

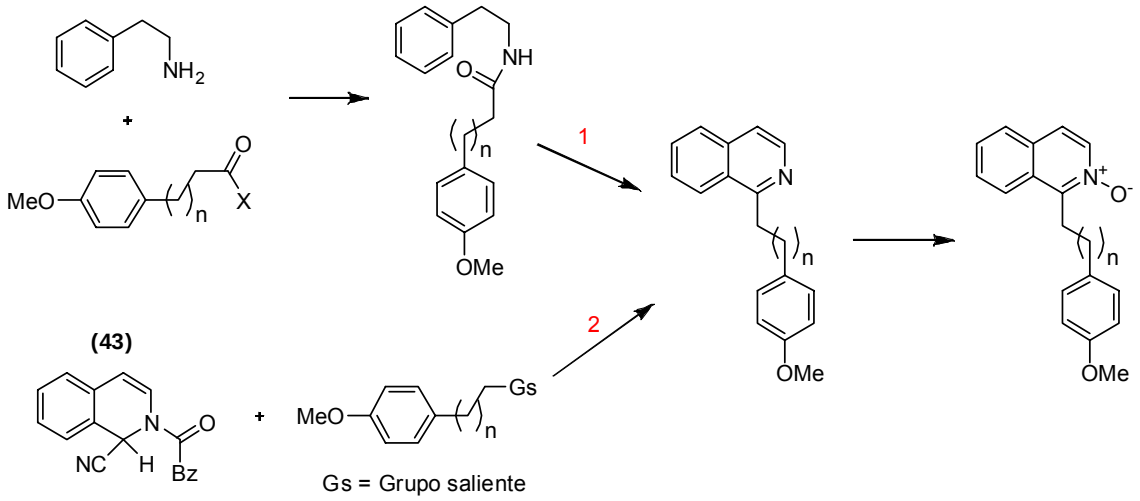

Fig. 27. Síntesis de isoquinolinas 1-sustituidas mediante reacción de Bischler-Napieralski **(1)** o mediante reacción de condensación de Reissert **(2)** como etapa clave.

La ciclación de Bischler-Napieralski, emplea como material de partida una β-fenetilamina, que se condensa con el haluro de ácido correspondiente y, en un posterior paso de reacción, se cicla mediado por un agente deshidratante como cloruro de fosforilo, pentóxido de fósforo u otros ácidos de Lewis.[57] Tras esto, se obtienen 3,4-dihidrobencilisoquinolinas 1-sustituidas que se aromatizan mediante un paso posterior de deshidrogenación mediada con un catalizador.

El método de la condensación del Reissert de isoquinolina con el compuesto correspondiente, origina isoquinolinas 1-sustituidas totalmente aromáticas.[56] El tratamiento del 2-benzoil-1-ciano-1,2-dihidroisoquinolina (Reissert de isoquinolina) con bases, genera un anión capaz de reaccionar con electrófilos para obtener análogos sustituidos en C-1. La posterior hidrólisis de la amida formada conduce a la rearomatización del anillo de isoquinolina.

[56] Shamma, M.; *The isoquinoline Alkaloids. Chemistry and Pharmacology*, vol. 25. Ed A. T. Blausuist y H. Wasserman. Academy Press. Nueva York y Londres **1972**, p. 45-89.
[57] Gilchrist, T.L.; *Heterocyclic Chemistry*, Longman Scientific & Technical, Essex **1992**, cap. 5.

SPICUM servicio de publicaciones

En nuestro caso, dada la conveniencia de síntesis y elaboración posterior, la reacción de condensación del Reissert es la ruta sintética que emplearemos para la obtención de los productos **(33)** y **(34)**.

El esquema para la síntesis de **(33)** y **(34)** se representa en la Fig. 28.

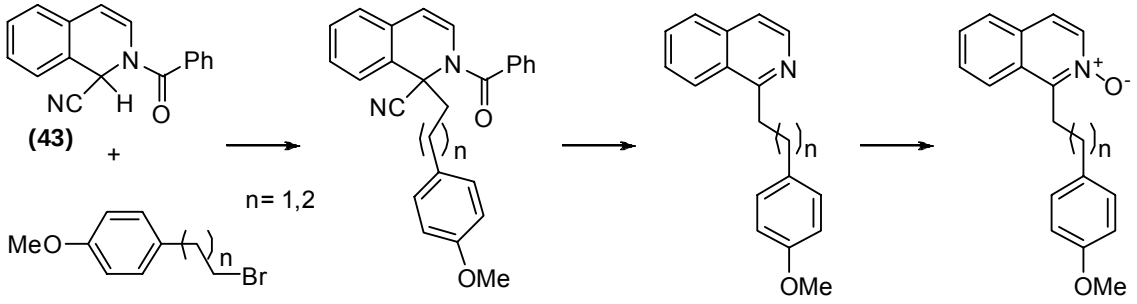

Fig. 28. Esquema sintético general de síntesis mediante reacción de acoplamiento Reissert

La formación del compuesto Reissert de isoquinolina **(43)**, inicialmente se llevaba a cabo mediante la reacción de isoquinolina con cloruro de ácido en una disolución acuosa de KCN.[58] Posteriormente se han mejorado los rendimientos de síntesis mediante modificaciones de la reacción inicial, empleando condiciones bifásicas y catalizadores de transferencia de fase,[59] siendo este método el que hemos empleado para su obtención.

- Síntesis de los bromuros de alquil-fenilo

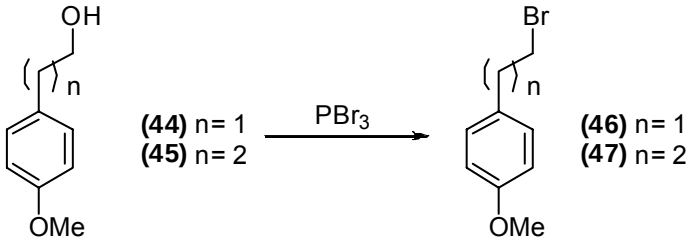

Fig. 29. Esquema de bromación de alcoholes

La síntesis de los bromuros de alquil-fenilo **(46)** y **(47)** se llevó a cabo partiendo de los alcoholes **(44)** y **(45)** mediante tratamiento con PBr_3, con unos rendimientos en torno al 65% en ambos casos. Estos haluros se caracterizaron por sus datos espectroscópicos, resultando coincidentes con los bibliográficos.

[58] Popp, F.; *Advances in Heterocyclic Chemistry*, vol.9, Ed. Academic Press, New York **1968**, p. 1-26.
[59] Koizumi, T.; Takeda, K.; Yoshida, K.; Yoshii, E.; *Synthesis* **1977**, 497.

SPICUM servicio de publicaciones

- Condensación del Reissert de isoquinolina y los bromuros de alquilfenilo

La generación del anión del compuesto Reissert **(43)** se ha llevado a cabo usando diversas bases como son NaH en DMF o THF, KOH en presencia de diciclohexil-18-corona-6 empleando benceno como disolvente o en condiciones bifásicas de NaOH (50%) en H_2O y benceno, utilizando un catalizador de transferencia de fase,[59] siendo los más empleados para transferencia de aniones las sales de amonio cuaternarias.[60]

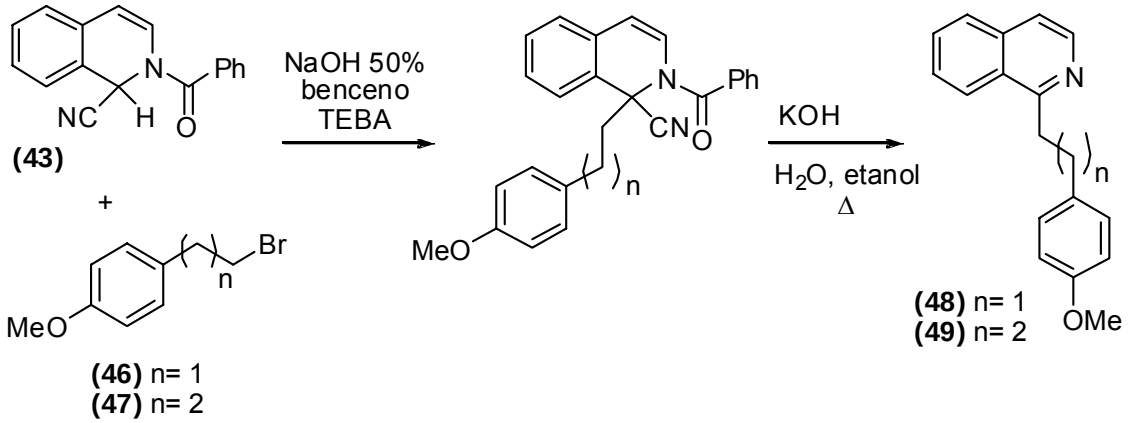

Fig. 30. Esquema reacción de acoplamiento Reissert

De esta forma, las reacciones de condensación de los cloruros con el compuesto Reissert se llevaron a cabo mediante catálisis de transferencia de fase (en nuestro caso, el catalizador empleado es el cloruro de bencil-trietilamonio, TEBA), entre una fase orgánica (benceno) y una acuosa de NaOH al 50%.[61] Esta reacción, nos da el aducto del compuesto Reissert, que debe hidrolizarse en condiciones acuosas básicas, para regenerar el anillo de isoquinolina (Fig. 30). De esta forma, obtuvimos los compuestos **(48)** y **(49)** con unos rendimientos del 78% y del 30% respectivamente.

[60] a) Starks, C.M.; *J. Am. Chem. Soc.* **1971**, *93*, 195. b) Herriott, A.W.; Picker, D.; *J. Am. Chem. Soc.* **1975**, *97*, 2345. c) Makosza, M.; *Pure. Appl. Chem.* **2000**, *72*, 1399.
[61] Makosza, M.; *Tetrahedron Lett.* **1969**, *10*, 677.

SPICUM servicio de publicaciones

- N-oxidación del anillo isoquinolínico

Existen diversos métodos de preparación de *N*-óxidos de heterociclos aromáticos. Todos ellos emplean un peróxido o un peroxiácido como agente oxidante, siendo comunes el ácido peracético, el *terc*-butilhidroperóxido,[62] los ácidos perfórmico,[63] peroxitrifluoroacético,[64] peroxidicloromaleico[65] y dimetildioxirano.[66] Más comúnmente, se emplean compuestos aromáticos como son ácidos perbenzoicos y sus derivados, siendo mucho más estables que los anteriores.

El oxidante más utilizado y el que nosotros hemos empleado es el ácido *m*-cloroperbenzoico. La reacción se realiza empleando $CHCl_3$ como disolvente a temperatura ambiente, con lo que obtuvimos los *N*-óxidos **(33)** y **(34)** como un sólido el primero y como un aceite denso el segundo, con unos rendimientos del 85 % y el 80% respectivamente (Fig. 31).

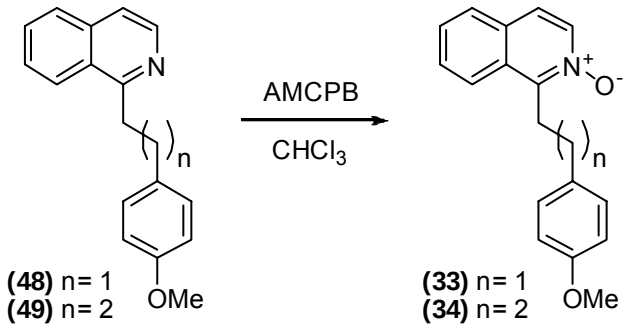

Fig. 31. Esquema de reacción de *N*-oxidación

[62] Sheng, M.N.; Zajacek, J.G.; *Org. Synth.* **1988**, *6*, 501.
[63] Roberts, S.M.; Suschitzky, H.; *J. Chem. Soc.C* **1969**, 1485.
[64] Chivers, G.E.; Suschitzky, H.; *J. Chem. Soc. C* **1971**, 2867.
[65] Pollak, A.; Zupan, M.; Sket, B.; *Synthesis* **1973**, 495.
[66] Murray, R.W.; Jeyaraman, R.; *J. Org. Chem.* **1985**, *50*, 2847.

SPICUM servicio de publicaciones

III.2.1.2. Propiedades fotofísicas

- Absorción electrónica

Estudiando los espectros de absorción electrónica en medio neutro de **(33)** y **(34)**, observamos que ambos son muy similares (Fig. 32) y de igual forma presentan gran semejanza con los espectros de los derivados 1-bencilisoquinolínicos estudiados previamente en nuestro laboratorio.[54]

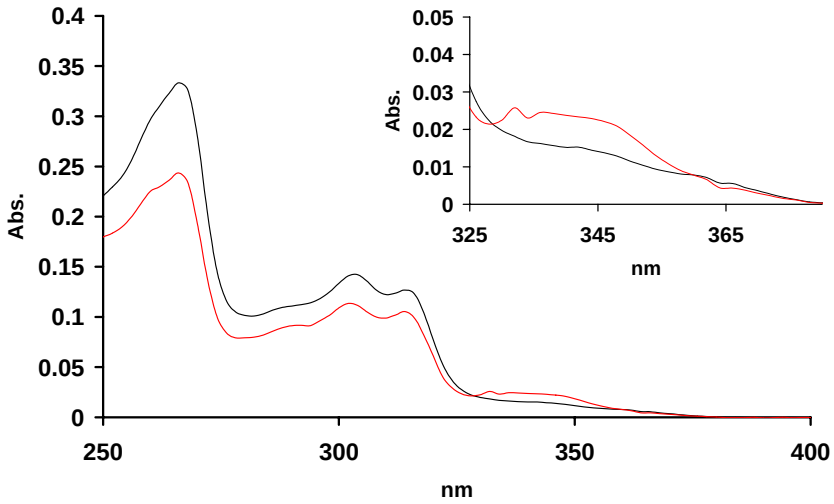

Fig. 32. Espectros de absorción en $CHCl_3$ de los *N*-óxidos **(33)** (—) y **(34)** (—)

En estos espectros, registrados empleando $CHCl_3$ como disolvente, a concentraciones 10^{-5}M de **(33)** y **(34)**, las bandas situadas a partir de 240 nm, corresponden mayoritariamente a la absorción del *N*-óxido de isoquinolina, siendo esta contribución total para longitudes de onda mayores a 300 nm. Por otro lado, la contribución del anillo de benceno es mucho mayor a longitudes de onda menores.

A partir de 330 nm, se observa una banda débil, correspondiente a una transición $\pi\pi^*$ de un orbital π localizado en el oxígeno a un orbital deslocalizado del anillo heterocíclico. Estas bandas están muy influenciadas por la polaridad del disolvente y sufren un desplazamiento hipsocrómico al aumentar la polaridad de éste.[40] Los máximos de absorción y los coeficientes de absorción molar de esta banda se muestran en la Table 1.

SPICUM servicio de publicaciones

Table 1. Coeficientes de absorción molar de **(33)** y **(34)** en $CHCl_3$

	(33)	**(34)**
λ_{max} (nm)	346	346
ε ($M^{-1}cm^{-1}$)	$1.38 \cdot 10^3$	$2.21 \cdot 10^3$

Las propiedades fotofísicas de los *N*-óxidos **(33)** y **(34)** vienen definidas por el sistema A-S-D formado por el *N*-óxido y el 4-metoxibenceno como Aceptor y Dador de electrones respectivamente y el etileno/propileno como Espaciador. Los sistemas aceptor-dador de electrones unidos covalentemente interaccionan tanto en el estado fundamental como en el estado excitado. Esta interacción es dependiente en gran medida de la forma en que están unidos A y D.

La unión mediante enlaces σ evita la conjugación entre A y D y hace que el espectro del sistema se asemeje a la suma de los espectros de los cromóforos individuales por separado, observándose pequeños desplazamientos hipsocrómicos respecto a los cromóforos por separado, que ponen de manifiesto cierta interacción aceptor-dador en el estado fundamental.

Estos datos, demostrados para los sistemas A-S-D donde S es una unidad de metileno,[54] pueden extrapolarse con fiabilidad a los sistemas **(33)** y **(34)** donde S es una unidad etileno o propileno.

En presencia de ácidos, se produce la protonación de la función *N*-óxido. Esto tiene una importante influencia en el carácter de transferencia de carga (CT) de las bandas de absorción del *N*-óxido que eran debidas a una transición $\pi\pi^*$ desde el orbital π del oxígeno hasta un orbital π^* del anillo, observándose un desplazamiento hipsocrómico hasta un máximo a 336 nm. De igual forma, la banda de absorción local del cromóforo, sufre un desplazamiento hipsocrómico, desde aproximadamente 310 nm a unos 280 nm.

SPICUM servicio de publicaciones

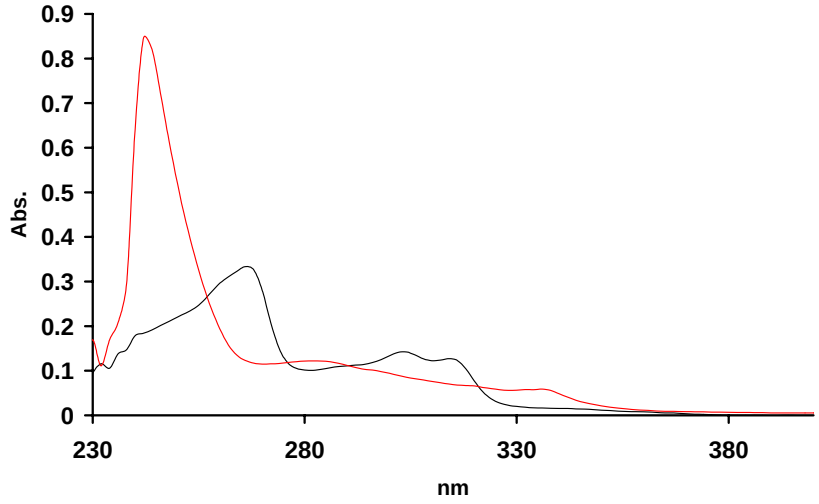

Fig. 33. Absorción en $CHCl_3$ neutro (—) y 0.1M TFA (—) de **(33)**

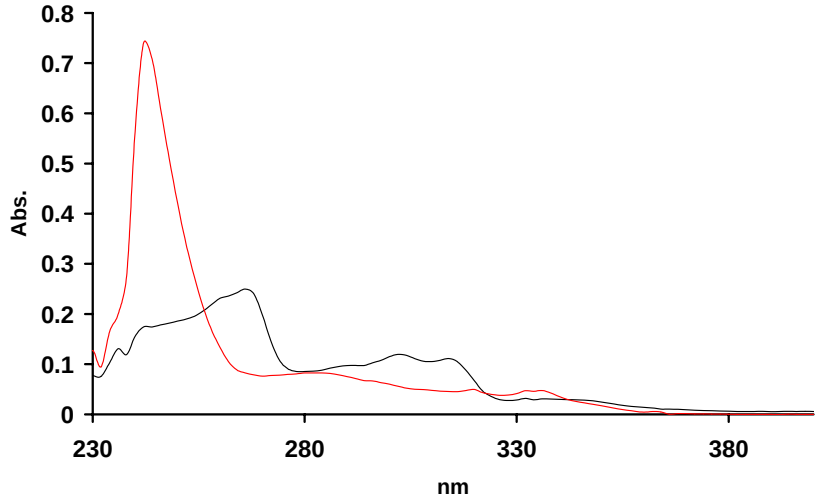

Fig. 34. Absorción en $CHCl_3$ neutro (—) y 0.1M TFA (—) de **(34)**

Se puede observar una gran similitud en el comportamiento de los productos **(33)** (Fig. 33) y **(34)** (Fig. 34) al registrarse su absorción electrónica en $CHCl_3$ a concentraciones 0.1M de ácido trifluoroacético.

SPICUM servicio de publicaciones

De igual forma, comparando los espectros de absorción de **(33)** y **(34)** en medio ácido entre sí, se observa que la extensión de la cadena espaciadora no influye de manera apreciable en el perfil de bandas de absorción (Fig. 35).

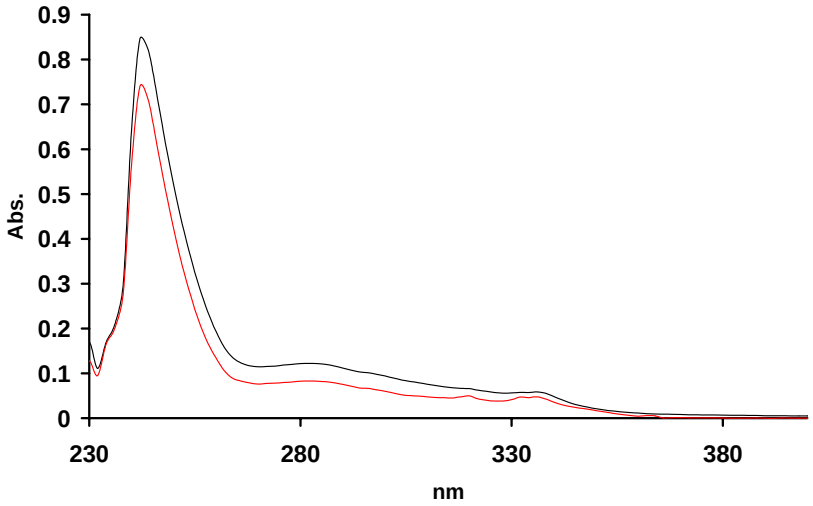

Fig. 35. Espectros de absorción de **(33)** (—) y **(34)** (—) en $CHCl_3$ 0.1M TFA

Los coeficientes de absorción molar de **(33)** y **(34)** en medio ácido, se muestran en la Table 2.

Table 2. Coeficientes de absorción molar de **(33)** y **(34)** en $CHCl_3$ (0.1M TFA)

	(33) (H^+)	**(34) (H^+)**
$\lambda_{máx}$ (nm)	336	336
ε ($M^{-1}cm^{-1}$)	$5.87 \cdot 10^3$	$7.11 \cdot 10^3$

SPICUM servicio de publicaciones

- Espectroscopía de fluorescencia

Los espectros de emisión de fluorescencia en medio neutro de los *N*-óxidos **(33)** y **(34)** se componen de una banda no estructurada, independiente de la longitud de onda de excitación, centrada a 396 nm (Fig. 36).

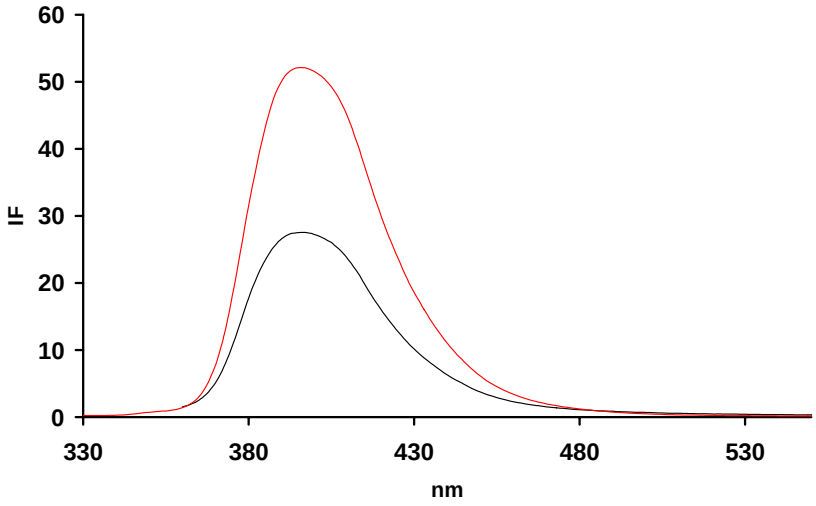

Fig. 36. Espectros de emisión de fluorescencia de **(33)** (—) y **(34)** (—) en $CHCl_3$ (escalado)

Esta banda es debida a la emisión local (LE) de la unidad de *N*-óxido de isoquinolina. Esta emisión local no se ve afectada por las características del espaciador y dador, de ahí que los espectros sean prácticamente idénticos, con independencia del aumento de distancia entre A y D.

Es interesante anotar que, estudiando los espectros de absorción electrónica, excitaciones a λ_{exc} > 330 nm producen la excitación directa del cromóforo de *N*-óxido de isoquinolina, detectando su correspondiente emisión de fluorescencia. Sin embargo, esta misma emisión es también detectada cuando se excita a λ_{exc} < 300nm (excitando el cromóforo 4-metoxibenceno), que indica un proceso de transferencia de energía efectivo desde el dador hasta el aceptor de electrones, al igual que el observado para el *N*-óxido de papaverina.[51b]

SPICUM servicio de publicaciones

Los rendimientos cuánticos de emisión de fluorescencia de **(33)** y **(34)** se muestran en la Table 3.

Table 3. Rendimientos cuánticos de emisión de fluorescencia **(ϕ)** de **(33)** y **(34)** en $CHCl_3$

	(33)	**(34)**
λ_{em} (nm) (λ_{exc} = 336nm)	396	396
ϕ	$4 \cdot 10^{-3}$	$5 \cdot 10^{-3}$

En los espectros de emisión de fluorescencia en medio ácido, se observan dos bandas de emisión, dependientes de la longitud de onda de excitación.

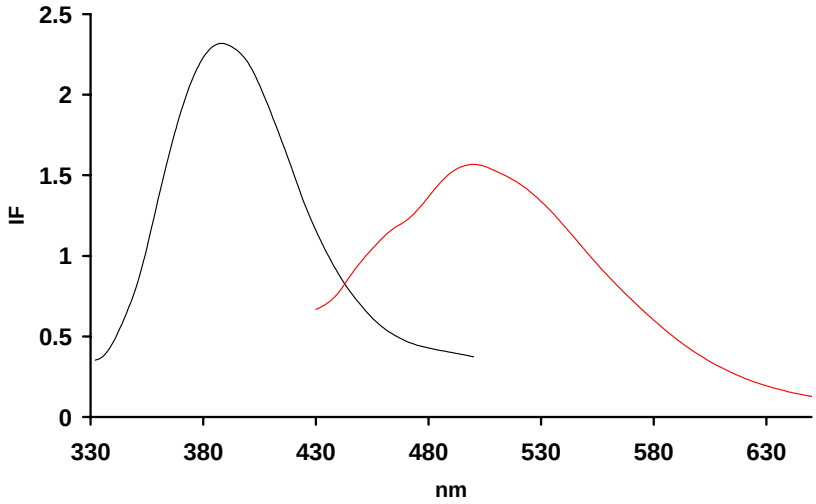

Fig. 37. Espectros de emisión de **(33)** en $CHCl_3$ 0.1M TFA λ_{exc}=330nm (—) y λ_{exc}= 400nm (—) (norm)

Como podemos observar en la Fig. 37, el compuesto **(33)** muestra dos bandas de emisión. Excitando a longitudes de onda λ_{exc}< 330 nm, se observa una banda con máximo a 388 nm que se corresponde con la LE del cromóforo de *N*-óxido de isoquinolina protonado que sufre un desplazamiento hipsocrómico con respecto a la misma banda de emisión en medio neutro. Excitando a longitudes de onda mayores ($\lambda_{exc} \geq$ 360 nm), observamos una nueva banda de emisión, centrada en torno a 500 nm y de menor intensidad, que se corresponde con la emisión desde un estado excitado de transferencia de carga (CT).

SPICUM servicio de publicaciones

Para **(34)**, se observa un perfil de bandas de emisión similar (Fig. 38). De nuevo observamos la banda de emisión correspondiente a la LE del cromóforo de *N*-óxido de isoquinolina, con máximo a 382 nm, y una banda de emisión débil desde el estado CT, que se encuentra a partir de 450 nm.

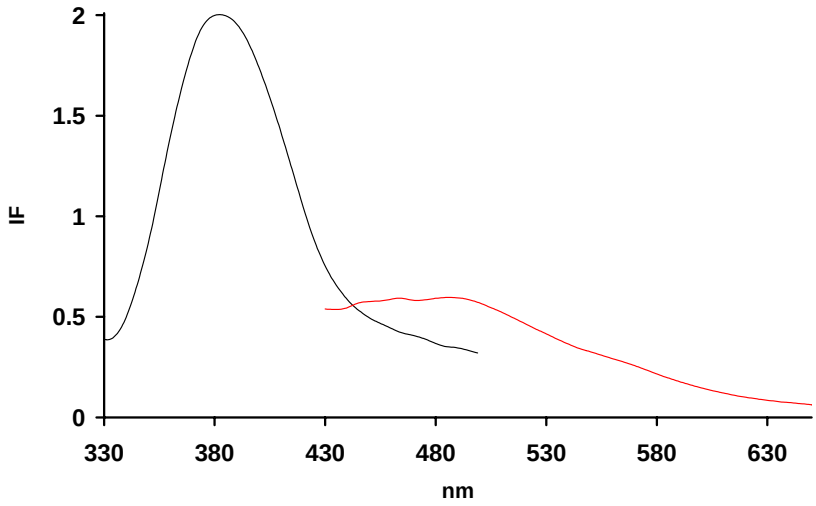

Fig. 38. Espectros de emisión de **(34)** en $CHCl_3$ 0.1M TFA λ_{exc}=330nm (—) y λ_{exc}= 400nm (—) (norm)

En la (Fig. 39) podemos observar la banda correspondiente a la LE excitando a longitudes de onda cortas (λ_{exc} < 330 nm) y la aparición de las bandas CT al excitar a longitudes de onda largas (λ_{exc} > 340 nm).

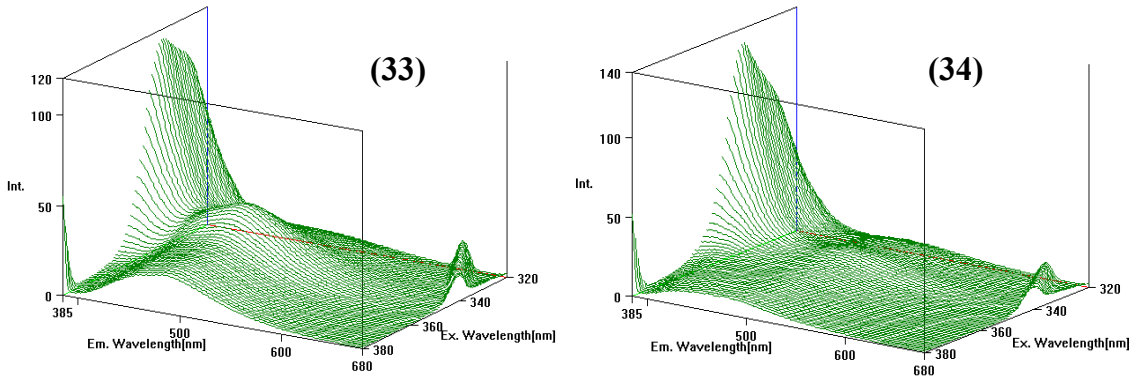

Fig. 39. Espectros 3D de la emisión de fluorescencia de **(33)** y **(34)** en $CHCl_3$ 0.1M TFA

SPICUM servicio de publicaciones

Al igual que en medio neutro, el aumento de la longitud del espaciador no afecta significativamente a las bandas de emisión del cromóforo. Así, como podemos observar en la Fig. 40, la excitación a λ_{exc}< 330, muestra los espectros de emisión desde el estado LE del cromóforo. Ambos presentan una banda de emisión experimentando un desplazamiento hipsocrómico de 6 nm **(34)** respecto a **(33)**.

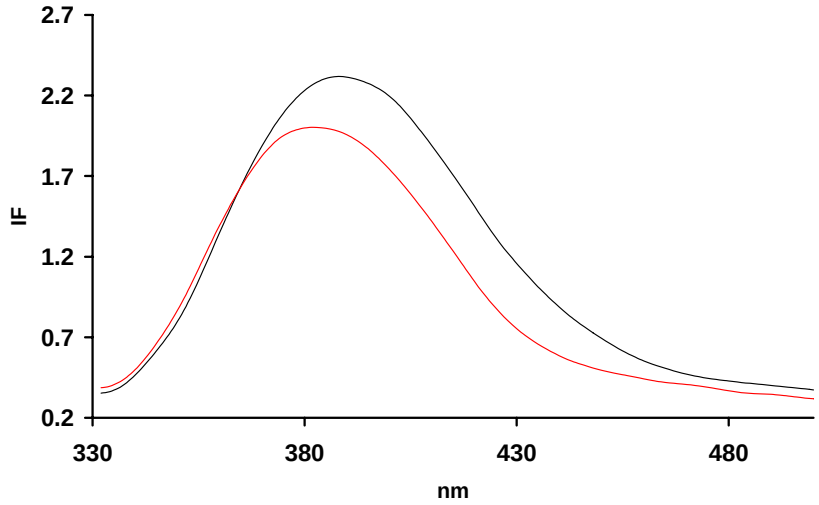

Fig. 40. Espectro de emisión de fluorescencia de **(33)** (—) y **(34)** (—) en $CHCl_3$ 0.1M TFA (λ_{exc}= 314 nm)

En cuanto a la emisión desde el estado CT, sí observamos diferencias entre **(33)** y **(34)**. La mayor dificultad de alcanzar el estado de transferencia de carga para **(34)** con respecto a **(33)** se ve reflejada en la diferencia entre las intensidades relativas de emisión de fluorescencia y los máximos de longitudes de onda de emisión a igual concentración de compuesto (10^{-5} M, 0.1M TFA). Así, la banda de emisión de **(34)** sufre un desplazamiento hacia el azul y una disminución en su rendimiento cuántico de emisión de fluorescencia (Fig. 41).

SPICUM servicio de publicaciones

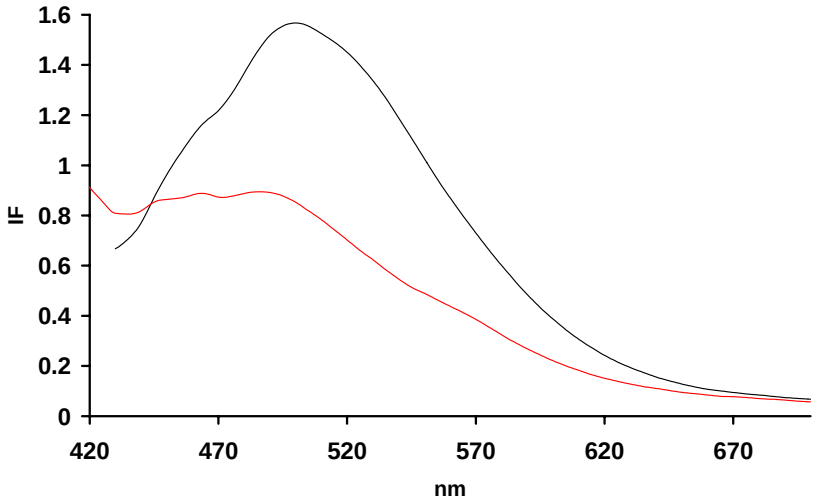

Fig. 41. Espectro de emisión de de **(33)** (—) y **(34)** (—) en $CHCl_3$ (0.1M TFA) (λ_{exc}= 400 nm)

La emisión desde el estado CT es más intensa que la observada desde el estado excitado de LE, siendo mucho más significativo este aumento para **(33)** que para **(34)** como podemos apreciar en la Table 4:

Table 4. Rendimientos cuánticos de emisión de fluorescencia **(ϕ)** de **(33)** y **(34)** en $CHCl_3$ 0.1M TFA

	(33) (H^+)	**(34) (H^+)**
λ_{em} (nm) (λ_{exc} = 314nm)	385	385
ϕ	$2\cdot10^{-3}$	$4\cdot10^{-3}$
λ_{em} (nm) (λ_{exc} = 400nm)	510	510
ϕ	$1.7\cdot10^{-2}$	$6\cdot10^{-3}$

SPICUM servicio de publicaciones

III.2.1.3. Reactividad fotoquímica

Los estudios de reactividad fotoquímica de papaverina y bencilisoquinolinas, mostraron que estos sistemas en medio ácido presentan dos caminos principales de reacción: desoxigenación para dar lugar a la isoquinolina libre de partida y un proceso de hidroxilación intramolecular hacia el anillo dador (Fig. 42).[51b,54,55]

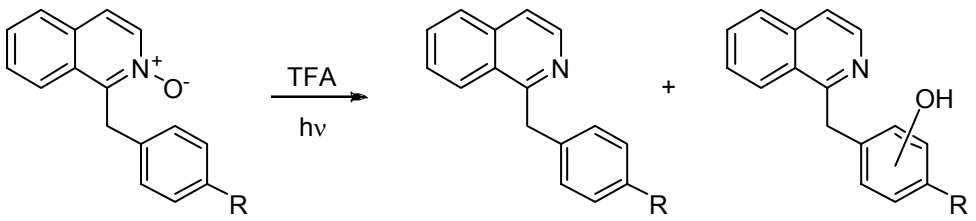

Fig. 42. Productos de irradiación de 1-bencilisoquinolinas

El proceso de desoxigenación está relacionado con la reactividad del estado excitado triplete, mientras que el proceso de hidroxilación se debe a la reactividad del estado excitado singlete. Ambos procesos, desoxigenación e hidroxilación se dan de forma paralela.

De igual forma, el proceso de hidroxilación consiste en la transferencia de oxígeno desde el anillo de *N*-óxido de isoquinolina protonado hasta el anillo bencénico, en un camino inverso al de la transferencia electrónica. Este proceso está determinado por las características energéticas (potenciales redox) del sistema que puede verse modificado mediante cambios en la sustitución del anillo dador o mediante cambios de pH, observándose un aumento del proceso de hidroxilación intramolecular al aumentar la concentración de ácido (TFA).

Mediante las reacciones de fotohidroxilación observadas en los derivados de 1-bencilisoquinolinas, se ha demostrado que, desde un punto de vista mecanístico, la reacción se produce mediante una serie de procesos, consistentes en la ruptura homolítica del enlace N-OH, seguida de liberación de radical hidroxilo y posterior acoplamiento radicalario en el anillo dador. Este mecanismo explica los productos detectados en posiciones *meta* y *para* al puente metilénico (Fig. 43).[54]

SPICUM servicio de publicaciones

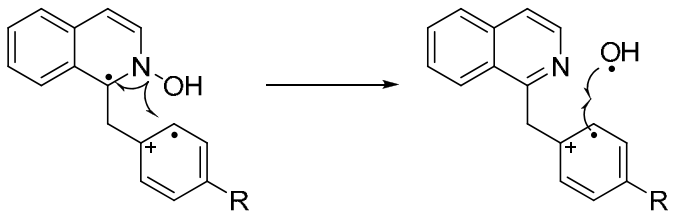

Fig. 43. Mecanismo secuencial de hidroxilación de 1-bencilisoquinolinas

La formación de productos de hidroxilación en el anillo dador para sistemas donde el espaciador es etileno o propileno, puede indicar que este mecanismo secuencial opera preferentemente, amparándonos en la distancia entre A y D.

- Irradiación en medio ácido

Los *N*-óxidos **(33)** y **(34)** se irradiaron durante un tiempo de 6 minutos en ambos casos. Tras irradiar, el crudo se lava con disolución acuosa de $NaHCO_3$ (5%). El crudo de reacción se separó mediante cromatografía en capa fina preparativa, empleando el eluyente adecuado en cada caso.
El progreso de la reacción se siguió por ccf y se estudiaron los crudos de reacción por RMN-^{1}H.

*- Irradiación de **(33)** en medio ácido*

La irradiación del compuesto **(33)** produjo dos productos principales de reacción, el producto de desoxigenación y un segundo producto de hidroxilación. Para **(33)** el producto de hidroxilación que se obtiene es el resultado de la inserción del radical ·OH en la posición bencílica de la cadena alquílica espaciadora **(50A)**. Esta estructura se confirma comparando sus datos experimentales con los bibliográficos.[67] En las condiciones ácidas de reacción, deshidrata para generar un doble enlace conjugado con el anillo de isoquinolina y el dador bencílico.

[67] Kaiser, E.M.; Knutson, P.L.; *Synthesis* **1978**, *2*, 148.

SPICUM servicio de publicaciones

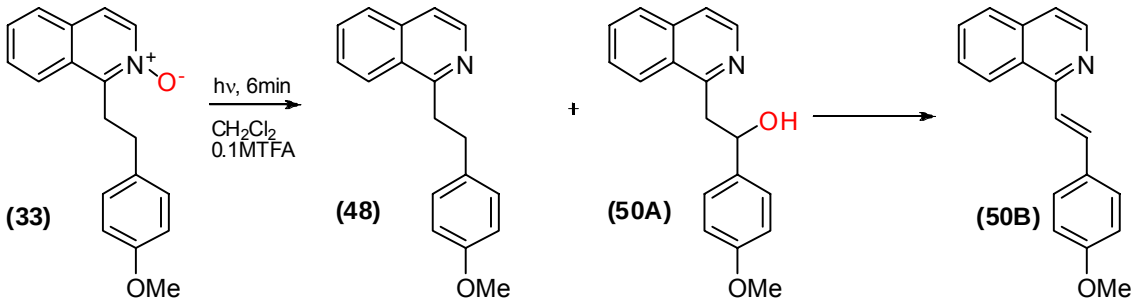

Fig. 44. Productos de irradiación del compuesto **(33)**

El estudio por RMN-^{1}H del crudo de reacción muestra las señales correspondientes al sistema de doble enlace centradas a 7.85 ppm y a 7.93 ppm, con *J*= 15.4 Hz, que confirma la formación del producto de deshidratación.

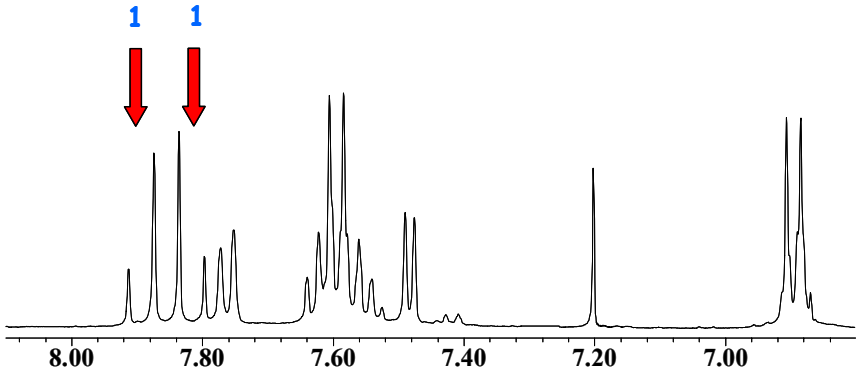

Fig. 45. RMN-^{1}H de producto de deshidratación **(50B)**. Detalle de las señales correspondientes a los H del doble enlace

También se detecta el producto correspondiente de hidroxilación en la cadena puente. Una cuidadosa elaboración de la reacción permite identificar el producto hidroxilado, pero dada su labilidad, su fácil deshidratación en el medio de reacción y que nuestro objetivo es el estudio de la posible hidroxilación del anillo dador, se llevó la reacción hasta la total desaparición de este producto y la obtención del producto de deshidratación, junto con la base libre anteriormente mencionada.

SPICUM servicio de publicaciones

En la Fig. 46, podemos observar el espectro RMN-^{1}H del producto hidroxilado en la cadena espaciadora **(50A)** para la irradiación del producto **(33)**. En el espectro se puede observar el doble doblete correspondiente al H metino unido al C-OH puente a 5.4 ppm, y el sistema de dos dobles dobletes del metileno correspondiente al -CH_2- de la cadena a 3.5 ppm. El tratamiento con ácido trifluoroacético a temperatura ambiente, conduce a la deshidratación y la obtención del producto **(50B)**.

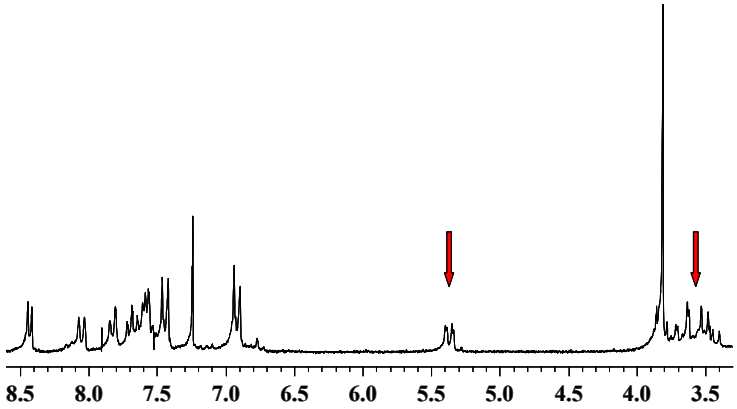

Fig. 46. RMN-^{1}H de producto hidroxilado en espaciador **(50A)**

En la Table 5, se muestran los rendimientos de reacción para la irradiación del compuesto **(33)**.

Table 5. Rendimientos de reacción para la irradiación del producto **(33)**

RENDIMIENTOS REACCIÓN FOTOQUÍMICA			
$t_{irradiacion}$= 6 min	Desoxigenación (%)	Deshidratación (%)	Conversión (%)
(33)	20	24	69

*- Irradiación de **(34)** en medio ácido*

La irradiación del compuesto **(34)** produjo tres productos principales de reacción, producto de desoxigenación y dos productos de hidroxilación. A diferencia de lo ocurrido con el compuesto **(33)**, en el caso de **(34)** los productos de hidroxilación se originan mediante la inserción del radical hidroxilo en el anillo dador. .

La separación mediante cromatografía en capa fina preparativa del crudo de reacción, dio como resultado la obtención de 3 productos mayoritarios. Al realizar el estudio por

SPICUM servicio de publicaciones

RMN del producto de R_f = 0.67 (CH_2Cl_2:MeOH 99:1) se confirmó que se trataba de la isoquinolina de partida **(49)**.

Un segundo producto, a R_f = 0.37 presentó un espectro de RMN-^{1}H (Fig. 47) donde se observa la desaparición del sistema AB correspondiente al sistema bencílico del producto de partida **(34)**, mientras que se observa la aparición de un doble doblete a 6.67 ppm (J_1 = 8.0 Hz, J_2 = 1.6 Hz) que integra por 1 H, un doblete a 6.75 ppm (J = 8.0 Hz) que integra por 1 H y un doblete a 6.79 ppm (J = 1.6 Hz) que integra por 1 H. Este sistema corresponde a un producto de hidroxilación del anillo dador.

La comparativa con el espectro de RMN-^{1}H del 2-metoxi-5-metilfenol,[68] que nos servirá como modelo de las señales del sistema aromático bencénico, permite asignar la estructura del producto de irradiación como la del producto **(52)**.

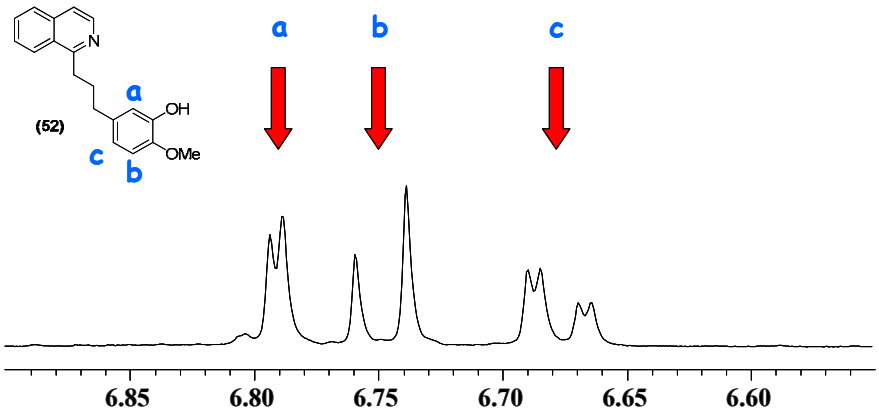

Fig. 47. Estructura y detalle del espectro RMN-^{1}H de **(52)**.
En azul, la asignación de los H bencénicos

Un tercer producto, a R_f = 0.80 presentó un espectro de RMN-^{1}H (Fig. 48) donde se observa la desaparición del sistema AB correspondiente al sistema bencílico del producto de partida **(34)**, mientras que se observa la aparición de un doble doblete a 6.41 ppm (J_1 = 2.4 Hz, J_2 = 8.4 Hz) que integra por 1H, un doblete a 6.58 ppm (J = 2.4 Hz) que integra por 1H y un doblete a 7.00 ppm (J = 8.4 Hz) que integra por 1H. Este espectro confirma la formación de un producto de hidroxilación en el anillo de benceno dador. El estudio de los desplazamientos químicos tabulados para compuestos

[68] Lai, C.-H., Shen, Y.-L.; Wang, M.-N.; Rao, N.S.K.; Liao, C.C.; *J. Org. Chem.* **2002**, *67*, 6493.

SPICUM servicio de publicaciones

aromáticos sustituidos,[69] señala que el desplazamiento del H bencénico situado en posición *orto* al espaciador propileno, se sitúa en torno a 7.00 ppm, que está de acuerdo con el valor registrado experimentalmente y que nos permite asignar la estructura de este producto a la del compuesto **(51)**.

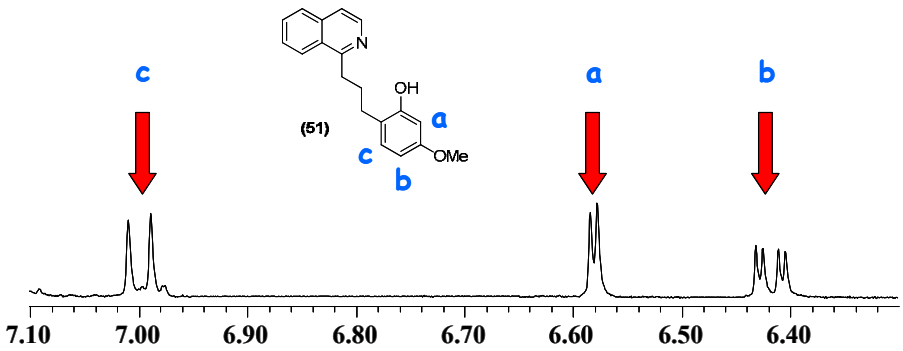

Fig. 48. Estructura y detalle del espectro ^{1}H-RMN de **(51)**.
En azul, la asignación de los H bencénicos

De esta forma, la irradiación de **(34)**, produce tres productos de reacción: el producto de desoxigenación, para dar lugar a la isoquinolina de partida, y dos productos de hidroxilación en las dos posiciones posibles del anillo dador (Fig. 49).

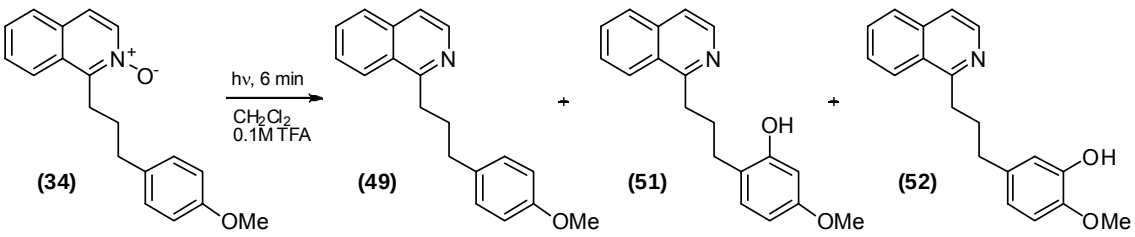

Fig. 49. Productos de irradiación de **(34).**

[69] Lambert, J.B.; Mazzola, E.P.; *Modern Nuclear Magnetic Resonance Spectroscopy: An Introduction to Principles, Applications, and Experimental Methods.* Pearson Prentice Hall, Upper Saddle River, NJ, (USA), **2004**.

SPICUM servicio de publicaciones

Los rendimientos de reacción, se muestran en la Table 6.

Table 6. Rendimientos de reacción para la irradiación del producto **(34)**

RENDIMIENTOS REACCIÓN FOTOQUÍMICA				
t_{irrad}= 6 min	Desoxigenación (%)	Hidroxilación *orto* a E (%)	Hidroxilación *meta* a E (%)	Conversión (%)
(34)	25	4	10	74

El mecanismo de hidroxilación secuencial propuesto en el que la inserción del radical hidroxilo en el anillo bencénico se produce tras la ruptura homolítica y posterior migración en el medio de reacción desde el anillo de isoquinolina (A) hasta el anillo de benceno (D), viene amparado por la formación de una caja de disolvente dentro de la cual se produce esta migración radicalaria.[54] El aumento de distancia entre A y D al aumentar la longitud del S, aumenta la probabilidad de que se produzcan procesos de escape de caja cuya consecuencia es la disminución en el rendimiento de formación de los productos de hidroxilación. Estos procesos de escape de caja, pueden explicar el bajo rendimiento de hidroxilación observado tras la irradiación del producto **(34)**.

Es interesante destacar que los procesos de hidroxilación pueden darse a distancias de hasta 5 enlaces sencillos entre A y D, como se observa para **(34)**. Este hecho, además del mecanismo secuencial mencionado anteriormente, admite la posibilidad de que la generación de estos productos hidroxilados se produzca mediante mecanismos concertados.

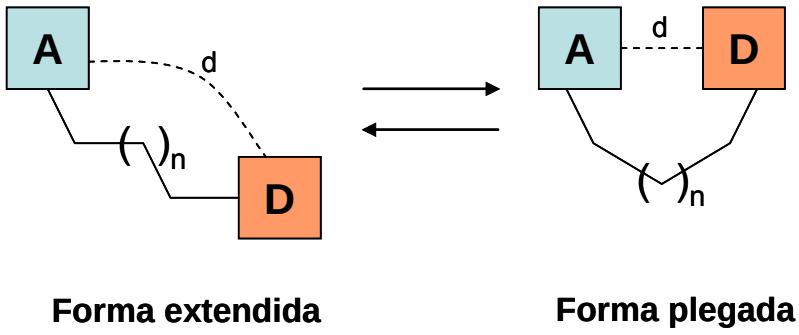

Fig. 50. Equilibrio entre forma extendida y plegada para los sistemas A-E-D con E superior a un metileno, apreciándose la reducción en la distancia *d*

SPICUM servicio de publicaciones

El mayor número de enlaces entre A y D, otorga al sistema mayor número de grados de libertad y con ello, mayor libertad de giro que puede producir el plegamiento de las estructuras de manera que los residuos A y D se coloquen a distancias cortas. Esta disposición espacial, más probable para **(34)** debido a su mayor libertad de giro, puede sustentarse en las interacciones electrostáticas que podrían producirse entre los residuos A y D cargados generados tras el proceso de transferencia electrónica. Esta orientación abre la posibilidad a que el proceso de hidroxilación pueda transcurrir, mediante un proceso concertado de manera similar al postulado para la hidroxilación del *N*-óxido de papaverina (Fig. 50)[51b]

SPICUM servicio de publicaciones

III.2.2. Sistemas A-S-D con espaciador amida

Continuando el estudio de sistemas A-S-D basados en *N*-óxido de isoquinolina, nos planteamos la síntesis de sistemas donde el espaciador consistiera en una cadena donde existiera un enlace amida.

Esta modificación persigue dos objetivos principales: conferir más rigidez al sistema en primer lugar y, en segundo lugar, buscar un sistema de conexión-desconexión para que, en el caso de que la reacción de hidroxilación se produjese, tener la posibilidad de utilizar nuevamente el residuo aceptor de electrones (*N*-óxido de isoquinolina) en un nuevo ciclo de reacción.

De esta forma sintetizamos los compuestos **(35)**-**(42)**, basándonos en la estructura de 1-isoquinolina-carboxamida, donde la separación entre A y D será de 3 enlaces (**(37)**,**(38)**), 4 enlaces (**(35)**,**(39)**,**(40)**) y 5 enlaces (**(36)**,**(41)**,**(42)**).

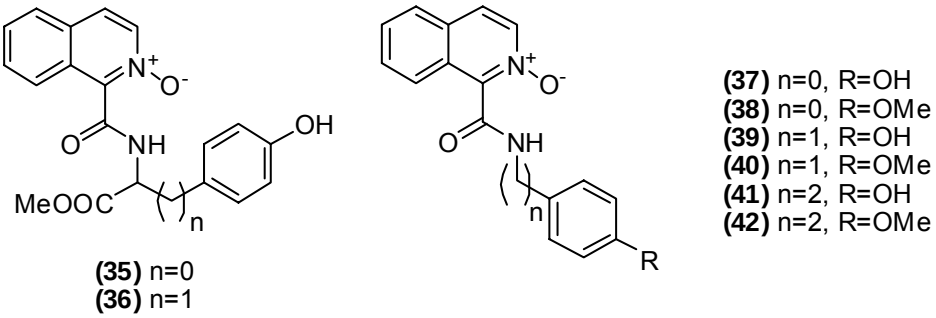

Fig. 51. Estructuras con S amida estudiadas

SPICUM servicio de publicaciones

III.2.2.1. Síntesis de sistemas con espaciador amida

La estructura de estos sistemas (Fig. 51) está formada por la unión de un anillo de isoquinolina y un benceno sustituido en posición *para* con un grupo hidroxilo o metoxilo. Esta unión se realiza mediante una cadena de longitud variable conteniendo un enlace amida, basándose en la estructura de 1-isoquinolina-carboxamida.

La ruta sintética que se ha empleado para la síntesis de estos compuestos presenta, como paso clave, la formación del enlace amida. La formación de enlaces amida es uno de los procesos sintéticos más estudiados debido a su importancia al ser los que forman los enlaces peptídicos, constituyentes de todas las proteínas.

Existen muchos métodos de síntesis de amidas, entre los que se encuentran la conversión directa al calentar a temperaturas elevadas una mezcla del ácido carboxílico y la amina correspondiente,[70] la activación del grupo amino como isocianato o isotiocianato,[71] y la activación de ácidos carboxílicos para posterior reacción con las aminas correspondientes. Esta activación de los ácidos puede hacerse en forma de haluros de ácido,[72] ésteres,[73] y de anhídridos.

Uno de los métodos más comunes es la síntesis mediante la formación de un *anhídrido mixto*, donde se produce la reacción del ácido carboxílico a emplear junto con un haloformiato, (que puede ser de etilo, isopropilo, etc.) para dar un anhídrido altamente reactivo que será atacado por la amina correspondiente,[74] o mediante el empleo de carbodiimidas.[75]

[70] a) Mitchell, J.A.; Reid, E.E.; *J. Am. Chem. Soc.* **1931**, *53*, 1879. b) Coleman, G.H.; Alvarado, A.M.; *Org. Synth. Coll. Vol.1*, **1948**, 3.
[71] a) Goldschmidt, S.; Wick, M.; *Justus Liebigs Ann. Chem.*, **1952**, *575*, 217. b) Blagbrough, I.S.; Mackenzie, N.E.; Ortiz, C.; Scott, A.I.; *Tetrahedron Lett.* **1986**, *27*, 1251. c) Ram, R.N.; Ashare, R.; Mukerjee, A.K.; *Chem. Ind. (London)* **1983**, 569.
[72] Cope, A.C.; Ciganek, E.; *Org. Synth., Coll. Vol.4,* **1963**, 339.
[73] a) Staab, H.A.; *Angew. Chem.* **1962**, *74*, 407. b) Matsumoto, K, Hashimoto, S.; Otani, S.; *Angew. Chem., Int. Ed. Engl.* **1986**, *25*, 565.
[74] a) Vaughan, J.R.Jr.; *J. Am. Chem. Soc.* **1951**, *73*, 3547. b) Boissonnas, R.A.; *Helv. Chim. Acta* **1951**, *34*, 874.
[75] Sheehan, J.C.; Hess, G.P.; *J. Am. Chem. Soc.* **1955**, *77*, 1067.

SPICUM servicio de publicaciones

El método que vamos a emplear es la síntesis mediante el empleo del *anhídrido mixto*, utilizando como generador del anhídrido el cloroformiato de isobutilo. El esquema sintético general se presenta en la Fig. 52.

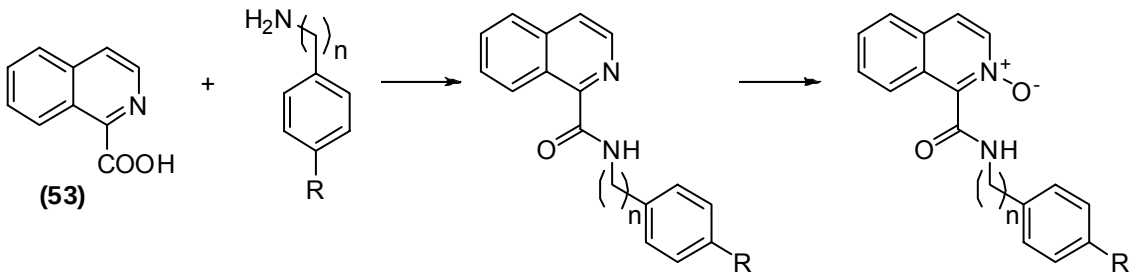

Fig. 52. Esquema sintético general de síntesis de *N*-óxidos de A-S-D con S amida

SPICUM servicio de publicaciones

- Reacción de formación de enlace amida mediante el método del anhídrido mixto

La reacción de formación del anhídrido mixto se lleva a cabo mediante reacción del ácido carboxílico, previamente desprotonado por la acción de una amina terciaria (en nuestro caso *N*-metilmorfolina), con cloroformiato de isobutilo. Esta reacción se mantiene a 0ºC durante 30 minutos. Tras este tiempo, se añade la amina correspondiente y se deja reaccionar durante 48 horas. Si la amina se presenta en forma de hidrocloruro o hidrobromuro, se añade simultáneamente un equivalente de *N*-metilmorfolina. De esta forma obtuvimos los productos **(54-61)** como sólidos con rendimientos superiores al 80%, a excepción de **(60)** que se obtuvo con un rendimiento del 50%.

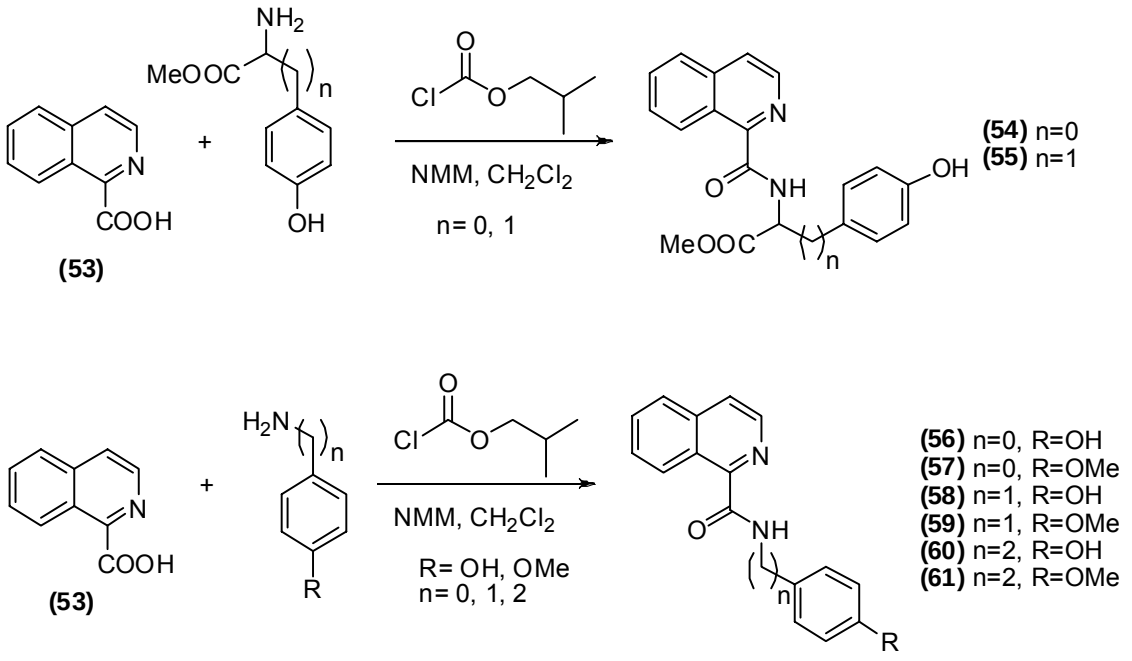

Fig. 53. Esquema de la síntesis de 1-isoquinolina-carboxamidas

SPICUM servicio de publicaciones

- Reacción de N-oxidación

La reacción se lleva a cabo empleando ácido *m*-cloroperbenzoico como oxidante en $CHCl_3$ como disolvente. Para obtener **(35)**, **(37)**, **(39)** y **(41)** empleamos como disolvente metanol, debido a la insolubilidad de los productos de partida en $CHCl_3$. De esta forma, obtuvimos los *N*-óxidos deseados como sólidos con rendimientos superiores al 70% salvo **(36)** y **(38)**, obtenidos con un 51 y 64% respectivamente.

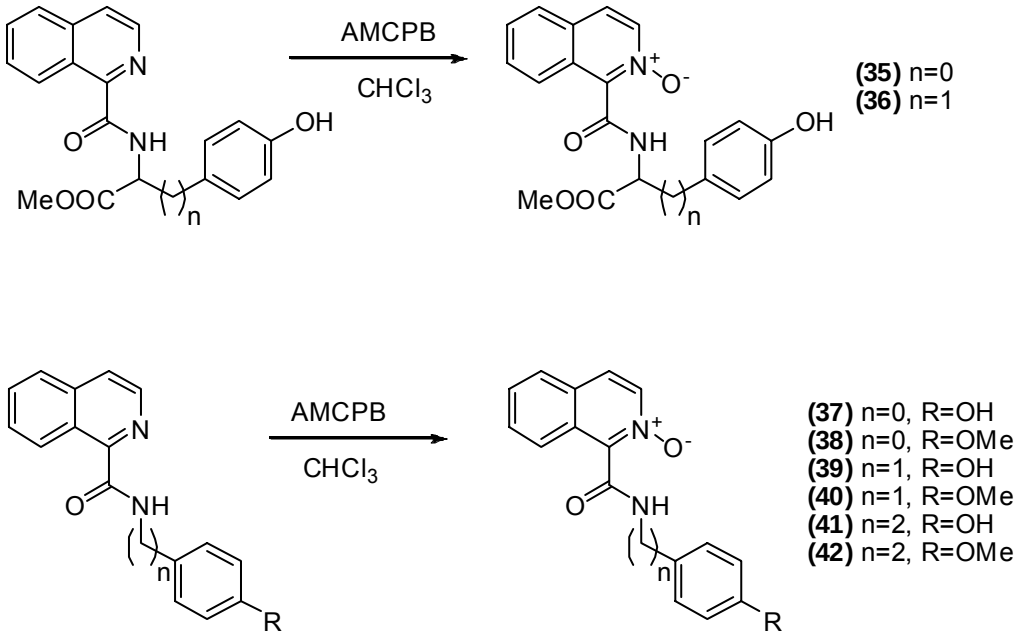

Fig. 54. Esquema de reacción de *N*-oxidación

III.2.2.2. Propiedades fotofísicas

Para el estudio de las propiedades fotofísicas de estos sistemas, vamos a dividir los compuestos estudiados en tres grupos, dependiendo de la distancia (número de enlaces) existente entre el Aceptor y el Dador electrónico. De esta forma, tendremos un primer grupo (Grupo I) formado por los derivados sintetizados a partir de anilinas **(37**, y **38)**, un segundo grupo (Grupo II) formado por los derivados sintetizados a partir de bencilaminas **(35**, **39** y **40)** y un tercer grupo (Grupo III) formado por los derivados sintetizados a partir de 2-feniletilaminas **(36**, **41** y **42)**.

SPICUM servicio de publicaciones

III.2.2.2.1. Grupo I. Compuestos (37) y (38)

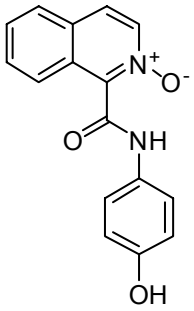

(37)

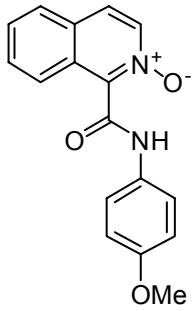

(38)

- Absorción electrónica

En medio neutro, observamos que las bandas de absorción de **(37)** y **(38)** son muy similares, apareciendo una banda entre 330 y 360 que se extiende hasta longitudes de onda mayores de 400 nm (Fig. 55).

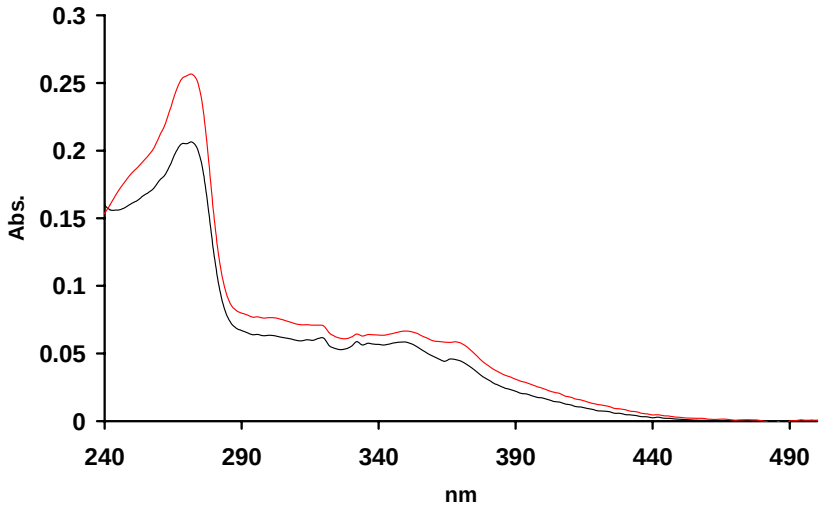

Fig. 55. Espectros de absorción electrónica de **(37)** (—) y **(38)** (—) en CH_2Cl_2

SPICUM servicio de publicaciones

Los coeficientes de absorción molar, registrados con soluciones 10^{-5}M en CH_2Cl_2, se presentan en la Table 7.

Table 7. Máximos de absorción y coeficientes de absorción molar de **(37)** y **(38)** (CH_2Cl_2)

	(37)	**(38)**
λ_{abs} (nm)	352	352
ε ($M^{-1}cm^{-1}$)	$5.71 \cdot 10^3$	$6.61 \cdot 10^3$

En medio ácido, (0.1M TFA) se observa un perfil similar para los dos compuestos (Fig. 56).

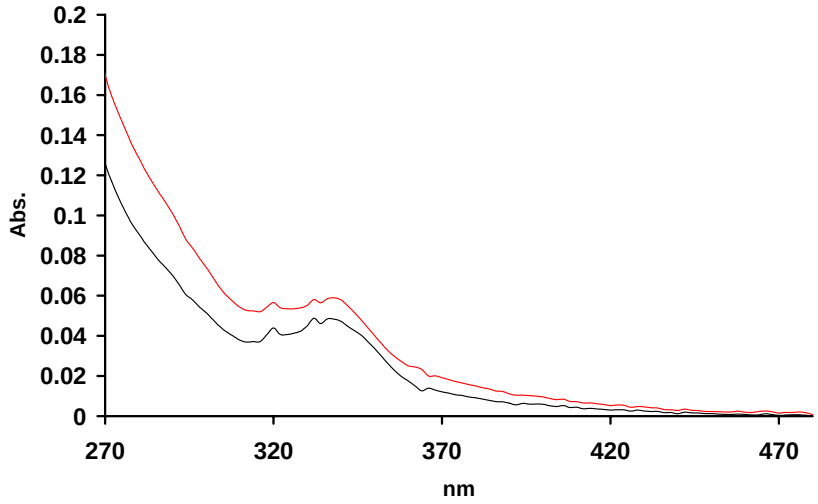

Fig. 56. Espectros de absorción electrónica de **(37)** (—) y **(38)** (—) en CH_2Cl_2 (0.1M TFA)

Los coeficientes de absorción molar, registrados con soluciones 10^{-5} M de **(37)** y **(38)** en CH_2Cl_2 y 0.1M TFA se presentan en la Table 8.

Table 8. Máximos de absorción y coeficientes de absorción molar en CH_2Cl_2 (0.1M TFA) de **(37)** y **(38)**

	(37) (H^+)	**(38) (H^+)**
λ_{abs} (nm)	336	338
ε ($M^{-1}cm^{-1}$)	$4.85 \cdot 10^3$	$5.90 \cdot 10^3$

SPICUM servicio de publicaciones

Tomando como modelo del Grupo I el compuesto **(37)** para comparar la absorción en medio neutro y ácido, se observa el comportamiento típico de estos sistemas. Al protonar el *N*-óxido, la banda de absorción situada en torno a 360-380 nm experimenta un desplazamiento hipsocrómico, situándose su máximo a 336 nm (Fig. 57).

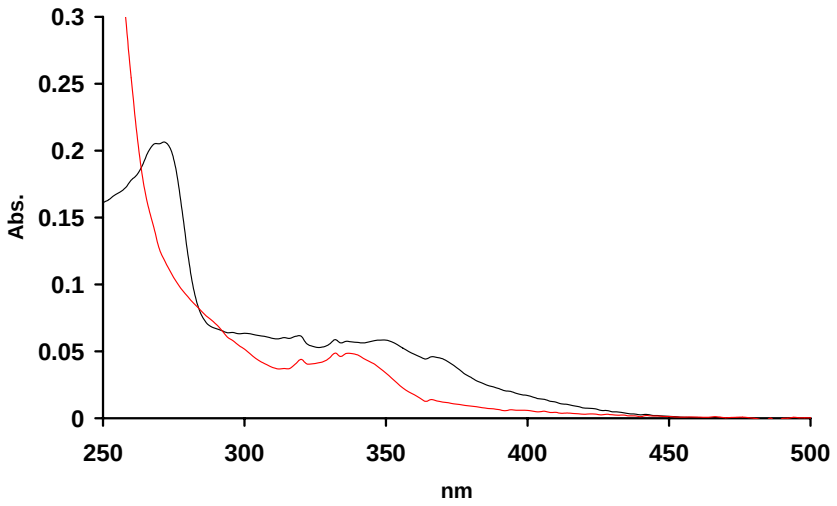

Fig. 57. Espectros de absorción de **(37)** en CH_2Cl_2 neutro (—) y 0.1M TFA (—)

- Emisión de fluorescencia

El estudio en medio neutro muestra una banda de emisión de fluorescencia, independiente de la longitud de onda de excitación, centrada en torno a 340 nm para ambos compuestos (Fig. 58).

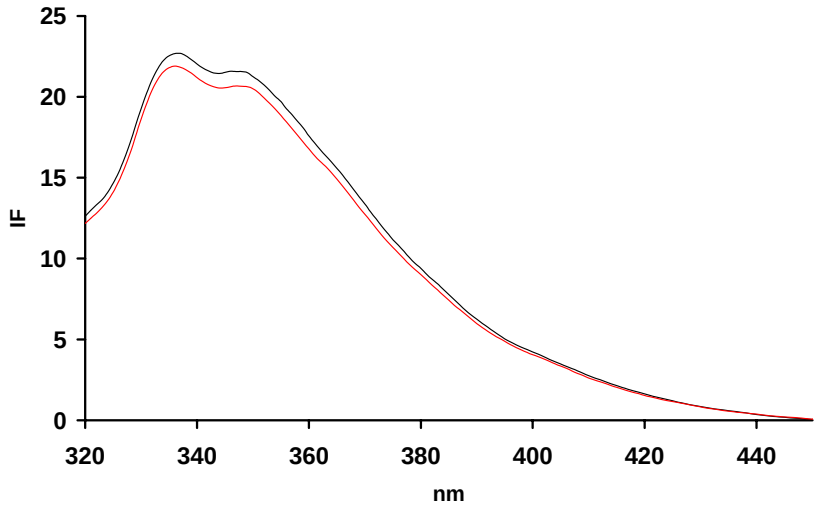

Fig. 58. Espectros de emisión de fluorescencia de **(37)** (—) y **(38)** (—) en CH_2Cl_2

SPICUM servicio de publicaciones

En medio ácido (0.1M TFA), excitando a longitudes de onda λ_{exc}< 340nm se observa una banda de emisión con máximo en torno a 345 nm para ambos compuestos, no detectándose variaciones significativas con respecto a los espectros registrados en medio neutro (Fig. 59).

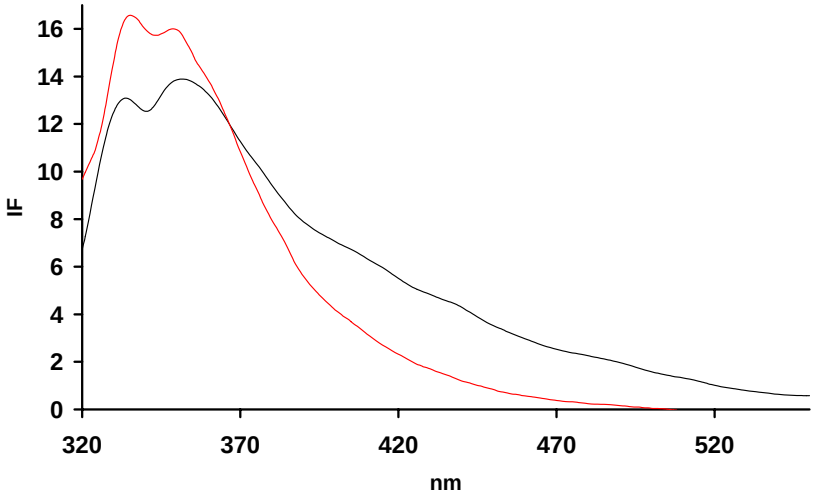

Fig. 59. Espectros de emisión de fluorescencia **(37)** (—) y **(38)** (—) en CH_2Cl_2 0.1M TFA (λ_{exc}< 340 nm)

Excitando a longitudes de onda $\lambda_{exc} \geq$ 360 nm, registramos una segunda banda de emisión, no observada en medio neutro (Fig. 60):

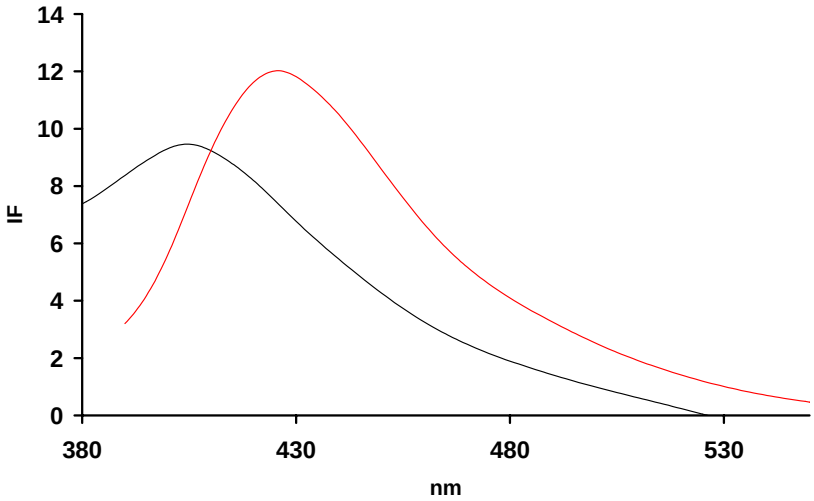

Fig. 60. Espectros de emisión de fluorescencia de **(37)** (—) y **(38)** (—) en CH_2Cl_2 0.1M TFA ($\lambda_{exc} \geq$ 360 nm)

SPICUM servicio de publicaciones

Para **(37)**, esta segunda banda se encuentra desplazada hacia el azul, situándose sus máximos de emisión a 405 nm para **(37)** y a 425 nm para **(38)**.

Las intensidades relativas de emisión de fluorescencia, son similares para ambos compuestos, siendo ligeramente inferiores para **(37)** en medio ácido. Los rendimientos cuánticos de emisión de fluorescencia se exponen en la Table 9:

Table 9. Rendimientos cuánticos de emisión de fluorescencia para los compuestos **(37)** y **(38)**

MEDIO NEUTRO		
	(37)	**(38)**
λ_{em} (nm) (λ_{exc} = 300nm)	345	345
ϕ	$1.9\cdot10^{-2}$	$1.5\cdot10^{-2}$
MEDIO ÁCIDO (0.1M TFA)		
	(37) (H^+)	**(38) (H^+)**
λ_{em} (nm) (λ_{exc} = 300nm)	345	345
ϕ	$1\cdot10^{-3}$	$1.2\cdot10^{-2}$
λ_{em} (nm) (λ_{exc} = 400nm)	405	425
ϕ	$5\cdot10^{-3}$	$1.2\cdot10^{-2}$

SPICUM servicio de publicaciones

III.2.2.2.2. Grupo II. Compuestos (35), (39) y (40)

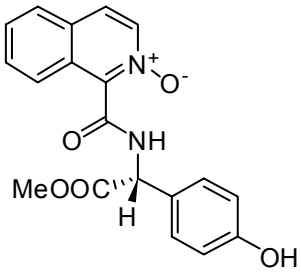

(35)

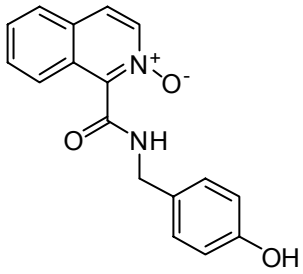

(39)

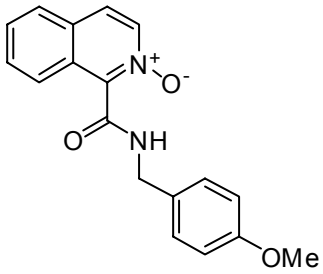

(40)

- Absorción electrónica

En medio neutro, los espectros de absorción electrónica de **(35)**, **(39)** y **(40)** son muy similares, presentando dos bandas de absorción de interés, localizadas con máximos a 314 y 366 nm. Estos espectros se asemejan más a los sistemas 1-bencil[54] y 1-alquilisoquinolínicos (ver Fig. 32), mostrándose un perfil de bandas similar (Fig. 61).

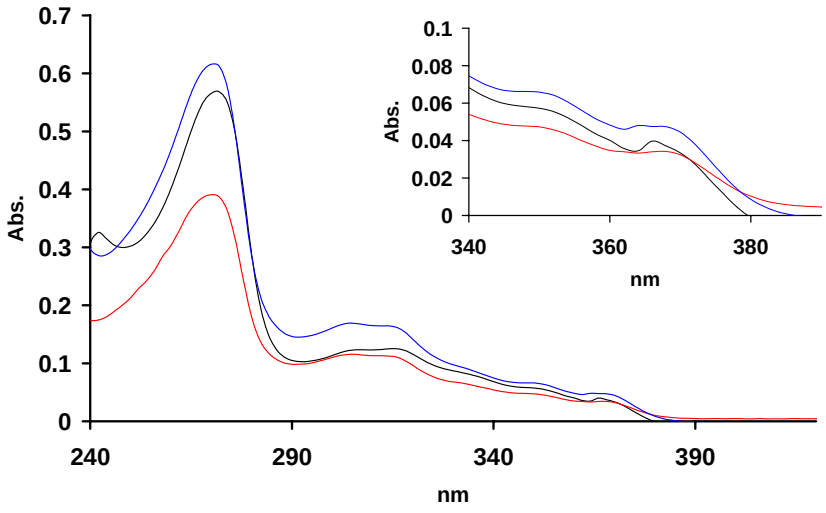

Fig. 61. Espectros de absorción en $CHCl_3$ de **(35)** (—) y CH_2Cl_2 de **(39)** (—) y **(40)** (—)

SPICUM servicio de publicaciones

De igual forma, los espectros de absorción electrónica en medio ácido (0.1M TFA) son muy similares para los tres compuestos, observándose un desplazamiento hipsocrómico de las bandas hasta una $\lambda_{máx}$ de absorción de 340 nm (Fig. 62), al igual que lo observado para los anteriores sistemas.

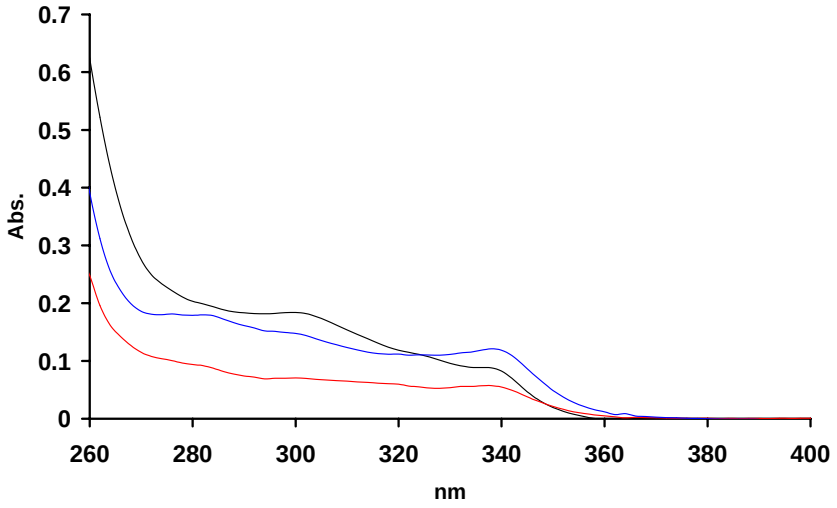

Fig. 62. Espectros de absorción en $CHCl_3$ de **(35)** (—) y CH_2Cl_2 **(39)** (—) y **(40)** (—) (0.1M TFA)

Los máximos de absorción y los coeficientes de absorción molar se muestran en la Table 10.

Table 10. Máximos de absorción y coeficientes de absorción molar de **(35)** en $CHCl_3$, **(39)** y **(40)** en CH_2Cl_2 en medio neutro y ácido (0.1M TFA)

MEDIO NEUTRO			
	(35)	**(39)**	**(40)**
λ_{abs} (nm)	368	368	368
ε ($M^{-1}cm^{-1}$)	$1.86 \cdot 10^3$	$1.03 \cdot 10^3$	$2.16 \cdot 10^3$
MEDIO ÁCIDO (0.1M TFA)			
	(35) (H^+)	**(39) (H^+)**	**(40) (H^+)**
λ_{abs} (nm)	338	338	338
ε ($M^{-1}cm^{-1}$)	$2.55 \cdot 10^3$	$2.91 \cdot 10^3$	$3.56 \cdot 10^3$

SPICUM servicio de publicaciones

- Emisión de fluorescencia

En medio neutro, se observa una única banda de emisión de fluorescencia, al excitar a cualquier longitud de onda, con máximo a 370 nm, debida a la emisión local del cromóforo *N*-óxido de isoquinolina (Fig. 63).

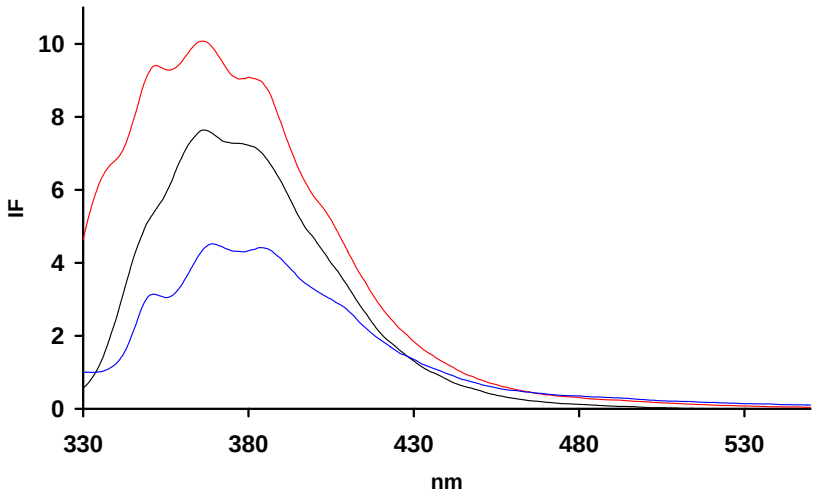

Fig. 63. Espectros de emisión en $CHCl_3$ de **(35)** (—) y CH_2Cl_2 de **(39)** (—) y **(40)** (—)

En medio ácido, se detectan de nuevo dos bandas de emisión de fluorescencia, dependientes de la longitud de onda de excitación. Así, al excitar a λ_{exc} < 330 nm, se observa una banda de emisión con máximo a 370 nm, correspondiente a la emisión LE y que no muestra una variación significativa con respecto a la emisión en medio neutro.

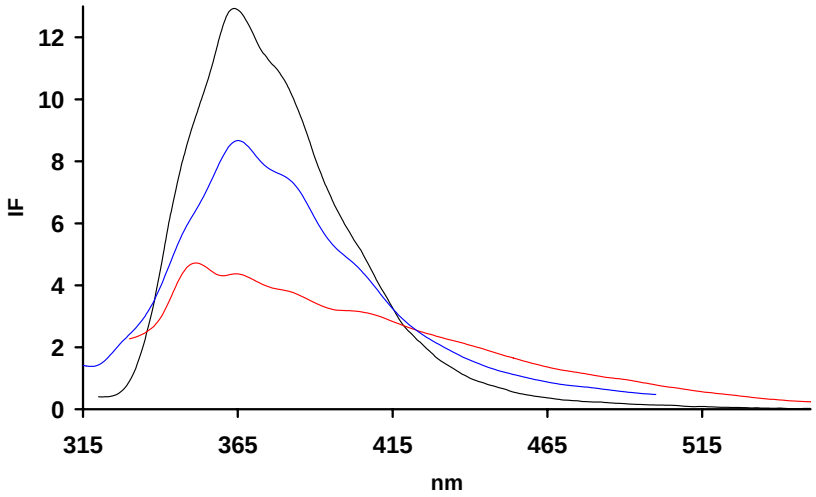

Fig. 64. Espectros de emisión en 0.1M TFA de **(35)** (—), **(39)** (—) y **(40)** (—) (λ_{exc}< 330 nm)

SPICUM servicio de publicaciones

Excitando a longitudes de onda mayores (λ_{exc} >360 nm) se observa una segunda banda de emisión, centrada a 410 nm para **(35)**, y a 415 para **(39)** y **(40)**, que se corresponde con la emisión desde el estado CT.

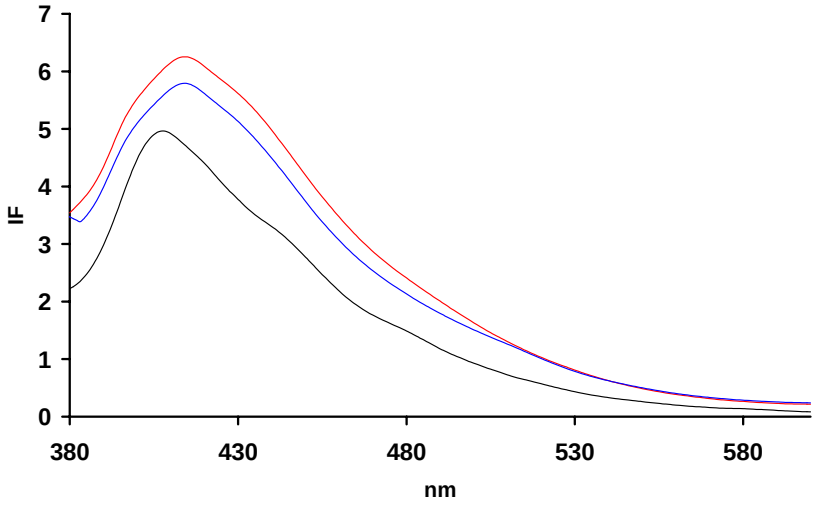

Fig. 65. Espectros de emisión en medio 0.1M TFA de **(35)** (—), **(39)** (—) y **(40)** (—) (λ_{exc} > 360 nm)

Los rendimientos cuánticos de estas emisiones se presentan en la Table 11.

Table 11. Rendimientos cuánticos de emisión de fluorescencia para **(35)** ($CHCl_3$) y **(39)** y **(40)** (CH_2Cl_2)

MEDIO NEUTRO			
	(35)	**(39)**	**(40)**
λ_{em} (nm) (λ_{exc} = 314nm)	370	370	370
ϕ	$2\cdot10^{-3}$	$2\cdot10^{-3}$	$4\cdot10^{-3}$
MEDIO ÁCIDO (0.1 M TFA)			
	(35) (H^+)	**(39) (H^+)**	**(40) (H^+)**
λ_{em} (nm) (λ_{exc} = 314nm)	365	365	365
ϕ	$3\cdot10^{-3}$	$2\cdot10^{-3}$	$2\cdot10^{-3}$
λ_{em} (nm) (λ_{exc} = 360nm)	415	415	415
ϕ	$5\cdot10^{-3}$	$7\cdot10^{-3}$	$4\cdot10^{-3}$

Estudiando los rendimientos cuánticos de emisión, se observa que las intensidades de emisión son bajas en todos los casos, siendo ligeramente superiores para la emisión a 415 nm en medio ácido. No se observan diferencias significativas entre medio neutro y ácido para la emisión con máximo a 370 nm.

SPICUM servicio de publicaciones

III.2.2.2.3. Grupo III. Compuestos (36), (41) y (42)

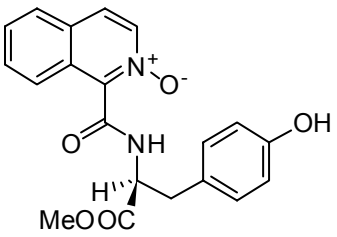

(36)

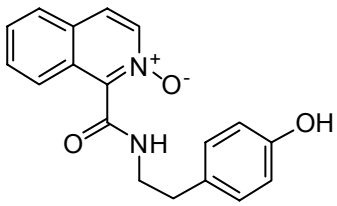

(41)

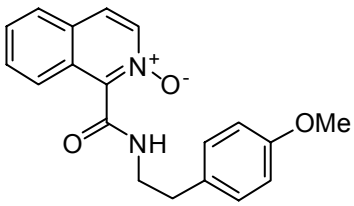

(42)

- Absorción electrónica

En medio neutro, los espectros de absorción electrónica de **(36)**, **(41)** y **(42)** son muy similares a todos los sistemas estudiados previamente, observándose bandas con máximos a 336 y 366 nm (Fig. 66).

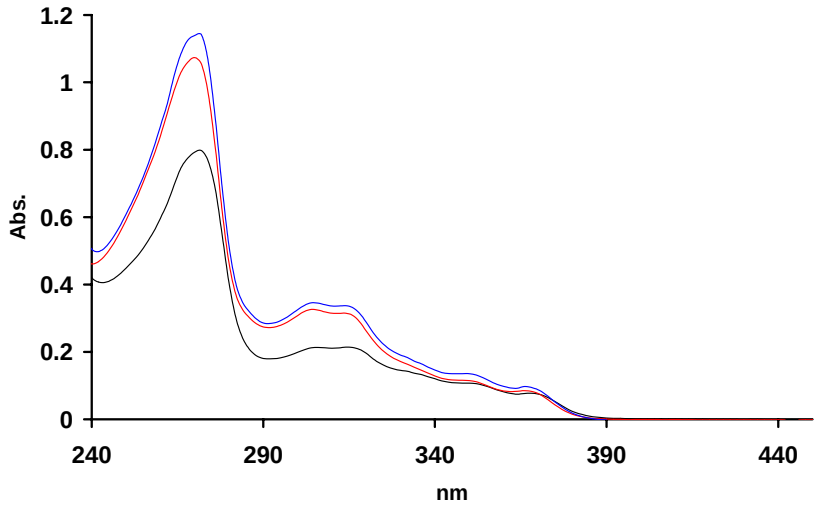

Fig. 66. Espectros de absorción en CH_2Cl_2 de **(36)** (—), **(41)** (—) y **(42)** (—)

En medio ácido (0.1M TFA), de nuevo los tres compuestos se comportan de manera similar entre sí y con respecto a los sistemas previos. Así, se observa un desplazamiento hipsocrómico de las bandas de absorción situándose las bandas antes centradas en 336 y 366 nm, a unos 304 y 338 nm respectivamente (Fig. 67).

SPICUM servicio de publicaciones

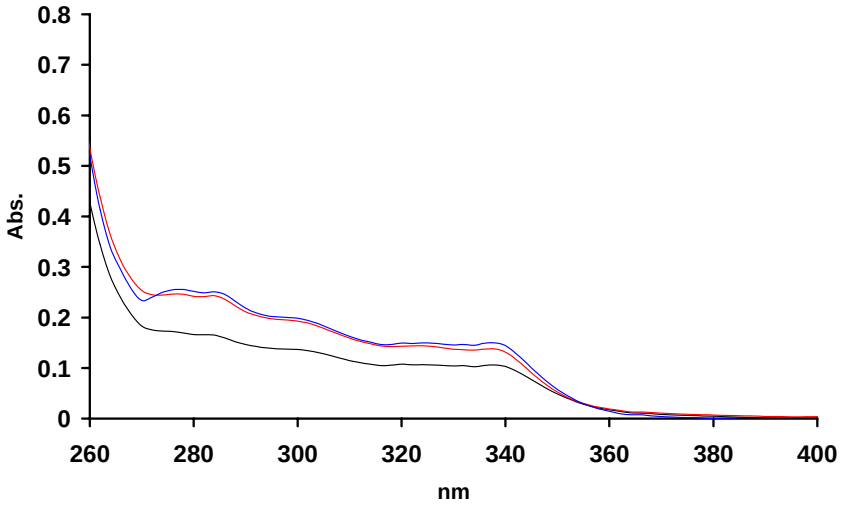

Fig. 67. Espectros de absorción en CH_2Cl_2 (0.1M TFA) de **(36)** (—), **(41)** (—) y **(42)** (—)

Los coeficientes de absorción molar y los máximos de absorción para **(36)**, **(41)** y **(42)** se presentan en la Table 12.

Table 12. Máximos de absorción y coeficientes de absorción molar de **(36)**, **(41)** y **(42)** en CH_2Cl_2 neutro y ácido (0.1M TFA)

MEDIO NEUTRO			
	(36)	**(41)**	**(42)**
λ_{abs} (nm)	366	366	366
ε ($M^{-1}cm^{-1}$)	$1.8 \cdot 10^3$	$1.7 \cdot 10^3$	$1.9 \cdot 10^3$
MEDIO ÁCIDO (0.1M TFA)			
	(36) (H^+)	**(41) (H^+)**	**(42) (H^+)**
λ_{abs} (nm)	338	338	338
ε ($M^{-1}cm^{-1}$)	$2.4 \cdot 10^3$	$2.8 \cdot 10^3$	$3.0 \cdot 10^3$

SPICUM servicio de publicaciones

- Emisión de fluorescencia

En medio neutro, el espectro de **(36)**, **(41)** y **(42)** está gobernado por una única banda de emisión, centrada a 345 nm para **(41)** y **(42)** y con un pequeño desplazamiento hacia el rojo, centrada a 352 nm para **(36)** (Fig. 68).

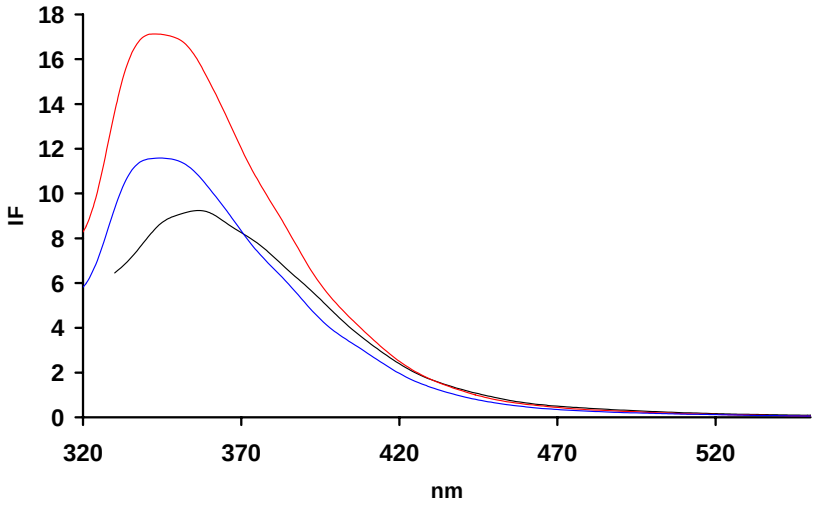

Fig. 68. Espectros de emisión en CH_2Cl_2 de **(36)** (—), **(41)** (—) y **(42)** (—)

En medio ácido se observan dos bandas de emisión, comportándose de manera similar a los sistemas previos. Así, al excitar a λ_{exc}< 330 nm, registramos una banda, centrada en 350 nm que no presenta variaciones significativas con respecto a la registrada en medio neutro (Fig. 69).

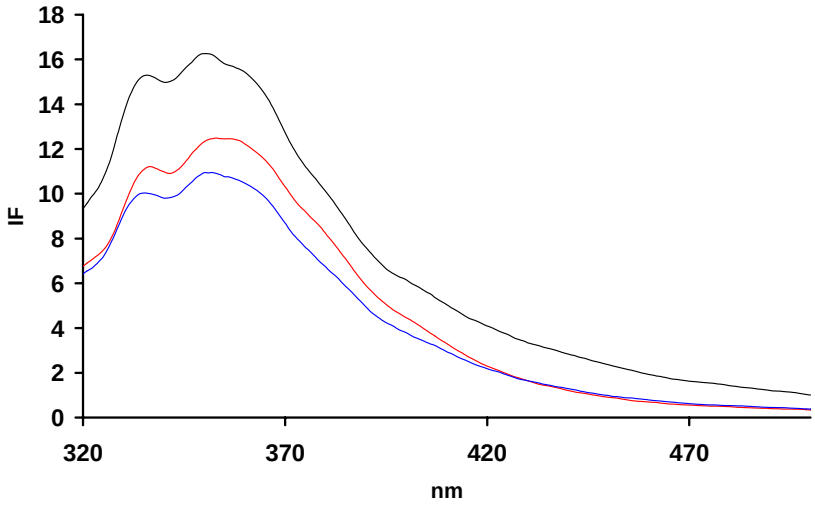

Fig. 69. Espectros de emisión en CH_2Cl_2 (0.1M TFA) de **(36)** (—), **(41)** (—) y **(42)** (—) (λ_{exc}< 330nm)

SPICUM servicio de publicaciones

Excitando a $\lambda_{exc} \geq 360$ nm, se registra una segunda banda de emisión, con máximo a 410 nm (Fig. 70).

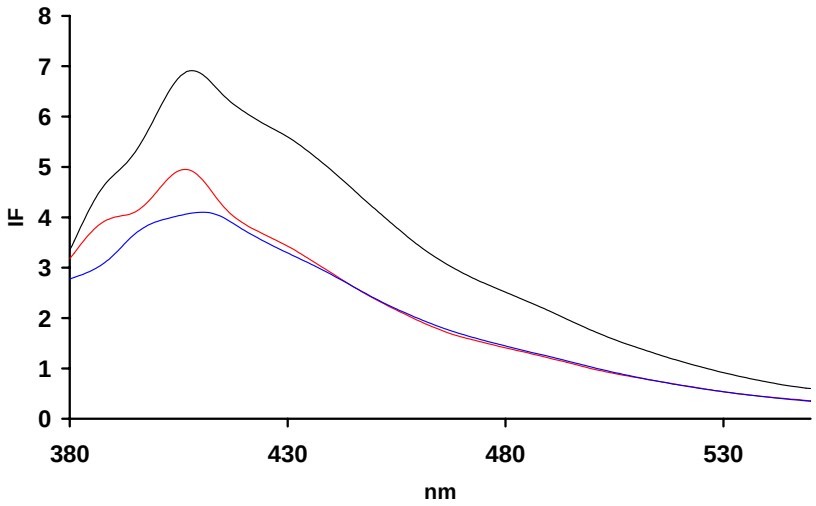

Fig. 70. Espectros de emisión en CH_2Cl_2 (0.1M TFA) de **(36)** (—), **(41)** (—) y **(42)** (—) ($\lambda_{exc} \geq 360$nm)

Los rendimientos cuánticos de emisión de fluorescencia se muestran en la Table 13.

Table 13. Rendimientos cuánticos de emisión de fluorescencia en CH_2Cl_2 neutro y 0.1M TFA para **(36)**, **(41)** y **(42)**

MEDIO NEUTRO			
	(36)	**(41)**	**(42)**
λ_{em} (nm) (λ_{exc} = 300nm)	350	350	350
ϕ	$3 \cdot 10^{-3}$	$4 \cdot 10^{-3}$	$2 \cdot 10^{-3}$
MEDIO ÁCIDO (0.1 M TFA)			
	(36) (H^+)	**(41) (H^+)**	**(42) (H^+)**
λ_{em} (nm) (λ_{exc} = 300nm)	350	350	350
ϕ	$9 \cdot 10^{-3}$	$5 \cdot 10^{-3}$	$4 \cdot 10^{-3}$
λ_{em} (nm) (λ_{exc} = 360nm)	410	410	410
ϕ	$1.4 \cdot 10^{-2}$	$8 \cdot 10^{-3}$	$1.0 \cdot 10^{-2}$

Como podemos observar, la segunda banda de emisión que aparece en medio ácido al excitar a $\lambda_{exc} \geq 360$ nm, sigue la tendencia observada en los compuestos del Grupo II, siendo de mayor intensidad que las registradas en medio neutro y ácido al excitar a $\lambda_{exc} < 330$ nm.

SPICUM servicio de publicaciones

III.2.2.3. Reactividad fotoquímica

Basándonos en los procesos de fotohidroxilación de los derivados de 1-bencilisoquinolinas,[54] sintetizamos los sistemas basados en 1-isoquinolina-carboxamidas. La unión mediante un enlace amida, nos da la posibilidad de una posterior ruptura y la reentrada en el ciclo de la isoquinolina, que se emplearía para hidroxilar una nueva unidad de amina bencílica.

Los *N*-óxidos **(35)**-**(42)** se irradiaron durante un tiempo de 35 minutos en CH_2Cl_2 como disolvente a concentraciones 0.1M de TFA en todos los casos. Tras este tiempo, la disolución se trata con $NaHCO_3$ sólido (1.5 eq), manteniéndolo en agitación durante 30 minutos. A continuación, se filtra y se concentra a sequedad. El crudo de reacción se separó mediante cromatografía en capa fina preparativa, empleando el eluyente adecuado en cada caso.

El progreso de la reacción se siguió por ccf y se estudiaron los crudos de reacción por ^{1}H-RMN. A diferencia de la irradiación para los *N*-óxidos **(33)** y **(34)**, en estos casos son necesarios tiempos de irradiación mayores para que se den los procesos fotoquímicos.

III.2.2.3.1. Grupo I. N-óxidos (37) y (38)

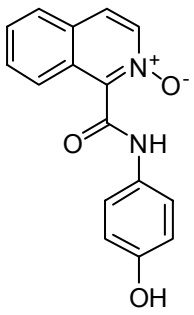

(37)

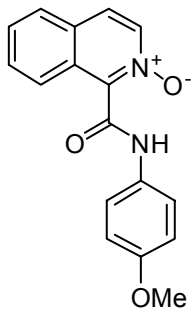

(38)

La irradiación de ambos compuestos en medio ácido produjo exclusivamente los productos de desoxigenación, sin detectar producto de hidroxilación (Fig. 71). En ambos casos se aumentó el tiempo de irradiación, llegando hasta los 180 minutos (para el compuesto **(38)**) sin detectar productos de hidroxilación.

SPICUM servicio de publicaciones

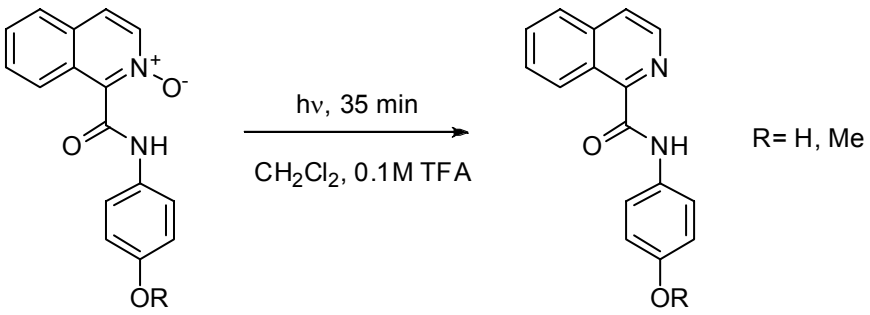

Fig. 71. Productos de irradiación de los *N*-óxidos de grupo I

Los rendimientos de reacción se muestran en la Table 14.

Table 14. Rendimientos de irradiación para los compuestos **(37)** y **(38)**

RENDIMIENTOS REACCIÓN FOTOQUÍMICA		
$t_{irradiación}$= 35 min	Desoxigenación (%)	Conversión (%)
(37)	35	44
(38)	37	30

Estos bajos valores de conversión unidos a que el aumento del tiempo de irradiación no aumenta significativamente el rendimiento de formación del producto desoxigenado, nos indica una baja reactividad fotoquímica de estos sistemas. Esto puede deberse a una cierta conjugación de los componentes A y D en las condiciones ácidas de reacción.

III.2.2.3.2. Grupo II. N-óxidos (35), (39) y (40)

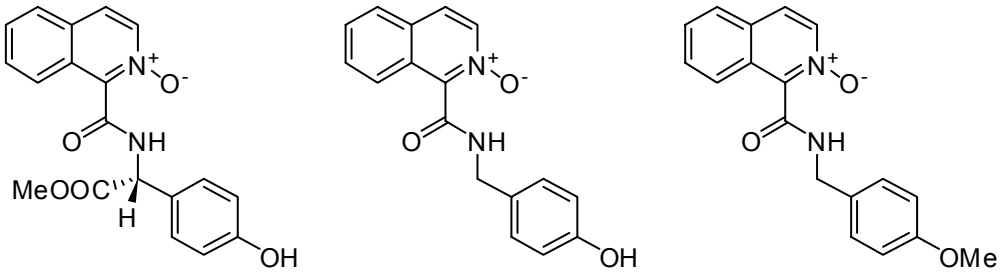

(35) **(39)** **(40)**

La irradiación de los compuestos **(35)**, **(39)** y **(40)** produjo diferentes resultados. Así, para el compuesto **(35)** exclusivamente fue posible identificar producto de desoxigenación, incluso aumentando el tiempo de reacción. Para **(39)** y **(40)**, además

SPICUM servicio de publicaciones

del producto de desoxigenación, se obtuvieron dos productos con R_f = 0.25 (AcOEt:Ciclohexano 4:6) para **(39)** y con R_f = 0.15 (AcOEt:Ciclohexano 3:7) para **(40)** que se corresponden con productos de hidroxilación en el anillo dador.

El estudio por RMN-^{1}H del producto de hidroxilación al irradiar **(39)** (Fig. 72), muestra un multiplete a 6.76 ppm que integra por 2 H y un doblete con J = 2.0 Hz a 6.86 ppm que integra por 1 H. Estas señales indican la sustitución en el anillo bencílico. La comparación con el producto de síntesis obtenido por la formación de amida a partir de la 3,4-dihidroxibencilamina, muestra cómo las señales correspondientes al anillo bencílico del producto obtenido de la irradiación, concuerdan con las del producto sintético, lo que confirma de esta forma que la estructura del producto de reacción es la del producto **(62)**.

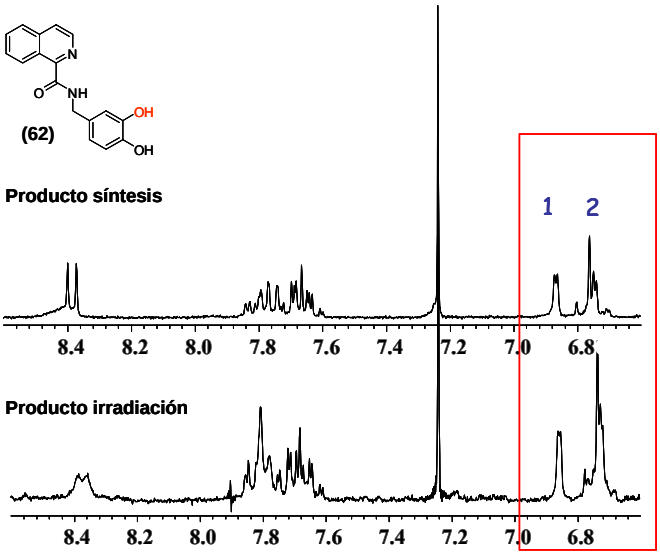

Fig. 72. Espectros RMN-^{1}H de **(62)**. En azul el valor de las integrales de los H del anillo dador

En el estudio por espectrometría de masas no se observa el ión molecular a *m/z* 294, aunque si podemos ver las señales a *m/z* 155 con una abundancia del 8% correspondiente a la fracción de 1-carbonilisoquinolina producto de la ruptura del enlace amida y la señal a *m/z* 138 correspondiente a la fracción de 3,4-dihidroxibencilamino procedente de la ruptura del enlace amida.

El espectro de RMN-^{1}H del producto de hidroxilación al irradiar **(40)** (Fig. 73), muestra un doblete a 6.81 ppm que integra por 1 H, un doble doblete a 6.89 ppm con J_1 = 8.4Hz y J_2 = 2.0Hz que integra por 1 H y un doblete a 6.97 ppm con J= 2.0Hz que

SPICUM servicio de publicaciones

integra por 1 H. La comparación del espectro con el del producto de síntesis obtenido por la formación de la amida a partir de la 3-hidroxi-4-metoxibencilamina, muestra la concordancia de las señales bencílicas entre el producto de irradiación y el de síntesis, que confirma la estructura del producto como la de **(63)**.

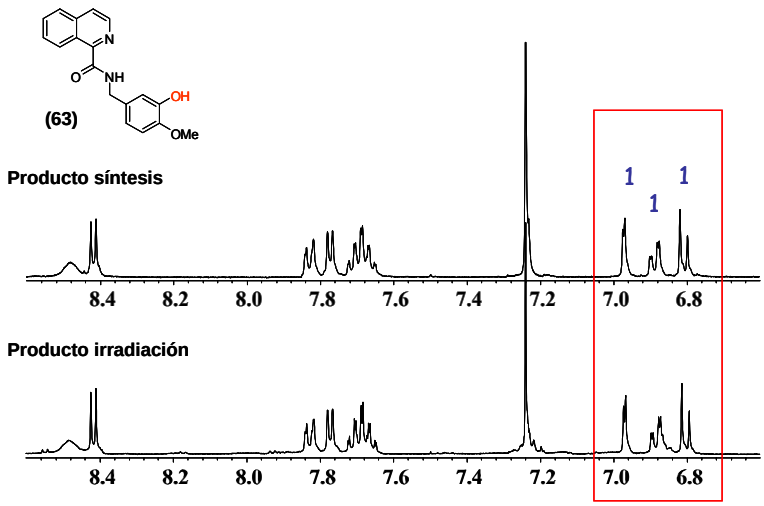

Fig. 73. Espectros RMN-^{1}H de **(63)**. En azul el valor de las integrales de los H del anillo dador

Al estudiar por espectrometría de masas el producto de irradiación se observa el pico correspondiente al ión molecular de *m/z* 308, así como el pico base del espectro a *m/z* 152, correspondiente a la fracción amina tras la ruptura del enlace amida.

El resultado de la reacción demuestra que el proceso de hidroxilación es regioselectivo y se produce en posición *orto* al sustituyente hidroxilo o metoxilo del anillo dador (Fig. 74).

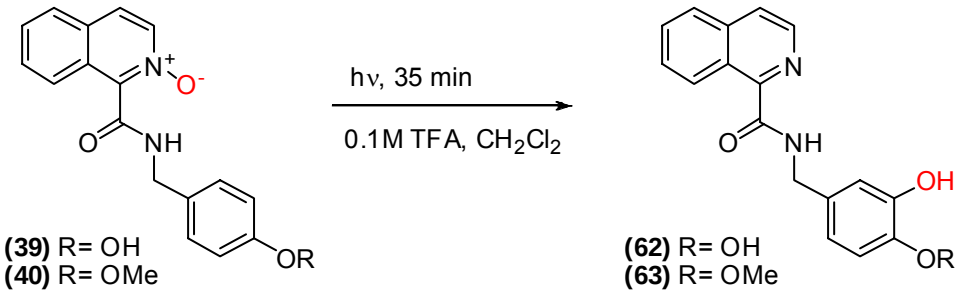

Fig. 74. Productos de irradiación de los *N*-óxidos **(39)** y **(40)**

SPICUM servicio de publicaciones

Los rendimientos de reacción se muestran en la Table 15.

Table 15. Rendimientos de irradiación para los compuestos **(35)**, **(39)** y **(40)**

RENDIMIENTOS REACCIÓN FOTOQUÍMICA			
$t_{irradiación}$= 35 min	Desoxigenación (%)	Hidroxilación (%)	Conversión (%)
(35)	16	-	70
(39)	27	41	65
(40)	32	23	75

III.2.2.3.3. Grupo III. N-óxidos (36), (41) y (42)

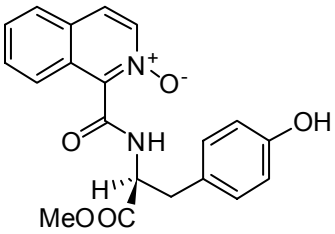

(36)

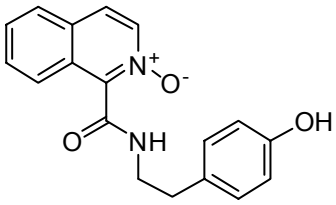

(41)

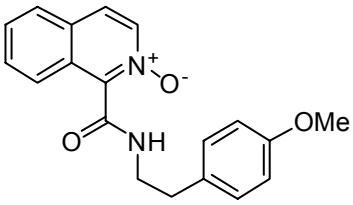

(42)

La irradiación de los compuestos **(36)**, **(41)**, y **(42)** dio como resultado exclusivo la obtención de los productos de desoxigenación, con unos rendimientos bajos.

Table 16. Rendimientos de irradiación para los compuestos **(36)**, **(41)** y **(42)**

RENDIMIENTOS REACCIÓN FOTOQUÍMICA		
$t_{irradiación}$= 35 min	Desoxigenación (%)	Conversión (%)
(36)	16	69
(41)	15	72
(42)	13	86

SPICUM servicio de publicaciones

A modo de conclusión del estudio de los tres modelos de amidas donde la separación es de 3 enlaces (Grupo I), 4 enlaces (Grupo II) o 5 enlaces (Grupo III), podemos decir que los resultados obtenidos en la fotoquímica de los compuestos basados en espaciadores amida siguen la tendencia marcada por los sistemas A-S-D con S etileno **(33)** y propileno **(34)**.

La irradiación de los sistemas basados en anilinas **(37)** y **(38)**, donde A y D están separados por 3 enlaces, exclusivamente genera productos de desoxigenación, no detectándose en ningún caso producto de hidroxilación en el anillo dador, incluso tras aumentar el tiempo de irradiación. Este resultado es similar al obtenido al irradiar el producto **(33)**, en el sentido de que no se obtiene producto de hidroxilación en el Dador. El proceso de hidroxilación en la cadena puente que se detecta en **(33)** no puede obtenerse para **(37)** y **(38)**.

La irradiación de los sistemas **(36)**, **(41)** y **(42)**, donde la separación entre A y D es a través de 5 enlaces, no produjo productos de hidroxilación en ninguno de los casos, detectándose exclusivamente productos de desoxigenación. Dado que la formación de productos de hidroxilación puede producirse por un proceso secuencial, el aumento de la distancia entre A y D puede resultar un factor clave para que los procesos de escape de caja del radical hidroxilo, impidan la formación de producto de hidroxilación.

Sin embargo, mientras que para los sistemas con espaciador alquílico se obtienen productos de hidroxilación en el anillo dador cuando la separación entre A y D es de 4 enlaces (S = propileno, **(34)**), la presencia de un enlace amida en S, no altera significativamente este resultado. Esto se comprueba al irradiar los compuestos **(39)** y **(40)**, obteniéndose los productos de hidroxilación en un sistema igualmente separado por 4 enlaces. Por el contrario, la presencia de un sustituyente metoxicarbonil en la cadena espaciadora, como sucede en el compuesto **(35)**, provoca que el único producto de fotólisis sea el producto de desoxigenación.

A la vista de estos resultados, podemos construir un diagrama simbolizando el proceso de hidroxilación fotoquímica (Fig. 75). En este diagrama se observa cómo el ácido 1-carboxilisoquinolínico, tras el proceso de formación de amida, *N*-oxidación, fotólisis e hidrólisis del producto hidroxilado, puede entrar en un nuevo ciclo de reacción, actuando de esta forma de manera similar a como se comporta una enzima en el medio biológico.

SPICUM servicio de publicaciones

El proceso de fotólisis, además del producto de hidroxilación, conlleva la formación de producto de desoxigenación, isoquinolina de partida, que se reincorpora al ciclo en el paso previo a la *N*-oxidación.

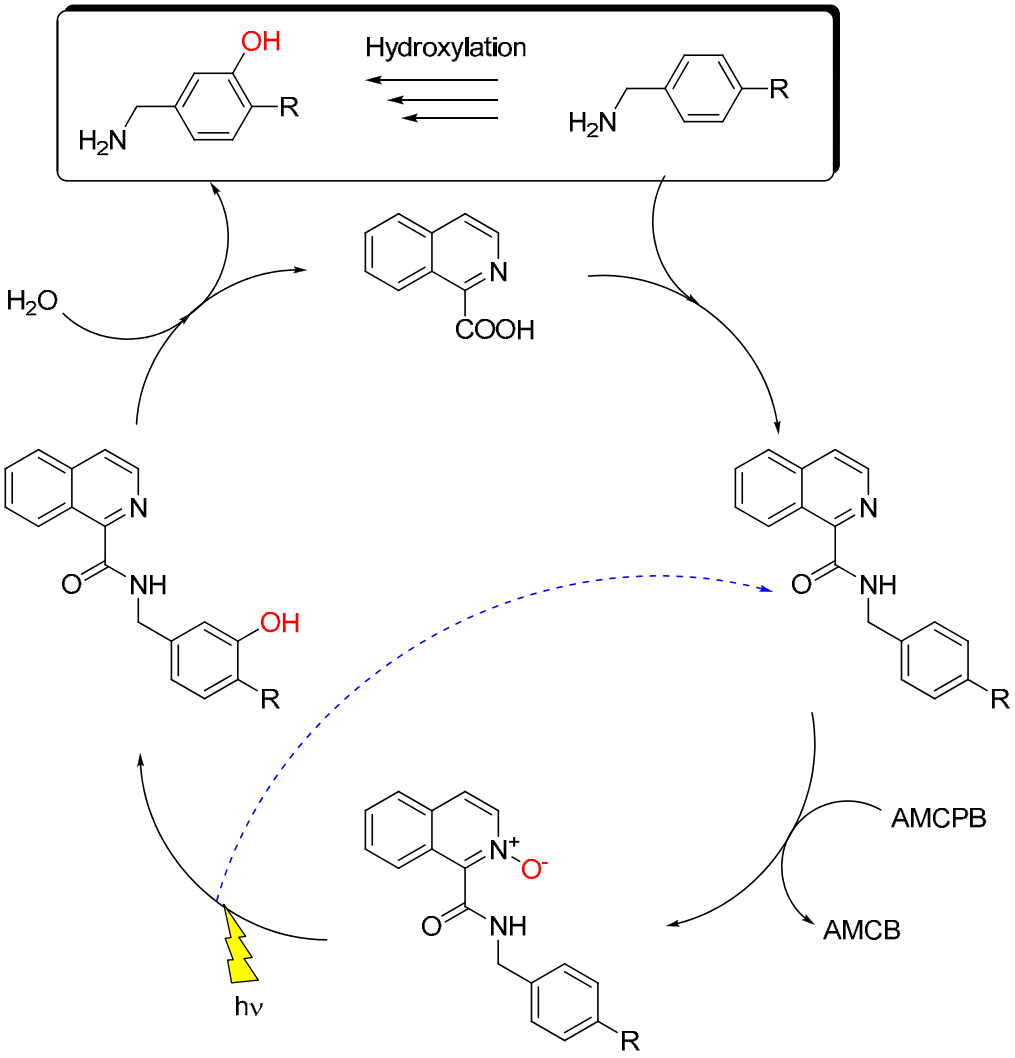

Fig. 75. Proceso de hidroxilación de amidas

SPICUM servicio de publicaciones

CHAPTER IV.

MOLECULAR LOGIC GATES

SPICUM
servicio de publicaciones

SPICUM
servicio de publicaciones

IV.1. Introduction

IV.1.1. A brief historical note

In December of 1943, a British scientist group working at Bletchley Park, to the north of London, built the *Colossus*, considered the first totally electronic digital computer. *Colossus* incorporated 1500 vacuum tubes and it was used to decode the encrypted German communications in II World War (Img. 1). Previously, in 1939, John Atanasoff and Clifford Berry, made an electronic machine prototype called the *Atanasoff Berry Computer* at Iowa State College (Iowa, USA), but it was dismantled (Img. 2).

In 1945, John Presper Eckert and John William Mauchly built a new computer called *ENIAC (Electronic Numeric Integrator and Computer)* that incorporated 17468 vacuum tubes and it could made 5000 additions and 300 multiplications per second, but it occupied a room of more than 200 m^2 and weighed 30 tons (Img. 3).

SPICUM servicio de publicaciones

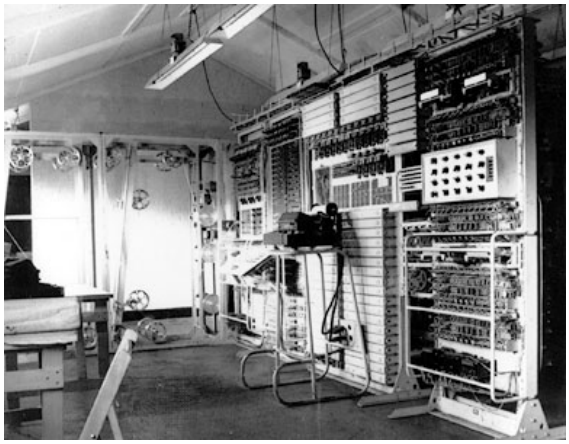

Img. 1. Colossus computer at Bletchley Park

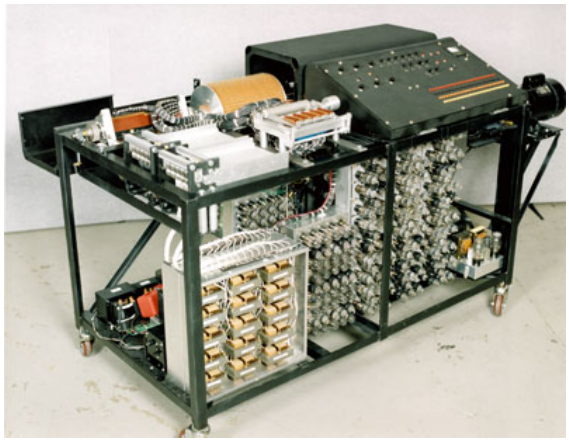

Img. 2. An Atanasoff-Berry computer (replica)

Img. 3. ENIAC computer

In 1959, Richard P. Feynman gave a talk at the annual meeting of the American Physical Society at the California Institute of Technology (Caltech), where he suggested that "*there is plenty of room at the bottom*",[76] meaning that the miniaturization of the devices is the way to improve these systems with the end on the atomic scale.

Since this time, the main goal on this research field was to improve the performance of these systems, focused in the reduction of the devices and machines size, and to increase the data storage as well as the processing bit rate. At the end of the 1940s the transistor appeared, in 1958, the integrated circuit, made by Noyce and Kilby and in the half of the 1970s, the microprocessors that enhanced the calculation capacity of these machines, reducing their size a lot.

[76] Feynman, R.P.; *Miniaturization* **1961**, 282. http://www.its.caltech.edu/~feynman/plenty.html

SPICUM servicio de publicaciones

IV.1.2. Devices miniaturization

Right now, the devices miniaturization (and consequently, the machines built with them), has been made by progressive devices size reduction using laser-based physical treatments, allowing the manipulation of smaller and smaller pieces (top-down, large-downward approach). Following Gordon Moore's prediction,[77] the capacity of a microprocessor is doubled each 18-24 months approximately, and it has been occurred since its appearance. The way to get that is packing a larger number of devices each time (mostly transistors) in the same space by reduction of their size, enhancing the component features.

This way to improve the electronic devices has intrinsic physical limitations located in the fact that we can't build devices smaller than 0.1 μm,[78] because to obtain regularly doped silicon on systems smaller than 50 nm is not possible. For this reason, we find an insurmountable barrier on the top-down processes that, if current trends continue this way, will find its limit around 2012.[79] With this handicap, the main goal now is not to reduce current components, but to develop new devices from the smallest possible entities: atoms and molecules (bottom-up, small-upward approach). This perspective, take us to the design of strategies through we could make structures simulating the electronic devices operation, starting with the atomic or molecular "bricks".

In the 1970s, the concept of *supramolecular chemistry* was born, enunciated by Jean Marie Lehn,[80] where he defined a new kind of chemistry, *"the chemistry beyond the molecule, based on organized entities of great complexity that are the result of the association of two or more chemical species, joined by intermolecular forces"* that is, not based in intermolecular covalent bonds, but in the bonds due to electrostatic interactions, hydrogen bonds, van der Waals forces, etc. This field is of key interest in the attempt to miniaturize electronic devices, because the supramolecular entities, give a great number of possibilities due to the different variety of components they can work, being very convenient building blocks for construction of nanoscale devices. In fact, we will see how the main advances in this field are based on supramolecular interactions.[81]

[77] Moore, G.E.; *Electronics* **1965**, Vol. 38, Nº 8, April 19.
[78] Balzani, V.; Credi, A.; Venturi, M.; *Chemphyschem* **2003**, *3*, 49.
[79] a) Ball, P.; *Nature* **2000**, *406*, 118. b) Service, R.F.; *Science* **2001**, *293*. 785.
[80] Lehn, J.M.; *Pure & Appl. Chem.* **1977**, *49*, 857.
[81] Toma, H.E.; *Curr. Sci.* **2008**, *95*, 1202.

SPICUM servicio de publicaciones

The individual molecules presenting potential barriers, strategically placed to originate a determined response can be used as switches or logic devices. The use of molecular-size systems would allow us 10^{13} logic gates/cm^2 approximately that, compared with the approximate quantity of 10^8 presented for the actual chips, suppose a reduction of 10^5 in the required size.

On the other side, other advantage lies in the response time of the molecular systems, placed in the femtoseconds range, while the present devices work in the nanosecond range. In this way, is possible to increase the speed around 10^6 times.[82]

Joining the size reduction with the speed increase is possible to enlarge the yields 10^{11} times. The advantage presented by the electronic systems is its speed and the input/output signal used, the electron, which permits an easy connection between the different electronic components.

Since Aviram et al. defined the first organic system acting as an electrical conductor,[83] organic compounds that work as wires,[84] rectifiers,[83,85] antennas[86] and memories[87] have been developed (Fig. 76).

[82] Tour, J.M.; Kozaki, M.; Seminario, J.M.; *J. Am. Chem. Soc.* **1998**, *120*, 8486.
[83] Aviram, A.; Ratner, M.A.; *Chem. Phys. Lett.* **1974**, *29*, 277.
[84] a) Pickaert, G.; Ziessel, R.; *Tetrahedron Lett.* **1998**, *39*, 3497. b) Grozema, F.C.; Huarner-Rassin, C.; Prins, P.; Siebbeles, L.D.A.; Anderson, H.L.; *J. Am. Chem. Soc.* **2007**, *129*, 13370. c) Hansen, M.R.; Schnitzler, T.; Pisula, W.; Graf, R.; Müllen, K.; Spiess, H.W.; *Angew. Chem. Int. Ed.* **2009**, *48*, 4621. d) Leary, E.; Zalinge, H.V.; Higgins, S.J.; Nichols, R.J.; Fabrizi de Biani, F.; Leoni, P.; Marchetti, L.; Zanello, P.; *Phys. Chem. Chem. Phys.* **2009**, *11*, 5198.
[85] a) Metzger, R.M.; *Acc. Chem.. Res.* **1999**, *32*, 950. b) Acharya, S.; Song, H.; Lee, J.; Kwon, P.S.; Lee, J.; Yogendranath, G.; Kim, Y.H.; Jang, Y.H.; Lee, T.; Samal, S.; Lee, J.-S.; *Org. Electron.* **2009**, *10*, 85.
[86] a) Li, F.; Yang, S.I.; Ciringh, Y.; Seth, J.; Martin III, C.H.M.; Singh, D.L.; Kim, D.; Birge, R.R.; Bocian, D.F.; Holten, D.; Lindsey, J.S.; *J. Am. Chem. Soc.* **1998**, *120*, 10001. b)Ajayaghosh, A.; Praveen, V.K.; Vijayakumar, C.; George, S.J.; *Angew. Chem. Int. Ed.* **2007**, *46*, 6260.
[87] Balzani, V. *Electron Transfer in Chemistry. Vol. 5.*, WILEY-VCH Verlag GmbH, Weinheim (Federal Republic of Germany), **2001**, pg.215-242.

SPICUM servicio de publicaciones

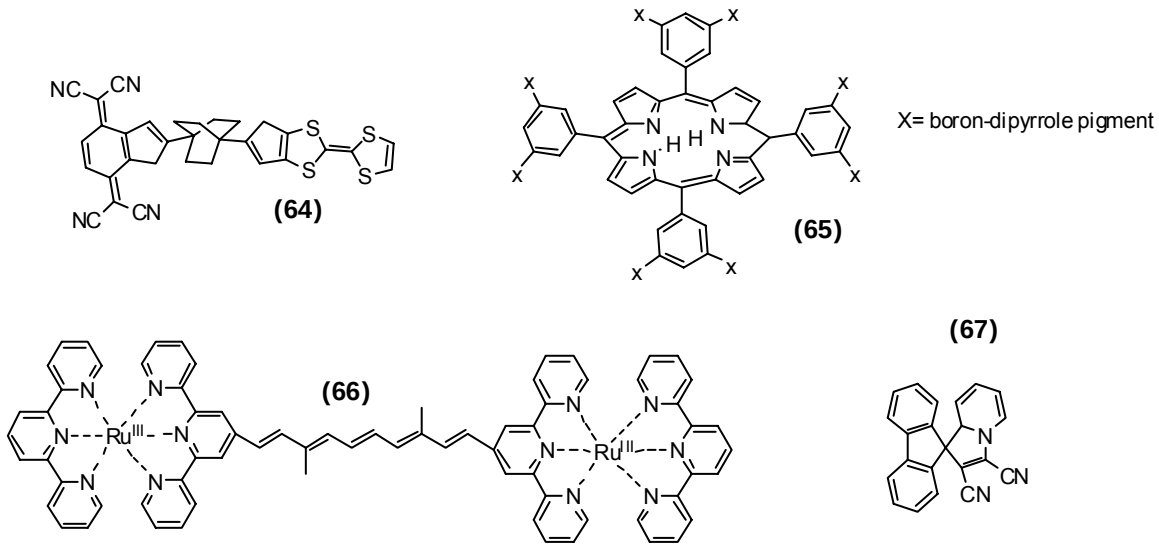

Fig. 76. Examples of rectifier **(64)**, antenna **(65)**, wire **(66)** and memory **(67)**

IV.1.3. Molecular logic gates

The data-process and the communication between devices, requires the codification of the information on electrical and optical signals expressed by binary digits (0 and 1). To face the study of these systems from the binary logic, is useful to understand that it's not necessary a total change (from high to null conductivity or from high to null fluorescence intensity, for example) in the measured signal, but it's necessary to establish appropriate thresholds and logic conventions. In a positive logic convention, a 0 is used to represent a signal lower than the threshold defined and a 1 is employed to indicate a higher signal value. In a negative logic convention, the assignment is reversed.

With this requirements and assuming that is not necessary that the components of a molecular computer must operate in the same way of conventional silicon-based computers, to simulate the silicon-based devices with molecular systems is searched.[79a,88]

[88] Clarkson, M.A.; *Byte* **1989**, *May*, 268.

SPICUM servicio de publicaciones

The response (output) to stimulation (input) is a very common phenomenon. The systems with this behaviour are called *molecular switches*. The result of a logic operation is only controlled by the binary digits value, without consider the nature of input-output signal. For this reason, the different kind of inputs and outputs are not compromising the use of one switch as a logic gate. On the other side, this fact can constitute an obstacle if the molecular logic gates must be connected sequentially, that is, if the output signal of one of them must be the input signal for the next one.

There are three kinds of signals that can be measured and used as 0 and 1 of binary code: electrical, optical and chemical. On the same way, the input and output signals can be optical, electrical or chemical. The handicap in the use of electrical signals is that, while electrical signal transport *via* cable is individual, the number of optical signals that can be transmitted on fibre optics cables is higher due to the non-interacting properties that these optical signals present. These advantages carry us to modify the strategies to obtain devices where the signals we apply and obtain are both optical.[89]

Logic gates are presented as a devices series capable to offer us different response (output) depending on the stimulation they are submitted (input). There are several types of different logic gates, which different properties lies on the number of inputs present and on the different response they offer to the presence of these inputs.

The input-output connection can be represented through tables, called *truth tables* where are shown the different possible combinations of input and outputs that each logic gate offers. These truth tables will be different depending on the logic gate considered.

[89] Nolte, D.D.; *J. Appl. Phys.* **1999**, *85*, 6259.

SPICUM servicio de publicaciones

IV.1.3.1. Basic logic gates

Since De Silva and co-workers reported the first organic structure that can be studied from the logic gates point of view (an AND logic gate),[90] many organic compounds have been synthesized which properties can be extended to the logic gates field. The supramolecular interactions between organic compounds have opened the door to the design of structures which properties can be analyzed from the logic gates point of view and used to define molecular systems which operation is comparable to the electronic logic systems.

There are many kinds of logic gates which properties can be unique (called basic logic gates) or are the result to combine several logic gates (called combined logic gates). First of all, we will start to study basic logic gates.

There are eight different logic functions that can be considered basics: YES, NOT, OR, AND, NOR, NAND, XOR and XNOR. Logic gates YES and NOT are the most simple, because they only present one input. The other present at least two different inputs.

IV.1.3.1.1. One input logic gates

- YES

YES logic gate presents one input and one output exclusively. When input value is 0, output value is 0 and when input is 1, output value is 1. This operation is not considered as such in an electronic context, and it's normally represented as a conductor or a switch.[91] In an input-output context, this operation is not trivial.

The action of many molecular fluorescent sensors is based on the fluorescence they show when an input substance is acting over them. With this base, all the fluorescent sensors than show fluorescence only when the target substance is present in the media, can be defined from the logic operations as YES logic gates.
Compound **(68)** (Fig. 77) is a fluorescent sensor of H^+ ions.

[90] De Silva, A.P.; Gunaratne, H.Q.N.; McCoy, C.P.; *Nature* **1993**, *364*, 42.
[91] Brown, G.J.; De Silva, A.P.; Pagliari, S.; *Chem. Commun.* **2002**, 2461.

SPICUM servicio de publicaciones

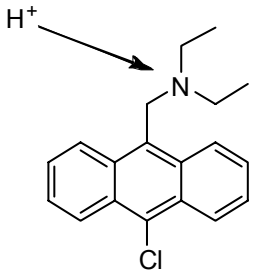

(68)

Fig. 77. Example of YES logic gate

This compound is conceptually a modular "fluorophore-spacer-receptor" system, based on an anthracene unit (fluorophore) with an electron-rich amine side chain (receptor). The amine is a base, acting as a selective receptor for H^+ ions. When H^+ is not present in the media, the excited fluorophore will not emit light because of the photo-induced electron transfer (PET) process from the electron-rich amine, to the anthracene across the spacer produced. This process can be so fast that light emission of the fluorophore is strongly quenched (output 0). Addition of H^+, produces the quaternization of the amine, making PET process impossible, and blue fluorescence emission of the anthracene derivative (output) is observed upon ultraviolet radiation (used as power supply to excite the molecule).

A truth table with the functionality of this system can be made (Table 17)

Table 17. Truth table of a YES logic gate

Input (H^+)	**Output** (Fluorescence)
0	0
1	1

And it's possible to draw a schematically circuit representation (Fig. 78)

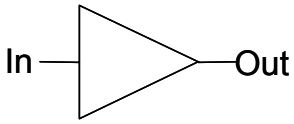

Fig. 78. YES logic gate representation

SPICUM servicio de publicaciones

The systems showing this behaviour present an added value, because the presence of the input is directly related with the apparition of the output signal, being more intuitive this way.

- NOT

NOT logic gate produces the reversal of the received signal, this is, the response to a positive input is a negative output. As in the YES gate, this kind of response is very common, and it's present in many already known systems. Thereby, the fluorescence emission quenching of a fluorophore by the presence of a chemical agent is very common.

This behaviour is seen for compound **(69)** (Fig. 79) as one example of a NOT logic gate.[92]

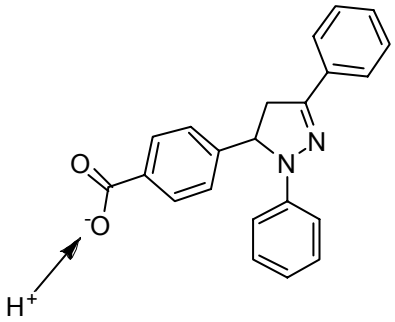

(69)

Fig. 79. Example of NOT logic gate

In this case, the fluorescence process is deactivated when the system is in presence of H^+ because the benzoic acid unit is protonated and the PET from the pirazolinic ring to the benzoic acid unit is given, reducing the fluorescence emission of the system. Absence of H^+, free the carboxylate anion inhibiting PET process and fluorescence emission is observed.

[92] De Silva, A.P.; de Silva, S.A.; Dissanayake, A.S.; Sandanayake, K.R.A.S.; *J. Chem. Soc., Chem. Commun*. **1989**, 1054.

SPICUM servicio de publicaciones

The truth table of this behaviour is shown on Table 18.

Table 18. Truth table of NOT logic function

Input (H^+)	Output (Fluorescence)
0	1
1	0

The schematically circuit representation for this logic gate is in Fig. 80.

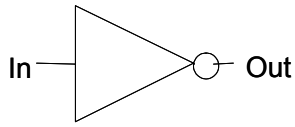

Fig. 80. NOT logic gate representation

IV.1.3.1.2. Two- input basic molecular logic gates.

The two-input basic molecular logic gates are the functions OR, AND, NOR, NAND, XOR and XNOR.

- OR

This logic gate, computes the logic sum of two input variables, giving one output as result. This system could be considered as a circuit made of two switches connected in parallel. The OR gate is the easiest to be implemented. Most of the all-chemical OR gates described, are based on fluorescent sensors that respond in the same way to at least two different molecular signals.

Several examples of OR logic gates based in fluorescence[93,115b] and enzymatic derivatives[94] have been reported. Desvergne and col.[95] made a system **(70)** where inputs are two metallic cations (Na^+ and Hg^{2+}) and output is the intramolecular photocyclization quantum yield to obtain **(71)**.

[93] De Silva, A.P.; Gunaratne, H.N.Q.; Maguire, G.E.M.; *J. Chem. Soc., Chem. Commun.* **1994**, 1213.
[94] a) Amir, R.J.; Popkov, M.; Lerner, R.A.; Barbas III, C.F.; Shabat, D.; *Angew. Chem. Int. Ed.* **2005**, *44*, 4378. b) Pita, M.; Katz, E.; *J. Am. Chem. Soc.* **2008**, *130*, 36.
[95] McSkimming, G.; Tucker, J.H.R.; Bouas-Laurent, H.; Desvergne, J.-P.; *Angew. Chem. Int. Ed.* **2000**, *39*, 2167.

SPICUM servicio de publicaciones

Each input acts in one different part of the molecule independently. Na^+ is complexed by the polyethyleneglycol chains of compound **(70)** (Fig. 81) fixing the molecule in a favourable position for the photocycloaddition. On the other hand, Hg^{2+} is complexed by bypiridyl unit, placing the compound in the right position to produce the photocyclization.

The output considered is the intramolecular photocyclization quantum yield to give product **(71)**, increased with the presence of Na^+, Hg^{2+} or both. The photocyclization from **(70)** to **(71)** is a thermically reversible process.

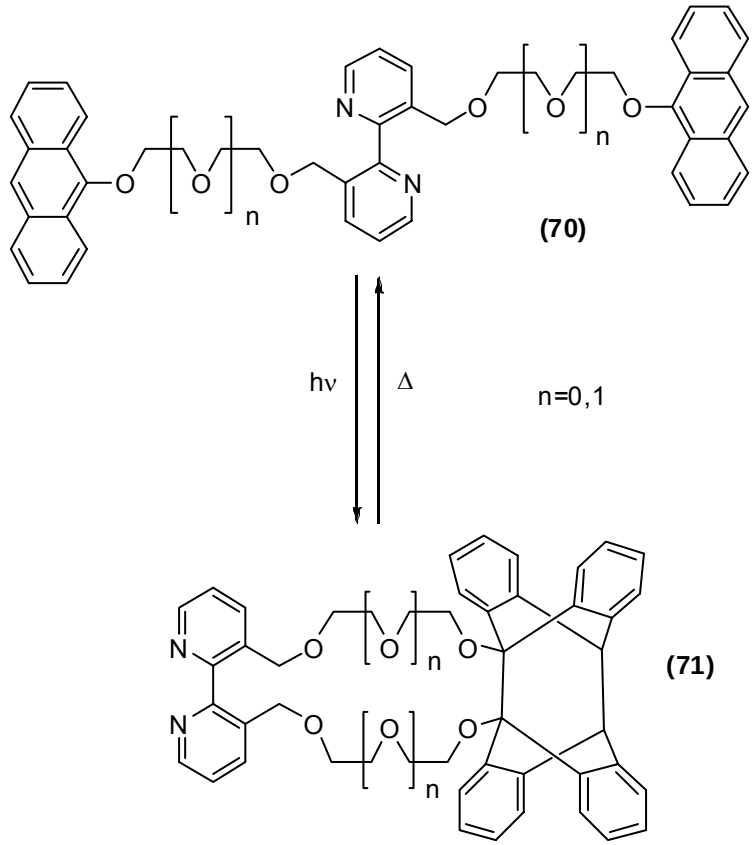

Fig. 81. Example of OR logic gate

For an OR gate behaviour, the photocyclization quantum yield must be necessary low when no metal input is present, but it must be high when either Na^+ or Hg^{2+} or both are bound to their receptors.

SPICUM servicio de publicaciones

The truth table that can be made is shown (Table 19):

Table 19. Truth table of OR logic function

In_1 (Hg^{2+})	In_2 (Na^+)	Output (ϕ)
0	0	0
0	1	1
1	0	1
1	1	1

A schematically device representation is in Fig. 82:

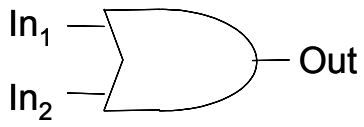

Fig. 82. OR Logic gate representation

- AND

From an electronic point of view, it can be represented as two switches connected in serial. Most of the molecular AND logic gates are based on ditopic receptors and a fluorescent unit linked covalently with both receptors.

The best examples for this type of logic gate are based on chemical inputs using fluorescence emission as output. Fluorescence should be switched on when both inputs bind with their corresponding receptors. Since the first molecular logic gate was reported,[90] an AND logic gate, many other systems have been designed with this functionality. A commonly used fluorophore is an anthranyl-based subunit,[96] that is bound to selective receptors for protons or metallic cations, but also based in TTF derivatives,[97] DNA,[98] in polymeric systems using temperature as input[99] or enzymes.[100]

[96] a) De Silva, A.P.; Gunaratne, H.Q.N.; McCoy, C.P.; *J. Am. Chem. Soc.* **1997**, *119*, 7891. b) Ji, H.-F.; Dabesgtani, R.; Brown, G.M.; *J. Am. Chem. Soc.* **2000**, *122*, 9306. c) Sadhu, K.K.; Bag, B.; Bharadwaj, P.K.; *J. Photochem. Photobiol. A* **2007,** *185*, 231.
[97] Fang, C.-J; Zhu, Z.; Sun, W.; Xu, C-H.; Yan, C.-H., *New J. Chem.* **2007**, *31*, 580.
[98] Frezza, B.M.; Cockroft, S.L.; Ghadiri, M.R.; *J. Am. Chem. Soc.* **2007**, *129*, 14875.
[99] Uchiyama, S.; Kawai, N.; de Silva, A.P.; Iwai, K.; *J. Am. Chem. Soc.* **2004**, *126*, 3032.

SPICUM servicio de publicaciones

It also have been reported several three-input AND gates,[101] and systems that switch on at ultrafast time scale using only optically controlled electron transport.[102]

The first reported computational chemical system confined to the nanometer scale entities was an AND molecular logic gate, based on the incorporation of the studied organic compound into tetramethylammonium dodecylsulfate-based micelles.[103]

The first AND and the first molecular logic gate defined, was designed by A.P. de Silva and it's shown on Fig. 83.[90]

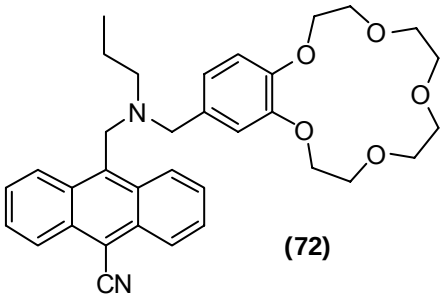

(72)

Fig. 83. Example of AND logic gate

In this case, inputs are H^+ and Na^+, while output is the anthracene subunit fluorescence emission of compound **(72)**. When H^+ and Na^+ are not present in the media, the fluorescence emission is quenched by photoinduced electron transfer from the tertiary amine residue and from benzocrown ether. When only one of the inputs is present, we can't see fluorescence emission, because it's quenched *via* PET from the tertiary amine (when Na^+, In2, is present) or from the benzocrown ether (when H^+, In1, is present). However, when both inputs are present, PET is not possible and anthracene ring fluorescence is observed.

[100] a) Margolin, A.A.; Stojanovic, M.N.; *Nature Biotechnology*, **2005**, *23*, 1374. b) Chen, X.; Wang, Y.; Liu, Q.; Zhang, Z.; Fan, C.; He, L., *Angew. Chem. Int. Ed.* **2006**, *45*, 1759.
[101] a) Guo, X.; Zhang, D.; Zhu, D., *Adv. Mater.* **2004**, *16*, 125. b) Magri, D.C.; Brown, G.J.; McClean, G.D.; de Silva, A.P., *J. Am. Chem. Soc.* **2006**, *128*, 4950.
[102] Andersson, M.; Sinks, L.E.; Hayes, R.T.; Zhao, Y.; Wasielewski, M.R., *Angew. Chem. Int. Ed.* **2003**, *42*, 3139.
[103] Uchiyama, S.; McLean, G.D.; Iwai, K.; de Silva, A.P.; *J. Am. Chem. Soc.* **2005**, *127,* 8920.

SPICUM servicio de publicaciones

The truth table we can make is shown on Table 20.

Table 20. Truth table of AND logic function

In_1 (H^+)	**In_2** (Na^+)	**Output** (Fluorescence)
0	0	0
0	1	0
1	0	0
1	1	1

It is also possible to see a schematically device representation on Fig. 84.

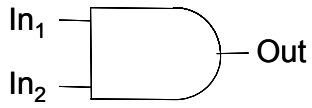

Fig. 84. AND logic gate representation

- NOR

This logic operation can be defined as the inverse of OR logic gate. It is an integration of NOT and OR functions. There are many examples of systems that work as NOR logic gates, based on fluorescence of TTF derivatives,[97] pH sensors with NOR function based on fluorine derivatives,[104] or calixarene-based systems.[105] One of the most clearly explained **(73)** was synthesized by de Silva et al.,[106] (Fig. 85).

[104] Wang, Z.; Zheng, G.; Lu, P.; *Org. Lett.* **2005**, *7*, 3669.
[105] Lee, S.H.; Kim, J.Y.; Kim, S.K.; Lee, J.H.; Kim, J. S.; *Tetrahedron* **2004**, *60*, 5171.
[106] De Silva, A.P.; Dixon, I.M.; Gunaratne, H.Q.N.; Gunnlaugsson, T.; Maxwell, P.R.S.; Rice, T.E.; *J. Am. Chem. Soc.* **1999**, *121*, 1393.

SPICUM servicio de publicaciones

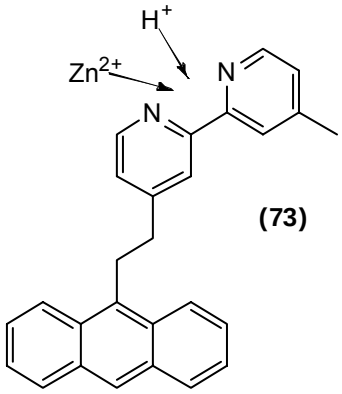

Fig. 85. Example of NOR logic gate

In this case, the bipyridyl moiety acts as H^+ (In1) or Zn^{2+} (In2) receptor. When any or both of these cations are present in the media, the anthracene fluorescence emission (Output) is deactivated. It is owed to the decreasing of the reduction potential of the system, producing PET from anthranyl moiety (acting as donor) to the bipyridyl. Only in the case that none of the inputs are present, the fluorescence is observed.

The truth table that can be made is shown (Table 21).

Table 21. Truth table of NOR logic function

In_1 (H^+)	**In_2** (Zn^{2+})	**Output** (Fluorescence)
0	0	1
0	1	0
1	0	0
1	1	0

And the device is schematically represented (Fig. 86).

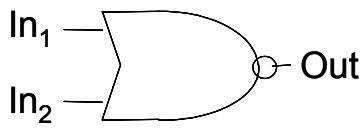

Fig. 86. NOR logic gate representation

SPICUM servicio de publicaciones

- NAND

This function can be defined as the inverse of AND logic gate. It is an integration of AND and NOT function. The NAND logic gate is one of the most commonly used in electronic systems because it can be treated as the simplest building block, since every other logic gates that can be generated by successive implementations of NAND gates. There are several chemical implementations of the NAND functionality, based on TTF derivatives,[97] the supramolecular base-paring interactions in nucleic acids[107] or supramolecular host-guest assemblies that are modified with the presence of cations.[108]

Yan et al. synthesized one TTF derivative[97] **(74)** (Fig. 87) that is fluorescent in its dicationic state. The absence or presence of Fe^{2+} or $NOBF_4$ individually has no effect on the emission and the fluorescent output remains high Out=1.

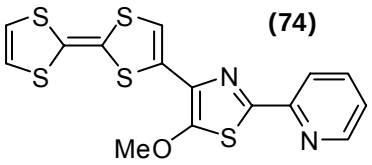

Fig. 87. Example of NAND logic gate

The presence of both Fe^{2+} and $NOBF_4$ inputs, leads to fluorescence quench, which is due to the sequential quenching effect of Fe^{3+} from the oxidation of Fe^{2+} by $NOBF_4$.
The truth table that can be made is shown (Table 22).

Table 22. Truth table of NAND logic gate

In_1 (Fe^{2+})	**In_2** ($NOBF_4$)	**Output** (Fluorescence)
0	0	1
0	1	1
1	0	1
1	1	0

[107] Baytekin, H.T.; Akkaya, E.U.; *Org. Lett.* **2000**, *2*, 1725.
[108] Chiang, P.-T.; Cheng, P.-N.; Lin, C.-F.; Liu, Y.-H.; Lai, C.-C.; Peng, S.-M.; Chiu, S.-H.; *Chem. Eur. J.* **2006**, *12*, 865.

SPICUM servicio de publicaciones

And the device is schematically represented (Fig. 88).

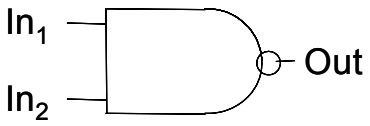

Fig. 88. NAND logic gate representation

- XOR

Implementation of the XOR gate in a chemical system is a particularly difficult task. It requires a chemical system that responds to two different stimuli in a complex way: any of these two stimuli should switch on the system, while simultaneously presence of both inputs should leave the system switched off.

Most of the devices described are not based on single molecular systems but on mixtures of compounds or supramolecular assemblies.[109,112] The most common case is that the two inputs react one with each other. Like that, input (0,0) and (1,1) have the same effect. Acid and base, used in stoichiometric proportions are commonly used and non-complementary chemical inputs are rarely described.

There have been synthesized many kinds of molecular XOR gates: based on molecular machines,[109] nucleotides,[110] systems that simulate neurons properties,[111] cyclam-cored dendrimers complexes,[112] internal charge transfer chromophores[115b] and optoelectronics structures, with optical inputs and electric outputs.[113]

[109] Credi, A.; Balzani, V.; Langford, S.J.; Stoddart, J.F.; *J. Am. Chem. Soc.* **1997**, *119*, 2679.
[110] Stojanovic, M.N.; Mitchell, T.E.; Stefanovic, D.; *J. Am. Chem. Soc.* **2002**, *124*, 3555.
[111] Pina, F.; Melo, M.J.; Maestri, M.; Passaniti, P.; Balzani, V.; *J. Am. Chem. Soc.* **2000**, *122*, 4496.
[112] Bergamini, G.; Saudan, C.; Ceroni, P.; Maestri, M.; Balzani, V.; Gorka, M.; Lee, S.-K.; van Heyst, J.; Vögtle, F.; *J. Am. Chem. Soc.* **2004**, *126*, 16466.
[113] Furtado, L.F.O.; Alexiou, A.D.P.; Gonçalves, L.; Toma, H.E.; Araki, K.; *Angew. Chem. Int. Ed.* **2006**, *45*, 3143.

SPICUM servicio de publicaciones

The only chemically driven molecular XOR logic gates not based on annihilation of input stimuli, was reported by A.P. de Silva et al. and one of these systems, **(75)** is presented in Fig. 89.[91]

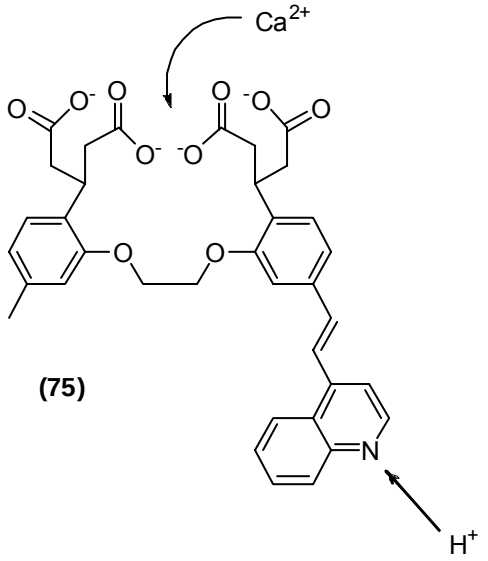

(75)

Fig. 89. Example of XOR logic gate

Ca^{2+} ions are complexed by carboxylic anions and H^+ interacts with quinoline moiety in an acid-basic equilibrium. When no input is present (Ca^{2+} or H^+), the chromophore shows a low transmittance at 390 nm. Presence of calcium, induce a hypsochromic shift while presence of protons produces a bathochromic shift, increasing transmittance at 390 nm. When both cations are in water, the result is the absorption at 390 nm.

The truth table is shown on Table 23.

Table 23. Truth table of XOR logic gate

In_1 (H^+)	**In_2** (Ca^{2+})	**Output** (transmittance)
0	0	0
0	1	1
1	0	1
1	1	0

SPICUM servicio de publicaciones

The schematically device representation is presented (Fig. 90).

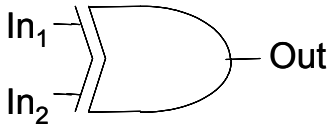

Fig. 90. XOR logic gate representation

- XNOR

The XNOR logic function, can be defined as the union between a XOR and a NOT function. There are several examples of this logic gate and are based in TTF derivatives,[97] fluorescence emission of pyrene-appended calixarenes[105] or based in electrochemically induced molecular motions in pseudorotaxanes.[114] (Fig. 91)

The pseudorotaxane **(76A)**, that consists on an electron rich tetrathiafulvalene derivative, inserts in an electron poor bipyridyl cyclophane cavity **(76B)**. The charge transfer interaction between both derivatives shows an absorption band at 830 nm, used as output signal. On the other hand, the inputs considered are the application of positive (+0.5V) or negative (-0.3V) electric voltage, with a strength enough to cause the oxidation of **(76A)** or reduction of **(76B)**. The application of any of these voltages produces the complex dissociation, with consequent disappearance of the absorption.

The value of input In_1=In_2= 1, means the application of both voltages simultaneously, that would lead to the oxidation of **(76A)** and reduction of **(76B)** in parallel, something unreal.

[114] Akasawa M.; Ashton, P.R.; Balzani, V.; Credi, A.; Mattersteig, G.; Matthews, O.A.; Montalti, M.; Spencer, N.; Stoddart, J.F.; Venturi, M.; *Chem. Eur. J.* **1997**, *3*, 1992.

SPICUM servicio de publicaciones

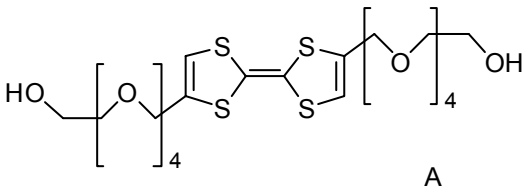

A

(76)

B

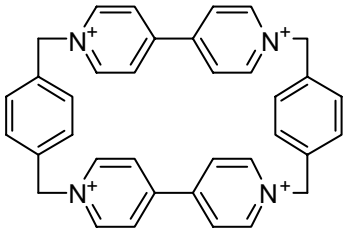

Fig. 91. Example of XNOR logic gate

The truth table is shown on Table 24:

Table 24. Truth table of XNOR logic gate

In_1 (+0.5V)	**In_2** (-0.3V)	**Output** (abs. 830 nm)
0	0	1
0	1	0
1	0	0
1	1	1

And the schematically device representation is shown on Fig. 92:

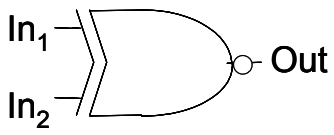

Fig. 92. XNOR logic gate representation

SPICUM servicio de publicaciones

IV.1.3.2. Logic gates combination

These functions are defined by the combination of several basic logic operations. The most important of them are Inhibit (INH), Half Adder, Half Subtractor, Full Adder and Full Subtractor.

- INH

This function is a simple AND system, where one of the inputs is inverted by a NOT function. There are several examples of INH logic gates, and are based in TTF derivatives,[97] pyrene-appended calixarenes,[105] with fluorescence outputs,[115] based in europium luminescence,[116] in DNA[117] and in phosphorescence.[118]

The example of Hirai et al. is shown on Fig. 93.[115a]

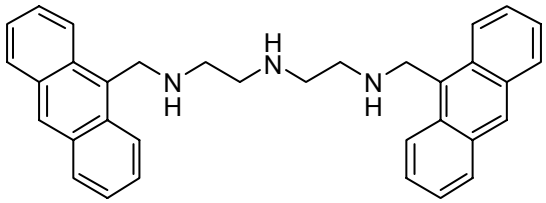

(77)

Fig. 93. Example of INH logic gate

This fluorophore is operated by two inputs, H^+ (In_1) and transition metal cations (In_2), in aqueous solution. Using Hg^{2+} or Cu^{2+} as In_2, we get an INH logic gate. Compound **(77)** at pH > 9, shows an excimer fluorescence emission (λ_{em}= 520nm), due to a direct photoexcitation of the ground-state intramolecular charge transfer (ICT) complex, formed *via* π-stacking interaction of the two anthracene moieties, associated with the pH-induced chain bending, and solvation of water molecules. At pH < 9, the compound shows anthracene monomer fluorescence emission (λ_{em}= 416nm). The study of the compound with both inputs previously mentioned gave as result the truth table showed on Table 25.

[115] a) Shiraishi, Y.; Tokitoh, Y.; Hirai, T.; *Chem. Commun.* **2005**, 5316. b) De Silva, A.P.; McClenaghan, N.D.; *Chem. Eur. J.* **2002**, *8*, 4935. c) Banthia, S.; Samanta, A.; *Eur. J. Org. Chem.* **2005**, 4967.
[116] de Sousa, M.; Kluciar, M.; Abad, S.; Miranda, M.A.; de Castro, B.; Pischel, U.; *Photochem. Photobiol. Sci.* **2004**, *3*, 639.
[117] a) Saghatelian, A.; Völcker, N.H.; Guckian, K.M.; Lin, V.S.-Y.; Ghadiri, M.R.; *J. Am. Chem. Soc.* **2003**, *125*, 346. b) Tang, Y.; He, F.; Wang, S.; Li, Y.; Zhu, D.; Bazan, G.C.; *Adv. Mater.* **2006**, *18*, 2105.
[118] Gunnlaugsson, T.; Mac Dónail, D.A.; Parker, D.; *Chem. Commun.* **2000**, 93.

SPICUM servicio de publicaciones

Table 25. INH truth table

In_1 (H^+)	**In_2** (Hg^{2+})	**Output** (Emission at 416nm)
0	0	0
0	1	0
1	0	1
1	1	0

The absence of both inputs keep pH higher than 9, so we can't see the monomer emission at 416 nm. Addition of Hg^{2+} (In_2) produces the monomer emission quenching because the coordination of these ions, lead to an energy transfer from the photoexcited anthracene to a *d*-orbital of the cations, even when H^+ is present. The emission at 416 nm can only be observed if H^+ (In_1) is present in absence of Hg^{2+}.

The schematically device representation is shown on Fig. 94.

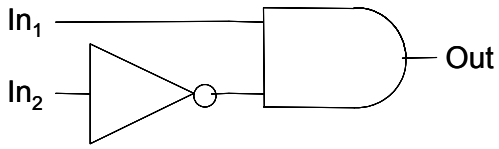

Fig. 94. INH logic gate representation

- Half-Adder

This function is defined as the addition operation of two binary digits. It is based on the combination of an AND and a XOR function working in parallel. Output of AND function is the first digit of the binary sum and the output of XOR function gives the second digit. To get this response, the considered molecules must present common inputs but they must generate different response (AND, XOR) in each of them.

Many systems have been synthesized since de Silva et al. defined the first one using two chromophores based in the combination of two different metallic cations receptors.[119] Rotaxanes,[120] fluorescent microfluidic devices,[121] tetrathiafulvalene and

[119] De Silva, A.P.; McClenaghan, N.D.; *J. Am. Chem. Soc.* **2000**, *122*, 3965.

SPICUM servicio de publicaciones

derivatives,[122] arylvinyl-bipyridyl fluorophores,[123] porphyrine based chromophores,[124] photochromic spiropyrans,[125] phenantroline pH-dependent systems[126] and biological modified systems with FRET processes[127] have been developed as useful systems with half-adder properties.

One interesting system was synthesized by Andréasson et al. integrating in one molecule (that consists of three covalently linked photochromic moieties, a spiropyran and two quinoline-derived dihydroindolizines) both AND and XOR functions (Fig. 95).[128]

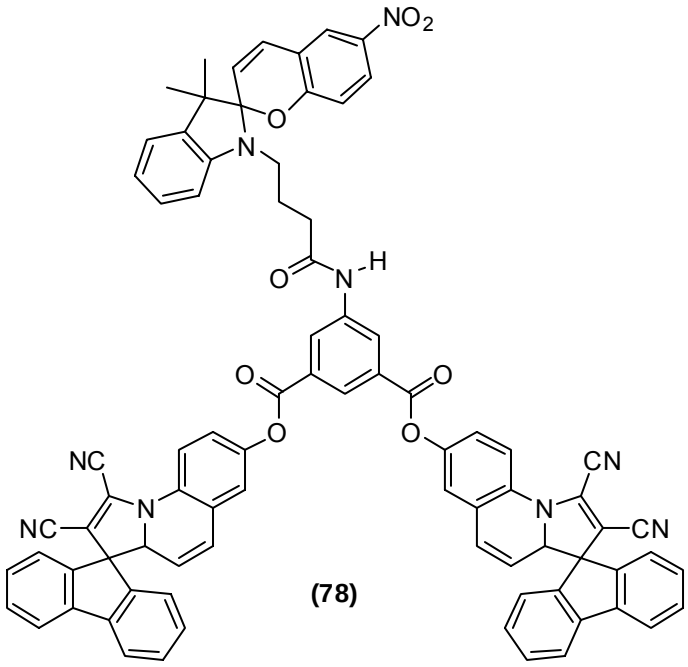

(78)

Fig. 95. Example of unimolecular Half-Adder logic gate

[120] Qu, D.-H.; Wang, Q.-C.; Tian, H.; *Angew. Chem. Int. Ed.* **2005**, *44*, 5296.
[121] Kou, S.; Lee, H.N.; van Noort, D.; Swamy, K.M.K.; Kim, S.H.; Soh, J.H.; Lee, K.-M.; Nam, S.-W.; Yoon, J.; Park, S.; *Angew. Chem. Int. Ed.* **2008**, *47*, 872.
[122] a) Zhou, Y.; Wu, H.; Qu, L.; Zhang, D.; Zhu, D.; *J. Phys. Chem. B* **2006**, *110*, 15676. b) Sun, W.; Xu, C.-H.; Zhu, Z.; Fang, C.-J.; Yan, C.-H.; *J. Phys. Chem. C.* **2008**, *112*, 16973.
[123] Zhang, L.; Whitfield, W.A.; Zhu, L.; *Chem. Commun.* **2008**, 1880.
[124] Andréasson, J.; Kodis, G.; Terazono, Y.; Liddell, P.A.; Bandyopadhyay, S.; Mitchell, R.H.; Moore, T.A.; Moore, A.L.; Gust, D.; *J. Am. Chem. Soc.* **2004**, *126*, 15926.
[125] Guo, X.; Zhang, D.; Zhang, G.; Zhu, D.; *J. Phys.Chem. B* **2004**, *108*, 11942.
[126] Liu, Y.; Jiang, W.; Zhang, H.-Y.; Li, C.-J.; *J. Phys. Chem. B* **2006**, *110*, 14231.
[127] Margulies, D.; Melman, G.; Felder, C.E.; Arad-Yellin, R.; Shanzer, A.; *J. Am. Chem. Soc.* **2004**, *126*, 15400.
[128] Andréasson, J.; Straight, S.D.; Kodis, G.; Park, C.D.; Hambourger, M.; Gervaldo, M.; Albinsson, B.; Moore, T.A.; Moore, A.L.; Gust, D.; *J. Am. Chem. Soc.* **2006**, *128*, 16259.

SPICUM servicio de publicaciones

Compound **(78)** is an all-photonic molecular half-adder. When **(78)** is irradiated at 355 nm, the open isomer of spiropyran and the quinoline-derived dihydroindolizines are populated. The open form of the spiropyran (merocyanine), absorbs strongly in the visible and it has a significantly fluorescence. The open form of the quinoline-derived dihydroindolizine absorbs at similar wavelengths that merocyanine emission, quenching the merocyanine fluorescence. The merocyanine form is the only form that absorbs at 581 nm. Selecting appropriated threshold values, the input signals are two identical light beams at 355 nm and the output signals are absorbance at 581 nm (AND gate) and fluorescence emission at 690 nm (XOR gate). Two 355 nm pulses are necessary to exceed the threshold value of absorbance at 581 nm.

The truth table of this system is shown on Table 26. The AND gate, generates the carry digit while the XOR gate produces the sum digit. This response produces the binary sum of the input digits.

Table 26. Truth table of Half-Adder logic gate

In_1 (λ= 355nm)	**In_2** (λ= 355nm)	"AND" **Out_1** (Carry digit) (Abs 581nm)	"XOR" **Out_2** (Sum digit) (Emiss 690 nm)	**Binary sum**
0	0	0	0	00
1	0	0	1	01
0	1	0	1	01
1	1	1	0	10

Considering In_1 and In_2 as the digits to be added, the operations that result are the following: 0+0 = 00 (0); 1+0 = 0+1 = 01 (1); and 1+1 = 10, that means "2" in binary.
The scheme of this function is shown on Fig. 96.

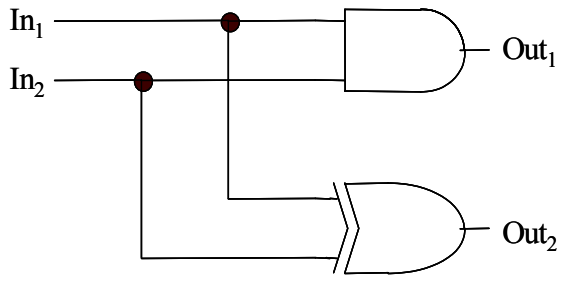

Fig. 96. Half-Adder logic gate representation

SPICUM servicio de publicaciones

- Half-Subtractor

The half-subtractor is defined as the difference between two numbers of a binary digit. This is a combinational circuit that subtracts two bit and results its difference. Half subtractors are composed of an INH and an XOR gate working in parallel. They produce a borrow (INH) and a difference (XOR) output.

Steven Langford et al. defined the first molecular half-subtractor based on the absorption of tetraphenylporphyrin upon addition of HCl or *t*-BuOK.[129] Systems based on BODIPY dyes,[130] fluorescent tetrathiafulvalene derivatives,[122b] modified biological systems,[127] and systems based on the absorption spectrum changes of phenanthroline derivatives *via* pH changes[126] have been developed.

One interesting system based on one hemicyanine monolayer supported on a modified indium-tin oxide (ITO) electrode with photocurrent outputs was developed by Li et al.[131] and is shown on Fig. 97.

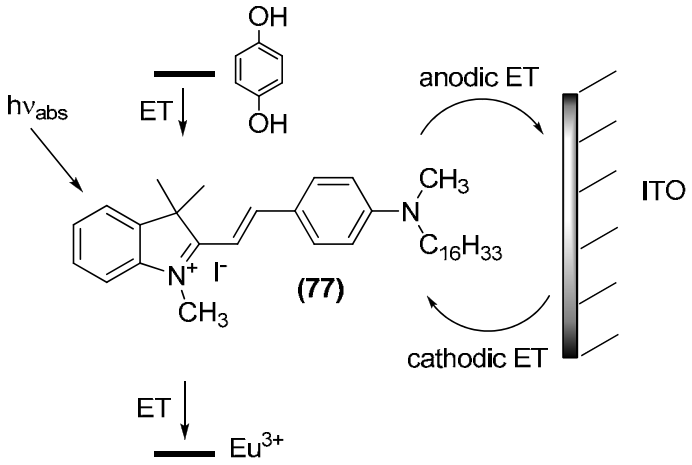

Fig. 97. Example of Half-Subtractor logic gate

Compound **(79)** is affected for two inputs: an electron donor (hydroquinone) and an electron acceptor (Eu^{3+}). The outputs considered are cathodic and anodic photocurrent. The truth table that can be made is shown on Table 27.

[129] Langford, S.J.; Yann, T.; *J. Am. Chem. Soc.* **2003**, *125*, 11198.
[130] Coskun, A.; Deniz, E.; Akkaya, E.U.; *Org. Lett.* **2005**, *7*, 5187.
[131] a) Li, F.; Shi, M.; Huang, C.; Jin, L.; *J. Mater. Chem.* **2005**, *15*, 3015. b) Pischel, U.; *Angew. Chem. Int. Ed.* **2007**, *46*, 4026.

SPICUM servicio de publicaciones

Table 27. Truth table of Half-Subtractor logic gate

In_1 (Hydroquinone)	**In_2** (Eu^{3+})	"INH" (Borrow) **Out 1.** (Cathodic photocurrent)	"XOR" (Difference) **Out 2.** (Current in absolute value)	**Subtraction**
0	0	0 (416 nA cm^{-2})	0 (416 nA cm^{-2})	00
0	1	1 (1010 nA cm^{-2})	1 (1010 nA cm^{-2})	11
1	0	0 (-2050 nA cm^{-2})	1 (2050 nA cm^{-2})	01
1	1	0 (-185 nA cm^{-2})	0 (185 nA cm^{-2})	00

The INH gate is generated taking as $Output_1$ the cathodic photocurrent. It is distinctly high only when the electron acceptor (Eu^{3+}) is present in the media and in absence of the donor (hydroquinone).

Considering the absolute value of the photocurrent as output, when hydroquinone is present in the media, the high anodic photocurrent associated to its presence, can be used as a "1" value for $Output_2$, to configure a XOR gate in association with the "1" value obtained by previous presence of Eu^{3+}.

The absence or simultaneously presence of both inputs produce a low anodic (In_1=In_2=1) or cathodic (In_1=In_2=0) photocurrent *via* electron transfer processes that involves the electron donor, the electron acceptor and the hemicyanine layer.
The subtraction between the two input bits, is shown on Table 27 where 0-0= 0; 1-0 = 1; 1-1= 0 and 0-1= 1 assuming that a borrow is performed from a higher state (represented for 11).

The scheme of this function is shown on Fig. 98.

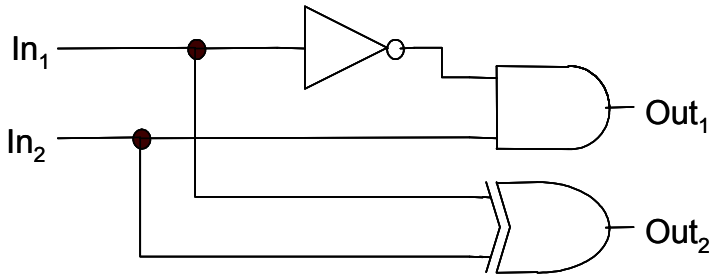

Fig. 98. Half-Subtractor logic gate representation

SPICUM servicio de publicaciones

- Full Adder

The full adder is a system that carries out an addition operation of three binary digits. It is a consequence of the concatenation of two half adder. This function produces a sum and a carry value, binary digits both of them. A binary full adder has three inputs, the two binary numbers (In_1, In_2) that have to be summed and the *carry in* (In_3), bit from the previous addition, where their sum is achieved. A full adder needs to produce two outputs, the "sum out", which is the XOR sum of the two inputs (In_1, In_2) and the *carry in* (In_3), and an output called the "carry out" which acts as the *carry in* input for the next addition cycle.

Remacle et al. theoretically defined the first full adder in a donor-acceptor system based in rhodamine 6G as donor and azulene as acceptor.[132] In 2006, Margulies et al. designed the first molecular full-adder.[133] It is based on the fluorescent indicator fluorescein **(80)** and use acids and bases as input signals, while changes in absorbance, transmittance and fluorescence are used as outputs (Fig. 99).

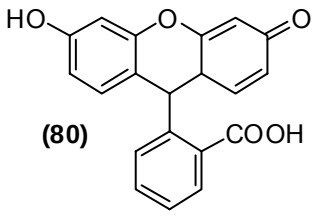

(80)

Fig. 99. Full-Adder based on Fluorescein

The basis on the operation of this system is to consider simultaneously absorbance (A) and transmittance (T) as output values, which can be observed even at the same wavelength. For example, if a YES operation is demonstrated through an absorbance output, a NOT operation will result from a transmittance output. Starting from a fluorescein cation, it can add two bits by processing identical chemical inputs (OH^-) and generating output signals at 447 and 474 nm.

Addition of just one of the inputs (NaOH) to the solution containing the cationic species, generates the neutral form. Insertion of a second chemical input, converts it to the monoanion. By introducing a third, identical chemical input, a fluorescein dianion is formed, leading to the correct sum and carry out signals for 1+1+1=11.

[132] Remacle, F.; Speiser, S.; Levine, R.D.; *J. Phys. Chem. B* **2001**, *105*, 5589.
[133] Margulies, D.; Melman, G.; Shanzer, A.; *J. Am. Chem. Soc.* **2006**, *128*, 4865.

SPICUM servicio de publicaciones

Table 28. Truth table of Full-Adder logic gate

In_1 (OH^-)	**In_2** (OH^-)	**In_3** (OH^-) (Carry in)	**Out_1** (Carry out) (A at 474)	**Out_2** (Sum) (T at 447nm)	**Sum**
0	0	0	0	0	00
0	1	0	0	1	01
1	0	0	0	1	01
1	1	0	1	0	10
0	0	1	0	1	01
0	1	1	1	0	10
1	0	1	1	0	10
1	1	1	1	1	11

The truth table of this full-adder is shown on Table 28 and the scheme of this function is shown on Fig. 100.

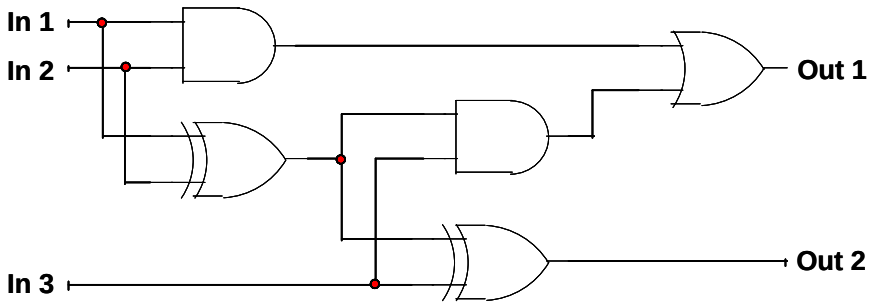

Fig. 100. Full Adder scheme

Several full-adder have been developed based on nucleotides,[134] an all optical molecular system based on a rhodamine-azulene bichromophoric molecule based on Remacle et al. studies,[135,132] a system based on sequence-specific photocleavage of DNA[136] and one system designed by Remacle group, with limited application because of the destruction of the molecules during its operation.[137]

[134] Lederman, H.; Macdonald, J.; Stefanovic, D.; Stojanovic, M.N.; *Biochemistry* **2006**, *45*, 1194.
[135] a) Kuznetz, O.; Salman, H.; Shakkour, N.; Eichen, Y.; Speiser, S.; *Chem. Phys. Lett.* **2008**, *451*, 63. b) Kuznetz, O.; Salman, H.; Eichen, Y.; Remacle, F.; Levine, R.D.; Speiser, S.; *J. Phys. Chem. C* **2008**, *112*, 15880.
[136] Ogasawara, S.; Kyoi, Y.; Fujimono, K.; *ChemBioChem* **2007**, *8*, 1520.
[137] Remacle, F.; Weinkauf, R.; Levine, R.D.; *J. Phys. Chem. A* **2006**, *110*, 177.

SPICUM servicio de publicaciones

- Full Subtractor

A full subtractor processes three inputs (x, y and borrow in B_{in}), in such a way that the difference and borrow out of x-y-B_{in} are obtained. This logic gate is the result to connect two half-subtractors and an additional OR gate. There are not many examples of this logic system being one of them the system reported by Margulies et al.[133] The use of fluorescein, **(80)** with its 4 pH-dependent ionization forms (cation, neutral, monoanion and dianion) and different optical properties in each form, allows having a wide variety of input-output signals to design logic systems.

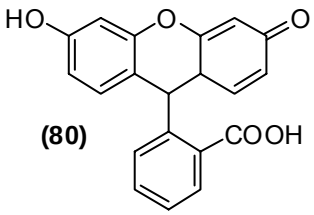

Fig. 101. Fluorescein-based full-subtractor

Starting from the neutral form of fluorescein and monitoring the absorption at 474 and 447 nm, the addition of H^+ or HO^- (1 or 2 eq) leads to the formation of the cation, the monoanion or the dianion. With these inputs and outputs, the truth table of the full-subtractor is shown on Table 29.

Table 29. Truth table of full-subtractor logic gate

In_1 (H^+)	**In_2** (HO^-)	**In_3** (OH^-) (Borrow in)	**Out_1** (Borrow out) (A at 474)	**Out_2** (Difference) (A at 447)	**Difference**
0	0	0	0	0	00
0	1	0	1	1	11
1	0	0	0	1	01
1	1	0	0	0	00
0	0	1	1	1	11
0	1	1	1	0	10
1	0	1	0	0	00
1	1	1	1	1	11

SPICUM servicio de publicaciones

Addition of H^+ produces the cationic fluorescein form, that absorbs at 447 nm while addition of HO^- (1 or 2 eq) leads to the formation of mono or dianionic form that absorbs at 447 and 474 nm or only at 474 nm respectively. Neutral form of fluorescein doesn't absorb at these wavelengths (with appropriated threshold value).

The full-subtractor can be represented by the following scheme (Fig. 102).

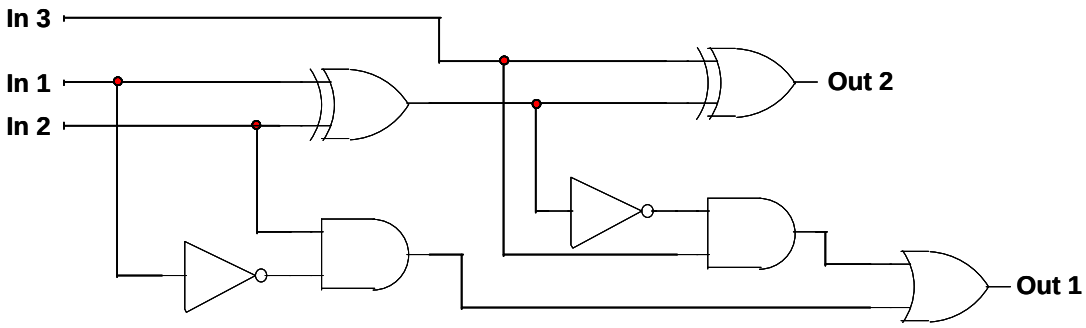

Fig. 102. Full-subtractor schematical representation

SPICUM servicio de publicaciones

IV.1.4. Advanced devices

Until now, we have described systems based on organic structures that can perform all Boolean operations to the top of full addition and subtraction. These structures are valuable synthetic approaches simulating logic gates behaviour, but their application by themselves is not usual. Nevertheless, it's possible to design molecular systems that can work as complex devices, completely functional by themselves. Moreover, it's not unusual to see how logic gates are redefined as higher complexity devices.

- Logic gates as diagnostic devices

One example of this last statement is the work presented by de Silva et al.[101b] where they redefined a three-input molecular AND logic gate as a "Lab-on-a-molecule" prototype. This prototype is formulated as a sensor that detects congregations of chemical species, with potential application in disease screening, making possible to test three disease parameters in a single rapid test, rather than testing for three disease parameters in three different and separated tests (Fig. 103).

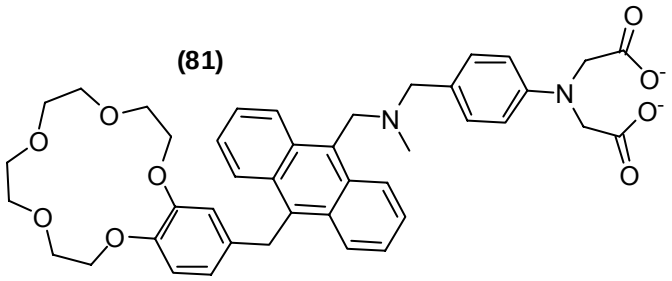

Fig. 103. A "Lab-on-a-molecule" prototype

Compound **(81)** is formed by three different inputs receptors: benzo-15-crown-5 ether for Na^+, tertiary amine for H^+ and a phenyliminodiacetate for Zn^{2+}; and one fluorophore (anthracene), separated by methylene spacers.

The simultaneous addition of Na^+, H^+ and Zn^{2+} produces a high fluorescence emission of anthracene in water. On the other hand, the addition of one or two inputs independently produces a low fluorescence output because of PET occurring from

SPICUM servicio de publicaciones

either the benzocrown ether if Na^+ is absent, the tertiary amine when there isn't H^+ or the anilinic moiety in absence of Zn^{2+}, to the excited anthracene fluorophore.
The truth table associated to this behaviour is shown on Table 30.

Table 30. Truth table of a three-input AND logic gate

In_1 (Na^+)	In_2 (H^+)	In_3 (Zn^{2+})	Out (ϕ_F)
0	0	0	0
0	1	0	0
0	0	1	0
0	1	1	0
1	0	0	0
1	1	0	0
1	0	1	0
1	1	1	1

Low levels of Inputs are either zero, or in the case of H^+, selecting a pH in which the tertiary amine was unprotonated.
This compound is a basic approach to systems where multiple inputs are jointly used to get a fast and reliable response.

A step forward in this field, developing intelligent medical diagnostics *via* molecular logic has been reported by Konry et al.[138] In this paper, the authors describe a way to detect respiratory infections *via* the interaction between a bacterial DNA and a protein (IL-8 protein) using a Boolean operator truth table. The use of these inputs is chosen because the IL-8 protein is secreted by several microorganisms involved in these diseases, especially *Haemophilus influenzae*, and it is studied together with the bacterial DNA.

The system is composed by a fiber-optic microarray, prepared by loading monoclonal antibody functionalized microspheres intro microwells. The microspheres are encoded with a fluorescent dye incorporated and is possible to determine whether both a protein and a nucleic acid simultaneously or only protein in the sample. The microspheres functionalized with antibodies, were used as selective receptors for the protein. The use of two different fluorescent probes allows the authors to detect protein-only and protein-DNA detection.

[138] Konry, T.; Walt, D.R.; *J. Am. Chem. Soc.* **2009**, *131*, 13232.

SPICUM servicio de publicaciones

The truth table of this behaviour is shown on Table 31.

Table 31. Truth table of the first molecular logic intelligent medical diagnosis

In 1 (Target DNA)	**In 2** (Protein)	**Out 1** AND gate	**Out 2** INH gate	**Out 3** OR gate
1	1	1	0	1
1	0	0	0	0
0	1	0	1	1

In the outputs are combined the fluorescence signals of both fluorophores used. The device scheme is represented in Fig. 104.

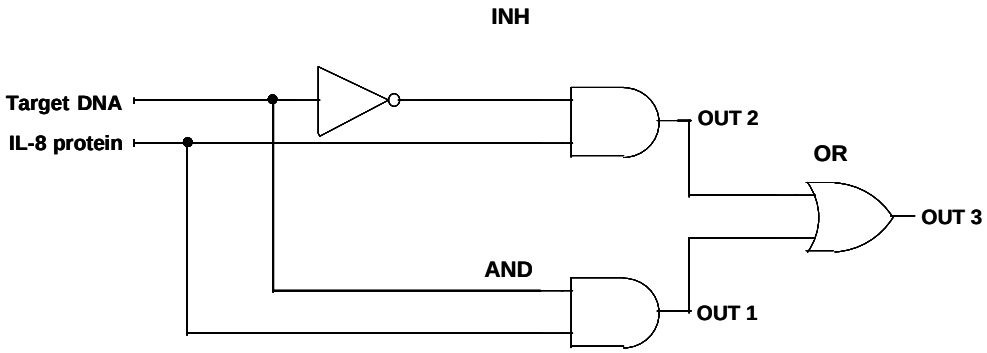

Fig. 104. Schematical representation

- Molecular calculators

Other interesting field, related to mathematical operations, is to integrate Boolean operations in the way to get systems capable to perform advanced arithmetic calculations onto single molecular species. In this way, Margulies et al.[133] designed the first advanced approach to a molecular scale calculator, called “Moleculator”. This system is the result to combine a molecular full-adder and full-subtractor into an individual molecular structure (Fig. 105).

SPICUM servicio de publicaciones

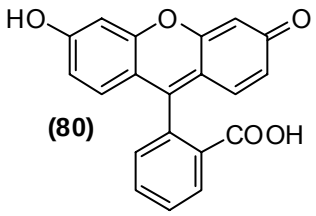

Fig. 105. Fluorescein used to build the first "Moleculator"

As seen previously, fluorescein has four ionization forms, with different optical properties each of them. Tuning between these sorts of forms is possible to obtain a full-adder and a full-subtractor, integrating two of the basic operations, addition and subtraction in a monomolecular system.

- Digital multiplexers and demultiplexers

Digital multiplexers combine several input signals into a single output signal, transmitted to a receiver. The presence of a control input, allows alternating between each input to be reported by the output. This switching input (*s*), reports the binary state of either one of these inputs or the other, depending on its own binary state.

For example, a 2:1 digital multiplexer (MUX) is composed by three inputs, two of them carrying the information and the third one selecting the carrier to be transmitted as output. The selected input showed as output, is determined by the binary state of the address input.

The first 2:1 digital multiplexer was developed by Andréasson et al.[139] and it was comprised of two photochromic moieties linked to a central porphyrin (Fig. 106). The opening of the colorless spiro form of the dihydroindolizine to a betaine form and the opening of the dihydropyrene to a colorless cyclophanediene form are the different modification possibilities of **(82)** (Fig. 106).

[139] Andréasson, J.; Straight, S.D.; Bandyopadhyay, S.; Mitchel, R.H.; Moore, T.A.; Moore, A.L.; Gust, D.; *Angew. Chem. Int. Ed.* **2007**, *46*, 958.

SPICUM servicio de publicaciones

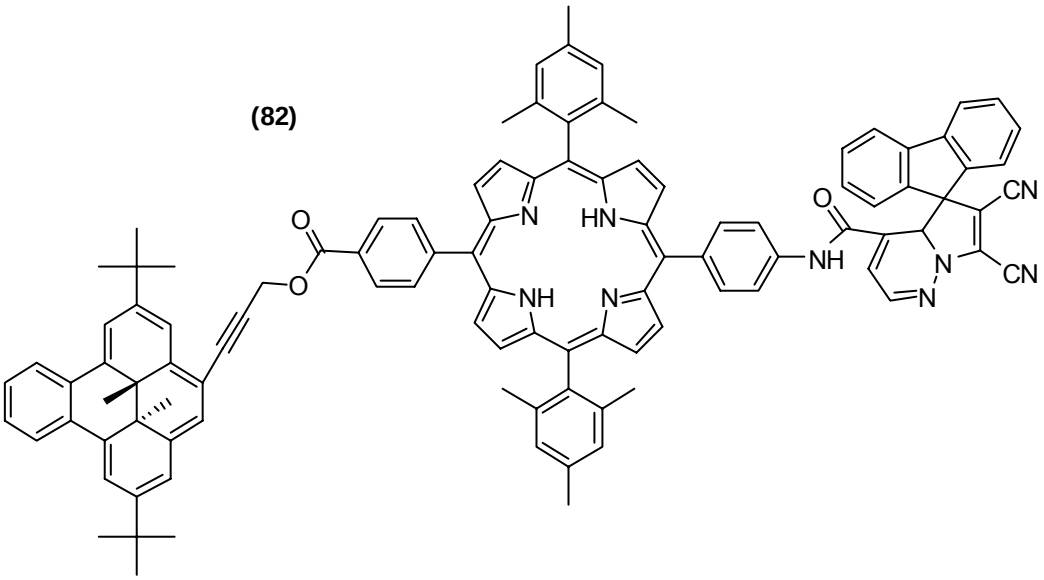

Fig. 106. Molecular 2:1 digital multiplexer

The truth table associated to 2:1 multiplexer is shown on Table 32.

Table 32. Truth table of 2:1 multiplexer

In_1 (heat)	**In_2** (red light)	**S** (green light)	**Out** (Fluo)
0	0	0	0
1	0	0	0
0	1	0	1
1	1	0	1
0	0	1	0
1	0	1	1
0	1	1	0
1	1	1	1

As we can see, when S is 0, the output reports the state of In_2. When S is 1, the output reports the state of In_1. Interconversion between the different fluorescent isomers *via* red light (opening of dihydropyranil derivative), heat (closing betaine to dihydroindolizine) and green light (opening of dihydroindolizine to betaine) and their fluorescence measurements, allows performing as a multiplexer.

SPICUM servicio de publicaciones

While a multiplexer encodes the digital state of each of two or more inputs into a single output through the use of a control input sending the encoded information to a receiver, this receiver must then decipher the entangled data streams from this single signal, directing the information from each of the initial inputs to a separate output. The device that carries this out is called demultiplexer (DEMUX).

A 1:2 demultiplexer can decode a single input signal *via* an additional input, called *address* or *control* input, that routes the signal between two different outputs selected by the binary state of the address input.

Andréasson et al., using compound **(82)** in combination with lasers and a third harmonic generating (THG) crystal, demonstrated the first molecular 1:2 digital demultiplexer.[140]

The truth table of this 1:2 demultiplexer system is presented on Table 33.

Table 33. Truth table of 1:2 demultiplexer

In_1 (Signal) λ= 532 nm	**In_2** (Address) λ= 1064 nm	**Out_1** (Fluo)	**Out_2** (Abs)
0	0	0	0
1	0	1	0
0	1	0	0
1	1	0	1

If we consider each output as a different communication route, when address input is *off* (In_2 = 0), then Out_1 reports the state of In_1 and Out_2 remains *off* (Out_2 = 0), whereas when address is *on* (In_2 = 1), Out_2 is the channel that report the state of In_1.

In this case, as in the multiplexer previously defined, the key of the behaviour of this compound lies in the isomerization of the spiro dihydroindolizine and the dihydropyrene moieties. Out_1 is the porphyrin fluorescence at 720 nm and Out_2 is the sample absorbance at 572 nm. When both photomodulable chromophores are closed, fluorescence at 720 nm (Out_1) is weak as absorbance at 572 nm (Out_2). Irradiation

[140] Andréasson, J.; Straight, S.D.; Bandyopadhyay, S.; Mitchell, R.H.; Moore, T.A.; Moore, A.L.; Gust, D.; *J. Phys. Chem. C* **2007**, *111*, 14274.

SPICUM servicio de publicaciones

with green light (532 nm wavelength, In_1) of the isomer with closed dihydropyrene and dihydroindolizine, produces the aperture of dihydropyrene to cyclophanediene form where porphyrin fluorescence is strong (Out_1 =1) but absorbance at 572 nm is still weak (Out_2 =0). If address input is turned on *via* exposing the sample to 1064 nm light, simultaneous passing of 532 nm (In_1) and 1064 nm (In_2, address) light *via* a third harmonic generator crystal generates a 355 nm light that produces isomerization of dihydroindolizine to betaine form keeping the low fluorescence emission but enhances the absorbance at 572 nm (Out_2 = 1). With these conditions, a digital demultiplexer is achieved.

Hence, a multiplexer encodes multiple data streams into a single data line for transmission, and a demultiplexer can decode entangled data streams from a single signal. If the output of the multiplexer can work as the input of the demultiplexer, and the control input of the multiplexer and the address input of demultiplexer are switched *on* and *off* in synchrony, demultiplexer output (Out_1) will accurately track the state of one of the multiplexer inputs, whereas the another demultiplexer output (Out_2) will report the state of the second multiplexer input.

Another additional step was given by Credi et al., designers of the first unimolecular multiplexer/demultiplexer (MUX-DEMUX) using a surprisingly simple molecular structure, the 8-methoxyquinoline **(83)**[141] (Fig. 107).

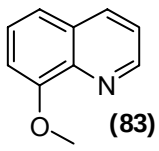

(83)

Fig. 107. 8-methoxyquinoline as MUX/DEMUX

8-Methoxyquinoline (8-MQ) is strongly fluorescent and the protonation of the quinoline, leads to the protonated form of 8-MQ-H^+ with absorption and fluorescence emission spectra clearly different from 8-MQ.

These changes in the optical properties, combined with the use of H^+ as *control* input for multiplexer and as *address* input for demultiplexer allows to define the following truth tables for multiplexer and demultiplexer functions. Inputs used are excitation wavelengths and outputs are fluorescence emission.

[141] Amelia, M.; Baroncini, M.; Credi, A.; *Angew. Chem. Int. Ed.* **2008**, *47*, 6240.

SPICUM servicio de publicaciones

Table 34. Truth table for 2:1 multiplexer function

In_1 (λ_{exc}= 285 nm)	**In_2** (λ_{exc}= 350 nm)	**In_3** "Switch" (H^+)	**Out** (λ_{em}= 474 nm)
0	0	0	0
1	0	0	1
0	1	0	0
1	1	0	1
0	0	1	0
1	0	1	0
0	1	1	1
1	1	1	1

Table 35. Truth table of 1:2 demultiplexer function

In_1 (λ_{exc}= 262 nm)	**In_2** "Address" (H^+)	**Out_1** (λ_{em}= 388 nm)	**Out_2** (λ_{em}= 500 nm)
0	0	0	0
1	0	1	0
0	1	0	0
1	1	0	1

For the multiplexer function, the output was monitored using fluorescence at 474 nm, where 8-MQ and 8-MQ-H^+ fluoresce and by means of changing excitation wavelength, since the different absorption properties of protonated and unprotonated form.

The demultiplexer operation is based on the different fluorescence emission of neutral and protonated 8-methoxyquinoline form.

SPICUM servicio de publicaciones

- "Plug and play" molecular logic

The "plug and play" systems are an important aim on the devices field, where the addition of new working modules to an operational system directly enables new functions. De Silva et al. recently applied the "plug and play" concept for molecular logic devices,[142] where different logic configurations are obtained by the easy addition of new modules under self-assembly conditions. In this way, PASS 0, PASS 1,[143] YES, NOT, OR, and AND gates are implemented with the minimal organic synthesis.

The device is designed using PET-based luminescent systems, because by definition, a "plug and play" device is necessary modular.

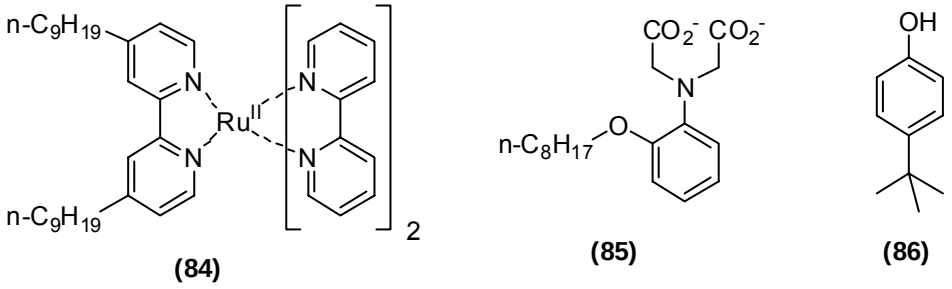

(84) **(85)** **(86)**

Fig. 108. "Plug and play" system components

Starting on a micellar dispersion of neutral detergent Triton X-100, and studying the emission at 625 nm when the sample is irradiated with 450 nm light excitation, this micellar dispersion shows a PASS 0 function. Addition of **(84)** produces the insertion of the complex inside the micelle and using H^+ as input, the systems works as a PASS 1 function: there is a high emission signal if H^+ concentration is low or high.

Further addition of **(85)** produces the insertion inside the micelle too. Using H^+ and Ca^{2+} as input, separately or simultaneously, leads this tricomponent system to work as a YES or an OR function respectively. Addition of **(86)** and studying the system with H^+ and Ca^{2+} produces an AND logic gate.

In conclusion, simple addition of selected compounds to a micellar dispersion produces several logic gates with minimal organic reactivity.

[142] De Silva, A.P.; Dobbin, C.M.; Vance, T.P.; Wannalerse, B.; *Chem. Commun.* **2009**, 1386.
[143] PASS 0 and PASS 1 are defined as two single-input, single-output binary gates with Out = 0 for any In value (PASS 0) or Out = 1 for any In value (PASS 1). More information: De Silva, A.P.; James, M.R.; McKinney, B.O.F.; Pears, D.A.; Weir, S.M.; *Nat. Mater.* **2006**, *5*, 2006.

SPICUM servicio de publicaciones

- Keypad lock

Data protection in the current society is of key interest in order to preserve the security of the information transfer and the personal details.

In order to this aim, Margulies et al. designed the first molecular device that simulates the operation of an electronic keypad lock (Fig. 109).[144] The distinction of this lock from a simple molecular logic gate is the fact that its output signals are dependent not only on the right combination of the inputs but also on the correct order by which these inputs are put in. This way of operation simulates a keypad lock because one needs to know the "password" that is, the right key combination (the right input sequence), to open the lock.

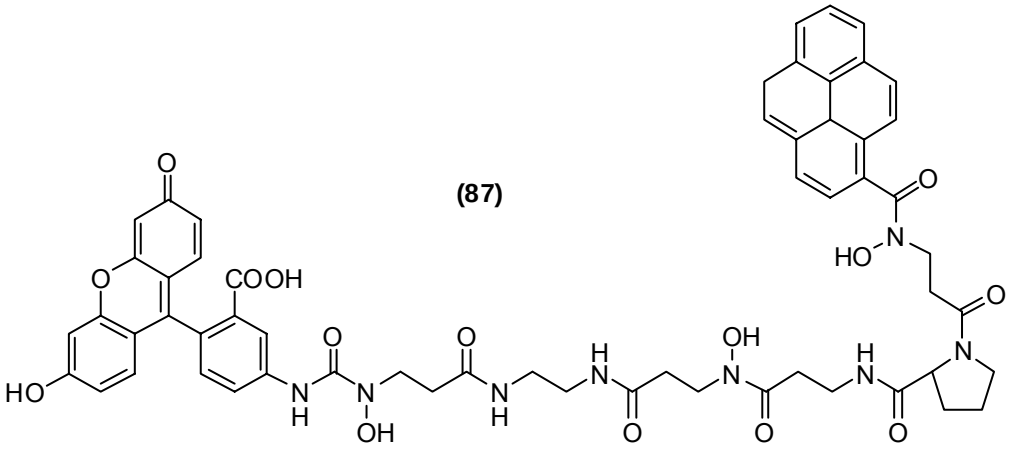

Fig. 109. Fluorescein-Linker-Pyrene used as a molecular keypad lock

The fluorescence of **(87)** is revealed only in response to correct sequences of three input signals. It is developed a kinetically controlled, priority-AND molecular logic gate, capable of authorizing different photoionic passwords.

Taking advantage of the high iron binding efficiency of the three hydroxamic acids joined to the acid-base properties of the fluorescein, Fe^{3+} and EDTA as acidic iron chelator will be used as inputs. The fluorescence of single fluorophores or *via* FRET processes between pyrene (donor) and fluorescein (acceptor) as outputs are the parameters studied.

[144] Margulies, D.; Felder, C.E.; Melman, G.; Shanzer, A.; *J. Am. Chem. Soc.* **2007**, *129*, 347.

SPICUM servicio de publicaciones

Starting from the iron complex in ethanol, the sequential addition of EDTA, base (AcO^- Na^+) and UV light in this order, produce the "keylock opening" generating a strong fluorescence at 525 nm.

Another keypad lock was synthesized by Kumar et al.[145] and recently, a new all-photonic molecular keypad lock has been reported by Andréasson et al.[146]

- Solid supported molecular logic gates

The development of miniaturized molecule-based devices requires systems capable to operate in the solid state in order to the design of useful devices. There are some examples of solid-state systems, which, nevertheless, demand chemical inputs.[141,147] Budyka et al., have recently reported a reconfigurable molecular logic system based on 2-styrylquinoline **(88)** operating in polymer film (Fig. 110).[148]

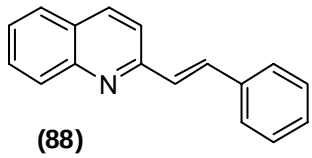

(88)

Fig. 110. 2-styrylquinoline

The *Z-E* isomerisation and the protonation of the isoquinoline, leads to four thermally stable forms that have different spectral properties and are easily interconvertible by irradiation at an appropriate wavelength and by protonation/deprotonation.
Studying the different absorption properties of these forms, the system is able to perform AND, OR, INH, NAND, NOR and IMPLICATION[149] and it also can operate as a 1:2 demultiplexer.

[145] Kumar, S.; Luxami, V.; Saini, R.; Kaur, D.; *Chem. Commun.* **2009**, 3044.
[146] Andréasson, J.; Straight, S.D.; Moore, T.A.; Moore, A.L.; Gust, D.; *Chem. Eur. J.* **2009**, *15*, 3936.
[147] a) Leigh, D.A.; Morales, M.A.F.; Pérez, E.M.; Wong, J.K.Y.; Saiz, C.G.; Slawin, A.M.Z.; Carmichael, A.J.; Haddleton, D.M.; Brouwer, A.M.; Buma, W.J.; Wurpel, G.W.H.; León, S.; Zerbetto, F.; *Angew. Chem. Int. Ed.* **2005**, *44*, 3062. b) Gupta, T.; van der Boom, M.E.; *Angew. Chem. Int. Ed.* **2008**, *47*, 5322.
[148] Budyka, M.F.; Potashova, N.I.; Gavrishova, T.N.; Lee, V.M.; *J. Mater. Chem.* **2009**, *19*, 7721.
[149] IMPLICATION (IMPL) is defined as the inverse of the INHIBIT (INH) logic gate.

SPICUM servicio de publicaciones

IV.2. Molecular logic gates design

The photophysical properties of A-S-D systems based on isoquinoline *N*-oxide electron Acceptor, methylene Spacer and modified benzene ring-based electron Donor developed in our research group, is the basis of chemical design that leads to develop molecular systems which behaviour can be defined from the molecular logic field. Protonation of isoquinoline *N*-oxide function leads to two different fluorescent excited states that can be reached by excitation at different wavelengths.

The interaction with these A-S-D systems *via* chemical or luminescent inputs in order to modify their photophysical behaviour, allows designing chemical structures with variable responses to external stimuli.

This way, there have been studied the compounds **(89)**, **(97)** and **(98)** (Fig. 111). The design of these compounds, includes different residues which response is variable depending on different stimuli presence in the media:

SPICUM servicio de publicaciones

- The *N*-oxide function (compounds **(89)**, **(97)** and **(98)**), that can response to the presence of acid (trifluoroacetic acid, TFA) of transition metallic cations as Zn^{2+}.

- The crown ether (compound **(89)**), that can response to the presence of alkaline and alkaline earth metallic cations (K^{+}, Ba^{2+}).

- The phenol function (compound **(97)**), that can response to the presence of base (tetrabutylammonium hydroxide, TBAOH).

Besides these chemical inputs, the different wavelengths producing different fluorescence emission can be used as input too.

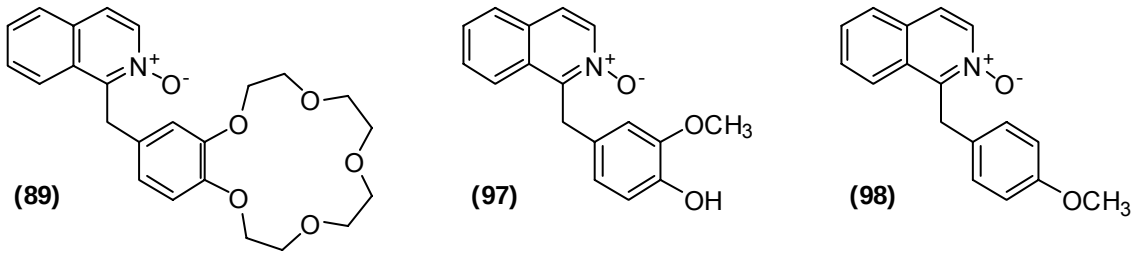

Fig. 111. Structures of the molecular logic systems designed

SPICUM servicio de publicaciones

IV.2.1. Logic gates combination *via* interaction with metal cations

IV.2.1.1. Synthesis of compound (89)

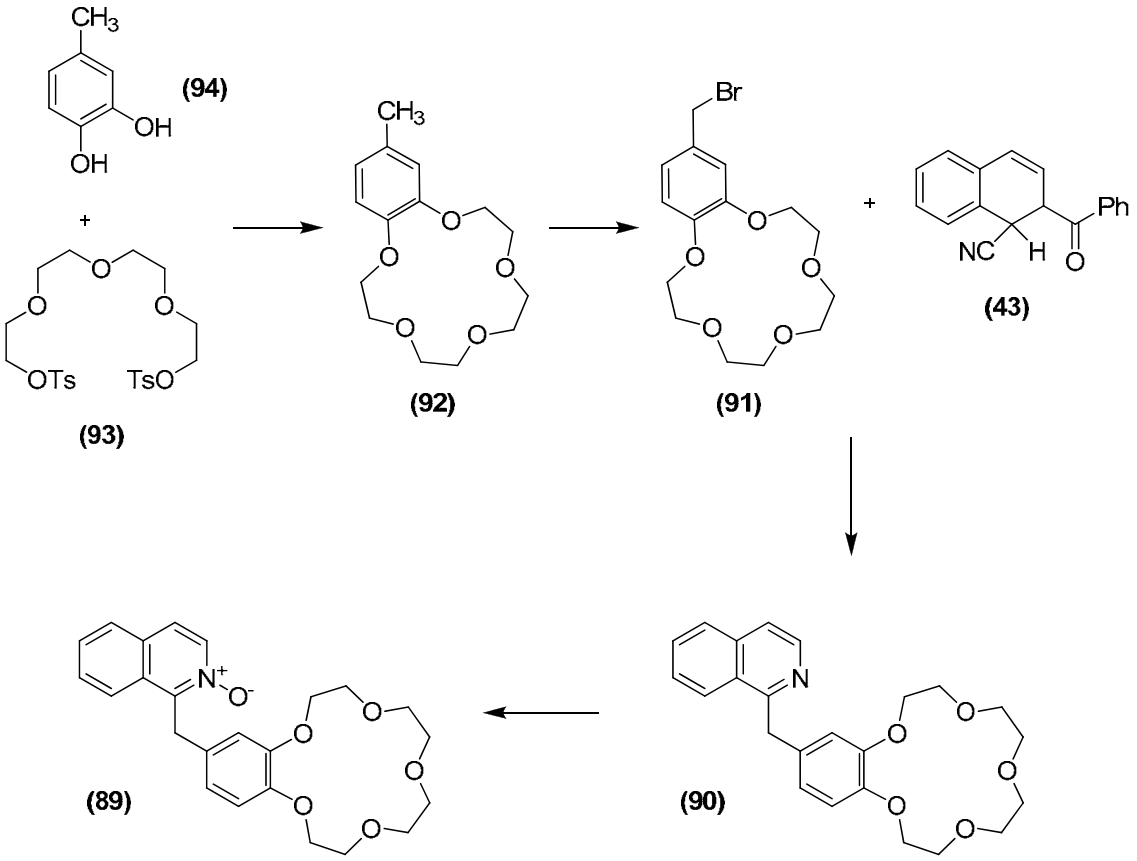

The first synthetic step is the benzo-15-crown-5 formation *via* cyclization of functionalized tetraethyleneglycol **(93)** over 4-methylcatechol **(94)**, using an alkaline cation template. A second step lies in the radical benzylic bromination of the 4-methyl-benzo-15-crown-5 **(92)**, carried out by treatment with *N*-bromosuccinimide using light as a radical initiator.

The formation of the 1-benzo-15-crown-5-isoquinoline **(90)** is made *via* Reissert coupling of the bromomethylbenzo-15-crown-5 **(91)** with isoquinoline Reissert **(43)**. A last step of *N*-oxidation using *m*-chloroperoxybenzoic acid to get **(89)** is required.

SPICUM servicio de publicaciones

- Synthesis of 4-methyl-benzo-15-crown-5 (92)

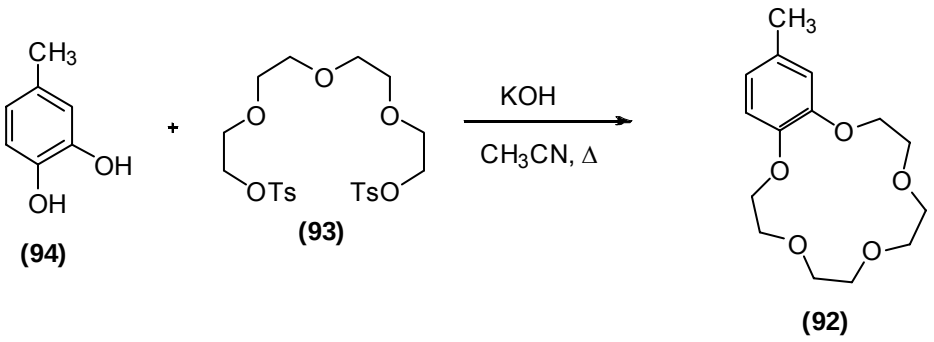

The reaction between 4-methylcatechol **(94)** and tetraethyleneglycol ditosylate **(93)** is carried out at 0.75M concentration of both reagents, using KOH as base and acetonitrile as solvent, obtaining **(92)** with 40% yield.

Using KOH as base responds to two main aspects:

- Use as base to produce the phenoxy anions that will carry out the substitution reaction over the tetraethyleneglycol ditosylate.

- Use of the K^+ as template, placing **(93)** and **(94)** in the right orientation to produce the cyclization (Fig. 112).

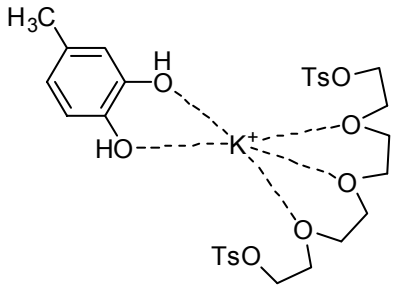

Fig. 112. Use of K^+ as template

SPICUM servicio de publicaciones

- Synthesis of 4-bromomethyl-benzo-15-crown-5 (91)

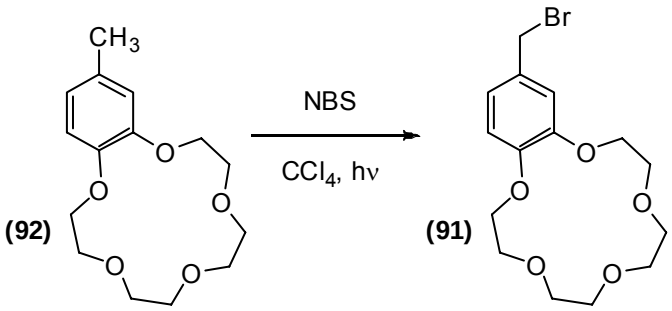

As allylic positions, benzylic positions are reactive to radical reactions. Like that, using bromine radical, will make possible the functionalization of the benzylic position.[150] There are several bromination reagents, as bromine, *N*-bromosuccinimide and 1,3-dibromo-5,5-dimethylhydantoine. The use of bromine entail the capture of a radical H$^{\cdot}$ from the benzylic position, generation of HBr and insertion of bromine radical Br$^{\cdot}$. The disadvantage to the use of Br_2 is the fact that many groups are sensitive to the presence of HBr in the reaction media.

To avoid this handicap one of the most useful methods is using *N*-bromosuccinimide (NBS) in combination with a radical initiator that can be chemical (benzoyl peroxide, *α,α'*-Azoisobutyronitrile), or a light source. In these conditions, bromine radicals selective for the benzylic position are generated. The side product formed in the radical reaction is succinimide, easy to remove in the reaction conditions and usually non-reactive to produce undesirable secondary products. The use of CCl_4 as solvent, where succinimide is not soluble, favours its elimination by filtration.

Selectivity of benzylic position against other positions, is based on the stability of the intermediate radicals formed.[151] This way, we use NBS and light as radical initiator, in CCl_4 as solvent, obtaining the product **(91)** with 98% yield.

The structure is confirmed by ^{1}H-NMR and ^{13}C-NMR with disappearing of the singlet at 2.25 ppm integrating for 3H, and the appearing of a 2H integrating singlet at 4.44 ppm, and disappearing of the methyl carbon at 20.8 ppm with new signal at 34.2 ppm for the methylene formed. Mass spectrometry, with two equal abundance peaks at *m/z* 360 and *m/z* 362 corresponding to both bromine isotopes, also confirms the structure.

[150] a) Corbin, T.F.; Hahn, R.C.; Shechter, H.; *Org. Synth. Coll.* **1973**, *5*, 328. b) Salir, A.; *Org. Synth. Coll.* **1973**, *5*, 825.
[151] Hendrickson, J.B.; de Vries, J.G.; *J. Org. Chem.* **1985**, *50*, 1688.

SPICUM servicio de publicaciones

- Synthesis of 1-(4'-methylenebenzo-15-crown-5) isoquinoline (90)

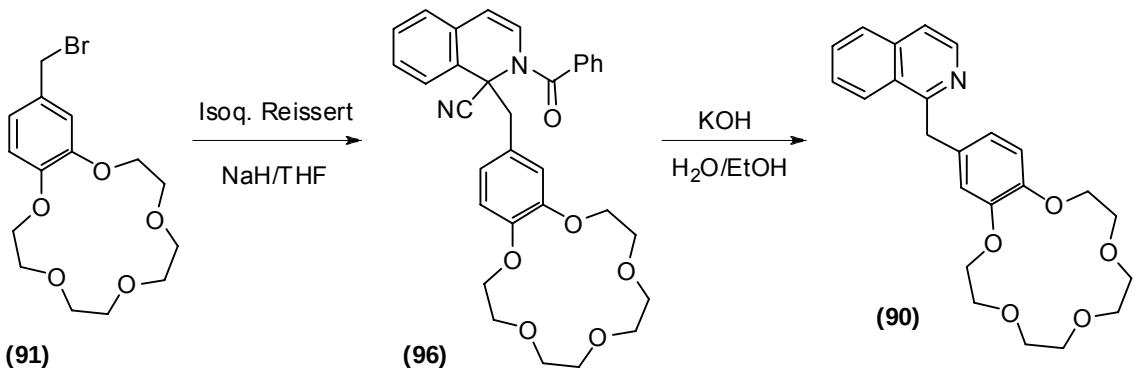

(91) **(96)** **(90)**

The synthesis of **(90)** is based on the reaction between isoquinoline Reissert and compound **(91)**. There are several reaction conditions depending on the base used. A widely used method lies in biphasic reaction conditions between an organic phase and a 50% NaOH aqueous phase, using a phase transfer catalyst. However, the most useful method in our case is the reaction in monophasic conditions, using NaH as base and THF as solvent. Two steps, coupling to obtain adduct **(96)** and hydrolysis to yield **(90)** are required.

- *Coupling reaction*

The reaction of **(91)** with isoquinoline Reissert, using NaH as base and anhydrous THF. The nucleophilic substitution of the benzylic bromine by the isoquinoline Reissert anion generated, lies to the adduct **(96)** formation. The formation of **(96)** is proved by ^{1}H-NMR, observing the double doublet of diasterotopic benzylic H and isoquinoline H_3 and H_4 doublets. The product is taken to hydrolysis without further purification to obtain **(90)**.

- *Hydrolysis*

Adduct **(96)** is hydrolyzed in a water/ethanol mixture using KOH as base heating under reflux for 4 hours. Extraction with CH_2Cl_2 and purification by alumina column chromatography give the desired product **(90)** as a sticky solid with 40% yield. ^{1}H-NMR, ^{13}C-NMR and MS spectra confirm the structure.

SPICUM servicio de publicaciones

- Synthesis of 1-(4'-methylenebenzo-15-crown-5) isoquinoline N-oxide (89)

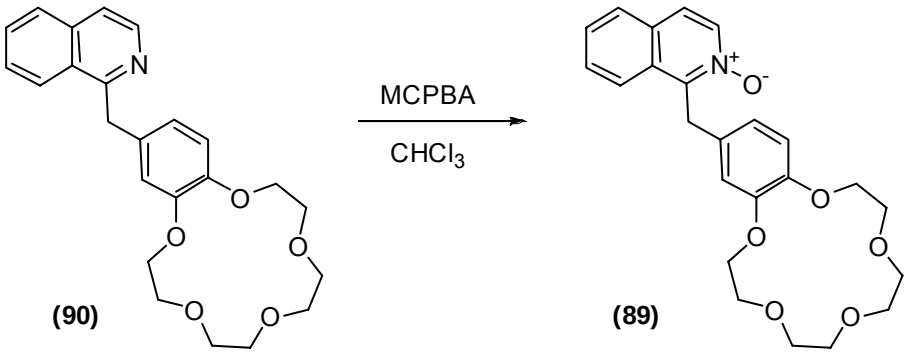

(90) **(89)**

The reaction was carried out using *m*-chloroperoxybenzoic acid as oxidizer because of its easy handle, easy workup and high reaction yields. This way, the product **(89)** is obtained with 75% yield. The formation of **(89)** is proved by the low field shift of methylene group in ^{1}H-NMR and the peak of the molecular ion at $M^{+\cdot}$ 425 in the mass spectrum.

SPICUM servicio de publicaciones

IV.2.1.2. Photophysical properties

The studies were carried out at 10^{-4} M concentrations of **(89)** and 0.1M TFA in $CHCl_3$ as solvent. Alkaline and alkaline earth salts were added to saturation. The assays carried out with Zn, were carried out at 10^{-4} M of **(89)** and $3 \cdot 10^{-4}$ M of $ZnCl_2$.

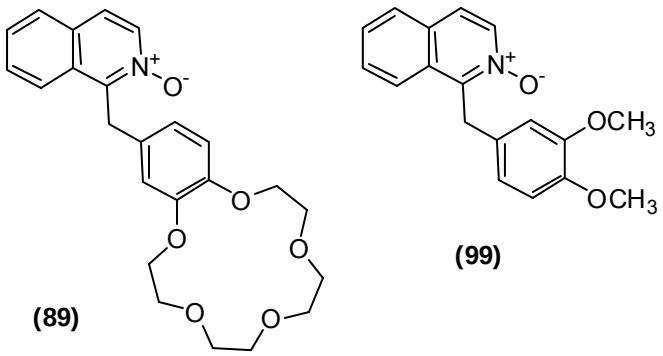

Fig. 113. Structure of compounds **(89)** and **(99)**

IV.2.1.2.1. Influence of alkaline and alkaline earth metallic cations

- Absorption spectra in neutral and acid media

The photophysical properties of A-S-D system **(89)** follow a similar pattern to the systems previously synthesized by our research group.[54] The comparison of the absorption spectrum of **(89)** and the derivative 1-(3,4-dimethoxybenzyl)isoquinoline *N*-oxide **(99)** shows the similarity between the spectra due to the presence of the same chromophoric structure and the low influence of the crown ether on **(89)** (Fig. 113).

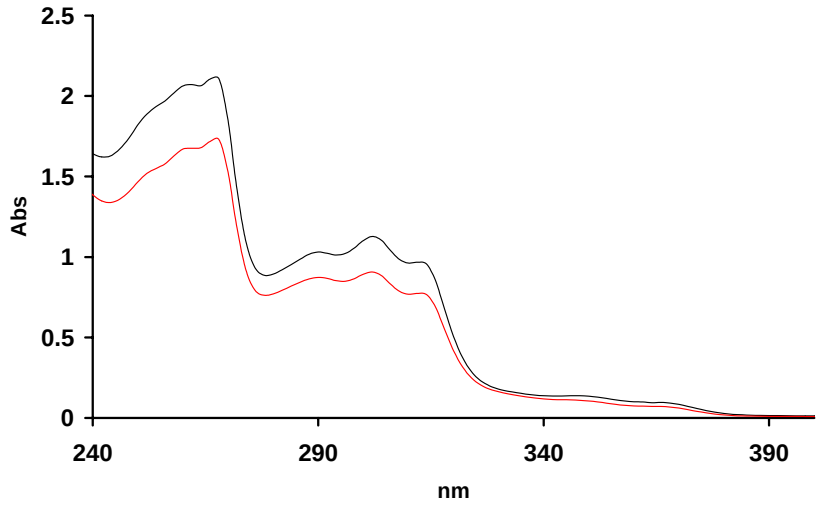

Fig. 114. Absorption spectra of **(89)** (—) and **(99)** (—) in acetonitrile

SPICUM servicio de publicaciones

The absorption spectra show the same bands pattern with the isoquinoline *N*-oxide absorption band from 300 nm, and the weak ππ* transition band at 330-360 nm.

The protonation of the *N*-oxide function,[40] leads to the generation of a formal positive charge on the isoquinoline ring. This charge formalization decreases the reduction potential of the isoquinoline moiety, increasing its electron acceptor ability.

The absorption spectrum of **(89)** in neutral and acidic media shows a general hypsochromic shift, displacing the band located up to 300 nm, to 280 nm and the 330-360 absorption band is displaced to a maximum of 340 nm (Fig. 115).

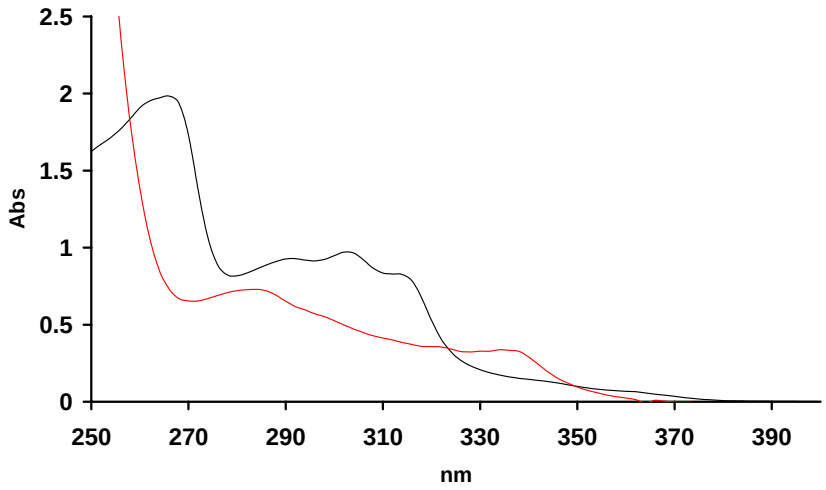

Fig. 115. Absorption spectra of **(89)** in $CHCl_3$ **(—)** and $CHCl_3$ 0.1M TFA (—)

Table 36. Molar absorption coefficient of **(89)** in neutral and acid media

	(89)	**(89) (H^+)**
λ_{max} (nm)	366	336
ε ($M^{-1}cm^{-1}$)	$0.49 \cdot 10^3$	$2.2 \cdot 10^3$

SPICUM servicio de publicaciones

- Absorption spectra in acidic media with metallic cations

The presence in the structure of **(89)** of a benzo-15-crown-5 residue, an alkaline and alkaline earth metal complexer, leads us to study the cation effect to the system photophysics.

All the measurements are carried out in acidic media, using the corresponding alkaline or alkaline earth perchlorates, added until saturation. Perchlorate is used as counterion because it doesn't absorb in the study region.
The low solubility of the perchlorates in chloroform could cause problems to carry out the study. Nevertheless, the benzo-15-crown-5 complexing capacity will act as solution coadjuvant of the inorganic salts.

A. Alkaline cations

The absorption spectra in acidic media are very similar when they are registered without or upon addition of Li^+, Na^+ or K^+ (Fig. 116).

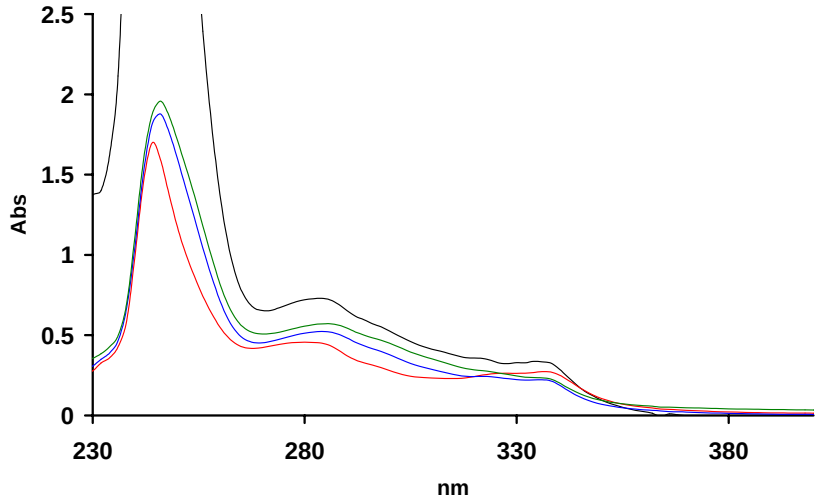

Fig. 116. Absorption spectra of **(89)** in $CHCl_3$ 0.1M TFA (—) and in the presence of Li^+ (—), Na^+ (—) and K^+ (—)

SPICUM servicio de publicaciones

B. Alkaline earth cations

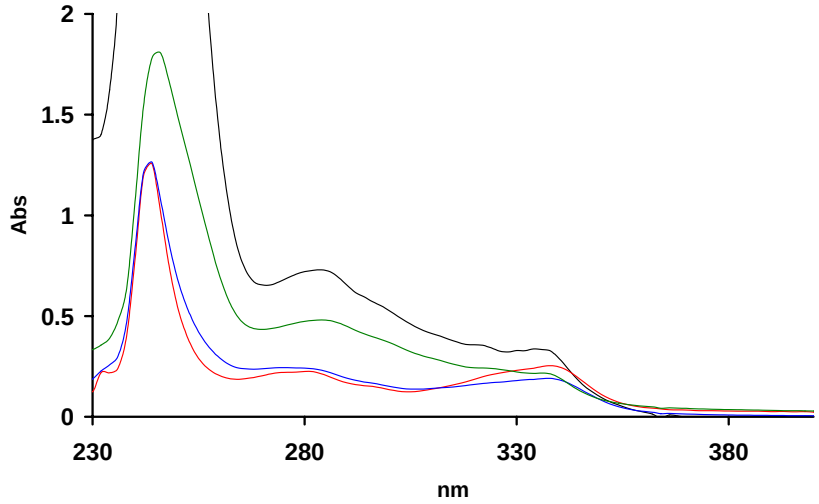

Fig. 117. Absorption spectra of **(89)** in $CHCl_3$ 0.1M TFA (—) and in the presence of Mg^{2+} (—), Ca^{2+} (—) and Ba^{2+} (—)

The addition of alkaline earth metallic cations shows the same effect than alkaline cations (Fig. 117). The absorption spectrum is not affected by the addition, probably due to the overlapping of D and A absorption bands that blocks the detection of any possible variation.

SPICUM servicio de publicaciones

- Fluorescence spectroscopy in neutral and acidic media

In neutral medium, the fluorescence emission of **(89)** is composed by a single emission band, with maximum at 392 nm upon excitation at any wavelength (Fig. 118).

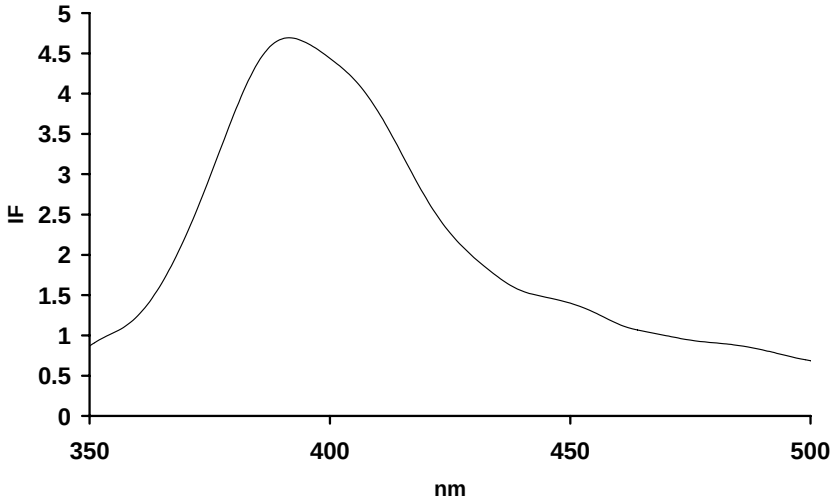

Fig. 118. Fluorescence emission of **(89)** in $CHCl_3$

This band corresponds to the isoquinoline *N*-oxide chromophore locally excited (LE) state emission.

In acidic media, two wavelength-dependent emission bands are observed.

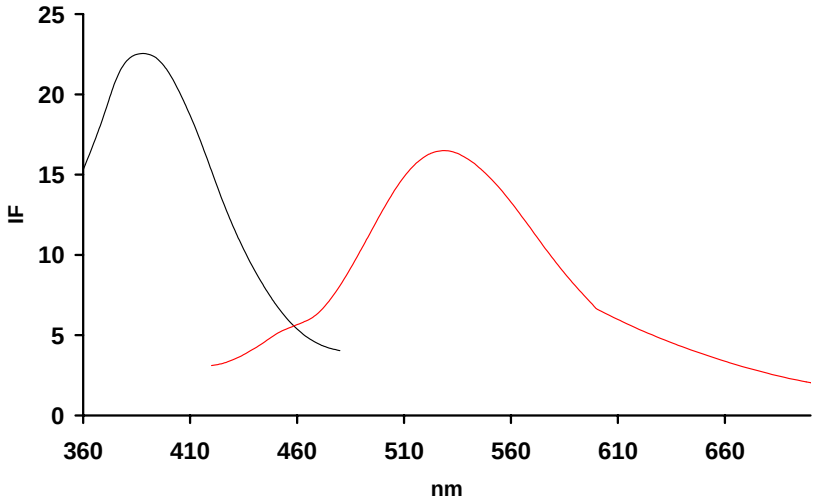

Fig. 119. Fluorescence emission of **(89)** in $CHCl_3$ 0.1M TFA λ_{exc} = 336 nm (—) and λ_{exc} = 400 nm (—)

SPICUM servicio de publicaciones

Excitation at short wavelengths ($\lambda_{exc} \leq 336$ nm) leads to the protonated isoquinoline *N*-oxide chromophore LE emission, a blue-shifted band compared with unprotonated **(89)** with maximum at 380 nm. Upon excitation at $\lambda_{exc} \geq 360$ nm, fast Photoinduced Electron Transfer (PET) between the positively charged electron acceptor and the bridged arene donor occurs, leading to a fluorescent CT state with an emission band at maximum of 530 nm.

Table 37. Fluorescence quantum yields of **(89)**

NEUTRAL	
	(89)
λ_{em} (nm) (λ_{exc} = 312nm)	400
ϕ	$0.4 \cdot 10^{-3}$
ACID (0.1 M TFA)	
	(89) (H^+)
λ_{em} (nm) (λ_{exc} = 336nm)	380
ϕ	$4 \cdot 10^{-3}$
λ_{em} (nm) (λ_{exc} = 400nm)	530
ϕ	$4.8 \cdot 10^{-2}$

- Fluorescence spectroscopy in acidic media with metallic cations

The red-shifted emission (emission from the CT excited state) is strongly dependent on the donor ability. The complexation of metallic cations, decrease the electron donor ability of benzo-15-crown-5 moiety, increasing the redox potential of the system. This effect involves a higher difficulty to reach the CT state that may produce changes in the fluorescence emission from this excited state.

The studies in presence of cations are carried out using alkaline and alkaline earth perchlorates as metallic cations source.

SPICUM servicio de publicaciones

A. Alkaline cations

● Fluorescence emission at λ_{exc} = 336 nm

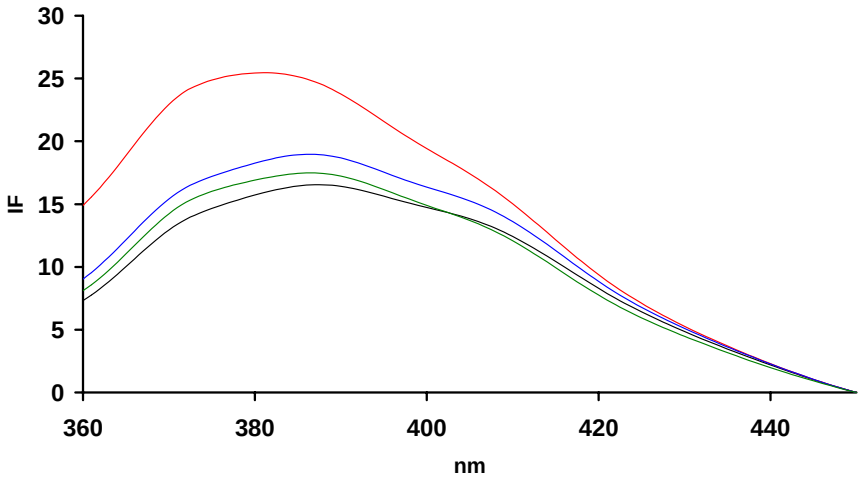

Fig. 120. Fluorescence emission of **(89)** in $CHCl_3$ 0.1M TFA (—), and in the presence of Li^+ (—), Na^+ (—) and K^+ (—) (λ_{exc} =336nm)

The presence of alkaline cations in the fluorescence emission of **(89)** upon excitation at λ_{exc} = 336 nm, shows a very similar spectrum in comparison to the absence of any cations with non-significant maximum blue shift for Li^+ addition from 386 to 381 nm.

● Fluorescence emission at λ_{exc} = 400 nm

The insertion of cations in the benzo-15-crown-5 cavity may reduce the fluorescence emission because the cationic complexation decreases its electron-donor ability. This way, an effective complexation, will make CT state reaching difficult. As shown on Fig. 121, the presence of K^+ produce a drastic fall in fluorescence emission at 550 nm, in comparison with the emission in absence of cations.

However, the addition of Li^+ and Na^+ present an opposite effect, enhancing the fluorescence emission. This effect can be explained because of the increase in the medium salinity. The CT excited states are polar and highly dependent of the medium polarity.[152] The increase of the ionic force leads to CT states stabilization that enhances its fluorescence emission.

[152] Goes, M.; Lauteslager, X.Y.; Verhoeven, J.W.; Hofstraat, J.W.; *Eur. J. Org. Chem.* **1998**, 2373.

SPICUM servicio de publicaciones

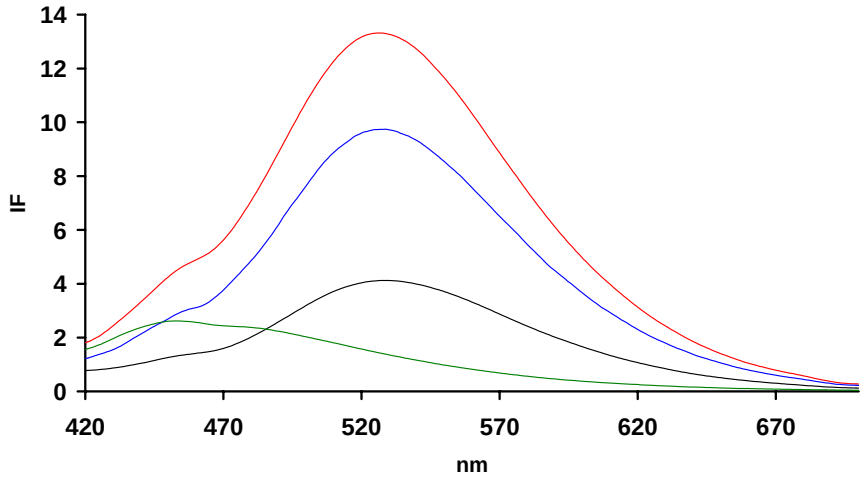

Fig. 121. Fluorescence emission of **(89)** in $CHCl_3$ 0.1M TFA (—), and in the presence of Li^+ (—), Na^+ (—) and K^+ (—) (λ_{exc}= 400nm)

Studying separately the effect of the addition of K^+, it is clearly shown the decrease in the fluorescence emission upon its addition.

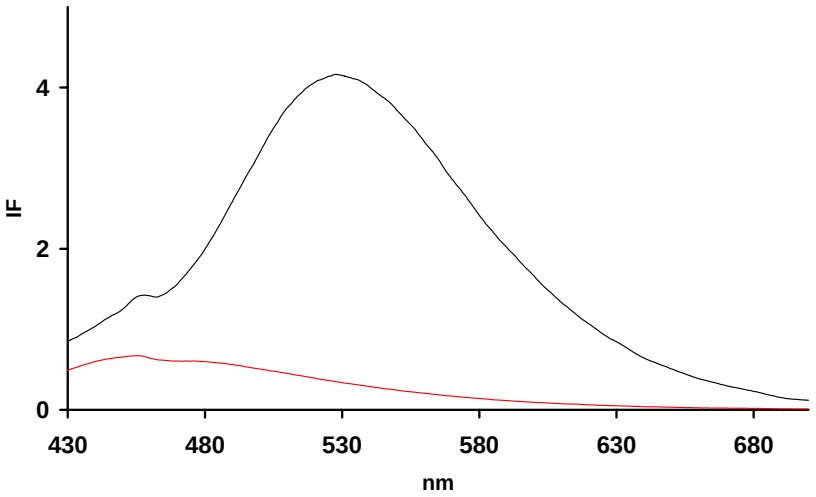

Fig. 122. Fluorescence emission of **(89)** in $CHCl_3$ 0.1M (—) and after K^+ addition (—)

The inclusion of K^+ in the chelating crown ether cavity, reduce the electronic availability, decreasing its charge donor potential. Like this, the reduction potential of the system increases and reaching the CT state is more difficult, quenching the fluorescence emission (λ_{em} = 550 nm).

SPICUM servicio de publicaciones

B. Alkaline earth cations

Just like the alkaline cations effect, it has been studied the presence of Mg^{2+},Ca^{2+} and Ba^{2+}.

● Fluorescence emission at λ_{exc} = 336 nm.

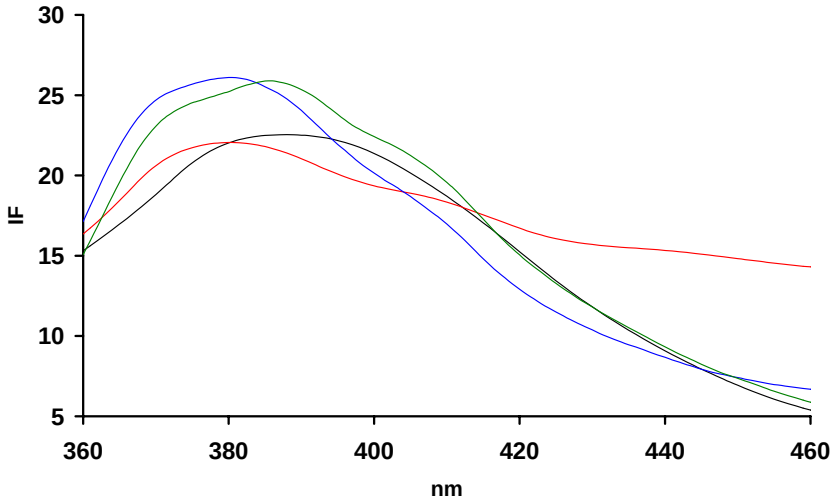

Fig. 123. Fluorescence emission of **(89)** in $CHCl_3$ 0.1M TFA (—), and upon addition of Mg^{2+} (—), Ca^{2+} (—) and Ba^{2+} (—) (λ_{exc}= 336 nm)

The addition of alkaline earth cations has a similar effect than alkaline cations addition. The emission spectrum is very similar, showing a low non-significant blue shift of the maximum for Mg^{2+} and Ca^{2+}.

SPICUM servicio de publicaciones

● Fluorescence emission at λ_{exc} = 400 nm.

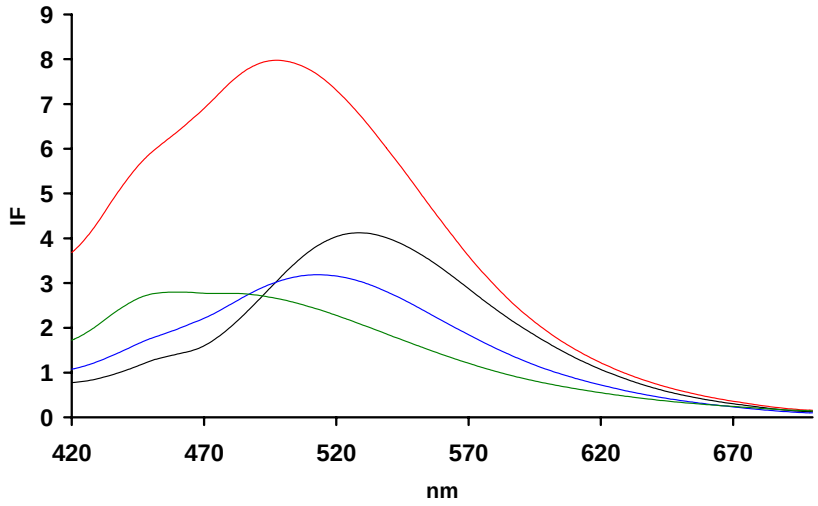

Fig. 124. Fluorescence emission of **(89)** in $CHCl_3$ 0.1M TFA (—), and in the presence of Mg^{2+} (—), Ca^{2+} (—) and Ba^{2+} (—) (λ_{exc}= 400nm)

As seen upon addition of Li^+ and Na^+ (Fig. 121), the presence of Mg^{2+} enhances the fluorescence emission. This behaviour is associated to an increase in the medium polarity. On the contrary, addition of Ca^{2+} shows a fluorescence emission reduction, more marked if the cation is Ba^{2+}. This effect is due to the inclusion of the cations in the crown ether cavity, reducing its donor ability (Fig. 125).

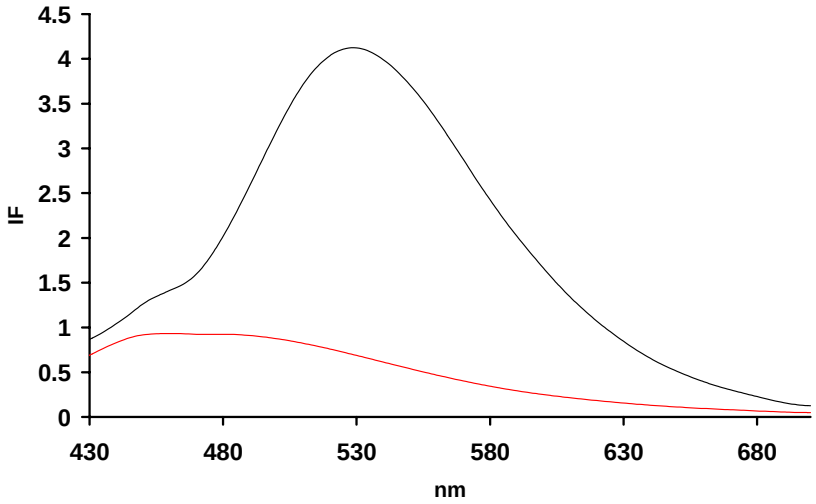

Fig. 125. Fluorescence emission of **(89)** in $CHCl_3$ 0.1M TFA (—) and upon addition of Ba^{2+} (—) (scaled)

SPICUM servicio de publicaciones

IV.2.1.2.2. Studies of (89) with Zn^{2+}

The *N*-oxide function is a weak ligand and can interact with transition metals like Zn^{2+}. The chelating ability of *N*-oxide for Zn^{2+} against crown ether, establish a preferred interaction leading to a similar effect than the H^+ addition. This behaviour can be used as the base to study the later addition of alkaline and alkaline earth effect on the system.

- Absorption spectra

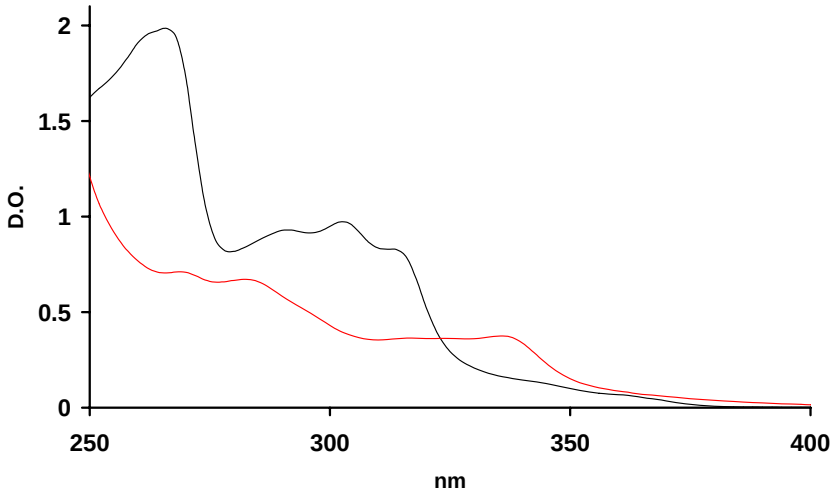

Fig. 126. Absorption spectra in $CHCl_3$ of **(89)** (—) and upon addition of Zn^{2+} (—)

The addition of Zn^{2+} has the same effect than the observed for the protonation of the *N*-oxide function, showing a hypsochromic shift of the bands (Fig. 126).

The comparison of **(89)** upon addition of Zn^{2+} and H^+ (Fig. 127) shows a very similar band pattern, demonstrating the Zn^{2+} preferred interaction for the *N*-oxide.

SPICUM servicio de publicaciones

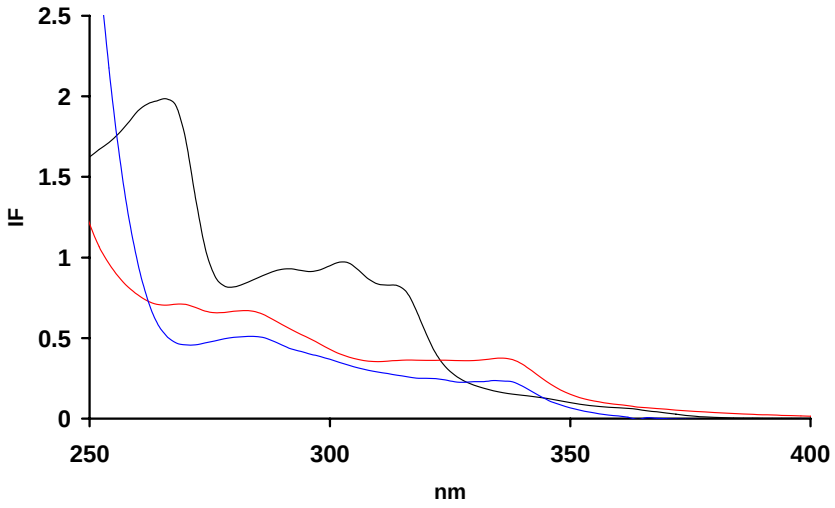

Fig. 127. Absorption spectra of **(89)** (—) and upon addition of Zn^{2+}(—) and H^{+} (—)

- Fluorescence emission

The emission spectra in the presence of Zn^{2+} present the characteristic dual channel emission bands, corresponding to the LE emission (blue-shifted at λ_{max} = 380 nm) and the CT emission state (λ_{max} = 530 nm) (Fig. 128). The best results were obtained when the Zn^{2+}: *N*-oxide relationship was 3:1. Higher Zn^{2+} concentrations interact with the crown ether moiety.

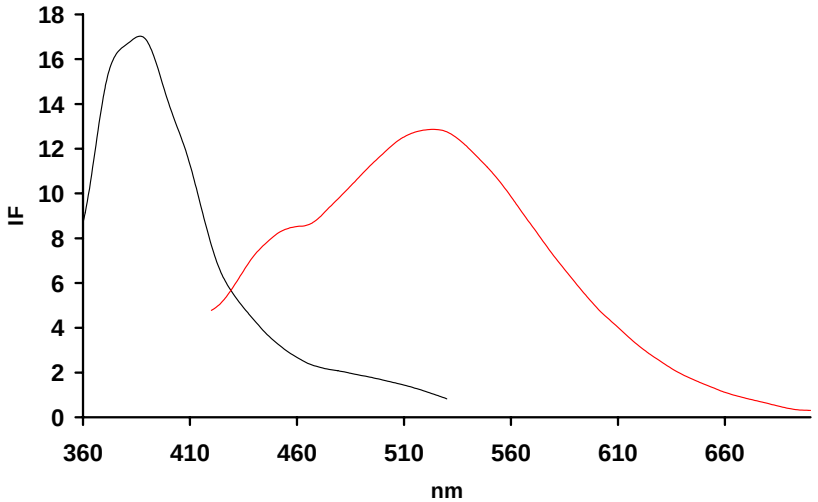

Fig. 128. Fluorescence emission of **(89)** in $CHCl_3$ upon addition of Zn^{2+}
λ_{exc} = 336 nm (—) and λ_{exc} = 400 nm (—)

SPICUM servicio de publicaciones

As seen, the Zn^{2+} addition has the same effect than the protonation of *N*-oxide. Our goal now is to observe the behaviour of the system upon addition of K^+. The presence of K^+, doesn't affect the LE emission of the isoquinoline *N*-oxide.

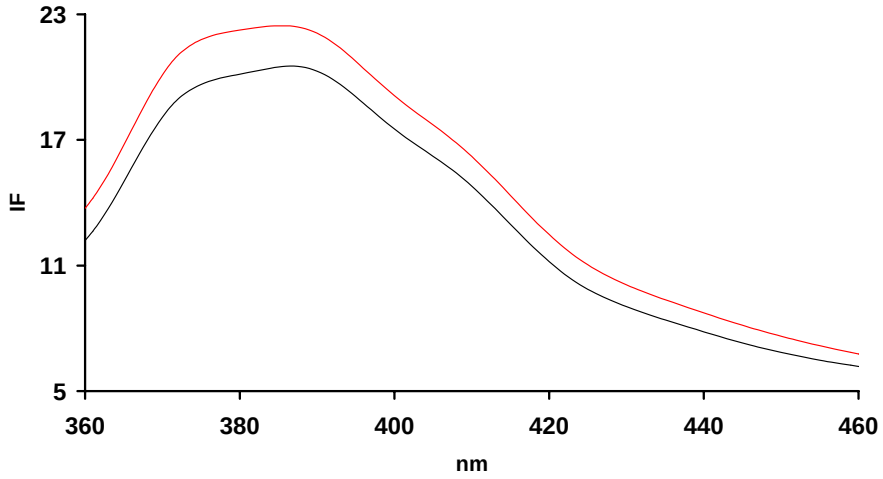

Fig. 129. Fluorescence emission of **(89)** upon addition of Zn^{2+} (—) and Zn^{2+}+K^+ (—). λ_{exc}= 336 nm

Studying the CT emission band, the addition of K^+ produce a decrease in the fluorescence intensity at λ_{em} = 550 nm because of the inclusion of K^+ in the chelating cavity of the crown ether.

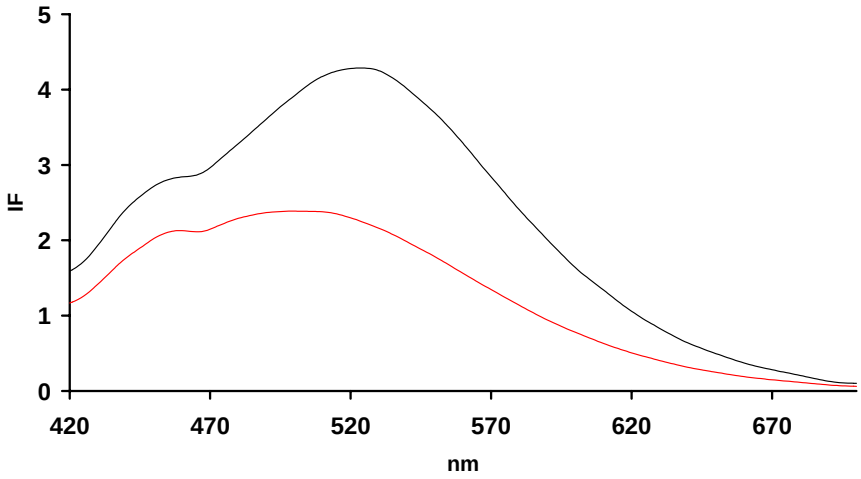

Fig. 130. Fluorescence emission of **(89)** upon addition of Zn^{2+} (—) and Zn^{2+}+ K^+ (—)

SPICUM servicio de publicaciones

IV.2.1.3. Interpretation from the Boolean logic

- Upon addition of alkaline cations

The fluorescence emission behaviour of **(89)** can be studied from the Boolean logic point of view. Like that, we can propose the binary convention shown on Fig. 131.

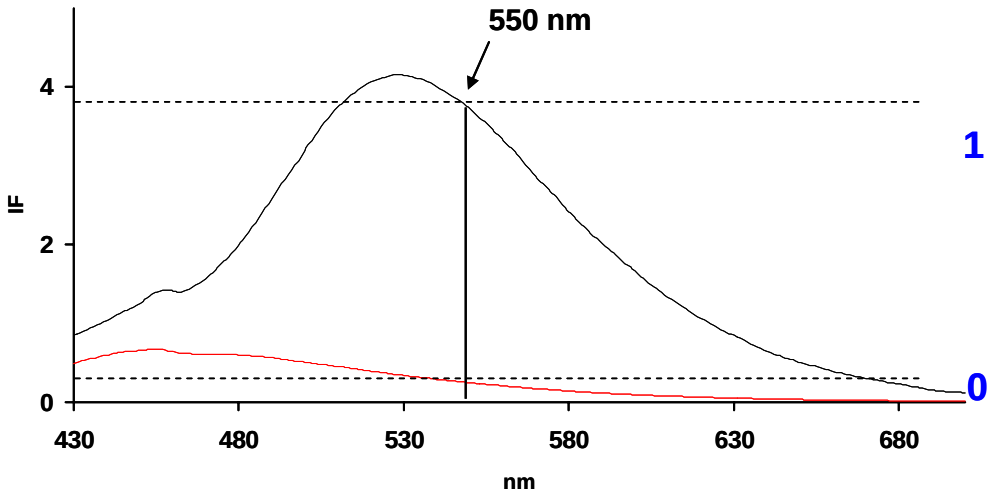

Fig. 131. Binary convention for fluorescence emission of **(89)** in $CHCl_3$ 0.1M TFA (—) and in the presence of K^+ (—) (scaled)

Considering the fluorescence emission at 550 nm like the system output, the threshold value shows the output pass from 0 to 1. It is defined at the fluorescence intensity value where the complex formed between **(89)** and K^+ doesn't emit.

The emission values below the threshold have assigned a "0". Values over this threshold have a value of "1". If two inputs, (In_1, H^+ and In_2, K^+), and one output (Out, λ_{em} = 550 nm) are considered, it is possible to define a truth table with the system operation. CT fluorescent emission at 550 nm (Output) is observed when the oxygen in the isoquinoline *N*-oxide is protonated. Upon addition of K^+, the donor ability of the benzo-crown-ether is cancelled. CT fluorescence can only be observed when protons rather than K^+ are present (Table 38). This operation is defined as an INH (Inhibit) logic gate.

SPICUM servicio de publicaciones

Table 38. Truth table of the INH logic function

In$_1$ (H^+)	**In$_2$** (K^+)	**Out** (λ_{em} = 550 nm)
0	0	0
0	1	0
1	0	1
1	1	0

The INH logic function is schematically represented on Fig. 132.

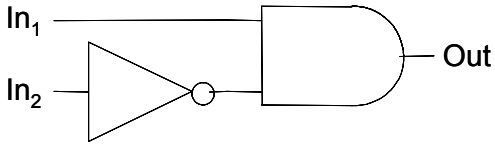

Fig. 132. INH (Inhibit) logic gate representation

- Upon addition of alkaline earth cations

Studying separately the Ba^{2+} effect, we can define a logic system, using the fluorescence emission at 550 nm as output.

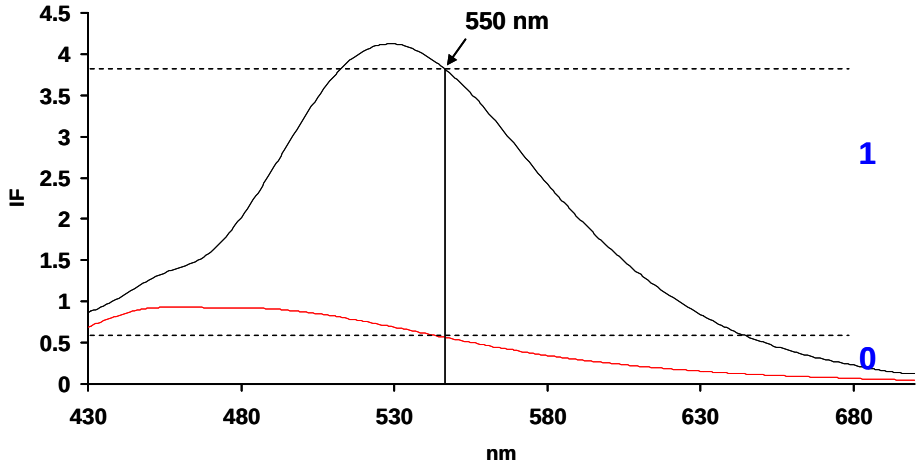

Fig. 133. Binary convention for the fluorescence emission of **(89)** in $CHCl_3$ 0.1M TFA (—) and in the presence of Ba^{2+} (—) (Scaled)

SPICUM servicio de publicaciones

Like addition of Ba^{2+} has a similar effect than addition of K^+, it is possible to design a system with three inputs (In_1, H^+; In_2, K^+; In_3, Ba^{2+}), one of them acting over the electron Acceptor (H^+), and two of them acting over the electron Donor (K^+ and Ba^{2+}), and one output (Out, λ_{em}=550 nm), presenting the truth table shown on Table 39.

Table 39. Truth table of the three inputs-one output system

In_1 (H^+)	**In_1** (K^+)	**In_1** (Ba^{2+})	**Out** (λ_{em}= 550 nm)
0	0	0	0
0	1	0	0
1	0	0	1
1	1	0	0
0	0	1	0
0	1	1	0
1	0	1	0
1	1	1	0

As both K^+ and Ba^{2+} work on the same way, the fluorescence emission is only observed when the oxygen in the isoquinoline *N*-oxide is protonated and there is not any cation in the media. Absence of H^+ or the simultaneously presence of H^+ and K^+ or Ba^{2+} inhibits this emission.

This operation can be expressed as a combination of a NOR and an AND logic gate.

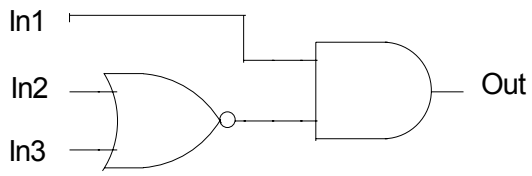

Fig. 134. Schematic representation of the system defined by Table 39

SPICUM servicio de publicaciones

- Upon addition of Zn^{2+}

The addition of Zn^{2+} has the same effect than the addition of H^+. Moreover, the hypsochromic shift shown on the LE state emission upon addition of H^+ can be used to define a new output channel studying the difference on LE between protonated and unprotonated form of isoquinoline *N*-oxide (Fig. 135).

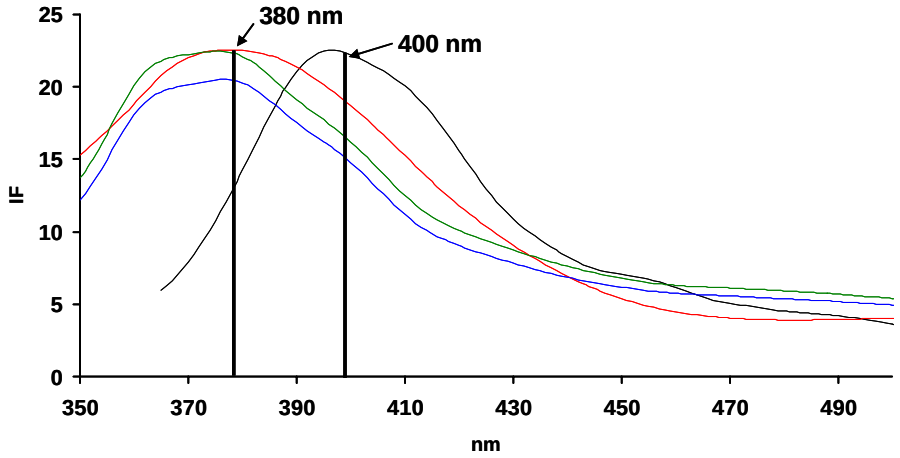

Fig. 135. Fluorescence emission of **(89)** in $CHCl_3$ (—) and upon addition of H^+ (—), Zn^{2+} (—) and Zn^{2+} + K^+ (—)

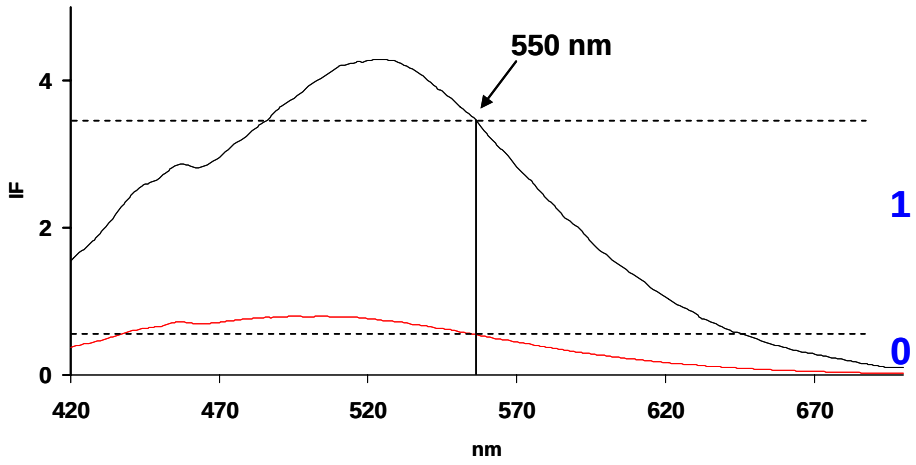

Fig. 136. Binary convention for the fluorescence emission of (89) with Zn^{2+} (—) and upon addition of K^+ (—)

Like addition of Zn^{2+} has a similar effect than addition of H^+, it is possible to design a system with three inputs (In_1, H^+; In_2, Zn^{2+}; In_3, K^+), two of them acting over the electron Acceptor (H^+ and Zn^{2+}), and one of them acting over the electron Donor (K^+), and three output (Out_1, λ_{em}= 400 nm; Out_2, λ_{em}= 380 nm; Out_3, λ_{em}= 550 nm) (Fig. 136). The truth table of this system is presented on Table 40.

SPICUM servicio de publicaciones

Table 40. Truth table of the three inputs-three outputs system

In$_1$ (H^+)	**In$_2$** (Zn^{2+})	**In$_3$** (K^+)	**Out$_1$** (λ_{em}= 400)	**Out$_1$** (λ_{em}= 380)	**Out$_1$** (λ_{em}= 550)
0	0	0	1	0	0
0	1	0	0	1	1
1	0	0	0	1	1
1	1	0	0	1	1
0	0	1	1	0	0
0	1	1	0	1	0
1	0	1	0	1	0
1	1	1	0	1	0

The emission at 400 nm is only achieved when the *N*-oxide is not combined with H^+ or Zn^{2+}, on the contrary than the emission at 380 nm. As previously seen, emission at 550 nm is achieved when the donor is not chelating K^+, in the presence of H^+ or Zn^{2+}. The operation of this system can be represented with the scheme shown on Fig. 137.

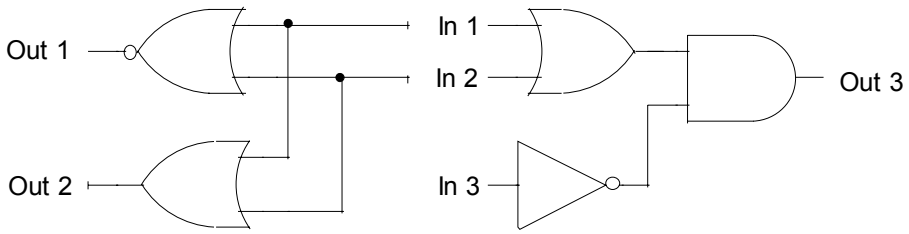

Fig. 137. Schematic representation of the system defined by Table 40

SPICUM servicio de publicaciones

IV.2.2. Toward molecular reversible logic gates

According to Landauer, every irreversible logic operation leads to minimum heat generation as the result of information loss.[153] In reversible logic, where input and output vectors are connected through a one-to-one mapping function, this is avoided. Reversible logic has its uses in quantum computing, low-power CMOS and optical and DNA computing.

By the reinterpretation of the photophysical properties of **(97)**, we demonstrate the integration of three logic gates (an XOR and two complementary INHIBIT gates) in a single molecule as a strategy toward developing molecules that can operate in a reversible logic mode by exploiting its four light-emissive electronic excited states.

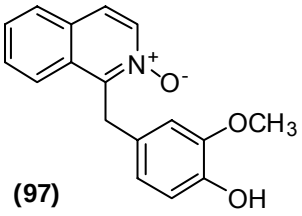

(97)

Fig. 138. Chemical structure of **(97)**

The photophysical properties of compound **(97)**, previously synthesized by our research group,[55] are not only driven by the modulation of the electron acceptor reduction capacity by protons or electrophile coordination. Basic reagents can operate over the donor moiety expressing the deprotonated phenolate form as a modulation of its oxidation capacity.

[153] Landauer, R.; *IBM J. Res. Develop.* **1961**, *5*, 183.

SPICUM servicio de publicaciones

IV.2.2.1. Photophysical properties

- Absorption spectra

The absorption spectroscopy of **(97)** has been studied in neutral, acidic (0.1M TFA) and basic media (0.1M tetrabutylammonium hydroxide, TBAH).

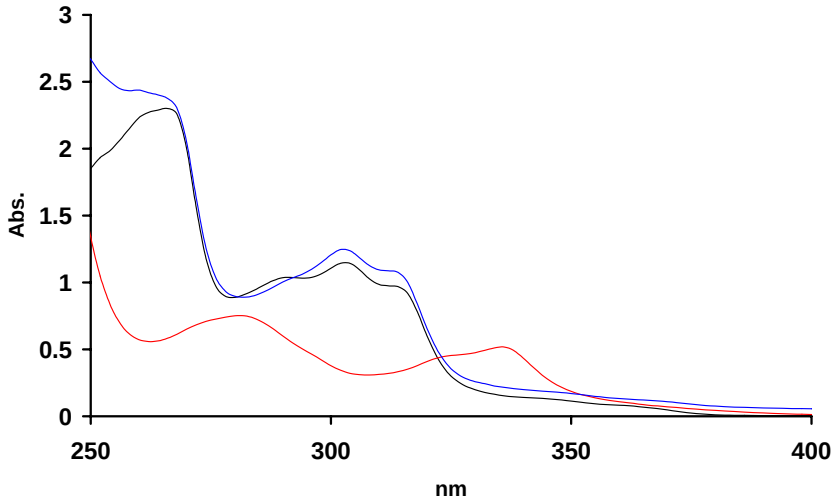

Fig. 139. Absorption spectra of **(97)** in CH_2Cl_2 (—), CH_2Cl_2 0.1M TFA (—) and CH_2Cl_2 0.1M TBAH (—)

The absorption spectra show the expected change between neutral and acidic media with the hypsochromic shift of the bands, associated to protonation of isoquinoline *N*-oxide function. However, addition of TBAH, doesn't significantly affect to the absorption spectra at wavelengths from 280 to 400 nm. This region is associated to the isoquinoline *N*-oxide chromophore and the addition of a base, acting over the phenol moiety, doesn't substantially modify its absorption spectrum.

Table 41. Molar absorption coefficient of **(97)** in neutral, acid and basic media

	(97)	**(97) (H^+)**	**(97) (HO^-)**
λ_{max} (nm)	366	336	366
ε ($M^{-1}cm^{-1}$)	$5.2 \cdot 10^2$	$2.68 \cdot 10^3$	$1.19 \cdot 10^3$

SPICUM servicio de publicaciones

- Fluorescence spectroscopy

One fluorescent-emitting channel in **(97)** corresponds to the emission of the isoquinoline *N*-oxide electron acceptor moiety. Its redox potential can be adjusted by coordinating the oxygen in the *N*-oxide to an electrophile such as the proton. Both unprotonated and protonated forms are fluorescent.

Neutral dichloromethane solutions of **(97)** exhibit an unstructured LE emission band centred at 400 nm. Addition of base remains unchanged the isoquinoline *N*-oxide electron acceptor chromophore and the LE emission is not affected, observing the 400 nm of the free isoquinoline *N*-oxide. However, in acidic medium (0.1M TFA in CH_2Cl_2), the band is replaced by a blue-shifted emission at 382 nm corresponding to the protonated form of the isoquinoline *N*-oxide upon excitation at $\lambda_{exc} \leq$ 330 nm (Fig. 140).

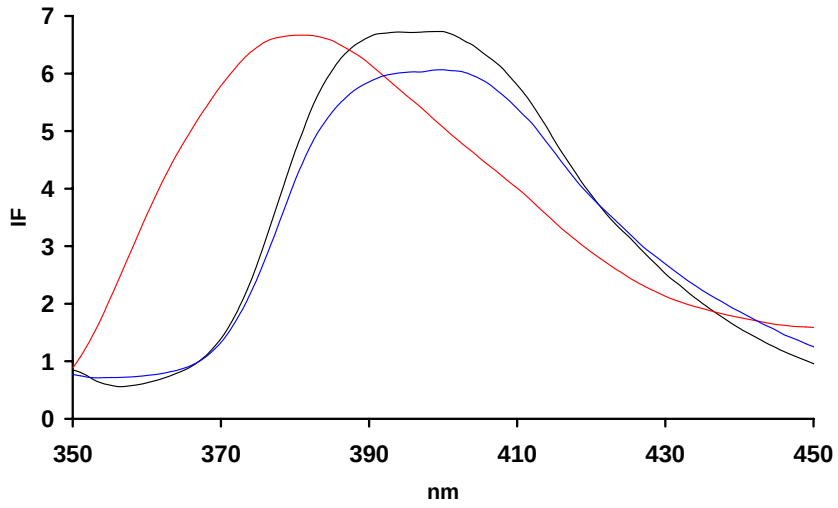

Fig. 140. Fluorescence emission of **(97)** in CH_2Cl_2 (—), CH_2Cl_2 0.1M TFA (—) and CH_2Cl_2 0.1M TBAH (—) $\lambda_{exc} \leq 330$ nm

The second fluorescence-emitting channel runs when the CT state is reached. The protonated form of the isoquinoline *N*-oxide can undergo PET from the electron-rich dioxygen-substituted aryl donor. The CT state generated by the electron transfer from the ground state donor moiety to the first excited singlet state of the protonated isoquinoline *N*-oxide (CT_{H+}) is light-emissive, so a fluorescent band at 490 nm appears upon excitation at $\lambda_{exc} > 360$ nm.

SPICUM servicio de publicaciones

In a basic medium (upon addition of 0.1M TBAH), the isoquinoline *N*-oxide electron acceptor chromophore remains unchanged and the LE emission is not affected (Fig. 140).

The possibility of reaching the CT state is determined by the Gibbs free energy change. The Rehm-Weller relationship ($\Delta G_{ET} = e[E_{ox}(D)-E_{red}(A)] - E_{00}$) determines the feasibility (driving force) of a PET process.[154]

The isoquinoline *N*-oxide moiety is a "poor" electron acceptor which ability is enhanced *via* protonation (addition of 0.1M TFA), decreasing its reduction potential and becoming a better electron acceptor. The proton enables the CT_{H+} emissive state. The increase of the net value of $E_{red}(A)$ favours the implementation of ΔG_{ET}.

ΔG_{ET} can also be implemented by lowering the value of $E_{ox}(D)$. Addition of 0.1M TBAH in dichloromethane, produces a similar red-shifted fluorescence emission at 491 nm upon excitation at λ_{exc} > 360 nm, assigned to a new fluorescent emissive CT_{HO-} state (Fig. 141).

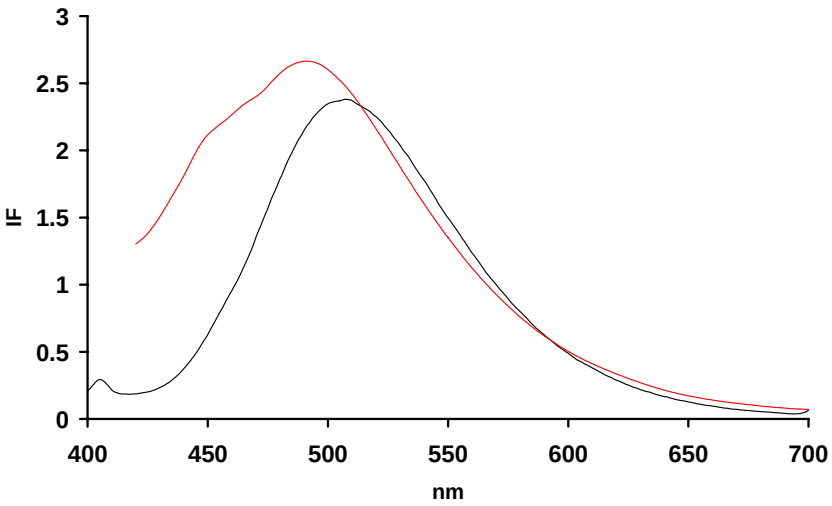

Fig. 141. Fluorescence emission of **(97)** in CH_2Cl_2 0.1M TFA (—) and CH_2Cl_2 0.1M TBAH (—) (λ_{exc} > 360 nm)

[154] Rehm, D.; Weller, A.; *Isr. J. Chem.* **1970**, *8*, 259.

SPICUM servicio de publicaciones

Table 42. Fluorescence quantum yields of **(97)**

NEUTRAL (97)		ACID (97) (H^+)		BASIC (97) (HO^-)	
λ_{em} (nm) (λ_{exc} = 312nm)	400	λ_{em} (nm) (λ_{exc} = 330nm)	380	λ_{em} (nm) (λ_{exc} = 312nm)	400
ϕ	$3 \cdot 10^{-3}$	ϕ	$3 \cdot 10^{-3}$	ϕ	$2 \cdot 10^{-3}$
-	-	λ_{em} (nm) (λ_{exc} = 400nm)	500	λ_{em} (nm) (λ_{exc} = 400nm)	490
-	-	ϕ	$1.7 \cdot 10^{-2}$	ϕ	$3 \cdot 10^{-3}$

IV.2.2.2. Electrochemistry

A comprehensive electrochemical study in neutral, acidic and basic media was carried out in order to gaining insight into the CT capabilities of the fluorescence-emitting states.

In neutral media, **(97)** exhibits one irreversible reduction at -1.46 V associated with the generation of the radical anion in the electron-acceptor *N*-oxide moiety, and one oxidation at +0.98 V, due to the generation of the radical cation in the electron-rich methoxy-phenol group (Fig. 142b).

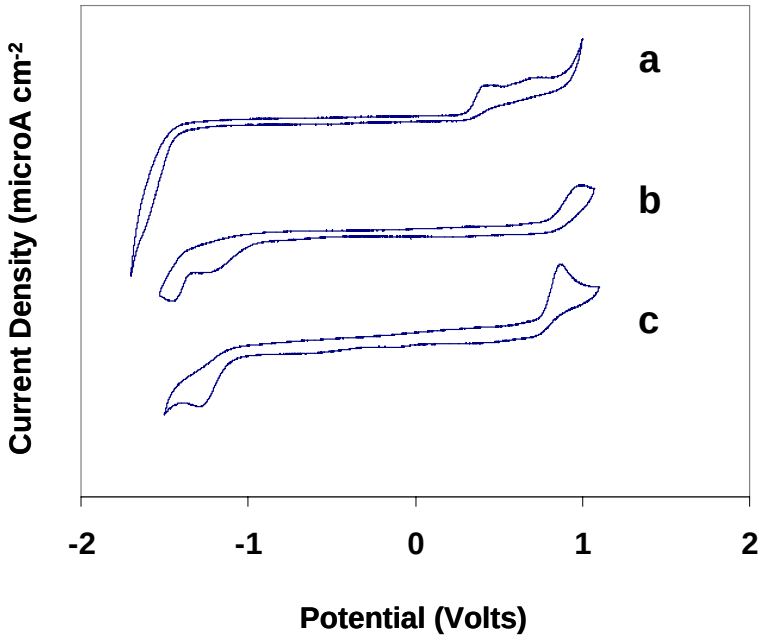

Fig. 142. Cyclic voltammetry of **(32)** in neutral **(b)**, 0.1M TBAH **(a)** and 0.1M TFA **(c)** media

SPICUM servicio de publicaciones

Upon addition of TFA, the reduction of the protonated form of the isoquinoline *N*-oxide electron acceptor is stabilized by 0.19 V. As a result, the Weller analysis (E_{ox}(D) = 0.98V, $E_{red}(A^+)$ = -1.27 V; E_{00} = 75.04 kcal·mol^{-1}) of the ET from the ground state of the phenolic form of the D to the first excited singlet state of the A^+ shows that the process is now favored by a reduction of 7.94 kcal·mol^{-1} compared to the same electron transfer for unprotonated *N*-oxide (Fig. 142c).

The presence of a base shifts the reduction of the *N*-oxide group to higher energy levels and significantly stabilizes (by 0.57 V) the oxidation of the methoxy-phenolate donor group. The deprotonated form of the phenolic donor is easier to oxidize and, although the free form of the isoquinoline *N*-oxide is more difficult to reduce than is its corresponding protonated form, the increased ability of the phenolate moiety to release one electron results in a favourable balance.

Weller analysis ($E_{ox}(D^-)$ = 0.41V, E_{red}(A) = -1.46V; E_{00} = 71.48 kcal·mol^{-1}) for this electron transfer process shows a more favourable process with a reduction of 13.14 kcal·mol^{-1} relative to the neutral form of the molecule. This behaviour is fully consistent with the presence of a negatively charged donor to neutral electron acceptor CT state and with the fluorescence data (Fig. 142a).

IV.2.2.3. Interpretation from the Boolean logic

The interaction of **(97)** with H^+ or HO^- produces four different fluorescent-emitting excited states. These states can be reached in an independent, nonannihilating way upon excitation at different wavelengths. Excitation at $\lambda_{exc} \leq 330$ nm runs the LE channel while excitation at $\lambda_{exc} \geq 360$ nm runs the CT channel.
The study of LE channel shows that, considering H^+ as In_1 and HO^- as In_2, the system can operate as an INHIBIT logic gate (Fig. 143).

SPICUM servicio de publicaciones

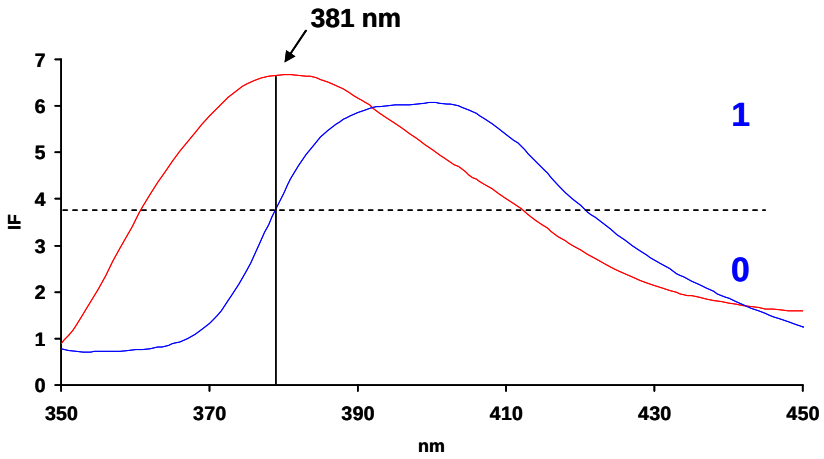

Fig. 143. Detail of fluorescence emission at λ_{em} = 500 nm of **(97)** in CH_2Cl_2 0.1M TFA (—) and CH_2Cl_2 0.1M TBAH (—)

The complementarity associated to the two signals has basically the same logic implications. Since both inputs in equimolar amounts leads to neutral solutions and emission at 381 nm (LE_{H+}) can only be reached in acidic media, the absence or simultaneously presence of both inputs (In_1=In_2 = 0; In_1=In_2 = 1) or the presence of TBAH expresses the unprotonated form of the isoquinoline *N*-oxide chromophore which emission (LE) is not observed at 381 nm. This behaviour is defined as an INHIBIT system (Fig. 144, Table 43).

Table 43. Truth table of INH logic gate studying emission at 381 nm

In_1 (H^+)	**In_2** (HO^-)	**Out** (λ_{em} = 381 nm)
0	0	0
0	1	0
1	0	1
1	1	0

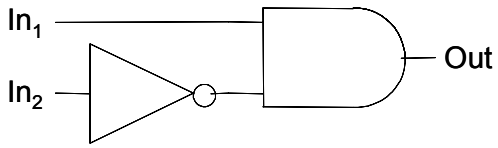

Fig. 144. INH schematic representation

SPICUM servicio de publicaciones

We can analyze CT_{H+} or CT_{OH}-, monitoring the fluorescence emission of **(97)** at 500 nm (Fig. 145). If we consider TFA as In_1 and TBAH as In_2, the absence (In_1 = 0; In_2 = 0) or simultaneous presence (In_1 = 1; In_2 = 1) of equimolecular amounts of both inputs leads to neutral solutions of **(97)** without possibility to reach CT state.

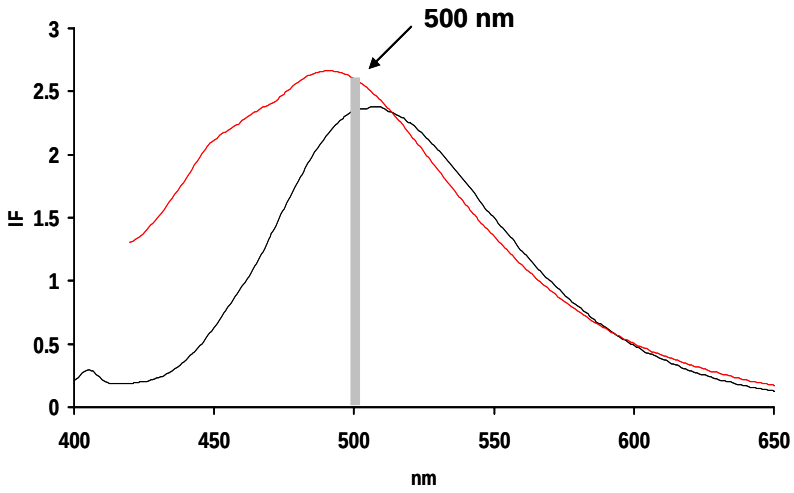

Fig. 145. Detail of fluorescence emission at λ_{em} = 500 nm of **(97)** in CH_2Cl_2 0.1M TFA (—) and CH_2Cl_2 0.1M TBAH (—)

However, the alternative presence of only one of the chemical inputs, TFA (In_1 = 1; In_2 = 0) or TBAH (In_1 = 0; In_2 = 1) affords the CT state. This behaviour can be defined as a XOR logic gate (Fig. 146), which truth table is shown on Table 44.

Table 44. Truth table of XOR logic gate studying emission at λ_{em} = 500 nm

In_1 (H^+)	**In_2** (HO^-)	**Out** (λ_{em} = 500 nm)
0	0	0
0	1	1
1	0	1
1	1	0

SPICUM servicio de publicaciones

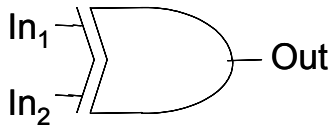

Fig. 146. XOR schematic representation

The consideration of both CT_{H+} and CT_{HO-} states are similar but not equivalent, increases the capabilities of **(97)** as a molecular logic gate. Both states are fluorescent on the same region (on 500 nm) but the emission corresponds in fact to radiative deactivation from two different excited states. Consequently, the outputs are circumstantially analogous, but intrinsically distinguishable (Fig. 147).

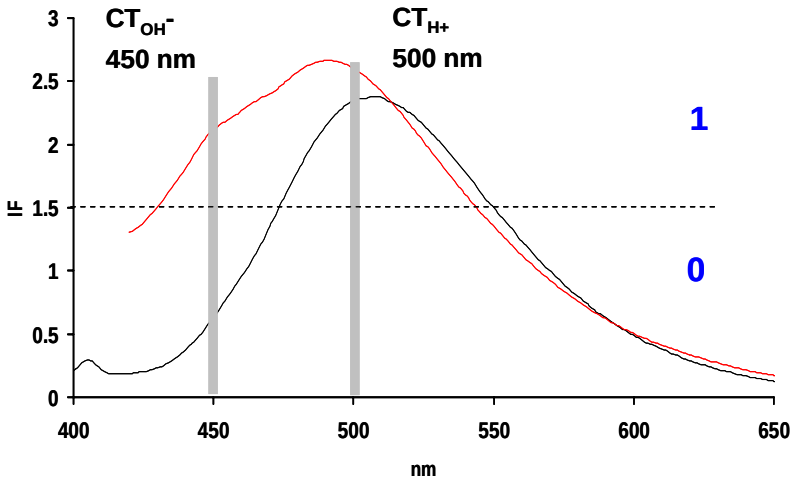

Fig. 147. Detail of fluorescence emission at λ_{em} = 500 nm of **(97)** in CH_2Cl_2 0.1M TFA (—) and CH_2Cl_2 0.1M TBAH (—)

Careful analysis of the CT fluorescence emission reveals that their maxima are 6 nm apart. This slight energy difference reflects the similarity of both CT states but is large enough to reflect that they are different electronic states.

By monitoring the CT fluorescence at 500 nm, there was defined a XOR logic gate. Nevertheless, by monitoring the fluorescence emission at 450 nm, we can discriminate the logical degeneracy of the two exclusive states, being distinguishable as only fluorescence emission will be observed in basic medium (TBAH) at this wavelength.

Using H^+ and HO^- as inputs and considering the requirements of a device to work in a reversible way, the 01 and 10 logical input states are operated by the XOR gate to get the same Output value (Out = 1) when monitoring the fluorescence emission at 500

SPICUM servicio de publicaciones

nm. With this output result, the reverse way cannot identify the originating input state. However, the 01 and 10 logical input states produce 1 and 0, respectively, as output if the fluorescence emission at 450 nm is monitored. These results indicate that it's possible to obtain two distinghishable outputs 11 and 10 states by monitoring the CT channel fluorescence emission of the 01 and 10 input states at 450 and 500 nm simultaneously (Table 45).

Table 45. Truth table of the system studying the emission at 500 and 450 nm

In$_1$ (H^+)	**In$_2$** (HO^-)	**Out$_1$** (λ_{em} 500 nm)	**Out$_2$** (λ_{em} 450 nm)	
0	0	0	0	
0	1	1	1	**1_1**
1	0	1	0	**1_0**
1	1	0	0	

The result of this combination is the suppression of the logical degeneracy of the CT fluorescent state by judiciously exploiting the different physical states they come. It's correct to state that the CT fluorescent state becomes logically reversible, but not the entire system, because 00 and 11 initial states result in 00 output.

This system is defined as a Half-Subtractor molecular logic gate (Fig. 148).

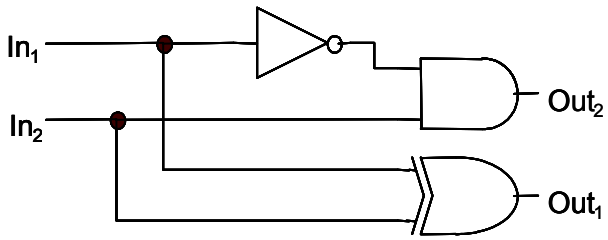

Fig. 148. Half-Subtractor schematic representation

There are two closely related types of reversibility: physical reversibility and logical reversibility. A physically reversible process is isentropic, that is, it results in keeping its physical entropy. A logically reversible process takes place with no loss of information. The connection between physical reversibility and logical reversibility is defined by the Landauer's principle: for a computational process to be physically reversible, it must also be logically reversible.[153]

SPICUM servicio de publicaciones

The studies carried out on the CT fluorescence emitting channel, open the possibility to develop reversible molecular logic gates owing to the fact that the number of possible logical states that run CT fluorescence (01 and 10) coincides with that CT_{HO^-} and CT_{H^+} physical states. This way, the total number of possible physical states is no smaller than the original number, the total entropy is not decreased and two distinguishable outputs 11 (1_1) and 10 (1_0), respectively, can be obtained.

The identification of the initial state of the system (inputs) studying the outputs keeps the information and permits to identify the initial states of the system, whenever the CT emission is active, providing a good approach to get a totally reversible system.

SPICUM servicio de publicaciones

IV.2.3. Design of advanced molecular switches

One interesting goal in the molecular devices research is the design of molecular structures that operates like microelectronic circuits, specially implementing molecules with decision-making capabilities.

The dual-channel fluorescence emission of the modified benzyl-isoquinoline *N*-oxide compounds synthesized in our laboratory allow us to design devices which behaviour can be used in order to simulate the electronic devices used in the control of bit data flow.

In digital signal processing, a multiplexer (MUX) takes several separate digital data streams and combines them into a single stream of a higher data rate. A complementary demultiplexer (DEMUX) is normally required at the receiving end of the data link. The practical applications of DEMUX are a key factor in the transmission data at a distance, since it steers an input to one of many possible outputs (Fig. 149).

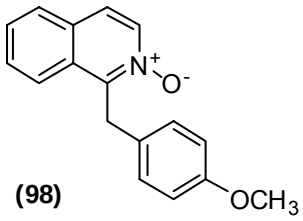

(98)

Fig. 149. Chemical structure of DEMUX

Reinterpretation of the photophysical properties of **(98)** have lead us to develop a molecular 1 : 2 demultiplexer studying the changes in the fluorescence emission between unprotonated and protonated form of isoquinoline *N*-oxide moiety where the sole presence of protons as input, can address the fluorescence response by switching the coding excitation wavelength in order to report the binary state of the input.

SPICUM servicio de publicaciones

IV.2.3.1. Photophysical properties

- Absorption spectra

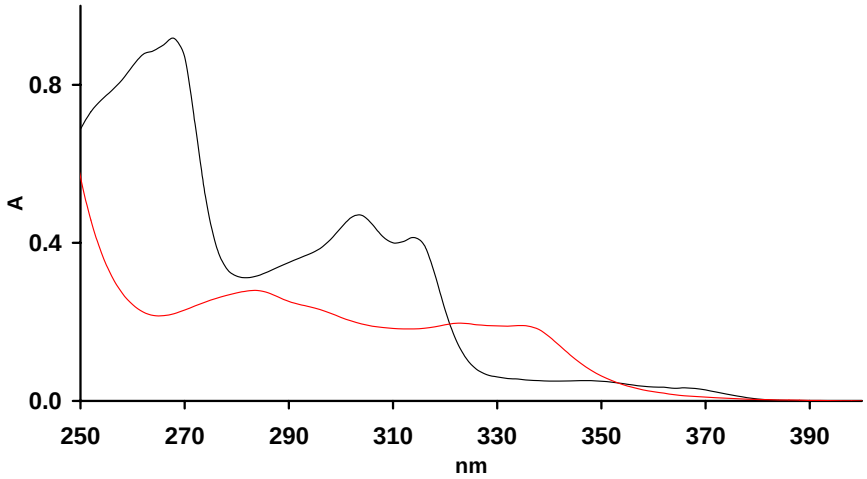

Fig. 150. Absorption spectra of **(98)** in CH_2Cl_2 (—) and CH_2Cl_2 0.1M TFA (—)

The absorption spectra in neutral and acidic media (Fig. 150) show the known behaviour of 1-benzyl-isoquinoline *N*-oxide where the addition of TFA produces a general hypsochromic shift of the absorption spectrum.[54]

Table 46. Molar absorption coefficient of **(98)** in neutral and acid media

	(98)	**(98)** (H^+)
λ_{max} (nm)	366	336
ε ($M^{-1}cm^{-1}$)	$0.95 \cdot 10^3$	$4.65 \cdot 10^3$

SPICUM servicio de publicaciones

- Fluorescence emission

In neutral media, the fluorescence emission of **(98)** is defined by a unique band corresponding to the LE state emission of isoquinoline *N*-oxide moiety at λ_{em} = 400 nm (Fig. 151).

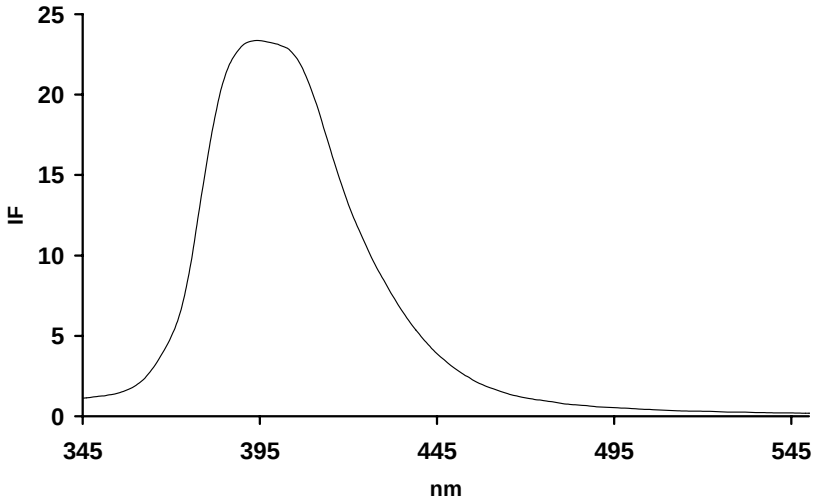

Fig. 151. Fluorescence emission of **(98)** in CH_2Cl_2 (λ_{exc} = 330 nm)

In acidic media, protonation of *N*-oxide produces an excitation wavelength-dependent dual-channel fluorescence composed by emission from the blue-shifted LE_{H+} (λ_{em} = 480 nm) excited state, exciting at λ_{exc}< 340 nm and the CT excited state emission (λ_{em} = 479 nm), reached upon a PET process from the electron Donor to the electron Acceptor exciting at λ_{exc} ≥ 360 nm (Fig. 152).

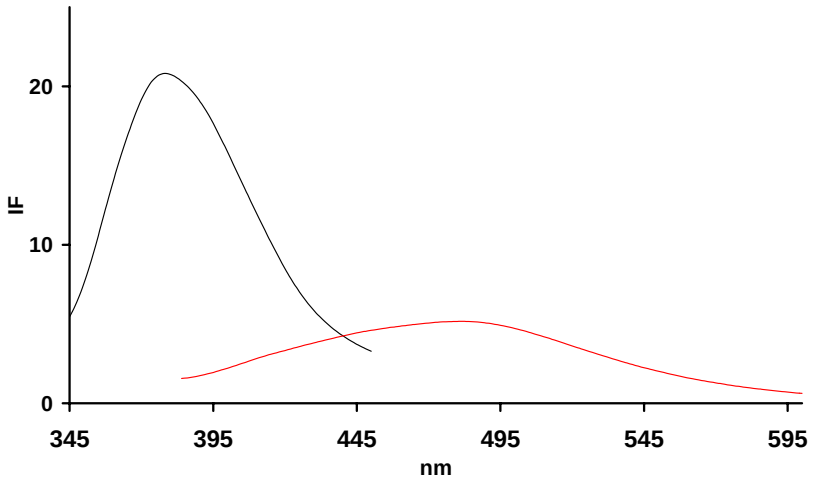

Fig. 152. Fluorescence emission of **(98)** in CH_2Cl_2 0.1M TFA.
λ_{exc} = 330 nm (—) and λ_{exc} = 360 nm (—)

SPICUM servicio de publicaciones

The fluorescence quantum yields are shown on the Table 47.

Table 47. Fluorescence quantum yields of **(98)** in neutral and acid media

NEUTRAL	
	(98)
λ_{em} (nm) (λ_{exc} = 330nm)	394
ϕ	$8 \cdot 10^{-3}$
ACID (0.1M TFA)	
	(98) (H^+)
λ_{em} (nm) (λ_{exc} = 330nm)	380
ϕ	$1 \cdot 10^{-3}$
λ_{em} (nm) (λ_{exc} = 400nm)	479
ϕ	$2 \cdot 10^{-2}$

IV.2.3.2. Interpretation from the Boolean logic

The Boolean algebraic expression for a one input-two output DEMUX switch is *In#c(Out₁, Out₂)*, the # symbol denoting a demultiplexer function. This expression means that, if *c* = 0, the first argument (Out_1) has the same value than *In* and the second argument (Out_2) is disabled. Conversely, if c = 1, then Out_2 is equal to *In* and Out_1 is disabled. *In* is the input variable and *c* is the control data variable. In brackets are represented the output variables of the two output demultiplexer (Out_1 and Out_2).
Two aspects of the chemical properties of **(98)** have been taking into account in order to the design of DEMUX switch: the tunable ability of the isoquinoline *N*-oxide moiety as an electron acceptor and the resulting fluorescent profile.

This way, the two emissive fluorescent channels for **(98)-H$^+$** can be operated independently by carefully selecting the excitation wavelength. It should be noted that the two fluorescent channels (LE_{H+} and CT) can be operated in an independent, no annihilating manner by taking the proton as a single input.

SPICUM servicio de publicaciones

Thus, the LE emission of the protonated isoquinoline *N*-oxide is blue-shifted to 380 nm at λ_{exc} = 330 nm and is completely displaced by a new CT band beyond 400 nm at λ_{exc} > 360 nm. The CT detectability is further increased by its significant Stokes shift, which tends to displace it to a region not overlapped by the residual LE emission from the electron acceptor.

The performance of compound **(98)** as a molecular digital demultiplexer (DEMUX) was assessed by using various combinations of protons and excitation light. Compound **(98)** can be excited to selectively reach LE_{H+} or CT fluorescent excited state and, because all its excited states are fluorescent, the molecule can communicate a selective response for these combinations.

The design of DEMUX is based on the use of H^+ as input and the different excitation wavelengths (λ_{exc} < 330 nm and λ_{exc} > 360 nm) as control digit "*c*". The outputs studied are the fluorescence emission at 380 and 479 nm.

The truth table generated with these considerations is shown on Table 48.

Table 48. Truth table of molecular DEMUX

In (H^+)	***c*** (λ_{exc})	**Out_1** (λ_{em} 380 nm)	**Out_2** (λ_{em} 479 nm)
0	λ_{exc} < 330 nm (*c* = 0)	0	0
1	λ_{exc} < 330 nm (*c* = 0)	1	0
0	λ_{exc} ≥ 360 nm (*c* = 1)	0	0
1	λ_{exc} ≥ 360 nm (*c* = 1)	0	1

The Table 48 shows that when control *c* was applied in the "off" mode (*c* = 0, λ_{exc} < 330 nm), the corresponding fluorescent emission of LE_{H+} at 380 nm was observed as a consequence of proton interaction. Owing to the fact that CT state cannot operate at *c* = 0, no signal was detected at 479 nm, remaining Out_2 = 0. When control *c* is in the "on" mode, (*c* = 1, λ_{exc} ≥ 360 nm), the LE_{H+} emission is not detected, observing the CT fluorescence emission at 479 nm.

SPICUM servicio de publicaciones

For an observer (or receptor), working at 380 nm (Out_1), the signal may be "on" only when the arriving proton coordinates the oxygen of the isoquinoline *N*-oxide and the control *c* is in the "off" state driving the signal *via* this fluorescent channel (Output is equal to input). However, only when *c* is in the "on" state, the signal is driven to the CT fluorescence channel at 479 nm.

The contour view analysis of the fluorescence emission with and without presence of acid, clearly show how the signal is addressed to one or another channel depending on the excitation wavelength.

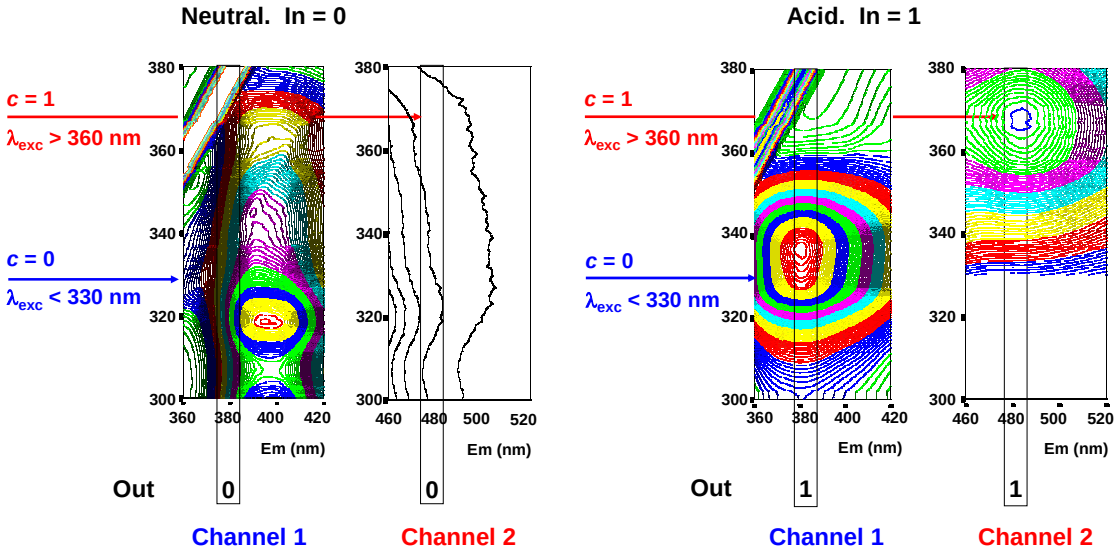

Fig. 153. Contour view graphics of the fluorescente emission of **(98)**

With these considerations, **(98)** meets the requirements of a 1 : 2 DEMUX where the input (H^+) can be photonically addressed to either Out_1 or Out_2 depending on the control *c* state. This behaviour is clearly shown in the Fig. 154 where is explained the job carried out by the control *c* to address the input signal.

SPICUM servicio de publicaciones

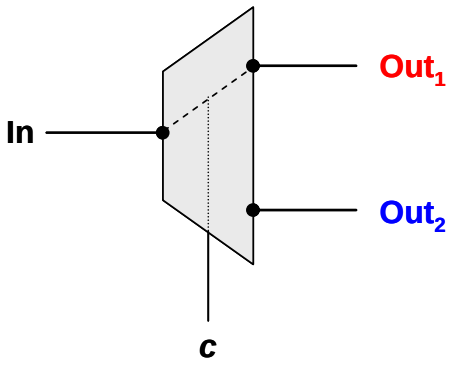

Fig. 154. DEMUX symbol

The schematical circuit representation is shown on Fig. 155.

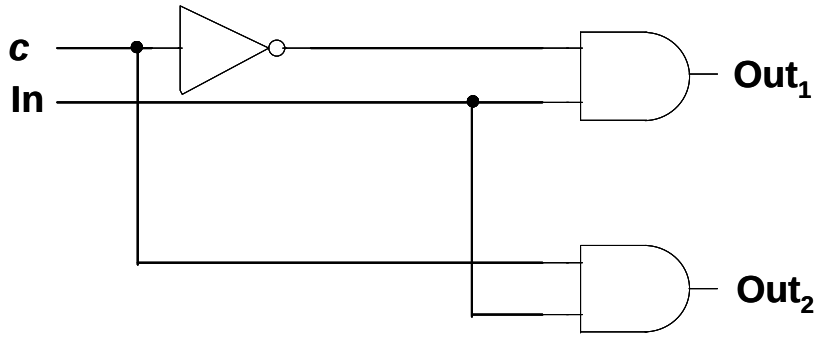

Fig. 155. DEMUX schematical representation

SPICUM servicio de publicaciones

CHAPTER V.

CONCLUSIONS

SPICUM
servicio de publicaciones

SPICUM
servicio de publicaciones

Conclusions

1. The photohydroxilation process of assembled systems comprising isoquinoline *N*-oxide bridged by alkyl chains to electron donor substituted aryls, forming an electron Acceptor-Spacer-Donor system, occurs to higher distances than two $\sigma_{C\text{-}C}$ bonds.

When the spacer is an ethylene, compound **33**, the hydroxyl radical insertion takes place in the alkyl chain. Under acidic reaction conditions the highly conjugated styrene derivative, *via* H_2O elimination, is the mainly isolated product.

When the spacer is a propylene chain, compound **34**, the hydroxylation takes place in the aryl electron donor ring and the two possible hydroxylation products, the methoxy *orto-* and *meta-* substituted are obtained.

2. The photohydroxilation process is also given in systems where the alkyl Acceptor-Donor connection is substituted by other functional groups as bridged units. This change allow us to define a “plug-unplug” system where, by the judicious selection of the corresponding functional group, like an amide group, the system can be integrated in a cyclic process. The sequence of: a) Connection of the electron Acceptor and Donor moieties; b) The Acceptor *N*-oxidation; c) Photolysis in acidic conditions; d) Disconnection to obtain the hydroxylated Donor moiety and the Acceptor returning to produce a new hydroxylation process; resembles biological behaviour.

SPICUM servicio de publicaciones

3. The study of the dual-channel fluorescence emission (LE and CT) of the electron A-S-D systems synthesized shows a significant behaviour:

a) The CT emission is observed even when the spacer length is increased, showing that this change is not a critical factor for its activation/deactivation.

b) The CT emission is highly dependent of the electron Donor reduction potential. The modulation of the electron Donor properties can be done in two different ways:

- An irreversible model *via* changes in the benzene ring substitution.
- A reversible model *via* interaction with chemical species present in the media: acids and bases (protonation/deprotonation) or metallic cations (complexation/ decomplexation).

4. By means of the judicious selection of the functional groups modulating the electron Donor ability of the substituted benzene ring, it is possible to control the on/off switching of the LE and CT fluorescence emission channels.

The interpretation of the interaction between the chemical species present in the media, called inputs, and its different LE and CT fluorescent response, called outputs, lead us to a careful Boolean logic analysis and interpretation:

a) By the interpretation of the photophysical properties **89** we can define an INH logic gate and two different complex logic systems.

b) By the photophysical interpretations of **97** behaviour, an INH, a XOR and a Half-Subtractor is defined, in order of the search toward a reversible logic system.

c) The photophysical interpretation of **98** behaviour leads us to develop a demultiplexer (DEMUX) switch.

SPICUM servicio de publicaciones

CHAPTER VI.

EXPERIMENTAL SECTION

SPICUM
servicio de publicaciones

SPICUM
servicio de publicaciones

VI.1. EXPERIMENTAL

VI.1.1. General considerations

The reagents and solvents were used without further purification. When dry solvents were needed, water was removed following the literature procedure.[155] The metallic salts used for the photophysical study of **(89)** were:

Salt	Purity
$LiClO_4$ anhydrous	98%
$NaClO_4$ anhydrous	99%
$KClO_4$ anhydrous	99%
$Mg(ClO_4)_2$ anhydrous	98%
$Ca(ClO_4)_2 \cdot 4\ H_2O$	-
$Ba(ClO_4)$ anhydrous	98%
$ZnCl_2$	98%

[155] Armarego, W.L.F.; Chai, C.L.L. *Purification of Laboratory Chemicals 5th Ed.*, Ed. Elsevier Butterworth-Heinemann, Oxford, **2003**.

SPICUM servicio de publicaciones

VI.1.2. General technics

Thin layer chromatography (TLC) was made using silica gel plates (SDS, 60 F_{254}) and alumina plates (Merck, 60 F_{254}). They were revealed using UV light (254 nm) or chemical revealing agents as potassium permanganate.

Purification *via* column chromatography was carried out with silica gel (Merck, silicagel 60, 0.040-0.063 mm, 230-400 mesh) for flash chromatography, silica gel (Merck, silicagel 60, 0.063-0.200 mm, 70-230 mesh) for gravity columns and alumina (SDS, 0.05-0.2 mm). The solvent employed is shown in each case.

- Nuclear Magnetic Resonance

^{1}H-NMR and ^{13}C-NMR were performed in a Bruker WP-200 SY at 200 MHz for ^{1}H and 50.3 MHz for ^{13}C or in a Bruker Biospin Avance III 400 at 400 MHz for ^{1}H and 100.6 MHz for ^{13}C. The chemical shifts are described in parts per million (δ, ppm). In ^{1}H-NMR are referred to the residual deuterated solvent signal in each case: residual $CHCl_3$ (7.24 ppm) in deuterated chloroform, CH_3OH residual (pentlet, 3.31 ppm) in deuterated methanol. The coupling constant value (*J*) is expressed in Hertzs (Hz). The chemical shifts on ^{13}C-NMR are referred to $CHCl_3$ (77.0 ppm), to methanol (49.0 ppm) or to dimethyl sulfoxide (39.4 ppm). The multiplicity of the signals is expressed with the following abbreviations: (s) singlet, (bs) broad singlet, (d) doublet, (t) triplet, (q) quartet, (qu) quintet, (dd) double doublet, (dt) double triplet, (m) multiplet.

- Mass spectrometry

Mass spectra were performed in a mass spectrometer with electronic impact ionization (70 eV) Thermo Scientific DSQ II Single Quadrupole GC/MS with Focus GC. The spectra are described in mass/charge (*m/z*) relationship, indicated relative intensities in brackets respect to the base peak, considered to 100%.

- High Resolution Mass Spectrometry

The HRMS (FAB) were carried out in a VG Autospec spectrometer in the C.A.C.T.I. of the University of Vigo.

SPICUM servicio de publicaciones

- Melting points

Melting points were determined in a Gallenkamp apparatus and are uncorrected.

- Electronic absorption

UV-VIS spectra were registered in a Hewlett Packard 8452A Diode Array spectrophotometer. Samples for absorption spectra were prepared in spectroscopic grade solvents and adjusted to a linear range response. Molar absorption coefficients were determined using concentrations of 10^{-4} or 10^{-5} M.

- Fluorescence measurements

The fluorescence emission spectra were recorded in a Jasco FP-750 spectrofluorometer. Samples for emission spectra were prepared in spectroscopic grade solvents and adjusted to a linear range response. No fluorescent contaminants were detected in the wavelength region of experimental interest upon excitation.
Fluorescence quantum yields were determined *via* comparison with quinine sulphate fluorescence in H_2SO_4 1N, using the next formula:

$$\Phi_F = \frac{S}{S_S} \cdot \frac{DO_S}{DO} \cdot \frac{n^2}{n_s^{\,2}} \cdot \Phi_{F_S}$$

Where:
S = fluorescence spectrum area of the target compound.
S_S = fluorescence spectrum area of the reference compound.
DO = optical density of the target compound solution at λ_{exc}.
DO_S = optical density of the reference compound solution at λ_{exc}.
n = refractive index of the solvent used for our target compound at 350 nm.
n_S = refractive index of H_2SO_4 1N at 350 nm.
Φ_{Fs} = quantum yield of quinine sulphate in H_2SO_4 1N (Φ_{Fs} = 0.55).

SPICUM servicio de publicaciones

VI.1.3. Synthesis of alkyl-bridged benzyl isoquinoline *N*-oxides

VI.1.3.1. Synthesis of 1-(4-methoxyphenethyl isoquinoline)-*N*-oxide (33)

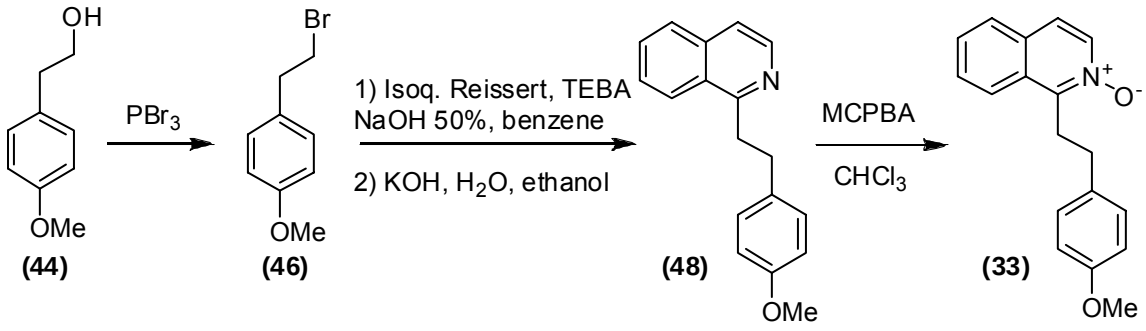

-Synthesis of 1-(2-bromoethyl)-4-methoxybenzene (46)

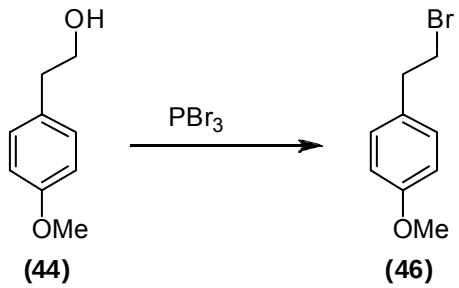

In a 25 mL round bottom flask, was placed 2-(4-methoxyphenyl)-ethyl alcohol (152 mg, 1.00 mmol) and cooled in an ice bath.

Then, PBr_3 (0.05 mL, 0.50 mmol) was added dropwise and the mixture was stirred at room temperature overnight. Then, CH_2Cl_2 was added and the organic layer was washed with 5% w/w $NaHCO_3$, dried over anhydrous $MgSO_4$ and the solvent was evaporated. The desired product was obtained as a yellowish oil with a 65% yield. The NMR data are identical to the literature.[156]

^{1}H-RMN ($CDCl_3$) δ 3.08 (t, *J*= 8.0 Hz, 2H); 3.51 (t, *J*= 8 Hz, 2H); 3.78 (s, 3H); 6.84 (d, *J*= 8.4 Hz, 2H); 7.11 (d, *J*= 8.4 Hz, 2H).

[156] Guziec, F.S.; Wei, D.; *J. Org. Chem.* **1992**, *57*, 3772.

SPICUM servicio de publicaciones

- Synthesis of 1-(4-methoxyphenethyl)-isoquinoline (48)

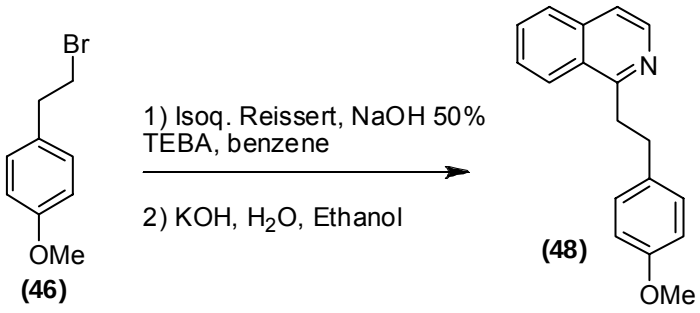

In a 25 mL round bottomed flask, 0.7 mL of 50% w/w NaOH were placed. Benzyl-triethylammonium chloride (8.3 mg, 0.04 mmol) was added and keeped under N_2 atm. A solution of isoquinoline Reissert (216 mg, 0.83 mmol) in 2.7 mL of benzene was added dropwise and stirred vigorously. After 20 minutes, a solution of 1-(2-bromoethyl)-4-methoxybenzene (215 mg, 1.00 mmol) in benzene (2 mL) was added dropwise, keeping stirred for 48h.

Then, H_2O and CH_2Cl_2 were added. The aqueous fraction was extracted, the organic layer was dried over anh. $MgSO_4$ and the solvent was evaporated. Then, 6 mL of H_2O, 10 mL of ethanol and 0.2 g of NaOH were added and heated under reflux for 3 hours. The aqueous fraction was extracted with CH_2Cl_2, the organic layer was dried over anh. $MgSO_4$ and solvent was evaporated. The crude was purified by silica gel column chromatography (Hexane:Ethyl acetate 7:3) to get the desired product as a yellow oil with a 78% yield.

1-(4-methoxyphenethyl)-isoquinoline (48)

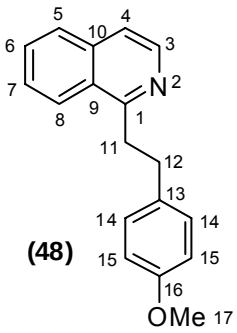

Yellow oil. 78% yield. R_f = 0.26 (Ethyl acetate : Cyclohexane 3:7). **^{1}H-RMN** ($CDCl_3$) δ 3.12 (t, *J*= 8.4 Hz, 2H, H_{12}); 3.55 (t, *J*= 8.4Hz, 2H, H_{11}); 3.78 (s, 3H, -OMe); 6.84 (d, *J*= 8.6 Hz, 2H, H_{15}); 7.21 (d, *J*= 8.6 Hz, 2H, H_{14}); 7.50-7.69 (m, 3H, $H_{4,6,7}$); 7.81 (d, *J*= 7.4 Hz, 1H, H_5); 8.14 (d, *J*= 8.2 Hz, 1H, H_8); 8.45 (d, *J*= 5.6Hz, 1H, H_3). **^{13}C-RMN** ($CDCl_3$) δ 24.6, 37.6, 55.2, 113.8, 119.4, 125.1, 126.9, 127.1, 127.4, 129.3, 129.8, 133.9, 136.2, 141.9, 157.9, 161.1. **MS-EI** *m/z* (%) 263 ($M^{+\cdot}$, 31), 262 (25), 248 (36), 121 (100). **FAB-HRMS** *m/z* Calculated for $C_{18}H_{18}NO$ (MH^+) 264.1383. Found: 264.1388.

SPICUM servicio de publicaciones

- Synthesis of 1-(4-methoxyphenethyl)-isoquinoline N-oxide (33)

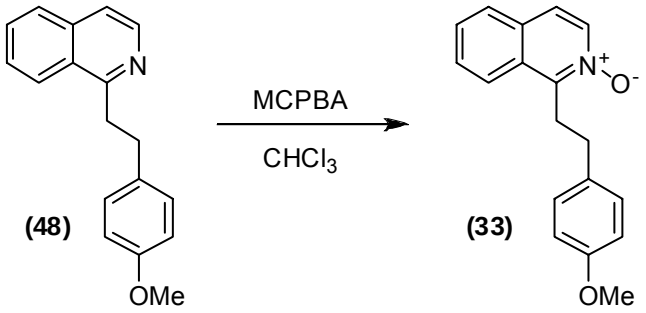

In a 50 mL round bottom flask 1-((4-methoxyphenethyl)-isoquinoline (258 mg, 0.98 mmol) was dissolved in 20 mL of $CHCl_3$. To the solution, 3-chloroperoxybenzoic acid (173 mg, 1.00 mmol) was added and stirred overnight under N_2 and light protected.

Then, the solution was washed with 5% $NaHCO_3$ and water, and the organic layer was dried over anh. $MgSO_4$ and the solvent was evaporated. The desired product was obtained as a white solid with 85% yield.

1-(4-methoxyphenethyl)-isoquinoline *N*-oxide (33)

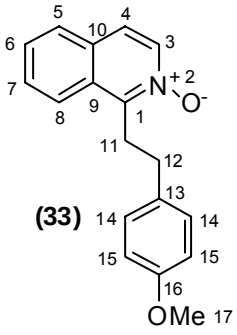

White solid. 85% yield. Mp (Ethyl acetate) 100-101ºC. R_f = 0.15 (Ethyl Acetate : Cyclohexane, 8 : 2) **^{1}H-RMN** ($CDCl_3$) δ 3.00 (t, *J*= 8.0 Hz, 2H, H_{12}), 3.63 (t, *J*= 8.0 Hz, 2H, H_{11}), 3.76 (s, 3H, -OMe), 6.80 (d, *J*= 8.5 Hz, 2H, H_{15}), 7.20 (d, *J*= 8.5 Hz, 2H, H_{14}), 7.50-7.56 (m, 3H, $H_{4,6,7}$), 7.72-7.79 (m, 2H, $H_{5,8}$), 8.20 (d, *J*= 7.4 Hz, 1H, H_3) **^{13}C-RMN** ($CDCl_3$) δ 28.9, 31.1, 55.2, 113.8, 122.1, 123.7, 127.3, 128.1, 128.5, 128.8, 129.0, 129.4, 133.1, 136.8, 148.0, 158.0. .**MS-EI** *m/z* (%) 279 ($M^{+\cdot}$, 23), 263 (24), 262 (100), 247 (15), 218 (19), 121 (42). **FAB-HRMS** *m/z* Calculated for $C_{18}H_{18}NO_2$ (MH^+) 280.1332. Found: 280.1339.

SPICUM servicio de publicaciones

-VI.1.3.2. Synthesis of 1-(3-(4-methoxyphenyl)propyl)-isoquinoline *N*-oxide (34)

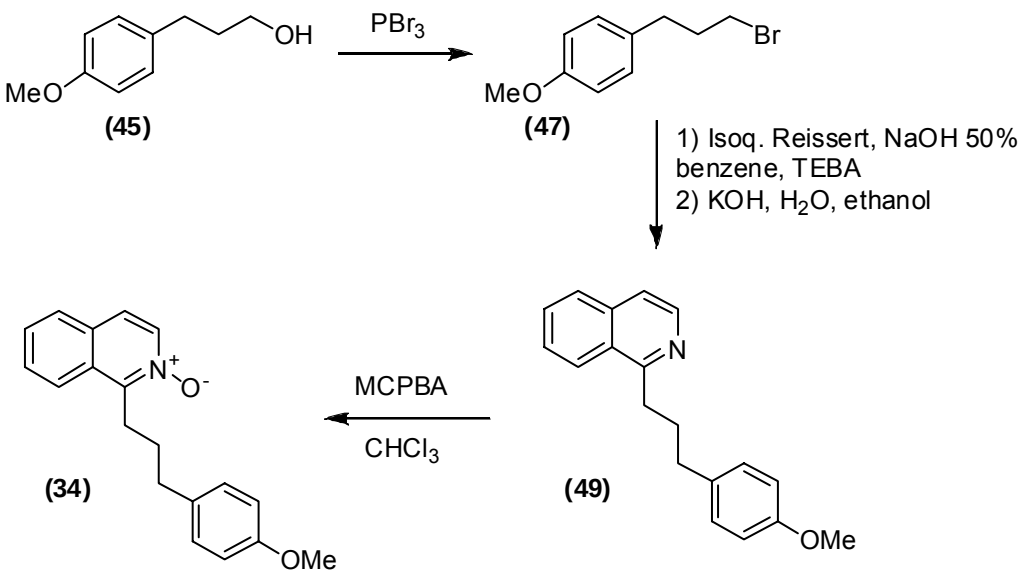

- Synthesis of 1-(3-bromopropyl)-4-methoxybenzene (47)

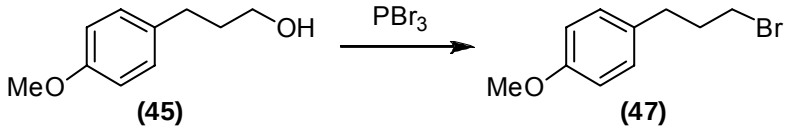

In a 10 mL round bottom flask, 3-(4-methoxyphenyl)-1-propyl alcohol (1.00 g, 6 mmol) was placed and the flask was cooled in an ice bath. Then, PBr_3 (0.28 mL, 3.00 mmol) was added and the mixture was stirred overnight at room temperature. Then, CH_2Cl_2 was added and the organic layer was washed with 5% w/w $NaHCO_3$, dried over anhydrous $MgSO_4$ and the solvent was evaporated. The desired product was obtained as a yellowish oil with a 67% yield. The NMR data are identical to the literature.[157]

^{1}H-RMN ($CDCl_3$) δ 2.11 (q, *J*= 7.2Hz, 2H); 2.70 (t, *J*=7.2Hz, 2H); 3.37 (t, *J*=7.2 Hz, 2H); 3.77 (s, 3H); 6.82 (d, *J*=8.6Hz, 2H); 7.10 (d, *J*=8.6Hz, 2H).

[157] Woscholski, R.; Hailes, H.; Numbere, M.; Rosivatz, E.; *PCT Int. Appl. 2006097744*, **21 Sep 2006**.

SPICUM servicio de publicaciones

- Synthesis of 1-(3-(4-methoxyphenyl)propyl)-isoquinoline (49)

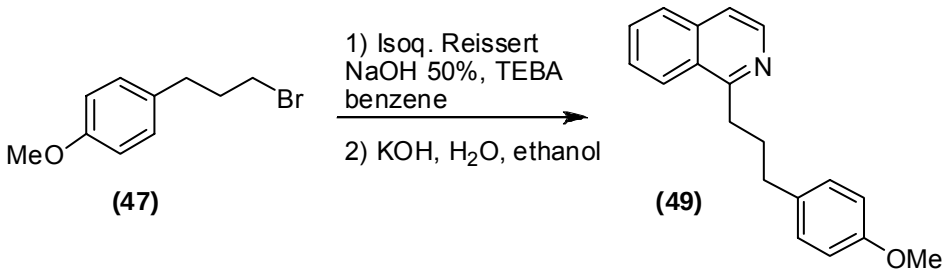

(47) **(49)**

In a 25 mL round bottom flask were added 1.7 mL of 50% w/w NaOH (1.70 g NaOH in 1.7 mL of water) and benzyl-triethylammonium chloride (23 mg, 0.10 mmol) and put under N_2. Then, isoquinoline Reissert (702 mg, 2.70 mmol) solved in 9 mL of benzene was added and kept energically stirred. After 20 minutes, 1-(3-bromopropyl)-4-methoxybenzene (687 mg, 3.00 mmol) dissolved in 1 mL of benzene was added. The mixture was stirred for one week.

Then, water was added and the crude was extracted with CH_2Cl_2. The organic layer was dried over anh. $MgSO_4$, and the solvent was evaporated.

To the crude were added 6 mL of water, 10 mL of ethanol and 0.2g of NaOH and the mixture was heated under reflux for 3 hours. Then, the solution was extracted with CH_2Cl_2, dried over anh. $MgSO_4$ and the solvent was evaporated. The crude was purified by silica gel column chromatography (Hexane : Ethyl Acetate 8:2) to give the desired product as a sticky solid with a 30% yield.

1-(3-(4-methoxyphenyl)propyl)-isoquinoline (49)

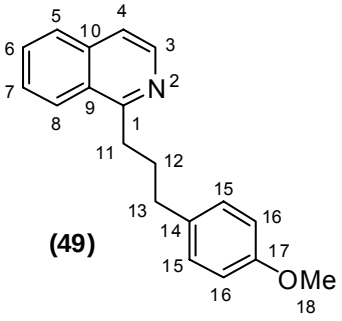

(49)

Sticky solid. **^{1}H-RMN** ($CDCl_3$) δ 2.15 (qu, *J*= 7.6 Hz, 2H, H_{12}); 2.73 (t, *J*= 7.6 Hz, 2H, H_{13}); 3.30 (t, *J*= 7.6 Hz, 2H, H_{11}) 3.77 (s, 3H, -OMe); 6.82 (d, *J*= 8.6 Hz, 2H, H_{16}); 7.13 (d, *J*= 8.6 Hz, 2H, H_{15}); 7.46-7.66 (m, 3H, $H_{4,6,7}$); 7.78 (d, *J*= 7.6 Hz, 1H, H_5); 8.03 (d, *J*= 8.6 Hz, 1H, H_8); 8.42 (d, *J*= 5.6 Hz, 1H, H_3). **^{13}C-RMN** ($CDCl_3$) δ 31.3, 34.8, 34.9, 55.2, 113.7, 119.2, 125.2, 126.8, 126.9, 127.3, 129.3, 129.7, 134.1, 136.2, 141.8, 157.7, 161.9. **MS-EI** *m/z* (%) 278 ($M^{+\cdot}$+H, 20), 143 (100). **FAB-HRMS** *m/z* Calculated for $C_{19}H_{20}NO$ (MH^+) 278.1539. Found: 278.1534.

SPICUM servicio de publicaciones

- Synthesis of 1-(3-(4-methoxyphenyl)propyl)-isoquinoline N-oxide (34)

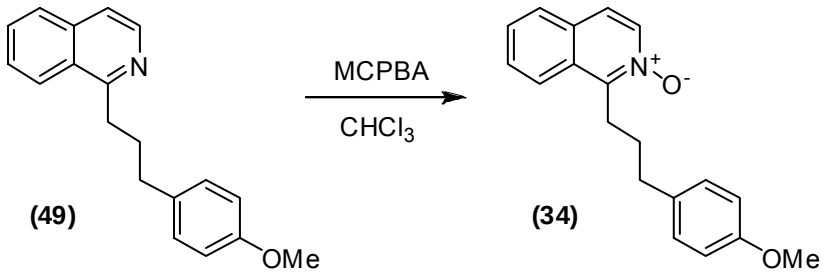

In a 25 mL round bottom flask, 1-(3-(4-methoxyphenyl)-propyl)-isoquinoline (189 mg, 0.68 mmol) was dissolved in 10 mL of $CHCl_3$. Then, 3-chloroperoxybenzoic acid (173 mg, 1.00 mmol) was added and the mixture was stirred overnight at room temperature light protected under N_2.

Then, the solution was washed with 5% $NaHCO_3$ and water, the organic layer was dried over anh. $MgSO_4$ and the solvent was evaporated. The desired product was obtained as a brown oil with a 85% yield.

1-(3-(4-methoxyphenyl)-propyl)-isoquinoline *N*-oxide (34)

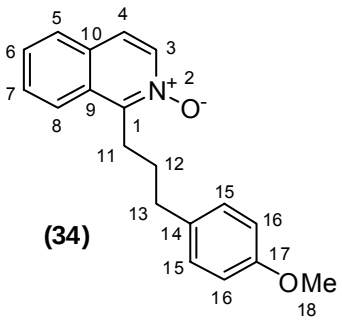

(34)

Brown oil. **^{1}H-NMR** ($CDCl_3$) δ 2.04 (p, *J*= 7.8 Hz, 2H, H_{12}), 2.78 (t, *J*= 7.8 Hz, 2H, H_{13}), 3.39 (t, *J*= 7.8 Hz, 2H, H_{11}), 3.77 (s, 3H, -OMe), 6.82 (d, *J*= 8.6 Hz, 2H, H_{16}), 7.15 (d, *J*= 8.6 Hz, 2H, H_{15}), 7.48-7.58 (m, 3H, $H_{4,6,7}$), 7.72 (t, *J*= 8.0 Hz, 2H, $H_{8,5}$), 8.16 (d, *J*= 7.2 Hz, 1H, H_3). **^{13}C-NMR** ($CDCl_3$) δ 25.7, 27.9, 34.8, 55.2, 113.7, 121.9, 123.7, 127.3, 128.2, 128.3, 129.0, 129.1, 129.3, 133.5, 136.5, 148.8, 157.7. **MS-EI** *m/z* (%) 293 ($M^{+\cdot}$, 7), 276 (5), 159 (100), 142 (67). **FAB-HRMS** *m/z* Calculated for $C_{19}H_{20}NO_2$ (MH^+) 294.1489. Found: 294.1490.

SPICUM servicio de publicaciones

VI.1.4. Synthesis of amide-bridged benzyl isoquinoline *N*-oxides

VI.1.4.1. General synthetic method for amide-bridged benzyl isoquinoline formation

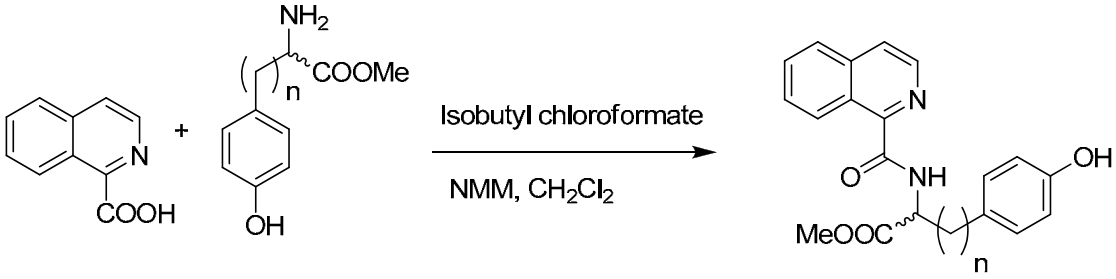

(54) n=1
(55) n=2

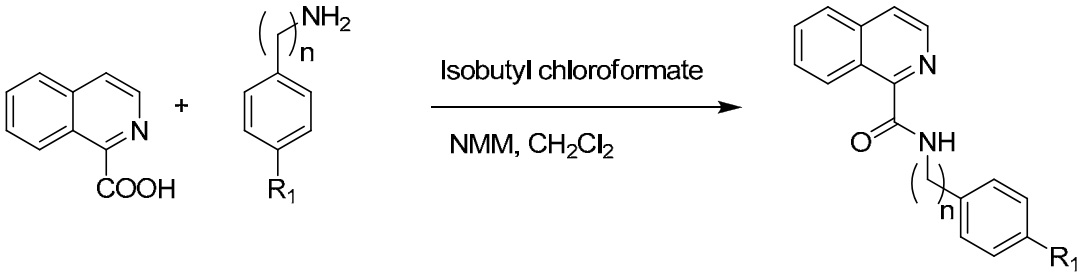

(56) n=0, R_2= OH
(57) n=0, R_2= OMe
(58) n=1, R_2= OH
(59) n=1, R_2= OMe
(60) n=2, R_2= OH
(61) n=2, R_2= OMe

In a 50 mL round bottom flask, 1-isoquinoline-carboxylic acid (1 mmol) was dissolved in 5 mL of CH_2Cl_2 and *N*-methyl-morpholine (1 mmol) was added, except for **(58)** where *N,N*-dimethylformamide was used as solvent. The mixture was cooled into an ice/salt bath. Then, isobutyl chloroformate (1 mmol) was added and cooled while stirring for 30 minutes. Amine (1 mmol) was added and the mixture was stirred at room temperature for 24 hours. When amine is presented as *p*-toluenesulfonyl **(54)** or hydrochloride, (**(55)** and **(60)**), *N*-methyl-morpholine (1 mmol) was added at the same time.

Then, the solvent was evaporated and the crude obtained was purified by silica gel column chromatography.

SPICUM servicio de publicaciones

(*R*)-*N*-1-((4-hydroxyphenyl)-1-methoxycarbonyl)-methyl-1-isoquinoline carboxamide (54)

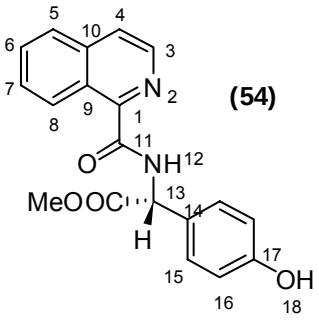

(54)

White solid. 78% yield. R_f = 0.37 (Ethyl acetate: Cyclohexane, 6:4). Mp (Ethyl acetate) 192-193 ºC. **^{1}H-NMR** ($CDCl_3$) δ 3.74 (s, 3H, -OMe), 5.64-5.66 (m, 1H, H_{13}), 6.79 (d, *J*= 8.4 Hz, 2H, H_{16}), 7.31 (d, *J*= 8.4 Hz, 2H, H_{15}), 7.61-7.69 (m, 2H, $H_{6,7}$), 7.77-7.82 (m, 2H, $H_{4,5}$), 8.45 (d, *J*= 5.6 Hz, 1H, H_3), 9.45 (d, *J*= 8.4 Hz, 1H, H_8). **^{13}C-NMR** (DMSO-d_6) δ 52.4, 56.0, 115.5, 123.5, 125.6, 126.2, 126.3, 127.1, 128.6, 129.2, 130.8, 136.5, 140.9, 150.3, 157.5, 165.7, 171.2. **MS-EI** *m/z* (%) 336 ($M^{+\cdot}$ 20), 277 (85), 180 (45), 156 (26), 128 (100). **FAB-HRMS** *m/z* Calculated for $C_{19}H_{17}N_2O_4$ (MH^+) 337.1183. Found: 337.1190.

(*S*)-*N*-(2-(4-hydroxyphenyl)-1-methoxycarbonyl)-ethyl-1-isoquinoline-carboxamide (55)

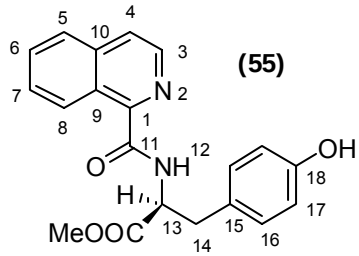

(55)

White solid. 90% yield. R_f = 0.40 (CH_2Cl_2 : MeOH, 98:2). Mp (Ethyl acetate) 142-143 ºC. **^{1}H-NMR** ($CDCl_3$) δ 3.19 (dd, J_1= 6.1 Hz, J_2= 3.5 Hz, 2H, H_{14}), 3.73 (s, 3H, -OMe), 5.04 (dt, J_1= 8.2 Hz, J_2= 6.1 Hz, 1H, H_{13}), 6.72 (d, *J*= 8.6 Hz, 2H, H_{17}), 7.07 (d, *J*= 8.6 Hz, 2H, H_{16}), 7.60-7.82 (m, 4H, $H_{4,5,6,7}$), 8.45 (d, *J*= 5.4 Hz, 1H, H_3), 8.64 (d, *J*= 8.2 Hz, 1H, NH), 9.49 (dd, J_1= 9.0 Hz, J_2= 2.0 Hz, 1H, H_8). **^{13}C-NMR** ($CDCl_3$) δ 37.5, 52.3, 53.7, 115.5, 124.5, 126.8, 127.0, 127.5, 127.6, 128.1, 128.7, 130.5, 137.4, 140.4, 147.4, 154.8, 165.6, 172.1. **MS-EI**: *m/z* (%) 350 ($M^{+\cdot}$, 3), 243 (16), 173 (71), 156 (24), 129 (44), 128 (100), 107 (14). **FAB-HRMS** *m/z* Calculated for $C_{20}H_{19}N_2O_4$ (MH^+) 351.1339. Found: 351.1354.

***N*-(4-hydroxyphenyl)-1-isoquinoline carboxamide (56)**

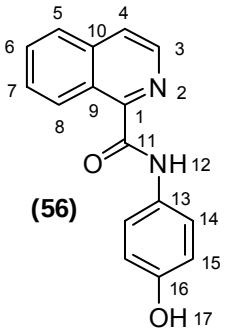

(56)

Pale yellow solid. 85% yield. R_f = 0.30 (Ethyl acetate : Cyclohexane, 3:7) Mp 199-200 ºC. **^{1}H-NMR** ($CDCl_3$) δ 6.87 (d, *J*= 8.8 Hz, 2H, H_{15}), 7.66 (d, *J*= 8.8 Hz, 2H, H_{14}), 7.69-7.75 (m, 2H, $H_{6,7}$), 7.83-7.87 (m, 2H, $H_{4,5}$), 8.51 (d, *J*= 5.2 Hz, 1H, H_3), 9.71 (d, *J*= 8.0 Hz, 1H, H_8), 10.2 (bs, 1H, NH). **^{13}C-NMR** (DMSO-d_6) δ 115.0, 121.6, 123.2, 125.3, 126.3, 127.1, 128.4, 130.3, 130.7, 136.5, 140.8, 151.8,

SPICUM servicio de publicaciones

153.8, 164.1. **MS-EI** *m/z* (%) 264 ($M^{+\cdot}$, 73), 129 (100), 128 (65). **FAB-HRMS** *m/z* Calculated for $C_{16}H_{13}N_2O_2$ (MH^+) 265.0972. Found: 265.0964.

N-(4-methoxyphenyl)-1-isoquinoline carboxamide (57)

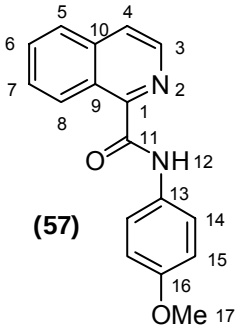

(57)

White solid. 96% yield. R_f = 0.40 (CH_2Cl_2 : MeOH, 98:2). Mp 105-106 ºC. **^{1}H-NMR** ($CDCl_3$) δ 3.82 (s, 3H, -OMe), 6.94 (d, *J*= 9.2 Hz, 2H, H_{15}), 7.68-7.75 (m, 4H, $H_{6,7,14}$), 7.83-7.88 (m, 2H, $H_{4,5}$), 8.51 (d, *J*= 5.6 Hz, 1H, H_3), 9.72 (d, *J*= 9.2 Hz, 1H, H_8), 10.20 (bs, 1H, NH). **^{13}C-NMR** ($CDCl_3$) 55.4, 114.1, 121.4, 124.7, 126.8, 127.2, 127.8, 128.7, 130.5, 131.2, 137.5, 139.9, 147.6, 156.3, 163.4. **MS-EI** *m/z* (%) 279 (23), 278 ($M^{+\cdot}$, 100), 129 (88), 128 (69). **FAB-HRMS** *m/z* Calculated for $C_{17}H_{15}N_2O_2$ (MH^+) 279.1128. Found: 279.1124.

N-(4-hydroxybenzyl)-1-isoquinoline carboxamide (58)

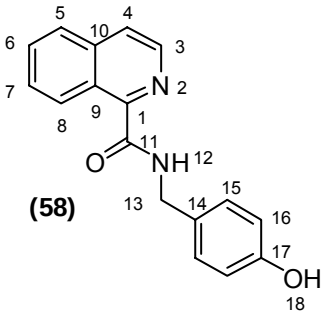

(58)

White solid. 93% yield. R_f = 0.23 (Ethyl Acetate : Cyclohexane, 3:7). Mp 174-175 ºC. **^{1}H-NMR** (CD_3OD) 4.57 (s, 2H, H_{13}), 6.77 (d, *J*= 8.4 Hz, 2H, H_{16}), 7.27 (d, *J*= 8.4 Hz, 2H, H_{15}), 7.70 (ddd, J_1= 8.6 Hz, J_2= 7.0Hz, J_3= 1.3 Hz, 1H, H_6), 7.79 (ddd, J_1= 8.6 Hz, J_2= 7.0 Hz, J_3= 1.3 Hz, 1H, H_7), 7.92 (d, *J*= 5.6 Hz, 1H, H_4), 7.97 (d, *J*= 8.0 Hz, 1H, H_5), 8.48 (d, *J*= 5.6 Hz, 1H, H_3), 8.90 (d, *J*= 8.6 Hz, 1H, H_8). **^{13}C-NMR** (CD_3OD) 43.9, 116.4, 124.9, 127.4, 127.8, 128.3, 129.6, 130.2, 130.6, 132.0, 138.7, 141.8,152.6, 127.9, 168.8. **MS-EI** *m/z* (%) 278 ($M^{+\cdot}$, 30), 235 (28), 129 (34), 122 (100). **FAB-HRMS** *m/z* Calculated for $C_{17}H_{15}N_2O_2$ (MH^+) 279.1128. Found: 279.1116.

N-(4-methoxybenzyl)-1-isoquinoline carboxamide (59)

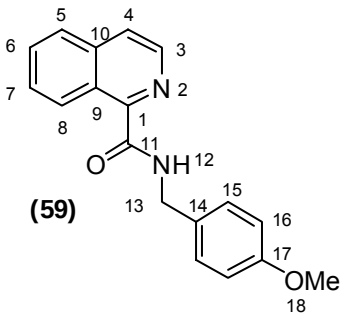

(59)

White solid. 81% yield. R_f = 0.24 (Ethyl acetate : Cyclohexane; 2:8). Mp 97-98 ºC. **^{1}H-NMR** ($CDCl_3$) δ 3.79 (s, 3H, -OMe), 4.63 (d, *J*= 6.0 Hz, 2H, H_{13}), 6.88 (d, *J*= 8.7 Hz, 2H, H_{16}), 7.33 (d, *J*= 8.7 Hz, 2H, H_{15}), 7.65-7.73 (m, 2H, $H_{6,7}$), 7.78 (d, *J*= 5.6 Hz, 1H, H_4), 7.83 (d, *J*= 7.6 Hz, 1H, H_5), 8.42 (d, *J*= 5.6 Hz, 1H, H_3), 8.448 (bs, 1H, NH), 9.63 (d, *J*= 8.3 Hz, 1H, H_8). **^{13}C-NMR** ($CDCl_3$) δ 43.0, 55.3, 114.1, 124.3, 126.7, 127.1, 127.8, 128.6, 129.2, 130.4, 130.5, 137.4, 140.1, 148.1, 159.0, 165.8. **MS-EI** *m/z* (%) 292 ($M^{+\cdot}$, 28), 136 (100), 129 (44). **FAB-HRMS** *m/z* Calculated for $C_{18}H_{17}N_2O_2$ (MH^+) 293.1285. Found: 293.1275.

SPICUM servicio de publicaciones

***N*-(2-(4-hydroxyphenyl)-ethyl)-1-isoquinoline carboxamide (60)**

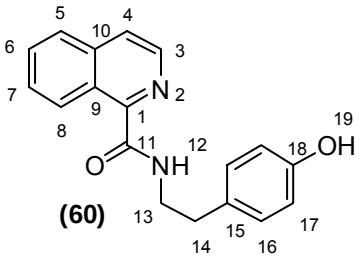

(60)

White solid. 50% yield. R_f = 0.25 (Ethyl acetate : Cyclohexane, 3:7) Mp 158-159 ºC. **^{1}H-NMR** ($CDCl_3$) δ 2.90 (t, *J*= 7.2 Hz, 2H, H_{14}), 3.71 (dd, J_1= 7.2 Hz, J_2= 6.2 Hz, 2H, H_{13}), 6.77 (d, *J*= 8.5 Hz, 2H, H_{16}), 7.13 (d, *J*= 8.5 Hz, 2H, H_{15}), 7.65-7.85 (m, 4H, $H_{4,5,6,7}$), 8.27 (bs, 1H, NH), 8.41 (d, *J*= 5.6 Hz, 1H, H_3), 9.55 (d, *J*= 7 Hz, 1H, H_8). **^{13}C-NMR** ($CDCl_3$) δ 35.8, 42.5, 116.4, 124.7, 127.3, 127.9, 128.2, 129.5, 131.0, 131.2, 132.0, 138.6, 141.8, 152.9, 157.1, 168.9. **MS-EI** *m/z* (%) 292 ($M^{+\cdot}$, 12), 185 (54), 173 (88), 156 (68), 128 (100). **FAB-HRMS** *m/z* Calculated for $C_{18}H_{17}N_2O_2$ (MH^+) 293.1285. Found: 293.1273.

***N*-(2-(4-methoxyphenyl)-ethyl)-1-isoquinoline carboxamide (61)**

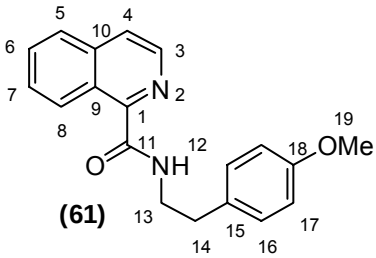

(61)

White solid. 90% yield. R_f = 0.30 (Cyclohexane : Ethyl Acetate, 8:2). Mp 68-69 ºC **^{1}H-NMR** ($CDCl_3$) δ 2.92 (t, *J*= 7.2Hz, 2H, H), 3.72 (dd, J_1= 7.2 Hz, J_2= 7.0 Hz, 2H, H_{13}), 3.78 (s, 3H, -OMe) 6.84 (d, *J*= 8.6 Hz, 2H, H_{17}), 7.19 (d, *J*= 8.6 Hz, 2H, H_{16}), 7.64-7.72 (m, 2H, $H_{6,7}$), 7.76 (d, *J*= 5.6 Hz, 1H, H_4), 7.82 (d, *J*= 7.6 Hz, 1H, H_5), 8.26 (bs, 1H, NH), 8.41 (d, *J*= 5.2 Hz, 1H, H_3), 9.58 (d, *J*= 8.0 Hz, 1H, H_8). **^{13}C-NMR** ($CDCl_3$) δ 35.0, 41.1, 55.2, 114.0, 124.2, 126.7, 127.0, 127.8, 128.6, 129.8, 130.4, 131.1, 137.4, 140.2, 148.3, 158.2, 166.0. **MS-EI** *m/z* (%) 306 ($M^{+\cdot}$, 10), 185 (23), 134 (100), 128 (63). **FAB-HRMS** *m/z* Calculated for $C_{19}H_{19}N_2O_2$ (MH^+) 307.1441. Found: 307.1446.

In order to study the hydroxylation products of the irradiation of *N*-oxides **(39)** and **(40)**, the amides **(62)** and **(63)** were synthesized, according to the synthetic general method for compounds **(54)**-**(61)**.

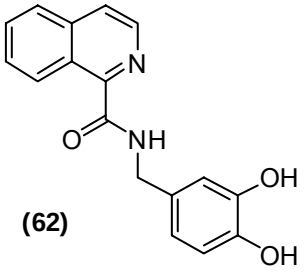

(62)

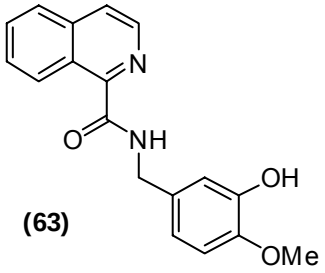

(63)

SPICUM servicio de publicaciones

N-(3,4-dihydroxybenzyl)-1-isoquinoline carboxamide (62)

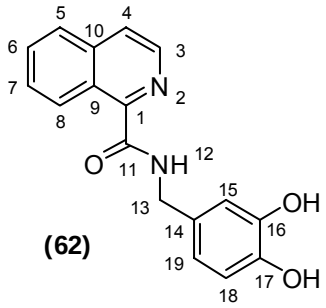

(62)

White solid. 50% yield. R_f = 0.25 (Cyclohexane : Ethyl acetate, 6:4). Mp (Ethyl Acetate) 198-199 ºC **^{1}H-NMR** ($CDCl_3$) δ 4.54 (d, *J*= 6.2 Hz, 2H, H_{13}), 6.77 (m, 2H, $H_{18,19}$), 6.89 (s, 1H, H_{15}), 7.62-7.84 (m, 4H), 8.39 (d, *J*= 5.4 Hz, 1H, H_3), 8.49 (bs, 1H, H_{12}), 9.50 (d, *J*= 7.4 Hz, 1H, H_8). **^{13}C-NMR** (DMSO-d_6) δ 42.0, 115.0, 115.3, 118.4, 123.2, 125.5, 126.5, 127.1, 128.3, 130.2, 130.6, 136.5, 140.8, 144.2, 145.1, 151.2, 165.9. **MS-EI** *m/z* (%) 155 (8), 139 (32), 138 (71), 129 (100), 128 (92). **FAB-HRMS** *m/z* Calculated for $C_{17}H_{15}N_2O_3$ (MH^+) 295.1077. Found: 295.1072.

N-(3-hydroxy-4-methoxybenzyl)-1-isoquinoline carboxamide (63)

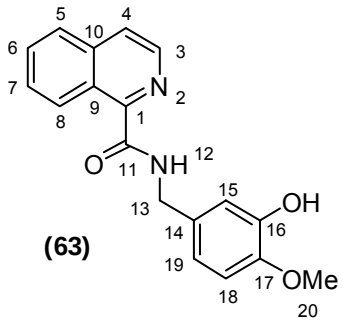

(63)

White solid. 75% yield. R_f = 0.15 (Cyclohexane : Ethyl acetate, 7:3). Mp (Ethyl Acetate) 139-140 ºC. **^{1}H-NMR** ($CDCl_3$) δ 3.86 (s, 3H, H_{20}), 4.60 (d, *J*= 6.0 Hz, 2H, H_{13}), 6.81 (d, *J*= 8.4 Hz, 1H, H_{18}), 6.89 (dd, J_1= 8.4 Hz, J_2= 2.0 Hz, 1H, H_{19}), 6.97 (d, *J*= 2.0 Hz, 1H, H_{15}), 7.65-7.73 (m, 2H, $H_{6,7}$), 7.77 (d, *J* = 5.4 Hz, 1H, H_4), 7.83 (d, *J* = 5.6 Hz, 1H, H_5), 8.42 (d, *J* = 5.4 Hz, 1H, H_3), 8.48 (bs, 1H, H_{12}), 9.63 (d, *J* = 8.0 Hz, 1H, H_8). **^{13}C-NMR** (DMSO-d_6) δ 41.9, 55.6, 112.1, 114.9, 118.1, 123.2. 125.5, 126.5, 127.1, 128.3, 130.6, 132.0, 136.5, 140.8, 146.3, 146.6, 151.1, 165.9. **MS-EI** *m/z* (%) 308 ($M^{+\cdot}$, 2), 152 (100), 129 (20). **FAB-HRMS** *m/z* Calculated for $C_{18}H_{17}N_2O_3$ (MH^+) 309.1234. Found: 309.1237.

SPICUM servicio de publicaciones

VI.1.4.2. General synthetic method for amide-bridged isoquinoline *N*-oxides formation

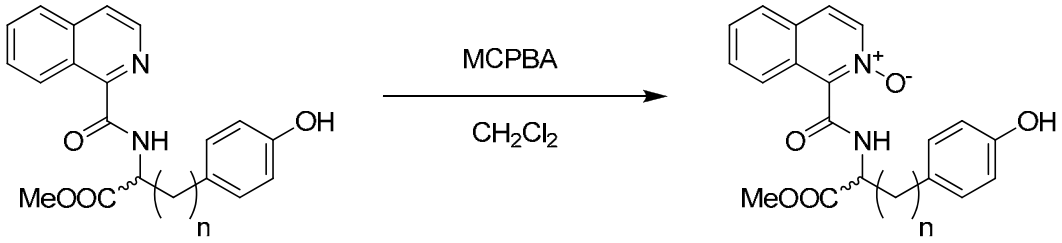

(35) n=0
(36) n=1

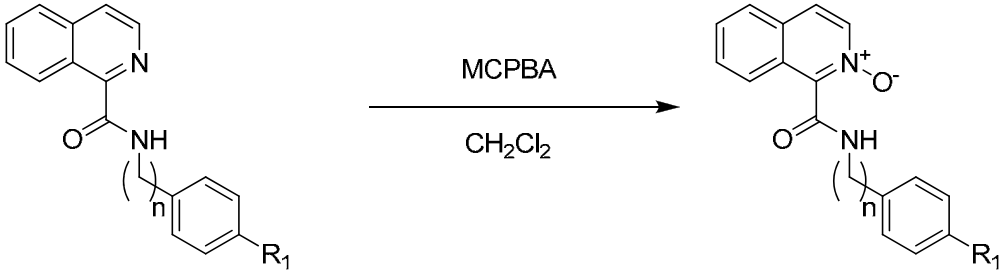

(37) n=0, R_2= OH
(38) n=0, R_2= OMe
(39) n=1, R_2= OH
(40) n=1, R_2= OMe
(41) n=2, R_2= OH
(42) n=2, R_2= OMe

In a 25 mL round bottom flask, isoquinoline carboxamide (1 mmol) was dissolved in CH_2Cl_2 except for carboxamides **(35)**, **(37)**, **(39)**, and **(41)** when methanol was used, and stirred. Then, 3-chloroperoxybenzoic acid (2 mmol) was added and the solution was stirred for 48 hours under N_2 and light protected.

Then, the solvent was evaporated and the crude was purified by silica gel column chromatography.

SPICUM servicio de publicaciones

(*R*)-*N*-1-((4-hydroxyphenyl)-1-methoxycarbonyl)-methyl-1-isoquinoline carboxamide-2-oxide (35)

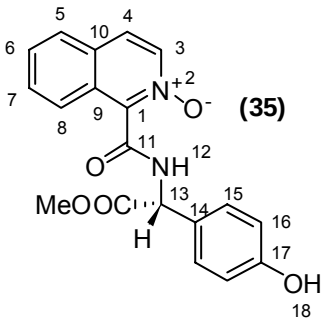

White solid. 91% yield. R_f = 0.58 (CH_2Cl_2:MeOH, 9:1). Mp 208-209 ºC (dec). **^{1}H-NMR** ($CDCl_3$) δ 3.71 (s, 3H, -OMe), 5.64 (s, 1H, H_{13}), 6.75 (d, *J*= 8.6 Hz, 2H, H_{16}), 7.27 (d, *J*= 8.6 Hz, 2H, H_{15}), 7.58-7.64 (m, 2H, $H_{6,7}$), 7.69 (d, *J*= 7.2 Hz, 1H, H_4), 7.75 (dd, J_1= 7.2 Hz J_2= 1.2 Hz, 1H, H_5), 8.04 (d, *J*= 6.8 Hz, 1H, H_3), 8.45 (d, *J*= 7.6 Hz, 1H, H_8). **^{13}C-NMR** (DMSO-d_6), δ 52.3, 56.3, 115.3, 123.3, 124.5, 125.0, 126.9, 127.0, 127.8, 128.3, 129.3, 129.6, 136.7, 140.2, 157.6, 161.1, 171.0. **MS-EI** m/z (%) 336 ($M^{+\cdot}$-16, 9), 335 (32), 293 (29), 277 (20), 128 (100). **FAB-HRMS** m/z Calculated for $C_{19}H_{17}N_2O_5$ (MH^+) 353.1132. Found: 353.1123.

(*S*)-*N*-(2-(4-hydroxyphenyl)-1-methoxycarbonyl)-ethyl-1-isoquinoline carboxamide-2-oxide (36)

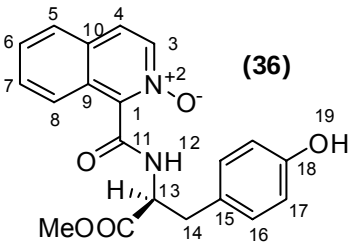

White solid. 51% yield. R_f = 0.53 (CH_2Cl_2:MeOH, 9:1). Mp 179-181 ºC (dec). **^{1}H-NMR** ($CDCl_3$) δ 3.07 (dd, J_1= 14.0 Hz, J_2= 6.8 Hz, 1H, H_{14a}), 3.22 (dd, J_1= 14.0 Hz, J_2= 5.0 Hz, 1H, H_{14b}), 3.75 (s, 3H, -OMe), 5.08 (ddd, J_1= 7.3 Hz, J_2= 6.8 Hz, J_3= 5.0 Hz, 1H, H_{13}), 6.68 (d, *J*= 8.4 Hz, 2H, H_{17}), 7.06 (d, *J*= 8.4 Hz, 2H, H_{16}), 7.57-7.74 (m, 4H, $H_{4,5,6,7}$), 8.07 (d, *J*= 6.9 Hz, 1H, H_3), 8.54 (d, *J*= 7.3 Hz, 1H, NH), 9.48 (d, *J*= 6.8 Hz, 1H, H_8). **^{13}C-NMR** (DMSO-d_6) δ 35.9, 51.9, 54.0, 115.1, 123.3, 124.5, 126.7, 126.8, 126.9, 127.7, 128.2, 129.4, 130.2, 136.7, 140.1, 156.1, 161.0, 171.6. **MS-EI** *m/z* (%) 350 ($M^{+\cdot}$-16, 5), 349 (19), 243 (12), 173 (32), 172 (25), 129 (30), 128 (100). **FAB-HRMS** *m/z* Calculated for $C_{20}H_{19}N_2O_5$ (MH^+) 367.1289. Found: 367.1298.

***N*-(4-hydroxyphenyl)-1-isoquinoline carboxamide-2-oxide (37)**

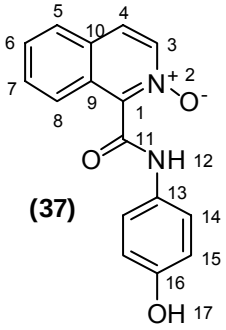

Yellowish solid. 83% yield. R_f = 0.43 (CH_2Cl_2:MeOH, 9:1) Mp 233-234ºC (dec). **^{1}H-NMR** ($CDCl_3$) δ 6.81 (d, *J*= 8.8 Hz, 2H, H_{15}), 7.54 (d, *J*= 8.8 Hz, 2H, H_{14}), 7.60-7.70 (m, 2H, $H_{6,7}$), 7.72 (d, *J*= 7.2 Hz, 1H, H_4), 7.79 (d, *J*= 8.4 Hz, 1H, H_5), 8.09 (d, *J*= 7.2 Hz, 1H, H_3), 8.69 (d, *J*= 8.8 Hz, 1H, H_8). **^{13}C-NMR** (DMSO-d_6) δ 115.2, 121.0, 123.1, 124.6, 126.5, 127.2, 128.0, 128.5, 130.0, 130.2, 136.8, 140.7, 153.9, 158.5. **MS-EI** *m/z* (%) 282 ($M^{+\cdot}$+2, 16), 281 ($M^{+\cdot}$+1,

SPICUM servicio de publicaciones

43), 280 ($M^{+\cdot}$, 50), 236 (21), 129 (18), 128 (100). **FAB-HRMS** *m/z* Calculated for $C_{16}H_{13}N_2O_3$ (MH^+) 281.0921. Found: 281.0912.

N-(4-methoxyphenyl)-1-isoquinoline carboxamide-2-oxide (38)

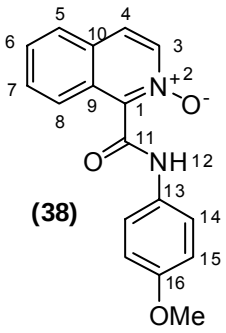

(38)

Yellowish solid. 64% yield R_f = 0.35 (Ethyl acetate : MeOH, 9:1). Mp 219-220 ºC. **^{1}H-NMR** ($CDCl_3$) δ 3.81 (s, 3H, -OMe), 6.92 (d, *J*= 9.1 Hz, 2H, H_{15}), 7.62-7.73 (m, 5H, $H_{4,6,7,14}$), 7.79 (d, *J*= 8.0 Hz, 1H, H_5), 8.15 (d, *J*= 7.3 Hz, 1H, H_3), 9.23 (d, *J*= 9.4 Hz, 1H, H_8). **^{13}C-NMR** ($CDCl_3$) δ 55.5, 114.2, 122.4, 125.4, 126.8, 126.9, 128.8, 129.6, 130.1, 130.3, 130.7, 136.4, 138.4, 156.7, 158.7. **MS-EI** *m/z* (%) 294 ($M^{+\cdot}$, 72), 278 (25), 250 (21), 129 (43), 128 (100). **FAB-HRMS** *m/z* Calculated for $C_{17}H_{15}N_2O_3$ (MH^+) 295.1077. Found: 295.1076.

N-(4-hydroxybenzyl)-1-isoquinoline carboxamide-2-oxide (39)

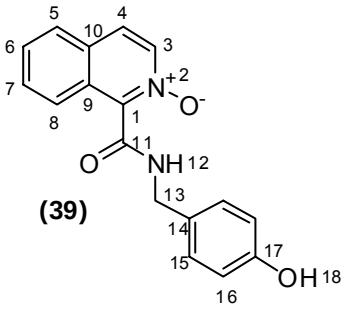

(39)

White solid. 93% yield, R_f = 0.30 (Ethyl acetate : MeOH, 9:1). Mp 249-250 ºC (dec). **^{1}H-NMR** (CD_3OD) δ 4.60 (d, *J*= 8.6 Hz, 2H, H_{13}), 6.79 (d, *J*= 8.4 Hz, 2H, H_{16}), 7.33 (d, *J*= 8.4 Hz, 2H, H_{15}), 7.73-7.77 (m, 3H, $H_{5,6,7}$), 8.01 (m, 2H, $H_{4,8}$), 8.19 (d, *J*= 7.2 Hz, 1H, H_3). **^{13}C-NMR** (DMSO-d_6) δ 42.0, 115.1, 123.2, 124.5, 126.6, 127.2, 127.9, 128.4, 128.7, 128.8, 129.8, 136.9, 140.8, 156.4, 160.9. **MS-EI** *m/z* (%) 278 ($M^{+\cdot}$-16, 4), 277 (23), 129 (30), 128 (100). **FAB-HRMS** *m/z* Calculated for $C_{17}H_{15}N_2O_3$ (MH^+) 295.1077. Found: 295.1069.

N-(4-methoxybenzyl)-1-isoquinoline carboxamide-2-oxide (40)

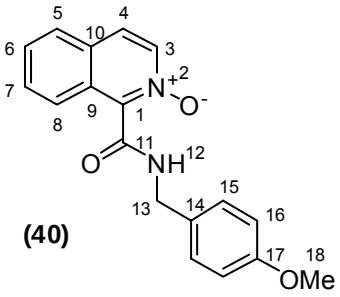

(40)

White solid. 83% yield. R_f = 0.33 (Ethyl acetate : MeOH, 9:1) Mp 179-180 ºC (dec). **^{1}H-NMR** ($CDCl_3$) δ 3.78 (s, 3H, -OMe), 4.69 (d, *J*= 5.6 Hz, 2H, H_{13}), 6.87 (d, *J*= 8.8 Hz, 2H, H_{16}), 7.35 (d, *J*= 8.8 Hz, 2H, H_{15}), 7.60-7.68 (m, 3H, $H_{4,6,7}$), 7.76 (d, *J*= 9.2 Hz, 1H, H_5), 8.09 (d, *J*= 7.2 Hz, 1H, H_3), 8.93 (d, *J*= 8.0 Hz, 1H, H_8), 9.82 (bs, 1H, NH). **^{13}C-NMR** ($CDCl_3$) δ 43.2, 55.3, 114.1, 125.3, 126.4, 126.9, 128.6, 129.1, 129.3, 129.7, 129.8, 130.2, 136.6, 138.4, 159.0, 161.3. **MS-EI** *m/z* (%) 309 ($M^{+\cdot}$+1, 6), 292 (18), 291 (81), 156 (28), 128 (100). **FAB-HRMS** *m/z* Calculated for $C_{18}H_{17}N_2O_3$ (MH^+) 309.1234. Found: 309.1233.

SPICUM servicio de publicaciones

***N*-(2-(4-hydroxyphenyl)-ethyl)-1-isoquinoline carboxamide-2-oxide (41)**

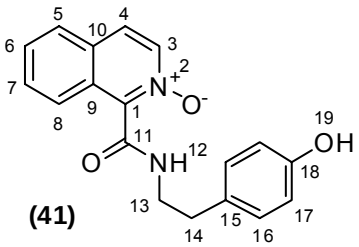

(41)

White solid. 86% yield. R_f = 0.26 (Ethyl acetate : MeOH, 9:1). Mp (Ethyl acetate) 189-190 ºC. **^{1}H-NMR** (CD_3OD) δ 2.90 (t, *J*= 7.0 Hz, 2H, H_{14}), 3.79 (t, *J*= 7.0 Hz, 2H, H_{13}), 6.76 (d, *J*= 8.6 Hz, 2H, H_{17}), 7.15 (d, *J*= 8.6 Hz, 2H, H_{16}), 7.24 (d, *J*= 8.6 Hz, 1H, H_4), 7.63 (t, *J*= 7.3 Hz, 1H, H_6), 7.71 (t, *J*= 7.3 Hz, 1H, H_7), 7.95-7.99 (m, 2H, $H_{3,5}$), 8.16 (d, *J*= 7.3 Hz, 1H, H_8). **^{13}C-NMR** (DMSO-d_6) δ 34.0, 40.4, 115.1, 123.5, 124.4, 126.5, 127.0, 127.8, 128.3, 129.2, 129.6, 129.7, 136.8, 141.0, 155.8, 160.7. **MS-EI** *m/z* (%) 292 ($M^{+\cdot}$-16, 3), 291 (16), 201 (11), 128 (92), 107 (100). **FAB-HRMS** *m/z* Calculated for $C_{18}H_{17}N_2O_3$ (MH^+) 309.1234. Found: 309.1243.

***N*-(2-(4-methoxyphenyl)-ethyl)-1-isoquinoline carboxamide-2-oxide (42)**

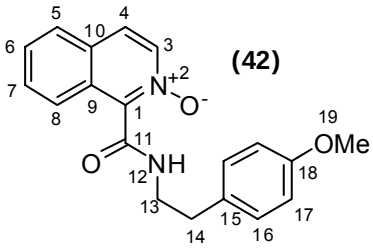

(42)

White solid. 84% yield R_f = 0.30 (Ethyl acetate : MeOH, 9:1). Mp (Ethyl acetate) 143-144 ºC. **^{1}H-NMR** ($CDCl_3$) δ 2.93 (t, *J*= 7.0 Hz, 2H, H_{14}), 3.76 (s, 3H, -OMe), 3.78 (m, 2H, H_{13}), 6.83 (d, *J*= 8.6 Hz, 2H, H_{17}), 7.20 (d, *J*= 8.6 Hz, 2H, H_{16}), 7.59-7.66 (m, 3H, $H_{4,6,7}$), 7.74 (d, *J*= 7.2 Hz, 1H, H_5), 8.08 (d, *J*= 6.8 Hz, 1H, H_3), 8.72 (d, *J*= 8.4 Hz, 1H, H_8), 9.38 (bs, 1H, NH). **^{13}C-NMR** ($CDCl_3$) δ 34.7, 41.2, 55.2, 114.0, 125.1, 126.3, 126.8, 128.4, 129.2, 129.6, 129.8, 130.1, 130.9, 136.5, 138.5, 158.2, 161.3. **MS-EI** *m/z* (%) 323 ($M^{+\cdot}$+1, 2), 306 (12), 305 (58), 201 (31), 172 (32), 134 (58), 128 (100). **FAB-HRMS** *m/z* Calculated for $C_{19}H_{19}N_2O_3$ (MH^+) 323.1390. Found: 323.1393.

SPICUM servicio de publicaciones

VI.1.5. Synthesis of 1-(4'-methylenebenzo-15-crown-5) isoquinoline *N*-oxide

- Synthetic scheme to obtain 1-(4'-methylenebenzo-15-crown-5) isoquinoline *N*-oxide (89)

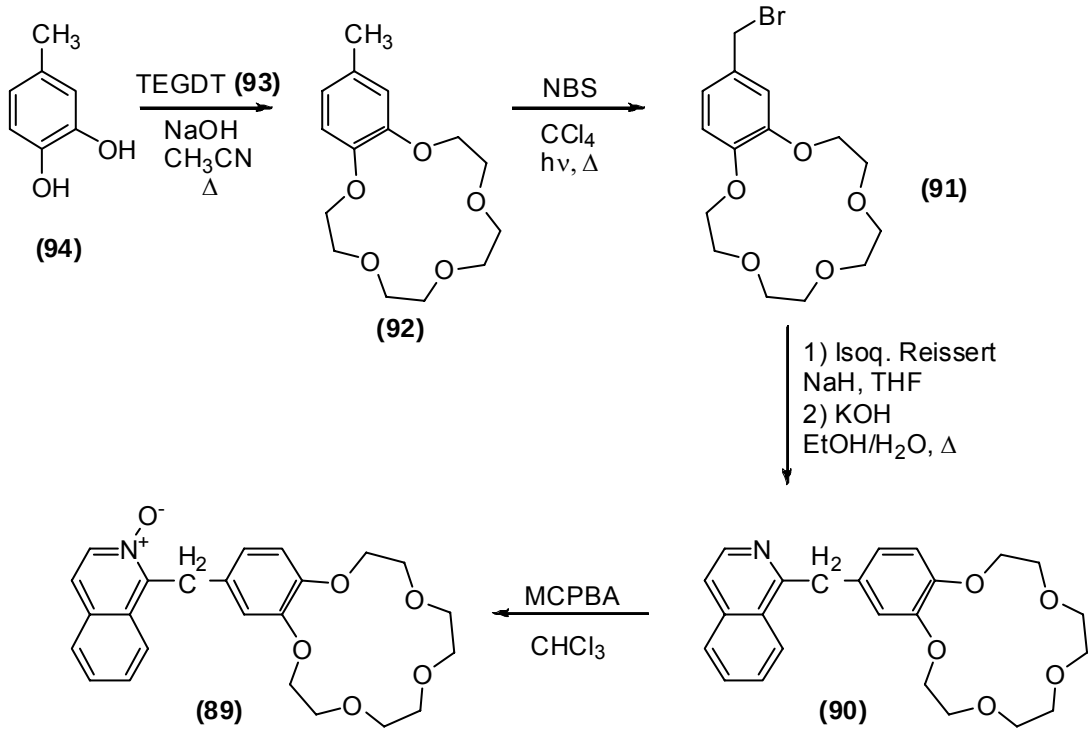

- Synthesis of 4-methyl-benzo-15-crown-5 (92)

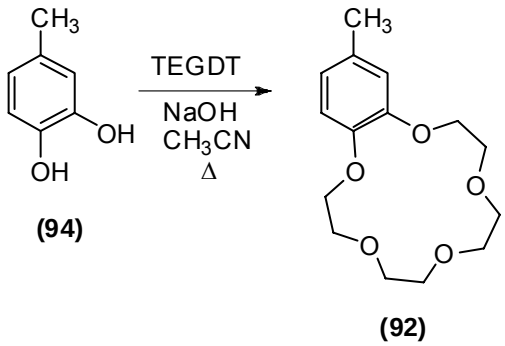

Tetraethylene glycol ditosylate (11.3 g, 22.5 mmol), 3-methylcatechol (2.8 g, 22.5 mmol) and NaOH (3.6 g, 0.09 mol) were dissolved in acetonitrile (40 mL) under nitrogen and heated under reflux for 3 h. The mixture was then filtered and the filtrate

SPICUM servicio de publicaciones

evaporated at reduced pressure. The resulting was dissolved in dichloromethane, washed with water, dried, evaporated and purified *via* column chromatography (silica gel, 99:1 dichloromethane:methanol) to obtain a sticky solid.

4-methyl-benzo-15-crown-5 (92)

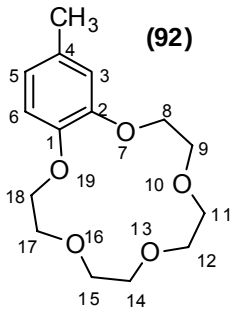

(92)

White slurry solid. 40% yield. **^{1}H-NMR** ($CDCl_3$) δ 2.25 (s, 3H, CH_3-), 3.73 (m, 8H, $H_{11, 12, 14, 15}$), 3.87 (m, 4H, $H_{9, 17}$), 4.10 (m, 4H, $H_{8, 18}$), 6.66 (m, 2H, $H_{3,5}$), 6.76 (d, *J*= 8.8 Hz, 1H, H_6). **^{13}C-NMR** ($CDCl_3$) δ 20.8, 68.8, 69.3, 69.5, 69..6, 70.3, 70.4, 70.8, 114.3, 115.0, 121.3, 130.9, 146.8, 148.0. **MS-EI** *m/z* (%): 282 ($M^{+\cdot}$, 29), 150 (100), 135 (63), 94 (78), 66 (38).

- Synthesis of 4-bromomethyl-benzo-15-crown-5 (91)

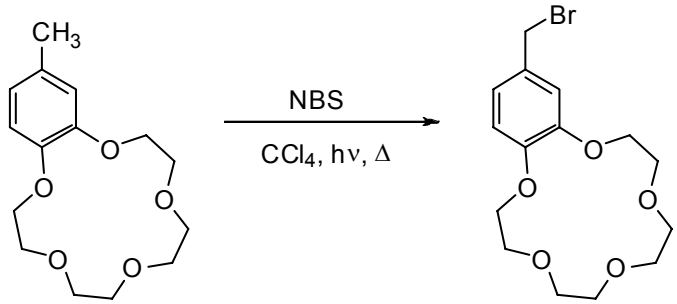

(92) **(91)**

In a round-bottomed flask fitted with a stirrer, nitrogen inlet tube, and reflux condenser were placed 4'-methylbenzo-15-crown-5 (282 mg, 1 mmol), NBS (186 mg, 1.1 mmol) and CCl4 (8 mL). The reaction mixture was stirred and heated under reflux in a nitrogen atmosphere for 7 h, while illuminated with a sunlamp. The succinimide was removed by suction filtration and washed twice with 10 mL portions of CCl_4 and the combined fractions evaporated.

SPICUM servicio de publicaciones

4-bromomethyl-benzo-15-crown-5 (91)

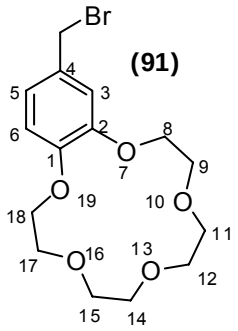

Yellowish sticky solid. 98% yield. **^{1}H-NMR** ($CDCl_3$) δ 3.73 (m, 8H, $H_{11,\ 12,\ 14,\ 15}$), 3.88 (m, 4H, $H_{9,17}$), 4.11 (m, 4H, $H_{8,18}$), 4.44 (s, 2H, -CH_2-Br), 6.76 (d, *J*= 8.2 Hz, 1H, H_6), 6.88 (s, 1H, H_3), 6.90 (d, *J*= 8.0 Hz, 1H, H_5). **^{13}C-NMR** ($CDCl_3$) δ 34.2, 68.7, 68.8, 69.3, 70.2, 70.9, 113.4, 114.6, 122.0, 130.6, 148.9, 149.1. **MS-EI** *m/z* (%) 360 ($M^{+\cdot}$, 7), 362 (7), 281 (28), 149 (100), 135 (18), 77 (24).

- Synthesis of 1-(4'-methylenebenzo-15-crown-5) isoquinoline (90)

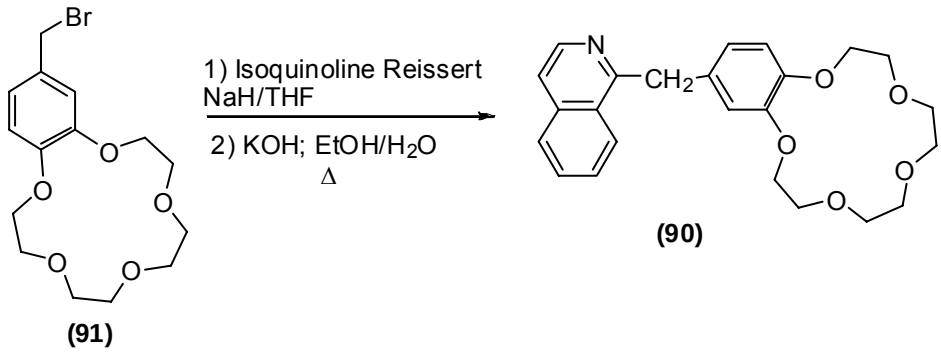

60 % NaH (40 mg, 1.01 mmol) was suspended in 5 mL anhydrous THF under N2. To the cooled suspension (0 ºC) a solution of isoquinoline Reissert (203 mg, 0.78 mmol) in 4 mL anhydrous THF was slowly added. After 10 min, 4'-bromomethylbenzo-15-crown-5 (271 mg, 0.75 mmol, dissolved in 4 mL anhydrous THF) was added and the reaction mixture allowed to warm to room temperature over 48 h. After addition of MeOH, the mixture was evaporated to dryness, leaving a residue that was washed with hexanes.

The oil obtained was suspended in a solution of 10 mL of EtOH, 5.5 mL of H_2O and 0.1 g of KOH, and the mixture was heated under reflux for 4 h. Upon cooling, the mixture was extracted with CH_2Cl_2 (3 x 10 mL) and the organic layers dried, filtered and evaporated to obtain an oil that was purified using alumina chromatography (*tert*-butyl methyl ether).

SPICUM servicio de publicaciones

1-(4'-methylenebenzo-15-crown-5) isoquinoline (90)

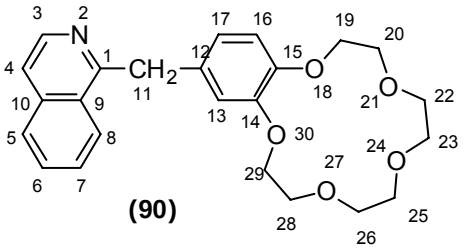

Yellowish sticky solid. 40% yield. **^{1}H-NMR** ($CDCl_3$) δ 3.69 (m, 8H, $H_{22,\ 23,\ 25,\ 26}$), 3.82 (m, 4H, $H_{20\text{-}28}$), 3.92 (m, 4H, $H_{19,29}$), 4.56 (s, 2H, H_{11}), 6.73-6.78 (m, 3H, $H_{13,16,17}$), 7.46-7.57 (m, 2H, $H_{4,6}$), 7.61 (t, *J*= 8.0 Hz, 1H, H_7), 7.78 (d, *J*= 8.0 Hz, 1H, H_5), 8.10 (d, *J*= 8 Hz, 1H, H_8), 8.45 (d, *J*= 5.8 Hz, 1H, H_3). **^{13}C-NMR** ($CDCl_3$) δ 41.7, 68.9, 69.1, 69.5, 69.6, 70.5, 71.0, 114.2, 114.6, 119.8, 121.2, 125.8, 127.2, 127.3, 129.8, 130.0, 132.7, 136.5, 141.9, 147.5, 149.1, 160.3. **MS-EI** *m/z* (%) 409 ($M^{+\cdot}$, 70), 276 (100), 204 (56), 193 (48), 149 (32), 77 (24). **FAB HRMS** *m/z* calculated for $C_{24}H_{28}NO_5$ (MH^+): 410.1967; Found 410.1981.

- Synthesis of 1-(4'-methylenebenzo-15-crown-5) isoquinoline N-oxide (89)

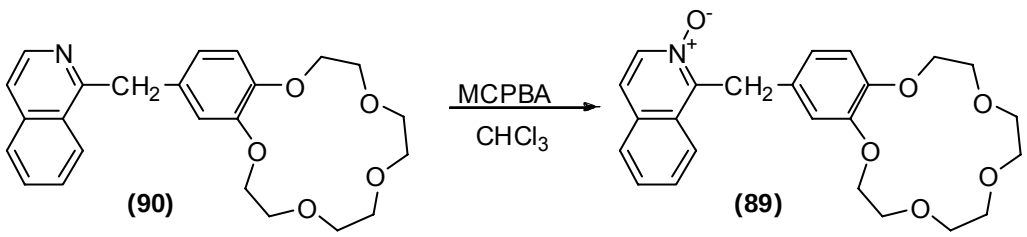

To a solution of 1-(4'-methylenebenzo-15-crown-5) isoquinoline (80 mg, 0.2 mmol) in 20 mL of chloroform, MCPBA (48 mg, 0.2 mmol) was added and the resulting solution stirred at room temperature for 24 h. The solution was then washed with saturated aqueous $NaHCO_3$ and water, dried and concentrated.

1-(4'-methylenebenzo-15-crown-5) isoquinoline *N*-oxide (89)

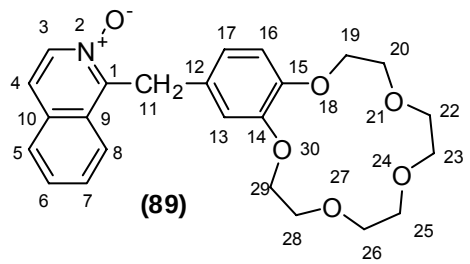

Yellow oil that solidifies on standing. 75% yield. **^{1}H-RMN** ($CDCl_3$) δ 3.70 (m, 8H, $H_{22,23,25,26}$), 3.83 (m, 4H, $H_{20,28}$), 4.04 (m, 4H, $H_{19,29}$), 4.71 (s, 2H, H_{11}), 6.70 (d, *J*= 8 Hz, 1H, H_{16}); 6.78 (dd, J_1= 8.0 Hz, J_2= 2 Hz, 1H, H_{17}), 6.97 (d, J_2= 2 Hz, 1H, H_{13}), 7.50-7.64 (m, 3H, $H_{4,6,7}$), 7.75 (dd, J_1= 6.8Hz, J_2= 2.0 Hz, 1H, H_5), 7.97 (d, *J*= 8.0 Hz, 1H, H_8), 8.20 (d, *J*= 8.0 Hz, 1H, H_3). **^{13}C-RMN** ($CDCl_3$) δ 31.2, 69.0, 69.1, 69.5, 70.5, 70.9, 114.2, 114.9, 121.2, 122.5, 124.0, 127.4, 128.2, 128.8, 129.0, 129.3, 130.2, 136.8, 147.1, 147.8, 149.2. **MS-EI** *m/z* (%): 425 ($M^{+\cdot}$, 20), 408 (100), 276 (80), 220 (40), 204 (70), 191 (40). **FAB HRMS** *m/z* calculated for $C_{24}H_{28}NO_6$ (MH^+): 426.1917. Found 426.1926

SPICUM servicio de publicaciones

VI.1.6. Irradiations

The irradiations were carried out using a water-cooled 150W medium pressure mercury lamp in two different immersion reactors with capacities of 120 and 150 mL. The time of irradiation is specified in each case.

- Irradiation of compounds (33) and (34)

A 10^{-3}M solution of the *N*-oxide and 0.1M of TFA in CH_2Cl_2 was degasified with Ar or N_2 for 10 min. The solution was irradiated for 6 minutes. The solution was washed with 5% $NaHCO_3$, dried over anh. $MgSO_4$, and the solvent was evaporated. The resulting crude was separated by preparative thin layer chromatography using a mixture of Ethyl acetate : Cyclohexane (3:7) as eluent for the irradiation of **(33)** and a mixture of CH_2Cl_2:Methanol (98:2) for the irradiation of **(34)**.

- Irradiation of (33)

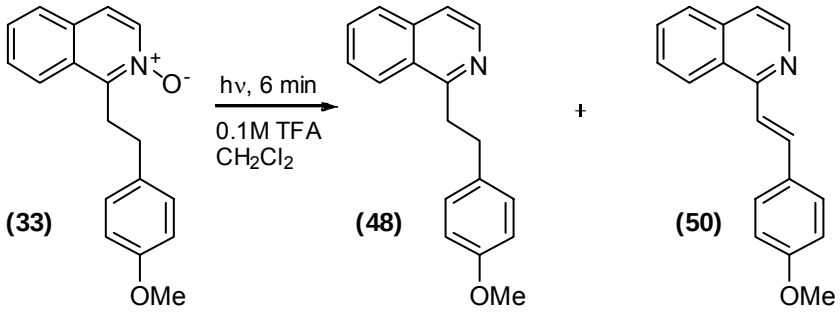

(33) **(48)** **(50)**

1-(4-methoxyphenethyl)-isoquinoline (48). Previously synthesized. 20% yield.

(*E*)-1-(4-methoxystyryl)isoquinoline (50B).

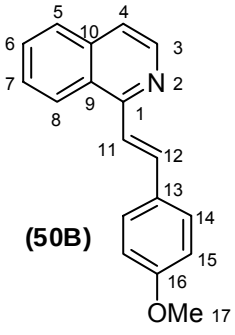

(50B)

24% yield. R_f = 0.70. Yellowish oil. **^{1}H-NMR** ($CDCl_3$) δ 3.84 (s, 3H, H_{17}), 6.93 (d, *J*= 8.8 Hz, 2H, H_{15}), 7.52 (d, *J*= 5.6 Hz, 1H, H_4), 7.58-7.68 (m, 4H), 7.80 (d, *J*= 8.4Hz, 1H, H_7), 7.85 (d, *J*= 15.4 Hz, 1H, H_{11}), 7.93 (d, *J*= 15.4 Hz, 1H, H_{12}), 8.35 (d, *J*= 8.4Hz, 1H, H_8), 8.52 (d, *J*= 5.6 Hz, 1H, H_3). **^{13}C-NMR** ($CDCl_3$) δ 55.3, 114.2, 119.6, 120.5, 124.5, 126.6, 127.0, 127.3, 128.8, 129.7, 129.8, 135.4, 136.7, 142.4, 154.8, 160.1. **MS-EI** *m/z* (%) 261 ($M^{+\cdot}$, 51), 260 (100), 246, (31), 217 (44). **FAB HRMS** *m/z* calculated for $C_{18}H_{16}NO$ (MH^+): 262.1226; Found: 262.1221.

SPICUM servicio de publicaciones

- Irradiation of (34)

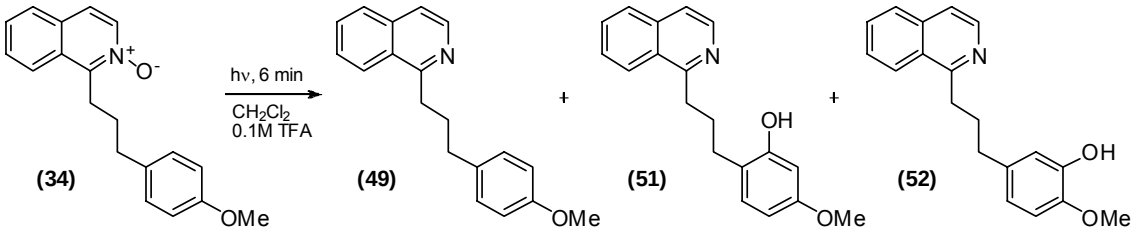

1-(3-(4-methoxyphenyl)-propyl)-isoquinoline (49). Previously synthesized. 25% yield.

1-(3-(2-hydroxy-4-methoxyphenyl)-propyl)-isoquinoline (51)

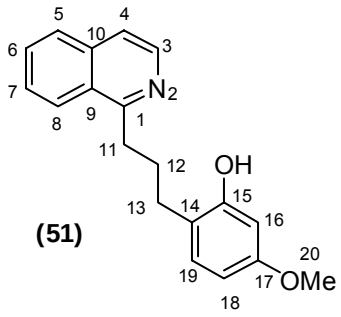

4% yield. R_f = 0.80. Brown oil. **^{1}H-NMR** ($CDCl_3$) δ 2.15 (qu, *J*= 7.2 Hz, 2H, H_{12}) 2.65 (t, *J*= 7.2 Hz, 2H, H_{13}), 3.33 (t, *J*= 7.2 Hz, 2H, H_{11}), 3.78 (s, 3H, H_{20}), 6.42 (dd, J_1= 8.2 Hz, J_2= 2.4 Hz, 1H, H_{18}), 6.58 (d, *J*= 2.4 Hz, 1H, H_{16}), 7.00 (d, *J*= 8.2 Hz, 1H, H_{19}), 7.62-7.66 (m, 2H, $H_{4,7}$), 7.73 (t, *J*= 8.0 Hz, 1H, H_6), 7.86 (d, *J*= 8.0 Hz, H_5), 8.19 (d, *J*= 8.6 Hz, H_8), 8.46 (d, *J*= 6.0 Hz, 1H, H_3). **^{13}C-NMR** ($CDCl_3$) δ 28.5, 29.7, 30.8, 55.2, 102.6, 105.7, 113.7, 120.2, 125.2, 127.2, 127.6, 127.7, 127.8, 130.6, 130.7, 130.9, 157.3, 159.5, 160.3. **FAB HRMS** *m/z* calculated for $C_{19}H_{20}NO_2$ (MH^+): 294.1489; Found: 294.1492.

1-(3-(3-hydroxy-4-methoxyphenyl)-propyl)-isoquinoline (52).

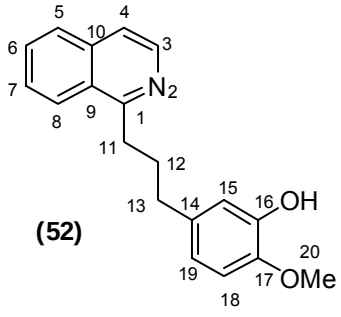

10% yield. R_f = 0.37. Brown oil. **^{1}H-NMR** ($CDCl_3$) δ 2.14 (qu, *J*= 7.8 Hz, 2H, H_{12}), 2.69 (t, *J*= 7.8 Hz, 2H, H_{13}), 3.30 (t, *J*= 7.8 Hz, 2H, H_{11}), 3.84 (s, 3H, H_{20}), 6.68 (dd, J_1= 8.0 Hz, J_2= 1.9 Hz, 1H, H_{19}), 6.75 (d, *J*= 8.0 Hz, 1H, H_{18}), 6.79 (d, *J*= 1.9 Hz, 1H, H_{15}), 7.49 (d, *J*= 5.6 Hz, 1H, H_4), 7.55 (t, *J*= 8.0 Hz, 1H, H_7), 7.65 (t, *J*= 8.0 Hz, 1H, H_6), 7.79 (d, *J*= 8.0 Hz, 1H, H_5), 8.04 (d, *J*= 8.0 Hz, 1H, H_8), 8.41 (d, *J*= 5.6 Hz, 1H, H_3). **^{13}C-NMR** ($CDCl_3$) δ 31.2, 34.8, 35.3, 56.0, 110.6, 114.7, 119.3, 119.8, 125.3, 126.9, 127.0, 127.4, 129.8, 135.4, 136.3, 141.7, 144.8, 145.5, 161.9. **FAB HRMS** *m/z* calculated for $C_{19}H_{20}NO_2$ (MH^+): 294.1489; Found: 294.1485.

SPICUM servicio de publicaciones

- Irradiation of compounds (35) - (42)

A 10^{-3}M solution of the *N*-oxide and 0.1M of TFA in CH_2Cl_2 was degasified with Ar or N_2 for 10 min. The solution was irradiated for 35 minutes. Then, $NaHCO_3$ was added to the solution and stirred for 30 minutes. The solid was filtered and the solvent was evaporated. The resulting crude was separated by preparative thin layer chromatography using the eluent specified in each case.

- Irradiation of (35)

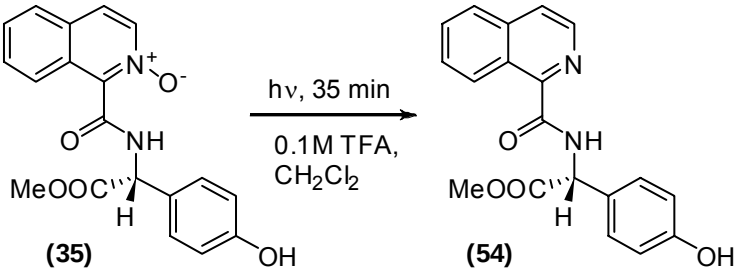

(*R*)-*N*-1-((4-hydroxyphenyl)-1-methoxycarbonyl)-methyl-1-isoquinoline carboxamide (54). Previously synthesized. 16% yield.

- Irradiation of (36)

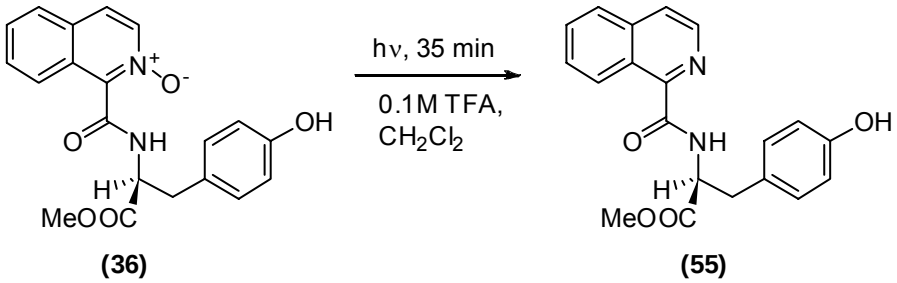

(*S*)-*N*-(2-(4-hydroxyphenyl)-1-methoxycarbonyl)-ethyl-1-isoquinoline carboxamide (55). Previously synthesized. 16% yield.

SPICUM servicio de publicaciones

- Irradiation of (37)

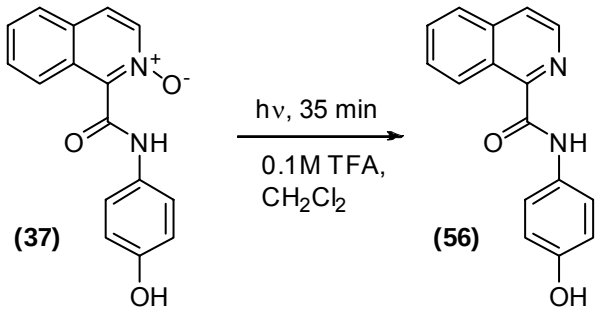

***N*-(4-hydroxyphenyl)-1-isoquinoline carboxamide (56).** Previously synthesized. 35% yield.

- Irradiation of (38)

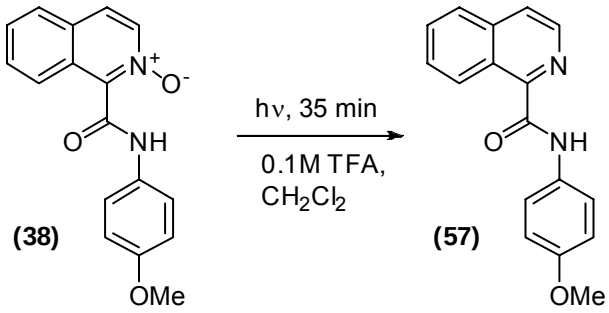

***N*-(4-methoxyphenyl)-1-isoquinoline carboxamide (57).** Previously synthesized. 37% yield.

SPICUM servicio de publicaciones

- Irradiation of (39)

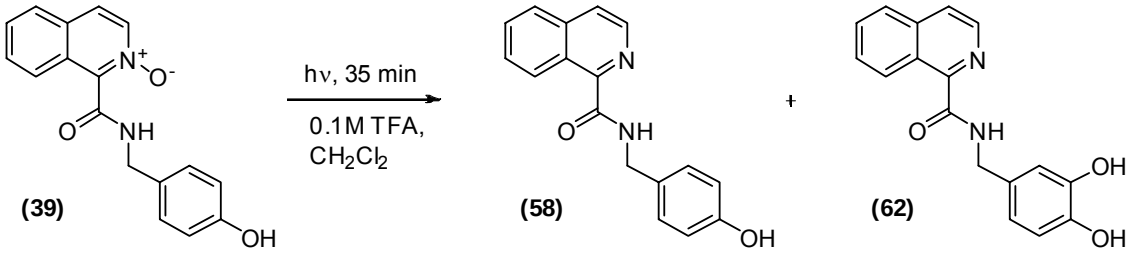

***N*-(4-hydroxybenzyl)-1-isoquinoline carboxamide (58).** Previously synthesized. 27% yield.

***N*-(3,4-dihydroxybenzyl)-1-isoquinoline carboxamide (62).** Previously synthesized. 41% yield.

- Irradiation of (40)

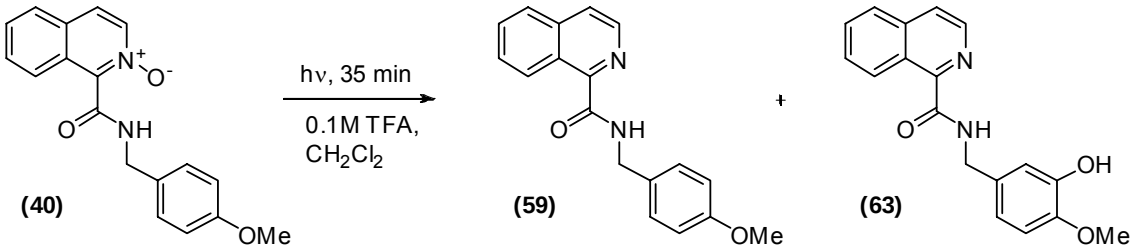

***N*-(4-methoxybenzyl)-1-isoquinoline carboxamide (59).** Previously synthesized. 32% yield.

***N*-(3-hydroxy-4-methoxybenzyl)-1-isoquinoline carboxamide (63).** Previously synthesized. 23% yield.

SPICUM servicio de publicaciones

- Irradiation of (41)

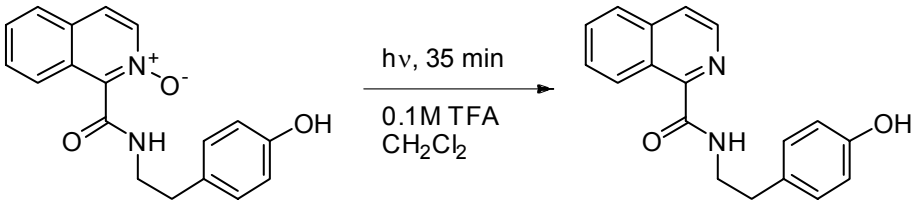

(41) **(60)**

***N*-(2-(4-hydroxyphenyl)-ethyl)-1-isoquinoline carboxamide (60).** Previously synthesized. 15% yield.

- Irradiation of (42)

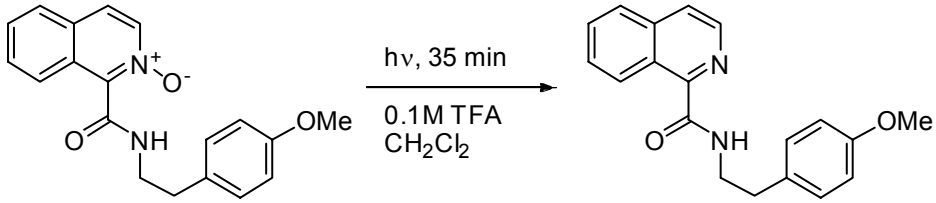

(42) **(61)**

***N*-(2-(4-methoxyphenyl)-ethyl)-1-isoquinoline carboxamide (27).** Previously synthesized. 13% yield.

SPICUM servicio de publicaciones

CHAPTER VII.

REFERENCES

SPICUM
servicio de publicaciones

SPICUM
servicio de publicaciones

VII. References

1. Newton, M.D.; *Electron transfer in Chemistry*, vol 1 (Ed. V. Balzani), Wiley-VCH, Weinheim (Federal Republic of Germany) **2001**, p. 3-63.

2. Braslavsky, S.E.; *Glossary of terms used in photochemistry 3rd Edition*, *Pure Appl. Chem.* **2007**, *79*, 293-465.

3. Nelsen, S.F.; *Electron transfer in Chemistry*, vol. 1 (Ed. V. Balzani), Wiley-VCH Weinheim (Federal Republic of Germany) **2001**, p. 342, 392.

4. Hubig, S.M.; Kochi, J.K.; *Electron transfer in Chemistry*, vol. 2 (Ed. V. Balzani), Wiley-VCH, Weinheim (Federal Republic of Germany) **2001**, p. 618-676.

5. a) Marcus, R.A.; *J. Chem. Phys.* **1956**, *24*, 966. b) Marcus, R.A.; *J. Chem. Phys.* **1957**, *26*, 867. c) Marcus, R.A.; *J. Chem. Phys.* **1957**, *26*, 872.

6. Balzani, V.; Scandola, F.; *Supramolecular Photochemistry*, Ellis Horwood Limited, Chichester (UK) **1991**, p. 51-75.

7. Marcus. R.A.; *Angew. Chem. Int. Ed.* **1993**, *32*, 1111.

8. Smith, T.A.; Lokan, N.; Cabral, N.; Davies, S.R.; Paddon-Row, M.N.; Ghiggino, K.P.; *J. Photochem. Photobiol. A: Chem.* **2002**, *149*, 55.

SPICUM servicio de publicaciones

9. Paddon-Row, M.N.; *Electron transfer in Chemistry*, vol. 3 (Ed. V. Balzani), Wiley-VCH, Weinhemi (Federal Republic of Germany) **2001**, p. 179-271.

10. Hush, N.S.; *Electrochimica Acta* **1968**, *13*, 1005.

11. Closs, G.L.; Miller, J.R.; *Science* **1988**, *240*, 440.

12. Paddon-Row, M.N.; Cotsaris, E.; Patney, M.K.; *Tetrahedron* **1986**, *42*, 1789.

13. Pasman, P.; Mes, G.F.; Koper, N. W.; Verhoeven, J.W.; *J. Am. Chem. Soc.* **1985**, *107*, 5839.

14. Jones II, G.; Farahat, M.S.; Greenfield, S.R.; Gosztola, D.J.; Wasielewski, M.R.; *Chem. Phys. Lett.* **1994**, *229*, 40.

15. a) Heitele, H.; Michel-Beyerle, M.E.; *J. Am. Chem. Soc.* **1985**, *107*, 8286. b) Nakamura, A.; Okutsu, s.; Oda, Y.; Ueno, A.; Toda, F.; *Tetrahedron Lett.* **1994**, *35*, 7241.

16. Pourtois, F.; Beljonne, D.; Cornil, J.; Ratner, M.A.; Brédas, J.L.; *J. Am. Chem. Soc.* **2002**, *124*, 4436.

17. a) Lewis, F.D.; Ho, T.-I.; Simpson, J.T.; *J. Org. Chem.* **1981**, 1077. b) Lewis, F.D.; Ho, T.-I.; *J. Am. Chem. Soc.* **1977**, *99*, 7991.

18. Su, Z.; Mariano, P.S.; Falvey, D.E.; Yoon, U.C.; Oh, S.W.; *J. Am. Chem. Soc.* **1998**, 120, 10676.

19. Berglund, J.; Pascher, T.; Winkler, J.R.; Gray, H.B.; *J. Am. Chem. Soc.* **1997**, *119*, 2464

20. Juris, A.; Balzani, V.; Barigelletti, F.; Campagna, S.; Belser, P.; von Zelewsky, A.; *Coord. Chem.Rev.* **1988**, *84*, 85.

21. Tokuyama, H.; Isobe, H.; Nakamura, E.; *J. Chem. Soc. Chem. Commun.* **1994**, 2753.

22. Yusuke, K.; Yoshikazu, K.; Masahiro, T.; Kazuhiro, C.; *Nippon Kagakkai Koen Yokoshu* **2001**, *79*, 730

23. a) Shigemitsu, Y.; Katsuhara, Y.; Odaira, Y.; *Tetrahedron Lett.* **1971**, *12*, 2887 b) Meggers, E.; Steckhan, E.; Blechert, S.; *Angew. Chem. Int. Ed.* **1995**, *34*, 2137. c) Majima, J.; Pac, C.; Nakasone, A.; Sakurai, H.; *J. Am. Chem. Soc.* **1977**, *99*, 5806.

24. Lakowicz, J.R.; *"Principles of fluorescence spectroscopy. 3rd Ed"* Springer Science+Business Media, LLC, New York (USA) **2006**, p. 335.

25. Valeur, B.; *"Molecular fluorescence: Principles and applications"* Wiley-VCH Verlag GMBH **2001**, p.286-292.

26. Szaciłowski, K.; *Chem. Rev.* **2008**, *108*, 3481.

27. Schmittel, M.; Ghorai, M.K.; *Electron transfer in chemistry*, vol. 2 (Ed. V. Balzani), Wiley-VCH, Weinhemi (Federal Republic of Germany) **2001**, p. 5-54.

SPICUM servicio de publicaciones

28. Rossi, R.A.; Pierini, A.B.; Peñéñory, A.B.; *Chem. Rev.* **2003**, *103*, 71.

29. Ahbala, M.; Hapiot, P.; Houmam, A.; Jouini, M.; Pinson, J.; Savéant, J.-M.; *J. Am. Chem. Soc*. **1995**, *117*, 11488.

30. a) Bunnett, J.F.; *Tetrahedron* **1993**, *49*, 4477. b) Rossi, R.A.; Palacios, S.M.; *Tetrahedron* **1993**, *49*, 4485.

31. Miyashi, T.; Takahashi, Y.; Konno, A.; Mukai, T.; Roth, H.D.; Schilling, M.L.; Abelt, C.J.; *J. Org. Chem.* **1989**, *54*, 1445.

32. Mizuno, K.; Ogawa, J.; Otsuji, Y.; *Chem. Lett.* **1981**, 741.

33. Arnold, D.R.; Du, X.; *Can. J. Chem.* **1994**, *72*, 403.

34. Weng, H.; Roth, H.D.; *J. Org. Chem.* **1995**, *60*, 4136.

35. Miao, X.-S.; March, R.E.; Metcalfe, C.D.; *Int. J. Mass Spectrom.* **2003**, *230*, 123.

36. Budzikiewicz, H.; Schaller, U.; Korth, H.; Pulverer, G.; *Monatsh. Chem.* **1979**, *110*, 947.

37. Gorrod, J.W.; Damani, L.A.; *J. Drug. Metab. Pharmacokinet.* **1980**, *5*, 53.

38. Bosin, T.R.; Maickel, R.P.; *Res. Commun. Chem. Pathol. Pharmacol.* **1973**, *6*, 813.

39. Antkowiak, W.Z.; Gessner, W.P.; *Tetrahedron Lett.* **1979**, *20*, 1931

40. Albini, A.; Pietra, S.; *Heterocyclic N-oxides*, CRC Press, Florida (USA) **1991**, p. 1-5.

41. a) Ulrich, G.; Hissler, M.; Ziessel, R.; *New J. Chem.* **1997**, *21*, 147. b) Lehn, J.-M.; Pietraszkiewicz, M.; Karpiuk, J.; *Helv. Chim. Acta* **1990**, *73*, 106. c) Collado, D.; Perez-Inestrosa, E.; Suau, R.; Desvergne, J.-P.; Bouas-Laurent, H.; *Org. Lett.* **2002**, *4*, 855.

42. Albini, A.; Alpegiani, M.; *Chem. Rev.* **1984**, *84*, 43.

43. Albini, A.; Fasani, E.; Dacrema, L.M.; *J. Chem. Soc., Perkin Trans. 1* **1980**, 2738.

44. Fasani, E.; Amer, A.M.; Albini, A.; *Heterocycles* **1994**, *37*, 985.

45. Tokumura, K.; Matsushita, Y.; *J. Photochem. Photobiol. A: Chem.* **2001**, *140*, 27.

46. Bucher, G.; Saciano, J.C.; *J. Phys. Chem.* **1994**, *98*, 12471.

47. Sako, H.; Shimada, K.; Hirota, K.; Maki, Y.; *J. Am. Chem. Soc.* **1986**, *108*, 6039.

48. a) Mitchell, K.H.; Rogge, C.E.; Gierahn, T.; Fox, B.G.; *Proc. Natl. Acad. Sci. USA* **2003**, *100*, 3784. b) Jerina, D.M.; Boyd, D.R.; Daly, J.W.; *Tetrahedron Lett.* **1970**, *11*, 457.

49. Sammes, P.G.; Serra-Errante, G.; Tinker, A.C.; *J. Chem. Soc., Perkin Trans. 1* **1978**, 853.

SPICUM servicio de publicaciones

50. Zadok, E.; Rubinraut, S.; Frolow, F.; Mazur, Y.; *J. Am. Chem. Soc.* **1985**, *107*, 2489.

51. a) Suau, R.; Rico-Gómez, R.; Souto-Bachiller, F.A.; Rodríguez-Rodríguez, L.A.; Ruiz, M.L.; *Tetrahedron Lett.* **1995**, *36*, 2653. b) Souto-Bachiller, F.A.; Perez-Inestrosa, E.; Suau, R.; Rico-Gómez, R.; Rodríguez-Rodríguez, L.A.; Coronado-Pérez, M.E.; *Photochem. Photobiol.* **1999**, *70*¸ 875.

52. Bremmer, J.B.; Wiriyachitra, P.; *Aust. J. Chem.* **1973** *26*, 437.

53. Jaffé, H.H.; Doak, G.O.; *J. Am. Chem. Soc.* **1955**, *77*, 4441.

54. Collado, D.; Perez-Inestrosa, E.; Suau, R.; *J. Org. Chem.* **2003**, *68*, 3574.

55. Collado, D.; Perez-Inestrosa, E.; Suau, R.; Lopez Navarrete, J.T.; *Tetrahedron* **2006**, *62*, 2927.

56. Shamma, M.; *The isoquinoline Alkaloids. Chemistry and Pharmacology*, vol. 25. Ed A. T. Blausuist y H. Wasserman. Academy Press. New York & London, **1972**, p. 45-89.

57. Gilchrist, T.L.; *Heterocyclic Chemistry*, Longman Scientific & Technical, Essex, **1992**, cap. 5.

58. Popp, F.; *Advances in Heterocyclic Chemistry*, vol.9, Ed. Academic Press, New York **1968**, p. 1-26.

59. Koizumi, T.; Takeda, K.; Yoshida, K.; Yoshii, E.; *Synthesis* **1977**, 497.

60. a) Starks, C.M.; *J. Am. Chem. Soc.* **1971**, *93*, 195. b) Herriott, A.W.; Picker, D.; *J. Am. Chem. Soc.* **1975**, *97*, 2345. c) Makosza, M.; *Pure. Appl. Chem.* **2000**, *72*, 1399.

61. Makosza, M.; *Tetrahedron Lett.* **1969**, *10*, 677.

62. Sheng, M.N.; Zajacek, J.G.; *Org. Synth.* **1988**, *6*, 501.

63. Roberts, S.M.; Suschitzky, H.; *J. Chem. Soc.C* **1969**, 1485.

64. Chivers, G.E.; Suschitzky, H.; *J. Chem. Soc. C* **1971**, 2867.

65. Pollak, A.; Zupan, M.; Sket, B.; *Synthesis* **1973**, 495.

66. Murray, R.W.; Jeyaraman, R.; *J. Org. Chem.* **1985**, *50*, 2847.

67. Kaiser, E.M.; Knutson, P.L.; *Synthesis* **1978**, *2*, 148.

68. Lai, C.-H.; Shen, Y.-L.; Wang, M.-N.; Rao, N.S.K.; Liao, C.C.; *J. Org. Chem.* **2002**, *67*, 6493.

69. Lambert, J.B.; Mazzola, E.P.; *Modern Nuclear Magnetic Resonance Spectroscopy: An Introduction to Principles, Applications, and Experimental Methods*. Pearson Prentice Hall, Upper Saddle River, NJ, (USA) **2004**.

70. a) Mitchell, J.A.; Reid, E.E.; *J. Am. Chem. Soc.* **1931**, *53*, 1879. b) Coleman, G.H.; Alvarado, A.M.; *Org. Synth., Coll. Vol.* **1948**, *1*, 3.

SPICUM servicio de publicaciones

71. a) Goldschmidt, S.; Wick, M.; *Justus Liebigs Ann. Chem.* **1952**, *575*, 217. b) Blagbrough, I.S.; Mackenzie, N.E.; Ortiz, C.; Scott, A.I.; *Tetrahedron Lett.* **1986**, *27*, 1251. c) Ram, R.N.; Ashare, R.; Mukerjee, A.K.; *Chem. Ind. (London)* **1983**, 569.

72. Cope, A.C.; Ciganek, E.; *Org. Synth., Coll. Vol.K* **1963**, *4*, 339.

73. a) Staab, H.A.; *Angew. Chem.* **1962**, *74*, 407. b) Matsumoto, K, Hashimoto, S.; Otani, S.; *Angew. Chem., Int. Ed. Engl.* **1986**, *25*, 565.

74. a) Vaughan, J.R.Jr.; *J. Am. Chem. Soc.* **1951**, *73*, 3547. b) Boissonnas, R.A.; *Helv. Chim. Acta* **1951**, *34*, 874.

75. Sheehan, J.C.; Hess, G.P.; *J. Am. Chem. Soc.* **1955**, *77*, 1067.

76. Feynman, R.P.; *Miniaturization* **1961**, 282.

77. http://www.its.caltech.edu/~feynman/plenty.html

78. Moore, G.E.; *Electronics* **1965**, Vol. 38, Nº 8, April 19.

79. Balzani, V.; Credi, A.; Venturi, M.; *Chemphyschem* **2003**, *3*, 49.

80. a) Ball, P.; *Nature* **2000**, *406*, 118. b) Service, R.F.; *Science* **2001**, *293*. 785.

81. Lehn, J.M.; *Pure & Appl. Chem.* **1977**, *49*, 857.

82. Toma, H.E.; *Curr. Sci.* **2008**, *95*, 1202.

83. Tour, J.M.; Kozaki, M.; Seminario, J.M.; *J. Am. Chem. Soc.* **1998**, *120*, 8486.

84. Aviram, A.; Ratner, M.A.; *Chem. Phys. Lett.* **1974**, *29*, 277.

85. a) Pickaert, G.; Ziessel, R.; *Tetrahedron Lett.* **1998**, *39*, 3497. b) Grozema, F.C.; Huarner-Rassin, C.; Prins, P.; Siebbeles, L.D.A.; Anderson, H.L.; *J. Am. Chem. Soc.* **2007**, *129*, 13370. c) Hansen, M.R.; Schnitzler, T.; Pisula, W.; Graf, R.; Müllen, K.; Spiess, H.W.; *Angew. Chem. Int. Ed.* **2009**, *48*, 4621. d) Leary, E.; Zalinge, H.V.; Higgins, S.J.; Nichols, R.J.; Fabrizi de Biani, F.; Leoni, P.; Marchetti, L.; Zanello, P.; *Phys. Chem. Chem. Phys.* **2009**, *11*, 5198.

86. a) Metzger, R.M.; *Acc. Chem.. Res.* **1999**, *32*, 950. b) Acharya, S.; Song, H.; Lee, J.; Kwon, P.S.; Lee, J.; Yogendranath, G.; Kim, Y.H.; Jang, Y.H.; Lee, T.; Samal, S.; Lee, J.-S.; *Org. Electron.* **2009**, *10*, 85.

87. a) Li, F.; Yang, S.I.; Ciringh, Y.; Seth, J.; Martin III, C.H.M.; Singh, D.L.; Kim, D.; Birge, R.R.; Bocian, D.F.; Holten, D.; Lindsey, J.S.; *J. Am. Chem. Soc.* **1998**, *120*, 10001. b)Ajayaghosh, A.; Praveen, V.K.; Vijayakumar, C.; George, S.J.; *Angew. Chem. Int. Ed.* **2007**, *46*, 6260.

88. Balzani, V. *Electron Transfer in Chemistry. Vol. 5.*, WILEY-VCH Verlag GmbH, Weinheim (Federal Republic of Germany) **2001**, pg.215-242.

89. Clarkson, M.A.; *Byte* **1989**, *May*, 268.

90. Nolte, D.D.; *J. Appl. Phys.* **1999**, *85*, 6259.

91. De Silva, A.P.; Gunaratne, H.Q.N.; McCoy, C.P.; *Nature* **1993**, *364*, 42.

SPICUM servicio de publicaciones

92. Brown, G.J.; De Silva, A.P.; Pagliari, S.; *Chem. Commun.* **2002**, 2461.

93. De Silva, A.P.; de Silva, S.A.; Dissanayake, A.S.; Sandanayake, K.R.A.S., *J. Chem. Soc., Chem. Commun*. **1989**, 1054.

94. De Silva, A.P.; Gunaratne, H.N.Q.; Maguire, G.E.M.; *J. Chem. Soc., Chem. Commun.* **1994**, 1213.

95. a) Amir, R.J.; Popkov, M., Lerner, R.A.; Barbas III, C.F.; Shabat, D.; *Angew. Chem. Int. Ed.* **2005**, *44,* 4378. b) Pita, M.; Katz, E.; *J. Am. Chem. Soc.* **2008**, *130*, 36.

96. McSkimming, G.; Tucker, J.H.R.; Bouas-Laurent, H.; Desvergne, J.-P.; *Angew. Chem. Int. Ed.* **2000**, *39*, 2167.

97. a) de Silva, A.P.; Gunaratne, H.Q.N.; McCoy, C.P.; *J. Am. Chem. Soc.* **1997**, *119*, 7891. b) Ji, H.-F.; Dabesgtani, R.; Brown, G.M.; *J. Am. Chem. Soc.* **2000**, *122*, 9306. c) Sadhu, K.K.; Bag, B.; Bharadwaj, P.K.; *J. Photochem. Photobiol., A* **2007,** *185*, 231.

98. Fang, C.-J; Zhu, Z.; Sun, W.; Xu, C-H.; Yan, C.-H.; *New J. Chem.* **2007**, *31*, 580.

99. Frezza, B.M.; Cockroft, S.L.; Ghadiri, M.R.; *J. Am. Chem. Soc.* **2007**, *129*, 14875.

100. Uchiyama, S.; Kawai, N.; de Silva, A.P.; Iwai, K.; *J. Am. Chem. Soc.* **2004**, *126*, 3032.

101. a) Margolin, A.A.; Stojanovic, M.N.; *Nature Biotechnology* **2005**, *23*, 1374. b) Chen, X.; Wang, Y.; Liu, Q.; Zhang, Z.; Fan, C.; He, L.; *Angew. Chem. Int. Ed.* **2006**, *45*, 1759.

102. a) Guo, X.; Zhang, D.; Zhu, D.; *Adv. Mater.* **2004**, *16*, 125. b) Magri, D.C.; Brown, G.J.; McClean, G.D.; de Silva, A.P.; *J. Am. Chem. Soc.* **2006**, *128*, 4950.

103. Andersson, M.; Sinks, L.E.; Hayes, R.T.; Zhao, Y.; Wasielewski, M.R.; *Angew. Chem. Int. Ed.* **2003**, *42*, 3139.

104. Uchiyama, S.; McLean, G.D.; Iwai, K.; de Silva, A.P.; *J. Am. Chem. Soc.* **2005**, *127,* 8920.

105. Wang, Z.; Zheng, G.; Lu, P.; *Org. Lett.* **2005**, *7*, 3669.

106. Lee, S.H.; Kim, J.Y.; Kim, S.K.; Lee, J.H.; Kim, J. S.; *Tetrahedron* **2004**, *60*, 5171.

107. De Silva, A.P.; Dixon, I.M.; Gunaratne, H.Q.N.; Gunnlaugsson, T.; Maxwell, P.R.S.; Rice, T.E.; *J. Am. Chem. Soc.* **1999**, *121*, 1393.

108. Baytekin, H.T.; Akkaya, E.U.; *Org. Lett.* **2000**, *2*, 1725.

SPICUM servicio de publicaciones

109. Chiang, P.-T.; Cheng, P.-N.; Lin, C.-F.; Liu, Y.-H.; Lai, C.-C.; Peng, S.-M.; Chiu, S.-H.; *Chem. Eur. J.* **2006**, *12*, 865.

110. Credi, A.; Balzani, V.; Langford, S.J.; Stoddart, J.F.; *J. Am. Chem. Soc.* **1997**, *119*, 2679.

111. Stojanovic, M.N.; Mitchell, T.E.; Stefanovic, D.; *J. Am. Chem. Soc.* **2002**, *124*, 3555.

112. Pina, F.; Melo, M.J.; Maestri, M.; Passaniti, P.; Balzani, V.; *J. Am. Chem. Soc.* **2000**, *122*, 4496.

113. Bergamini, G.; Saudan, C.; Ceroni, P.; Maestri, M.; Balzani, V.; Gorka, M.; Lee, S.-K.; van Heyst, J.; Vögtle, F.; *J. Am. Chem. Soc.* **2004**, *126*, 16466.

114. Furtado, L.F.O.; Alexiou, A.D.P.; Gonçalves, L.; Toma, H.E.; Araki, K., *Angew. Chem. Int. Ed.* **2006**, *45*, 3143.

115. Akasawa M.; Ashton, P.R.; Balzani, V.; Credi, A.; Mattersteig, G.; Matthews, O.A.; Montalti, M.; Spencer, N.; Stoddart, J.F.; Venturi, M.; *Chem. Eur. J.* **1997**, *3*, 1992.

116. a) Shiraishi, Y.; Tokitoh, Y.; Hirai, T.; *Chem. Commun.* **2005**, 5316. b) de Silva, A.P.; McClenaghan, N.D.; *Chem. Eur. J.* **2002**, *8*, 4935. c) Banthia, S.; Samanta, A.; *Eur. J. Org. Chem.* **2005**, 4967.

117. de Sousa, M.; Kluciar, M.; Abad, S.; Miranda, M.A.; de Castro, B.; Pischel, U.; *Photochem. Photobiol. Sci.* **2004**, *3*, 639.

118. a) Saghatelian, A.; Völcker, N.H.; Guckian, K.M.; Lin, V.S.-Y.; Ghadiri, M.R.; *J. Am. Chem. Soc.* **2003**, *125*, 346. b) Tang, Y.; He, F.; Wang, S.; Li, Y.; Zhu, D.; Bazan, G.C.; *Adv. Mater.* **2006**, *18*, 2105.

119. Gunnlaugsson, T.; Mac Dónail, D.A.; Parker, D.; *Chem. Commun.* **2000**, 93.

120. De Silva, A.P.; McClenaghan, N.D.; *J. Am. Chem. Soc.* **2000**, *122*, 3965.

121. Qu, D.-H.; Wang, Q.-C.; Tian, H.; *Angew. Chem. Int. Ed.* **2005**, *44*, 5296.

122. Kou, S.; Lee, H.N.; van Noort, D.; Swamy, K.M.K.; Kim, S.H.; Soh, J.H.; Lee, K.-M.; Nam, S.-W.; Yoon, J.; Park, S.; *Angew. Chem. Int. Ed.* **2008**, *47*, 872.

123. a) Zhou, Y.; Wu, H.; Qu, L.; Zhang, D.; Zhu, D.; *J. Phys. Chem. B* **2006**, *110*, 15676. b) Sun, W.; Xu, C.-H.; Zhu, Z.; Fang, C.-J.; Yan, C.-H.; *J. Phys. Chem. C* **2008**, *112*, 16973.

124. Zhang, L.; Whitfield, W.A.; Zhu, L.; *Chem. Commun.* **2008**, 1880.

125. Andréasson, J.; Kodis, G.; Terazono, Y.; Liddell, P.A.; Bandyopadhyay, S.; Mitchell, R.H.; Moore, T.A.; Moore, A.L.; Gust, D.; *J. Am. Chem. Soc.* **2004**¸*126*, 15926.

126. Guo, X.; Zhang, D.; Zhang, G.; Zhu, D.; *J. Phys.Chem. B* **2004**, *108*, 11942.

127. Liu, Y.; Jiang, W.; Zhang, H.-Y.; Li, C.-J.; *J. Phys. Chem. B* **2006**, *110*, 14231.

SPICUM servicio de publicaciones

128. Margulies, D.; Melman, G.; Felder, C.E.; Arad-Yellin, R.; Shanzer, A.; *J. Am. Chem. Soc.* **2004**, *126*, 15400.

129. Andréasson, J.; Straight, S.D.; Kodis, G.; Park, C.D.; Hambourger, M.; Gervaldo, M.; Albinsson, .; Moore, T.A.; Moore, A.L., Gust, D.; *J. Am. Chem. Soc.* **2006**, *128*, 16259.

130. Langford, S.J.; Yann, T.; *J. Am. Chem. Soc.* **2003**, *125*, 11198.

131. Coskun, A.; Deniz, E.; Akkaya, E.U.; *Org. Lett.* **2005**, *7*, 5187.

132. a) Li, F.; Shi, M.; Huang, C.; Jin, L.; *J. Mater. Chem.* **2005**, *15*, 3015. b) Pischel, U.; *Angew. Chem. Int. Ed.* **2007**, *46*, 4026.

133. Remacle, F.; Speiser, S.; Levine, R.D.; *J. Phys. Chem. B* **2001**, *105*, 5589.

134. Margulies, D.; Melman, G.; Shanzer, A.; *J. Am. Chem. Soc.* **2006**, *128*, 4865.

135. Lederman, H.; Macdonald, J.; Stefanovic, D.; Stojanovic, M.N.; *Biochemistry* **2006**, *45*, 1194.

136. a) Kuznetz, O.; Salman, H.; Shakkour, N.; Eichen, Y.; Speiser, S.; *Chem. Phys. Lett.* **2008**, *451*, 63. b) Kuznetz, O.; Salman, H.; Eichen, Y.; Remacle, F.; Levine, R.D.; Speiser, S.; *J. Phys. Chem. C* **2008**, *112*, 15880.

137. Ogasawara, S.; Kyoi, Y.; Fujimono, K.; *ChemBioChem* **2007**, *8*, 1520.

138. Remacle, F.; Weinkauf, R.; Levine, R.D.; *J. Phys. Chem. A* **2006**, *110*, 177.

139. Konry, T.; Walt, D.R.; *J. Am. Chem. Soc.* **2009**, *131*, 13232.

140. Andréasson, J.; Straight, S.D.; Bandyopadhyay, S.; Mitchel, R.H.; Moore, T.A.; Moore, A.L.; Gust, D.; *Angew. Chem. Int. Ed.* **2007**, *46*, 958.

141. Andréasson, J.; Straight, S.D.; Bandyopadhyay, S.; Mitchell, R.H.; Moore, T.A.; Moore, A.L.; Gust, D.; *J. Phys. Chem. C* **2007**, *111*, 14274.

142. Amelia, M.; Baroncini, M.; Credi, A.; *Angew. Chem. Int. Ed.* **2008**, *47*, 6240.

143. De Silva, A.P.; Dobbin, C.M.; Vance, T.P.; Wannalerse, B.; *Chem. Commun.* **2009**, 1386.

144. PASS 0 and PASS 1 are defined as two single-input, single-output binary gates with Out = 0 for any In value (PASS 0) or Out = 1 for any In value (PASS 1). More information: De Silva, A.P.; James, M.R.; McKinney, B.O.F.; Pears, D.A.; Weir, S.M.; *Nat. Mater.*, **2006**, *5*, 2006.

145. Margulies, D.; Felder, C.E.; Melman, G.; Shanzer, A.; *J. Am. Chem. Soc.* **2007**, *129*, 347.

146. Kumar, S.; Luxami, V.; Saini, R.; Kaur, D.; *Chem. Commun.* **2009**, 3044.

147. Andréasson, J.; Straight, S.D.; Moore, T.A.; Moore, A.L.; Gust, D.; *Chem. Eur. J.* **2009**, *15*, 3936.

148. a) Leigh, D.A.; Morales, M.A.F.; Pérez, E.M.; Wong, J.K.Y.; Saiz, C.G.; Slawin, A.M.Z.; Carmichael, A.J.; Haddleton, D.M.; Brouwer, A.M.; Buma, W.J.; Wurpel,

SPICUM servicio de publicaciones

G.W.H.; León, S.; Zerbetto, F.; *Angew. Chem. Int. Ed.* **2005**, *44*, 3062. b) Gupta, T.; van der Boom, M.E.; *Angew. Chem. Int. Ed.* **2008**, *47*, 5322.

149. Budyka, M.F.; Potashova, N.I.; Gavrishova, T.N.; Lee, V.M.; *J. Mater. Chem.* **2009**, *19*, 7721.

150. IMPLICATION (IMPL) is defined as the inverse of the INHIBIT (INH) logic gate.

151. a) Corbin, T.F.; Hahn, R.C.; Shechter, H.; *Org. Synth. Coll.* **1973**, *5*, 328. b) Salir, A.; *Org. Synth. Coll.* **1973**, *5*, 825.

152. Hendrickson, J.B.; de Vries, J.G.; *J. Org. Chem.* **1985**, *50*, 1688.

153. Goes, M.; Lauteslager, X.Y.; Verhoeven, J.W.; Hofstraat, J.W.; *Eur. J. Org. Chem.* **1998**, 2373.

154. Landauer, R.; *IBM J. Res. Develop.* **1961**, *5*, 183.

155. Rehm, D.; Weller, A.; *Isr. J. Chem.* **1970**, *8*, 259.

156. Armarego W.L.F.; Chai,.C.L.L., *Purification of Laboratory Chemicals 5th Ed.*, Ed. Elsevier Butterworth-Heinemann, Oxford, **2003**.

157. Guziec, F.S.; Wei, D.; *J. Org. Chem.* **1992**, *57*, 3772.

158. Woscholski, R.; Hailes, H.; Numbere, M.; Rosivatz, E.; *PCT Int. Appl. 2006097744*, **21 Sep 2006**.

SPICUM servicio de publicaciones

SPICUM
servicio de publicaciones

APPENDIX I

BOOLEAN LOGIC AND REVERSIBILITY

SPICUM
servicio de publicaciones

SPICUM
servicio de publicaciones

In the middle of the 19th century, George Boole, an English mathematician and philosopher, defined an algebraic system, known as Boolean algebra, where he stablished the mathematical treatment of logic.
With the advent of digital computation in the 20th century, this mathematics area has been widely used in devices and switches design, being the basis of the digital electronics development.

The logical propositions are based in the fact that only can take two possible values (called Yes/Not or True/False) as answer to a given question (with two possible values too). This way, the Boolean logic is a mathematical system using binary digits 0 and 1 (false/true or not/yes), as well as the used in computation. The logical response (called output) to their different combination (called input) is given *via* logical operators.

The logical operators, moved to the digital circuit design, are defined as *logic gates* where every possible input-output behaviour can be modeled by a Boolean expression. The Boolean algebra only use three logical operators, AND, OR and NOT. However, with the judicious combination of these logical operators is possible to design any other Boolean operator. These logic gates, defined apart from the classical ones, can be

SPICUM servicio de publicaciones

used by themselves and have been incorporated into the Boolean logic definition as XOR logic gates, and the inverse YES, NAND, NOR or XNOR. With the combination of this main logic gates, is possible to define a serie of logic systems with operation by themselves as INH, Half-Adder, Half-Subtractor, Full-Adder and Full-Subtractor as well as especifical systems.

The set formed by the input-output relationship defined by each logic gate, can be expressed with a table called *truth table* where the logic propositions are clearly shown in form of binary digits.

In_1	In_2	Out
0	0	0
0	1	0
1	0	0
1	1	1

This truth table represents the AND function and show all the possible combinations of on/off input states (the two first columns), and the result of this combination (output) depending on the logic gate we are talking about (the third column). This way, the output is only in *"on"* state (Out = 1) when In_1 and In_2 is *"on"* ($In_1 + In_2 = 1$).

All the Boolean logic has direct application to physical devices and for this reason there is a convention of symbols, defined by ANSI/IEEE (American National Standards Institute / Institute of Electrical and Electronics Engineers) Std 91/1984 and its supplement Std 91a/1991, used by researchers and developers to draw circuitry schemes.

These symbols, readed from left to right represent a two-inputs OR logic gate (left) and a three-inputs AND logic gate. The sticks going in and out these symbols represent the input and output of the system and can be connected one with others *via* wires, making complexes operational devices this way.

SPICUM servicio de publicaciones

The operation of switches and all the devices made with them have the handicap that information processing, like all processes, is inevitably accompanied by a certain minimum amount of heat generation.

The heat generation is a characteristic side effect of irreversible logic systems. This way, reversible computing is a main goal in the devices development. Its operating way improves the energy efficiency to the top that a totally reversible logic gate, theoretically avoids energy dissipation because a logically reversible process involves a physically reversible behaviour.
In terms of molecular logic gates, a system is logically reversible when the output present no degeneracy states compared with the input, this is, it's possible to unequivocally know the input state only studying the output of the system.

There have been defined several reversible logic gates depending on the number of inputs and outputs considered as the Feynman gate that has two inputs and two outputs and the Fredkin gate, presenting three inputs and three outputs. It is also possible to stablish a universal reversible logic series with the use of the Toffoli gates. This means that is possible to use Toffoli gates to build systems that will perform any Boolean function in a reversible manner and with a significant improve efficiency.

SPICUM servicio de publicaciones

SPICUM
servicio de publicaciones

APPENDIX II.

^{1}H-NMR AND ^{13}C-NMR SPECTRA

SPICUM
servicio de publicaciones

SPICUM
servicio de publicaciones

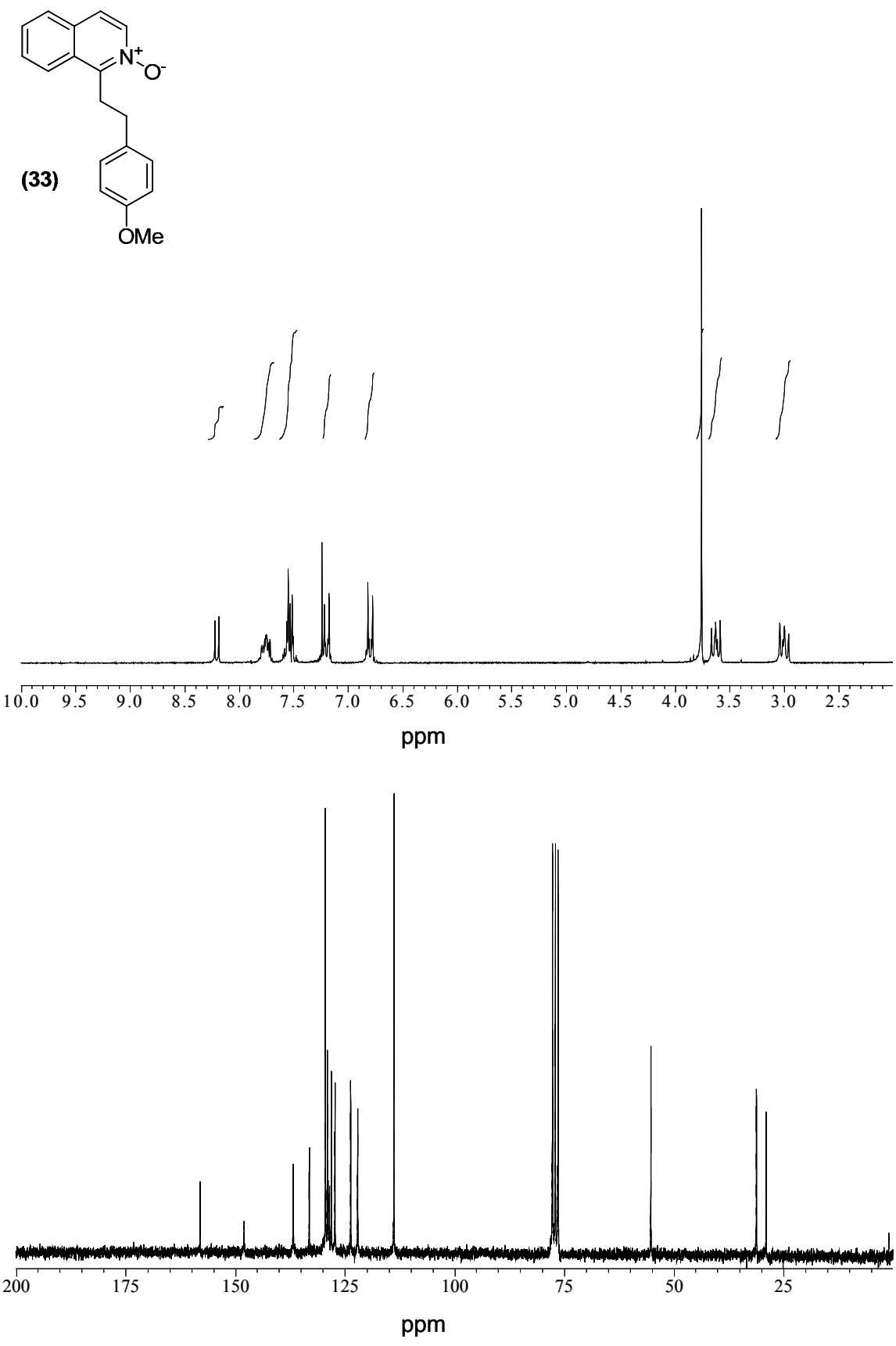

^{1}H-NMR and ^{13}C-NMR in $CDCl_3$ of **(33)**

SPICUM servicio de publicaciones

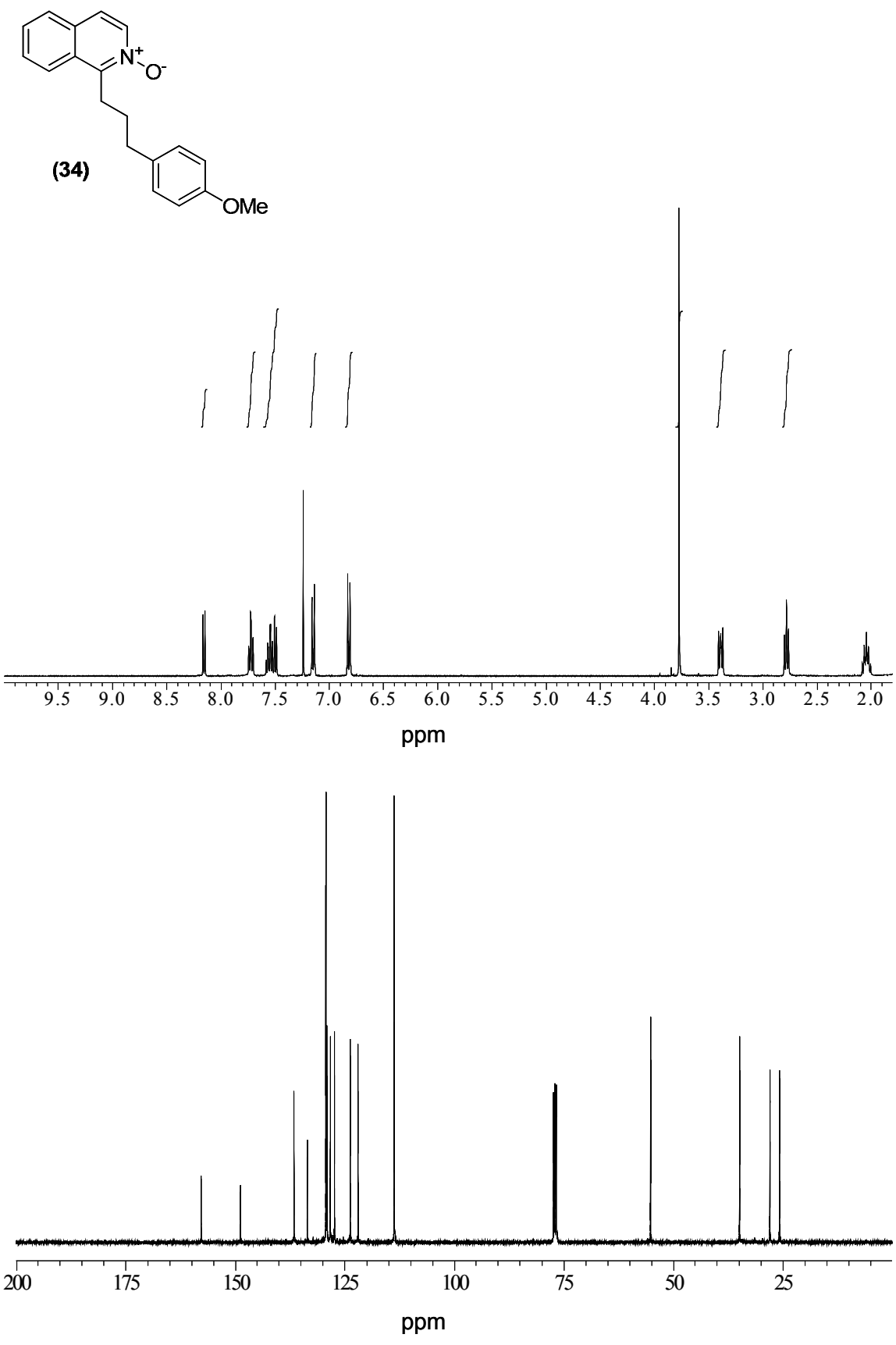

^{1}H-NMR and ^{13}C-NMR in $CDCl_3$ of **(34)**

SPICUM servicio de publicaciones

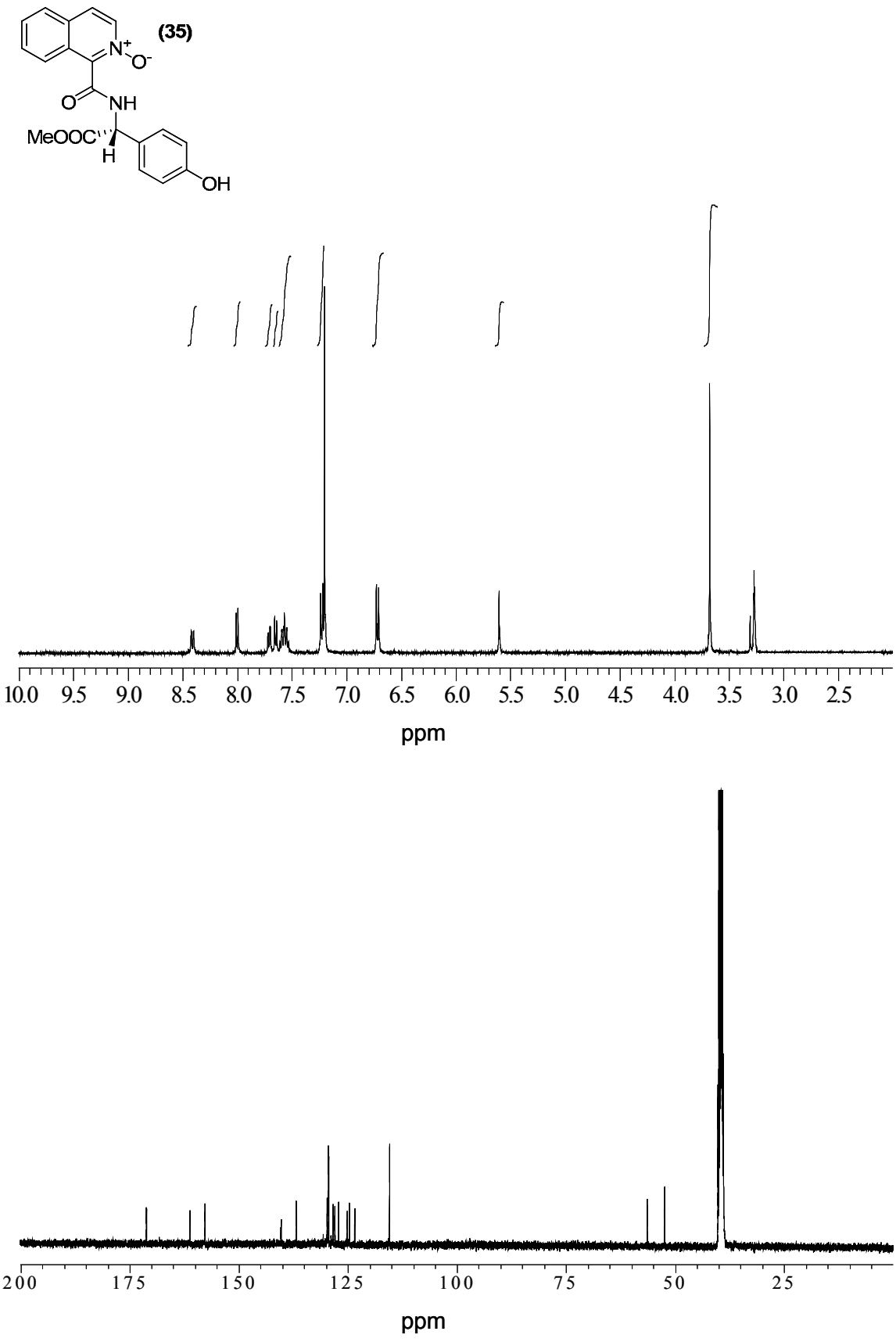

^{1}H-NMR in $CDCl_3$ and ^{13}C-NMR in *DMSO-d_6* of **(35)**

SPICUM servicio de publicaciones

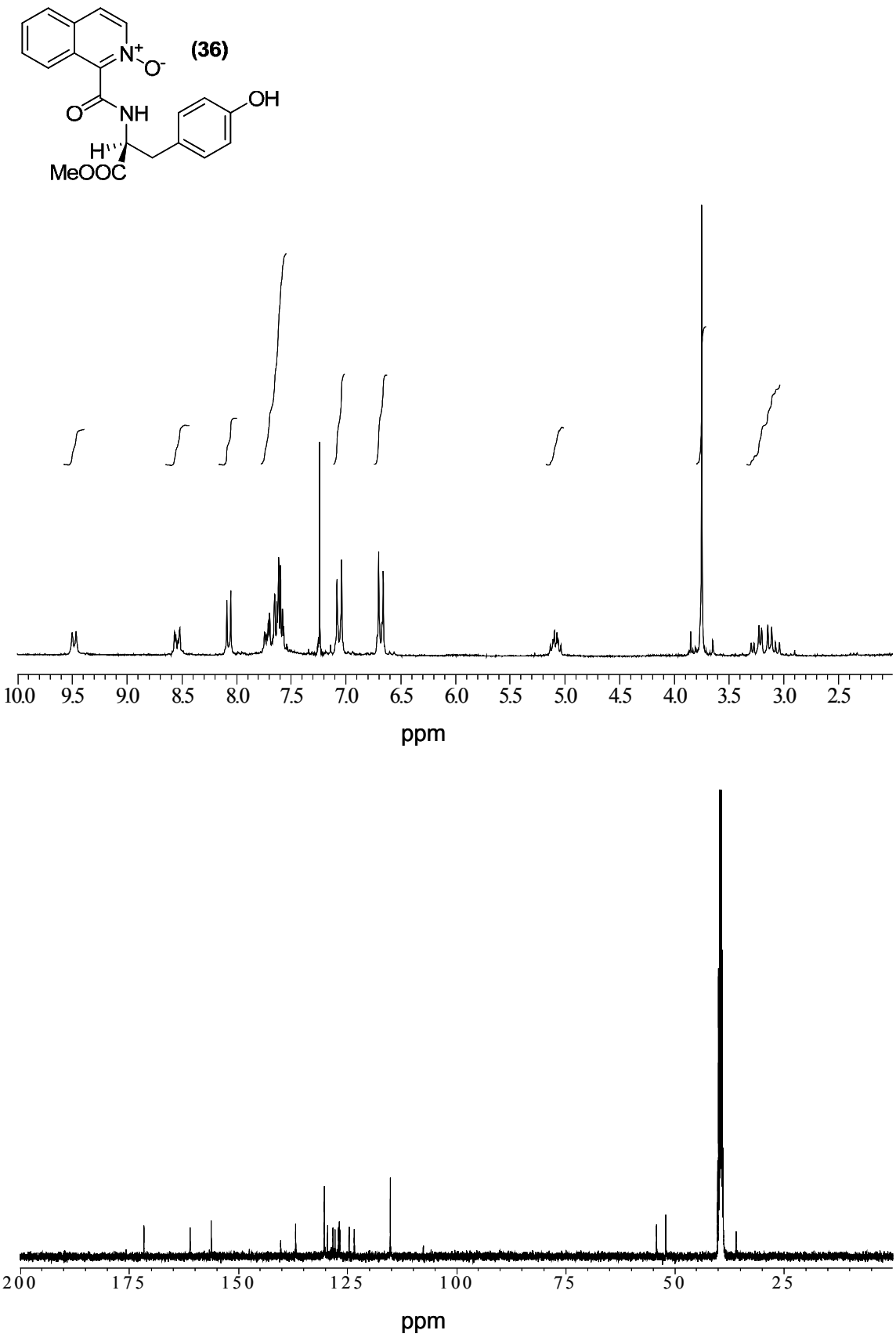

^{1}H-NMR in $CDCl_3$ and ^{13}C-NMR in DMSO-d_6 of **(36)**

SPICUM servicio de publicaciones

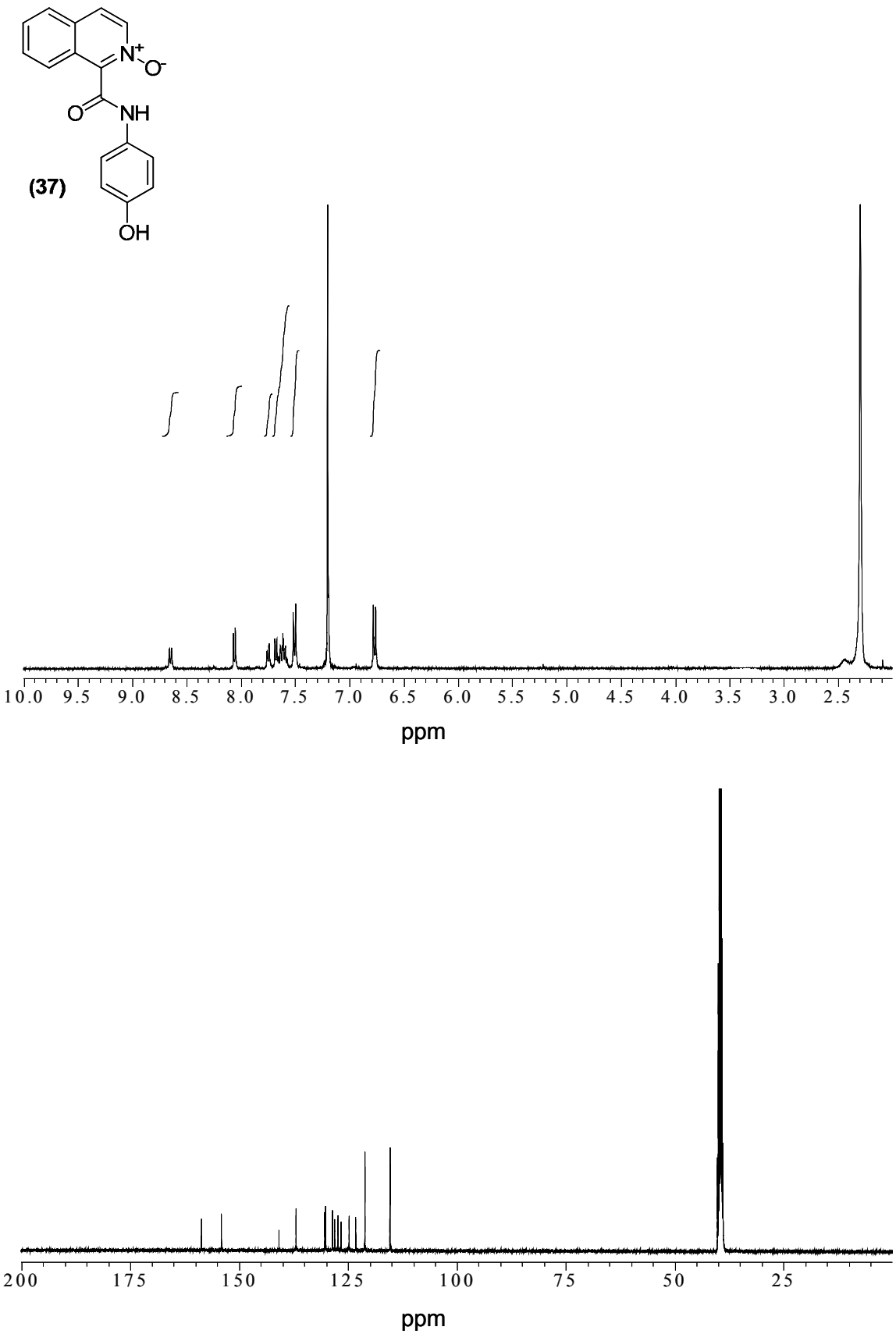

^{1}H-NMR in $CDCl_3$ and ^{13}C-NMR in DMSO-d_6 of **(37)**

SPICUM servicio de publicaciones

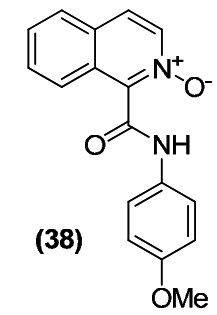

(38)

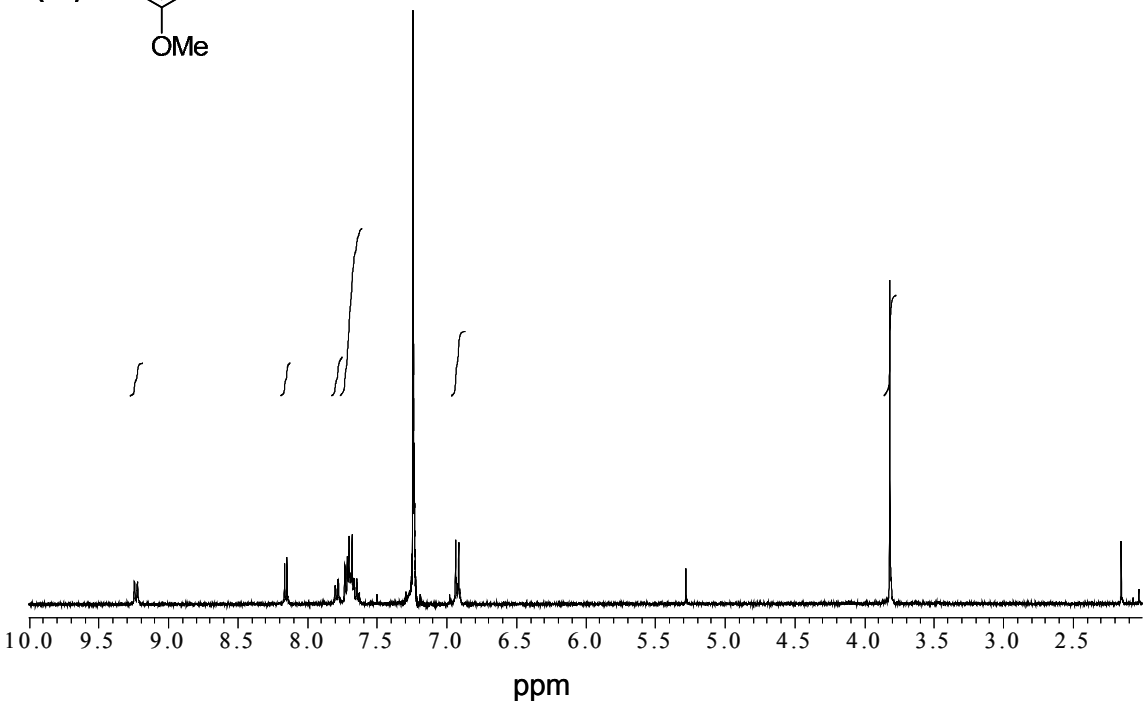

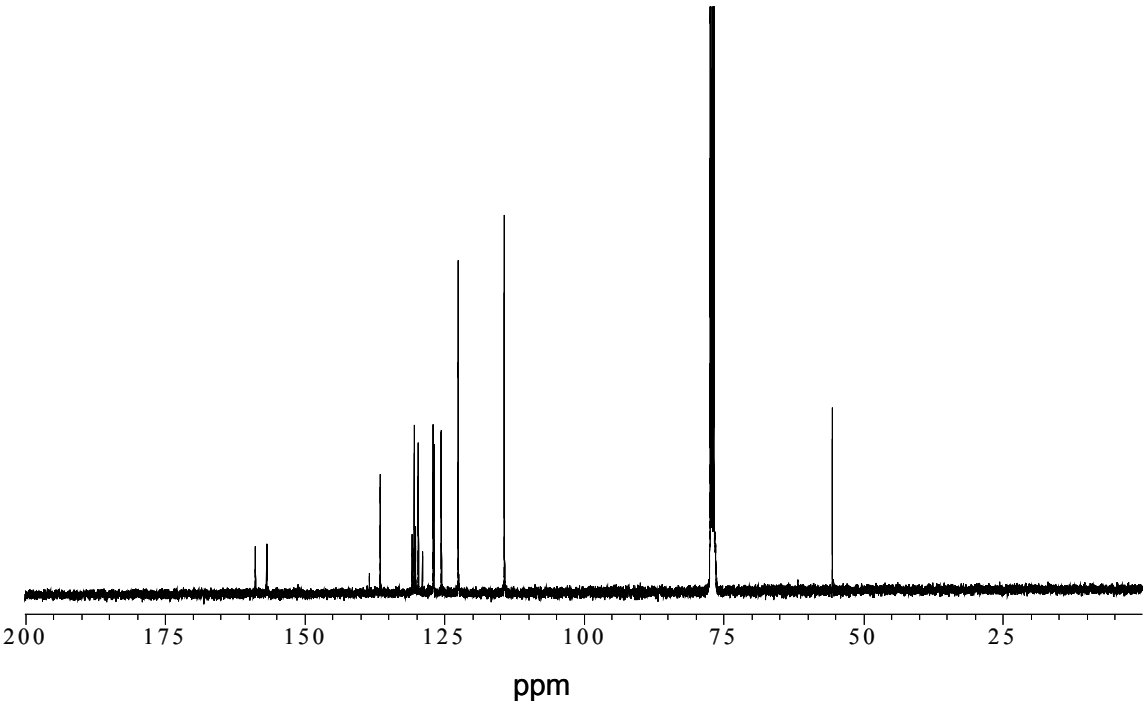

^{1}H-NMR and ^{13}C-NMR in $CDCl_3$ of **(38)**

SPICUM servicio de publicaciones

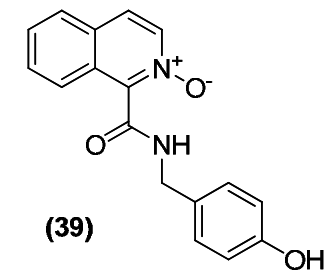

(39)

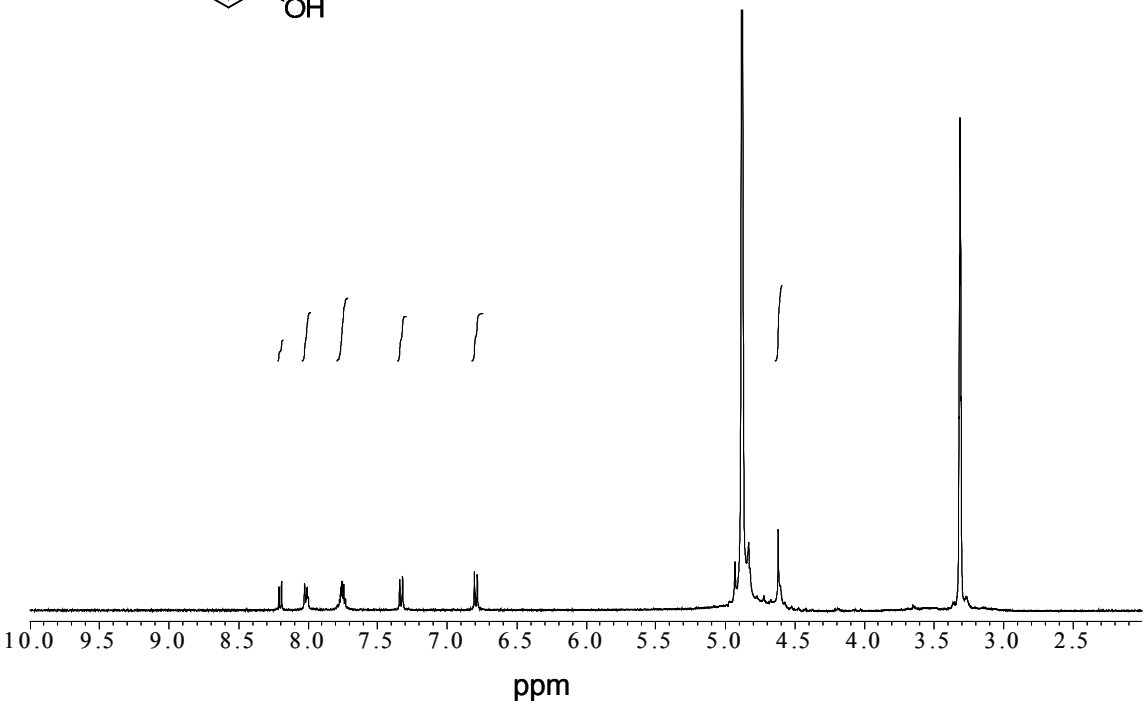

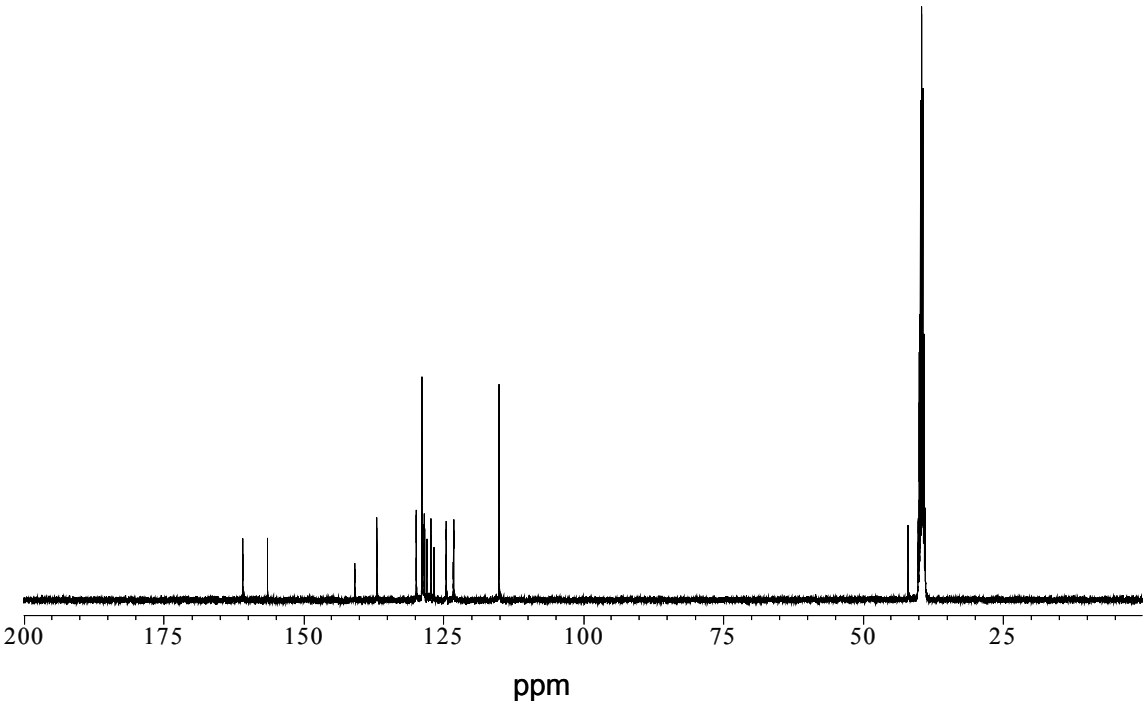

^{1}H-NMR in CD_3OD and ^{13}C-NMR in DMSO-d_6 of **(33)**

SPICUM servicio de publicaciones

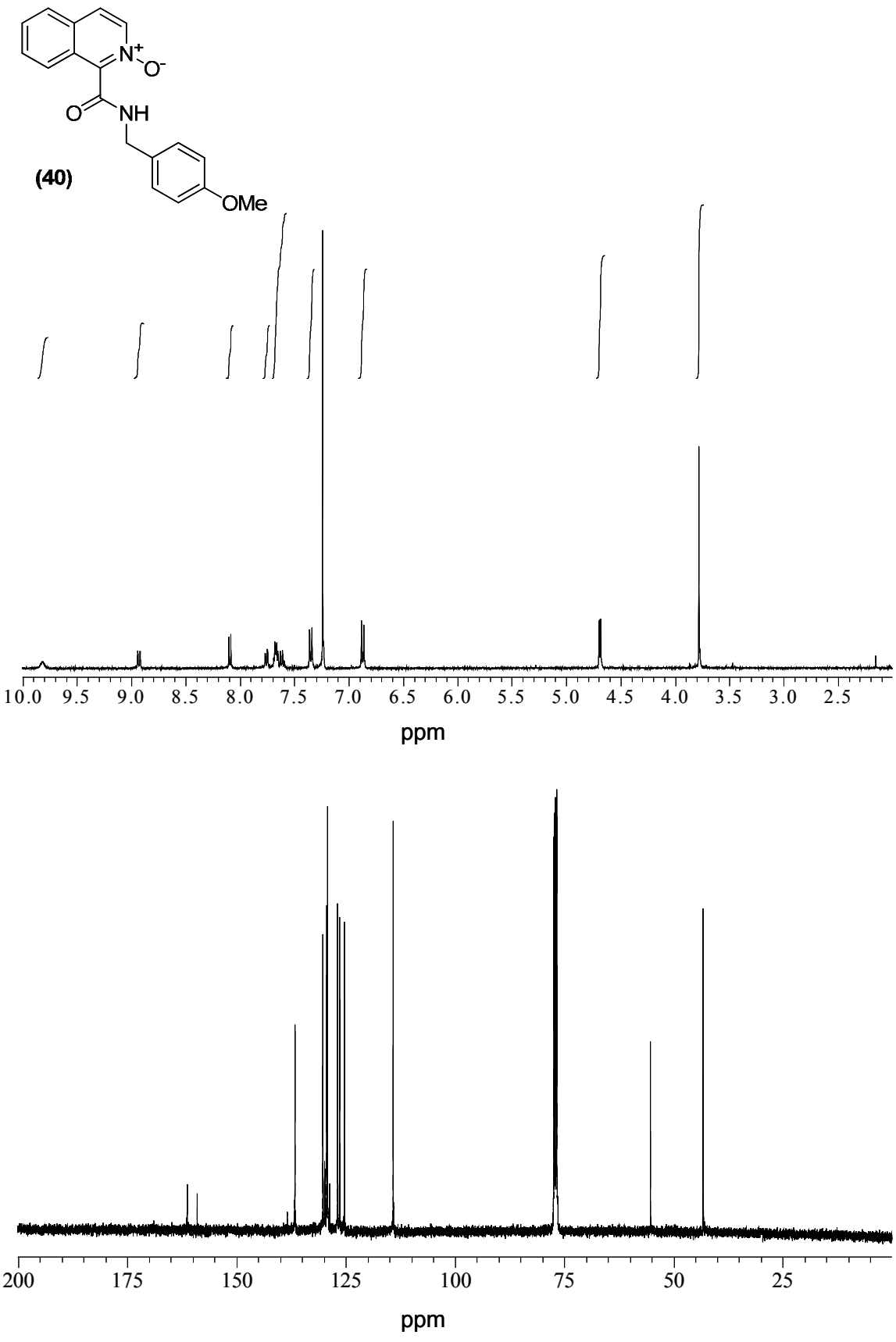

^{1}H-NMR and ^{13}C-NMR in $CDCl_3$ of **(40)**

SPICUM servicio de publicaciones

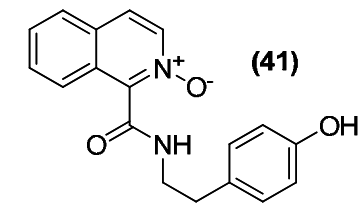

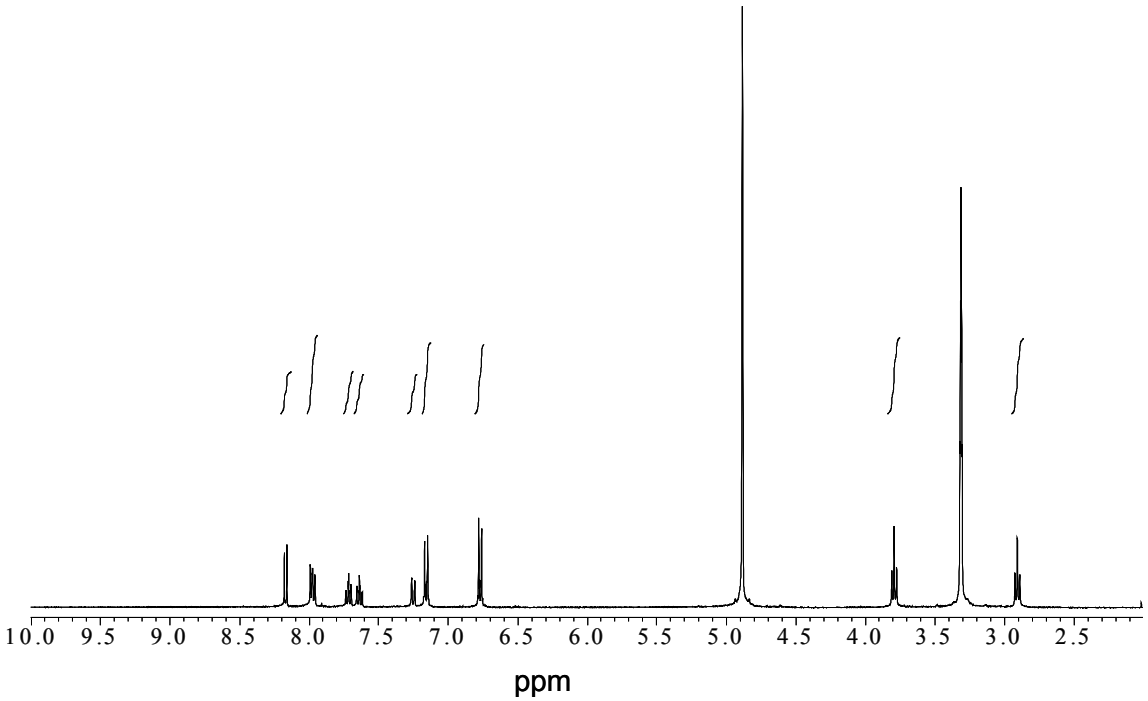

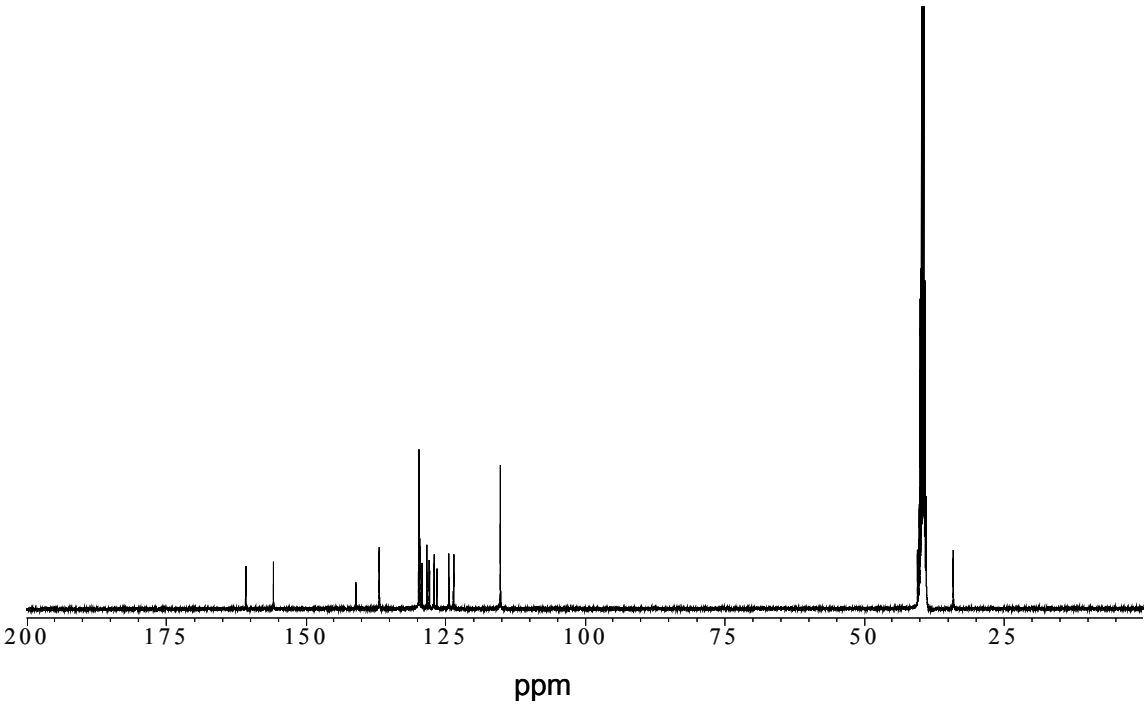

^{1}H-NMR in CD_3OD and ^{13}C-NMR in DMSO-d_6 of **(41)**

SPICUM servicio de publicaciones

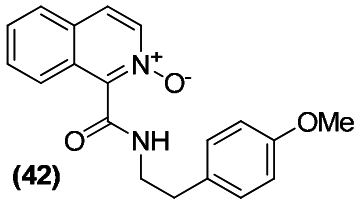

(42)

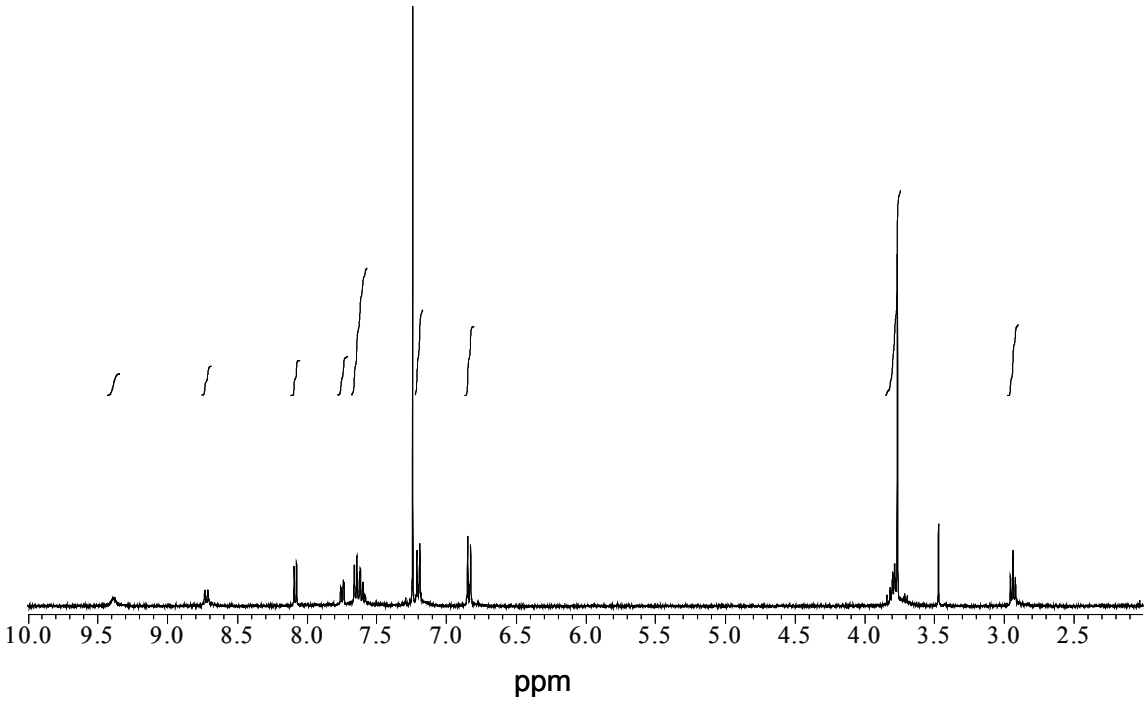

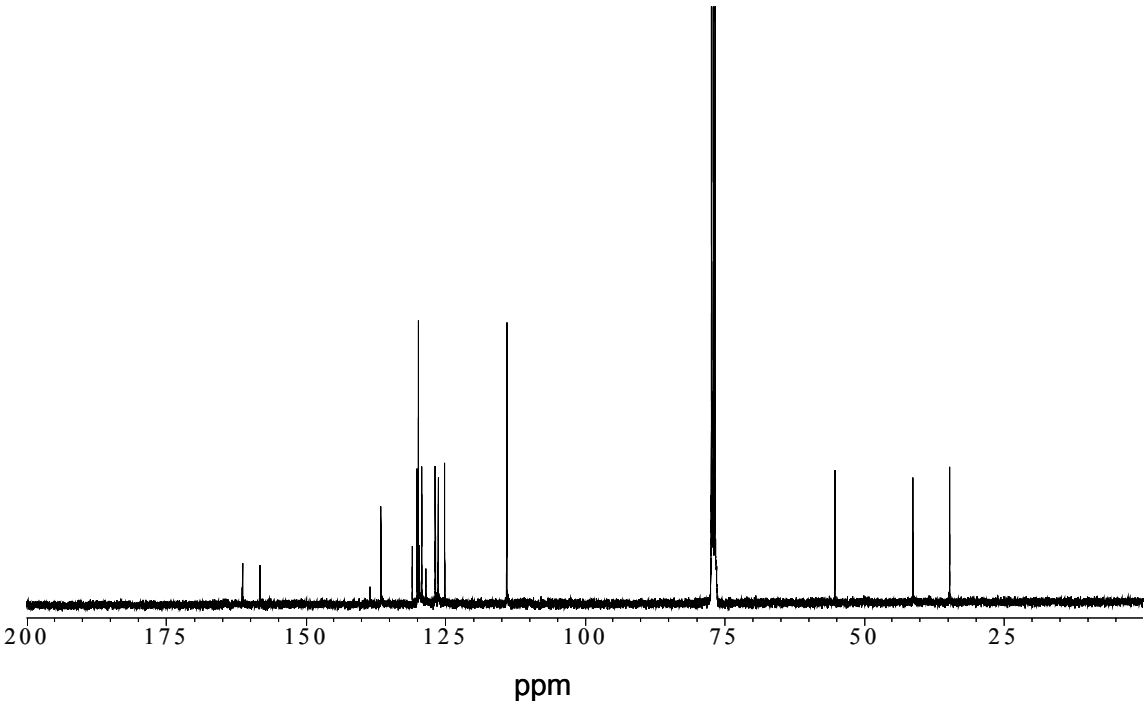

^{1}H-NMR and ^{13}C-NMR in $CDCl_3$ of **(42)**

SPICUM servicio de publicaciones

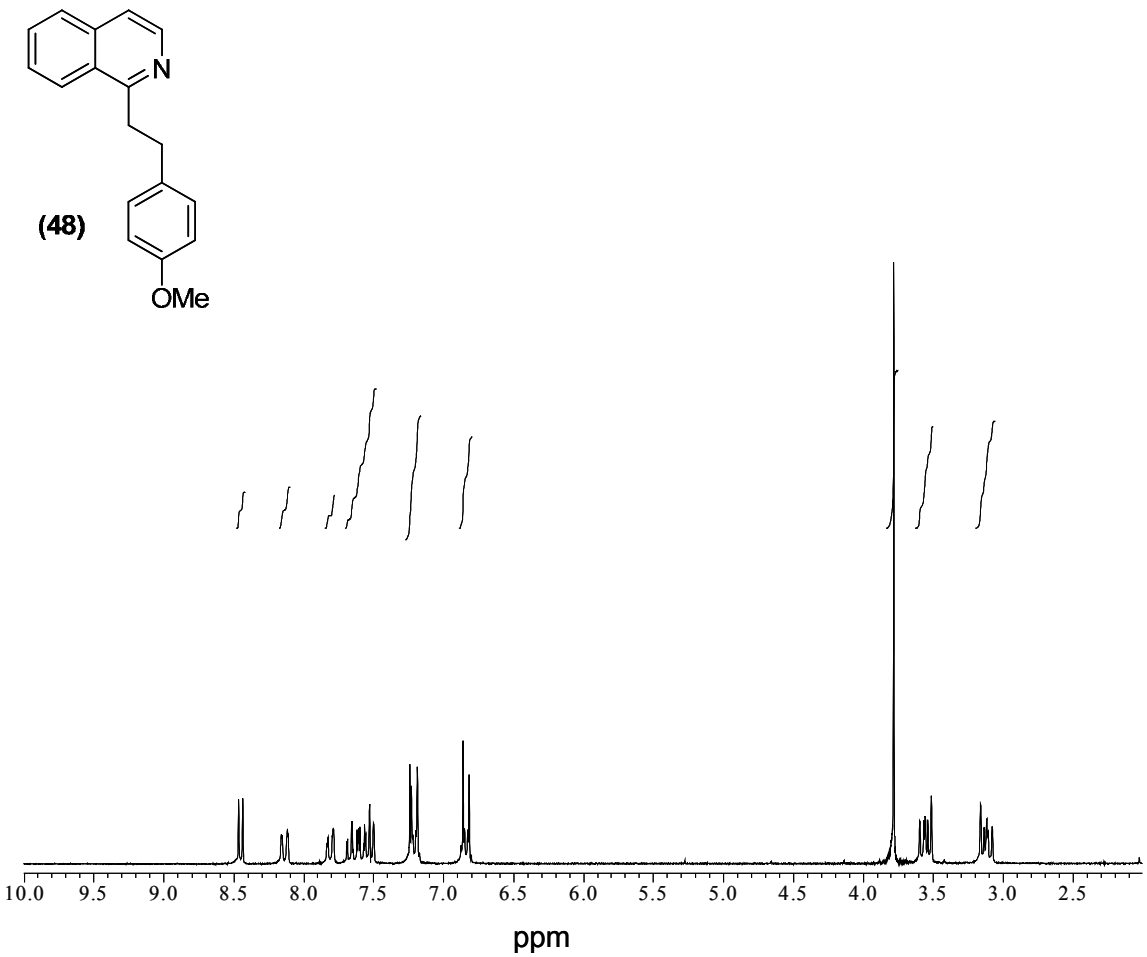

^{1}H-NMR and ^{13}C-NMR in $CDCl_3$ of **(48)**

SPICUM servicio de publicaciones

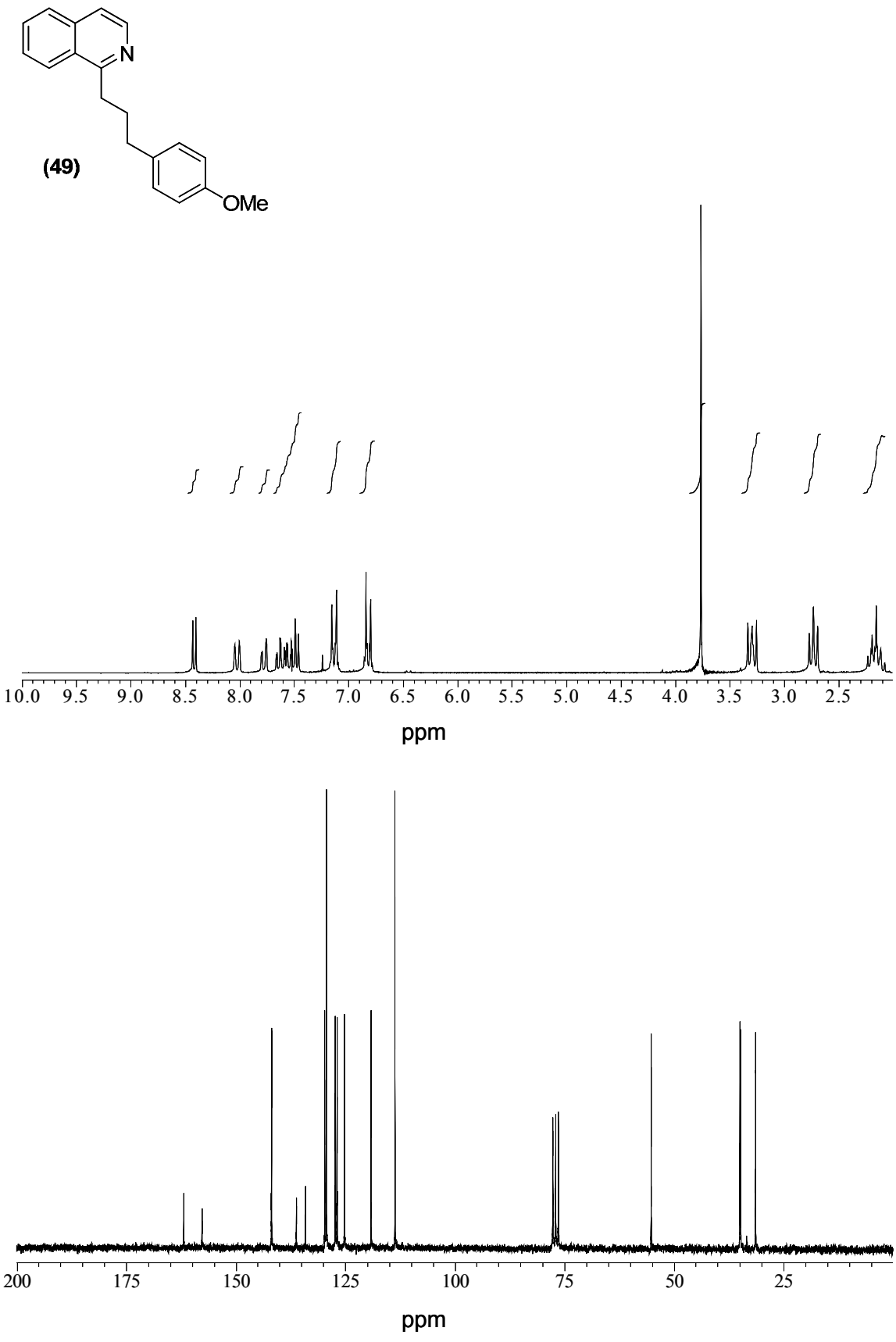

^{1}H-NMR and ^{13}C-NMR in $CDCl_3$ of **(49)**

SPICUM servicio de publicaciones

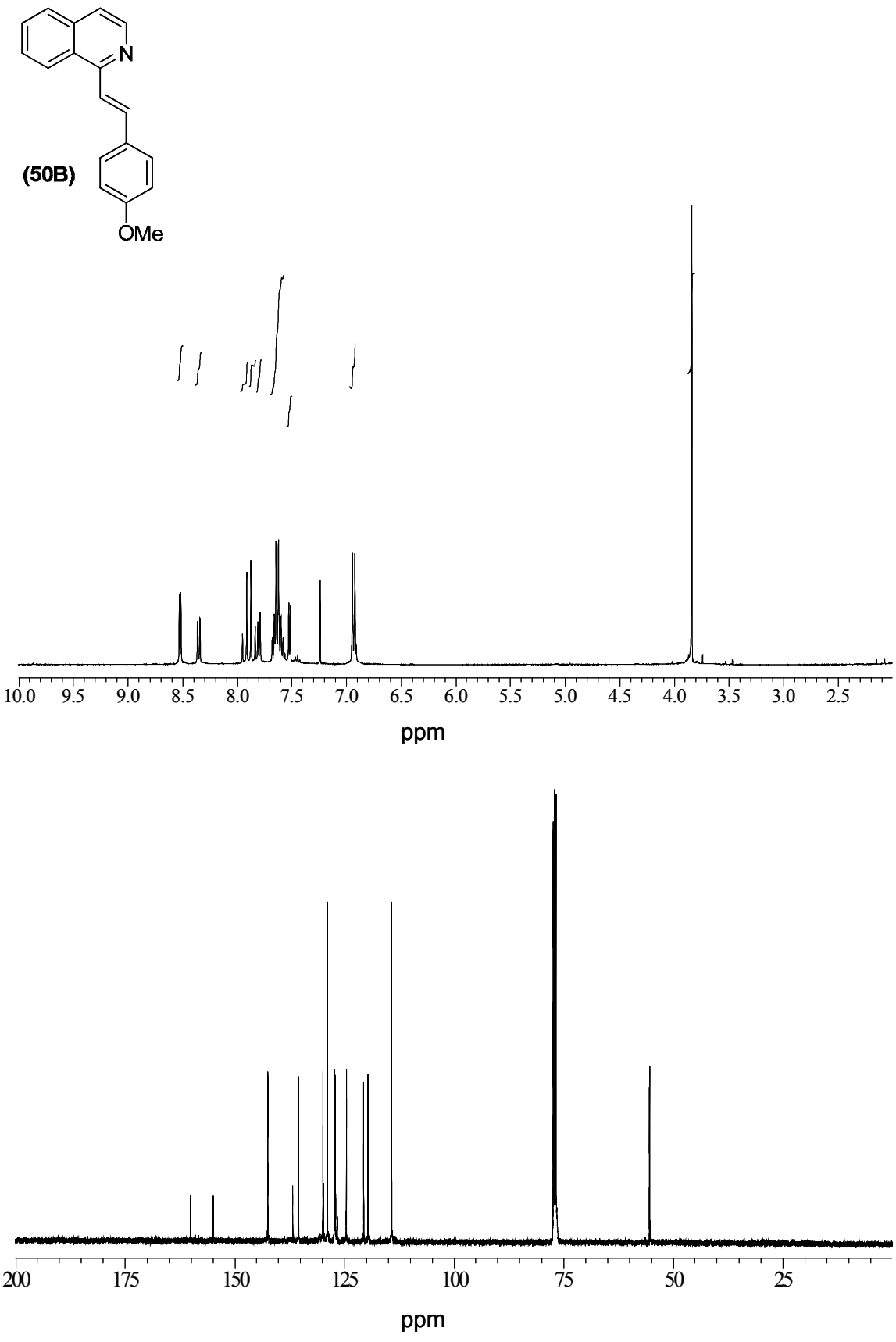

^{1}H-NMR and ^{13}C-NMR in $CDCl_3$ of **(50B)**

SPICUM servicio de publicaciones

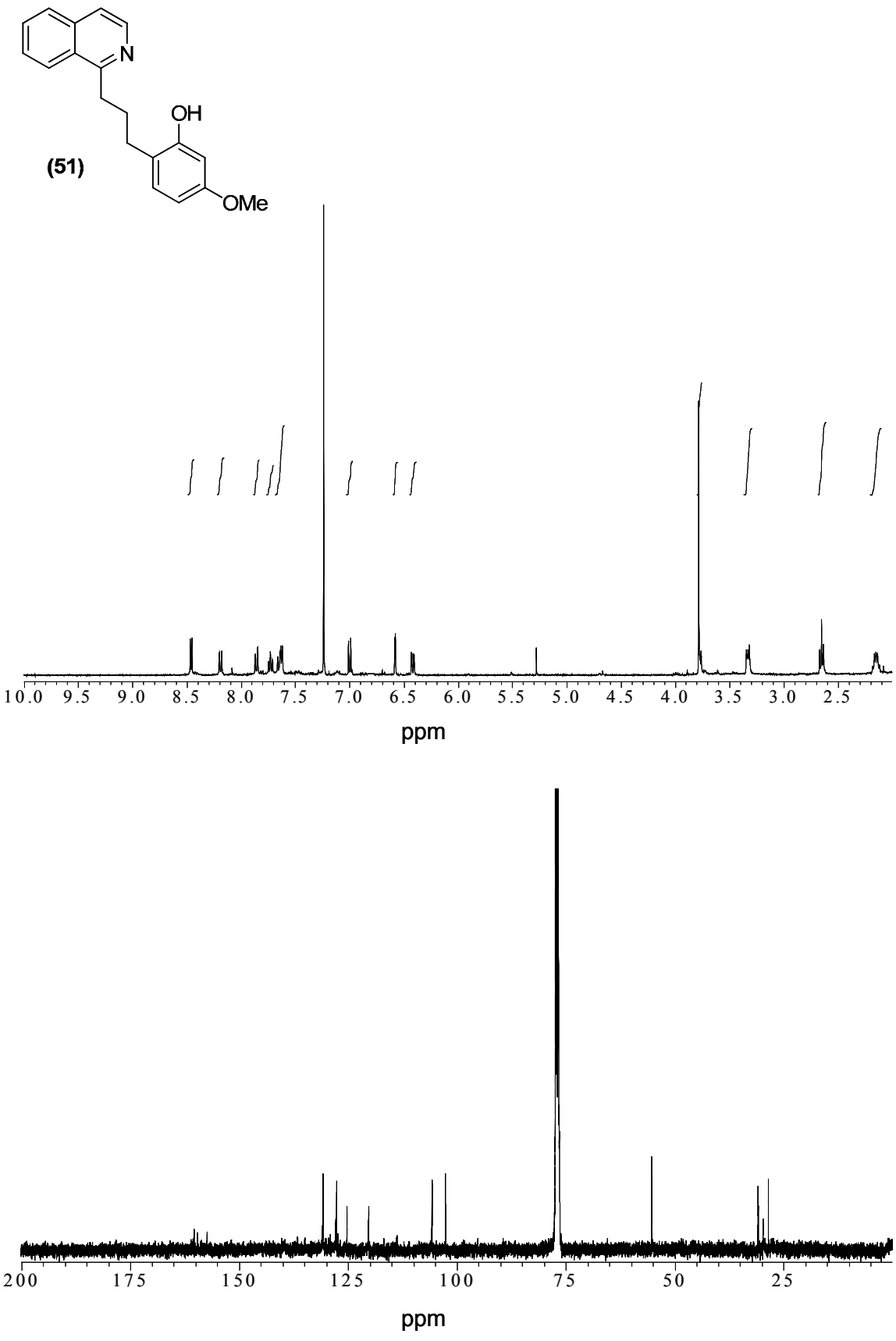

^{1}H-NMR and ^{13}C-NMR in $CDCl_3$ of **(51)**

SPICUM servicio de publicaciones

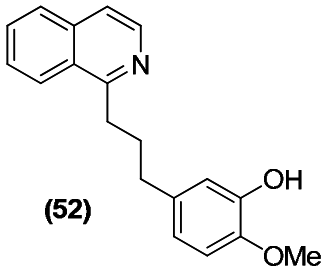

(52)

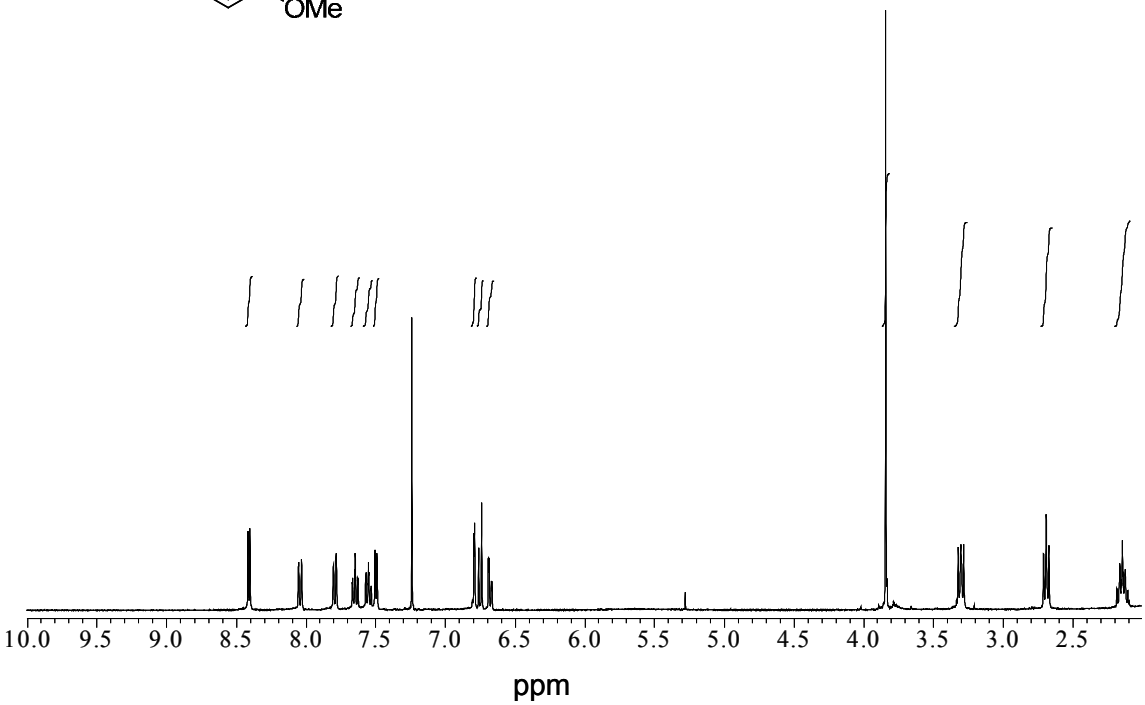

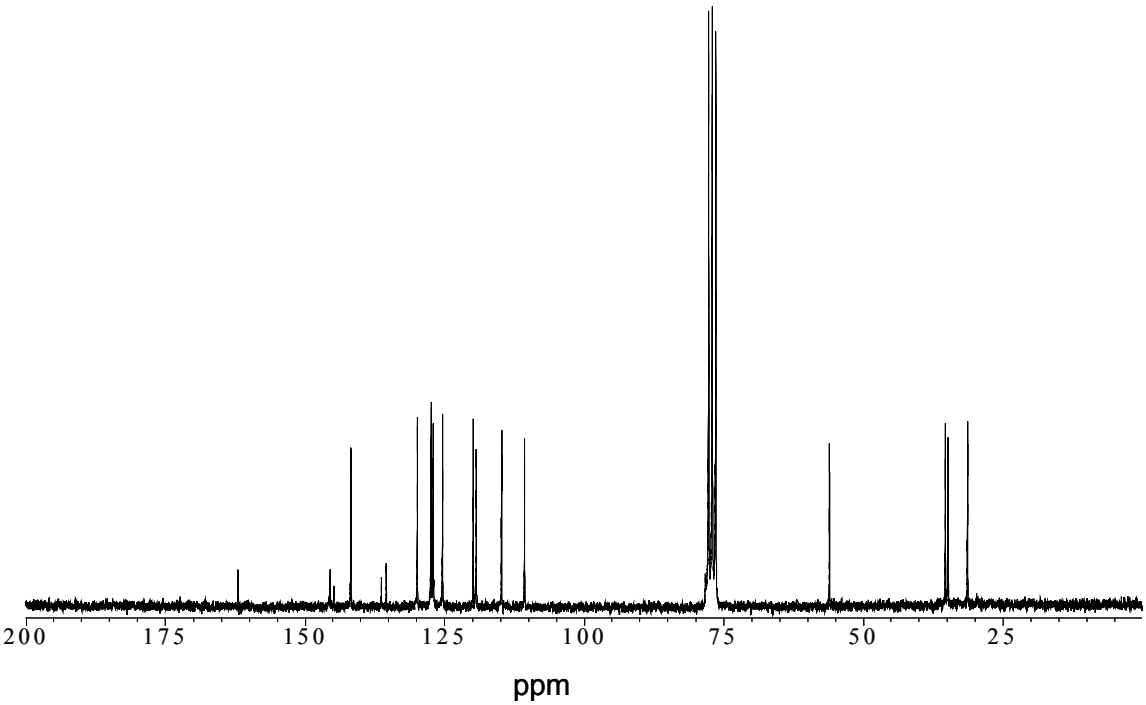

^{1}H-NMR and ^{13}C-NMR in $CDCl_3$ of **(52)**

SPICUM servicio de publicaciones

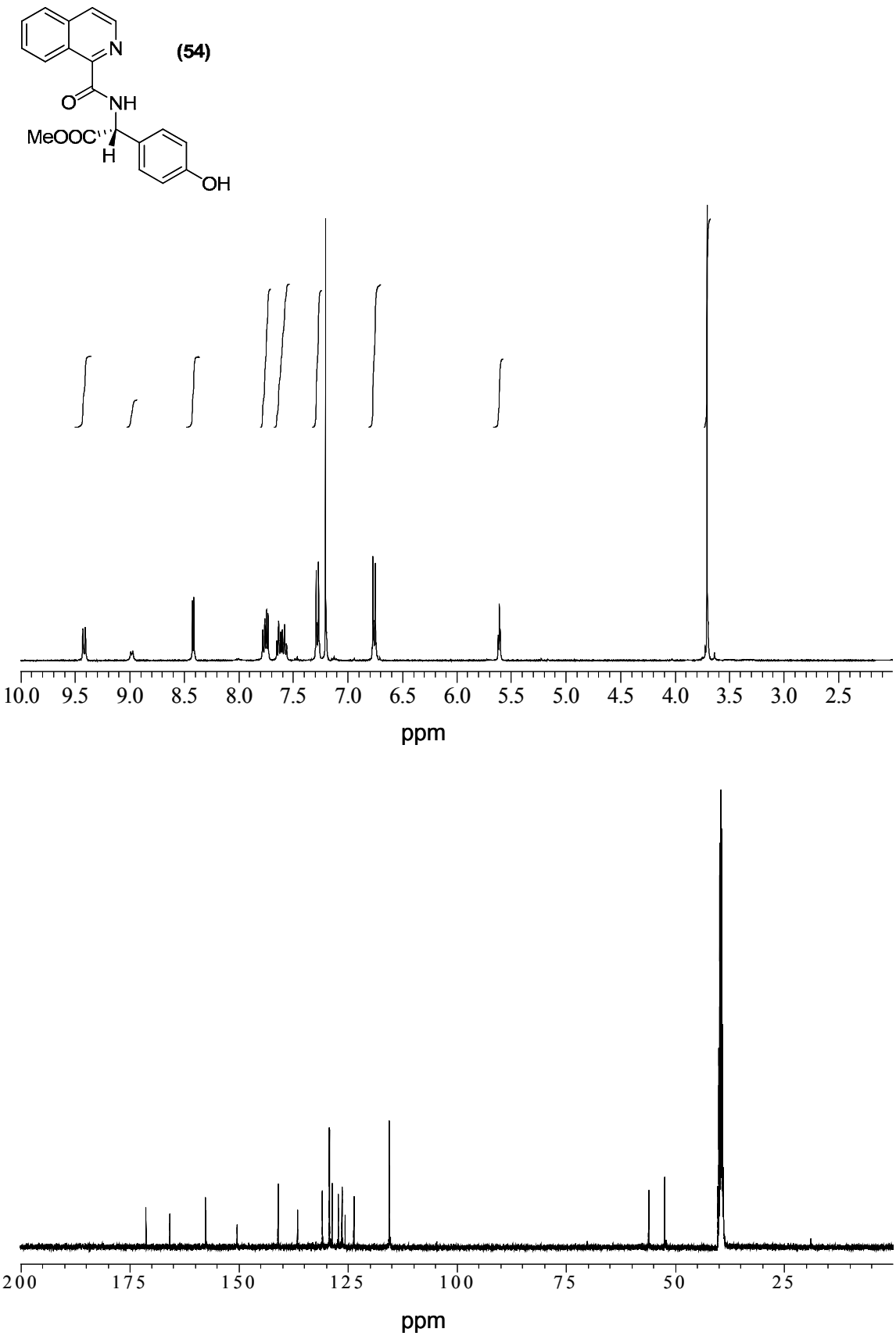

^{1}H-NMR in $CDCl_3$ and ^{13}C-NMR in DMSO-d_6 of **(54)**

SPICUM servicio de publicaciones

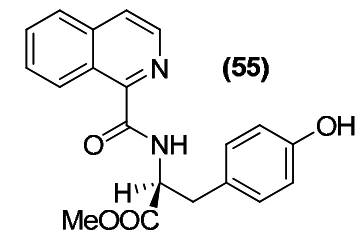

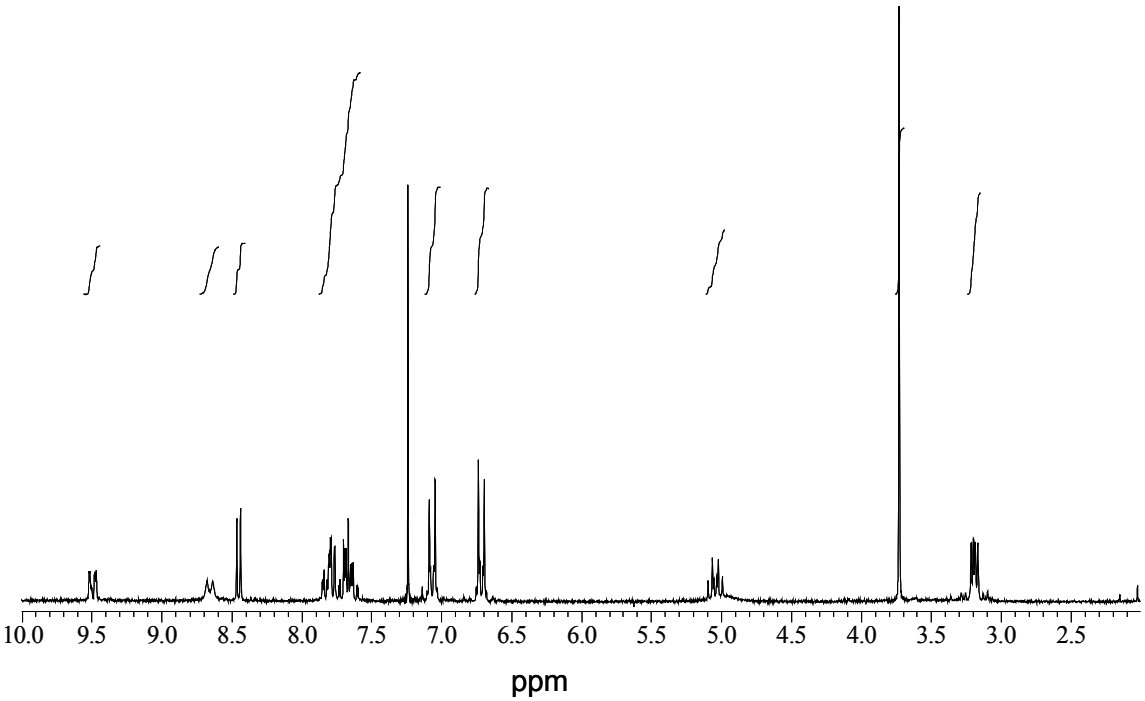

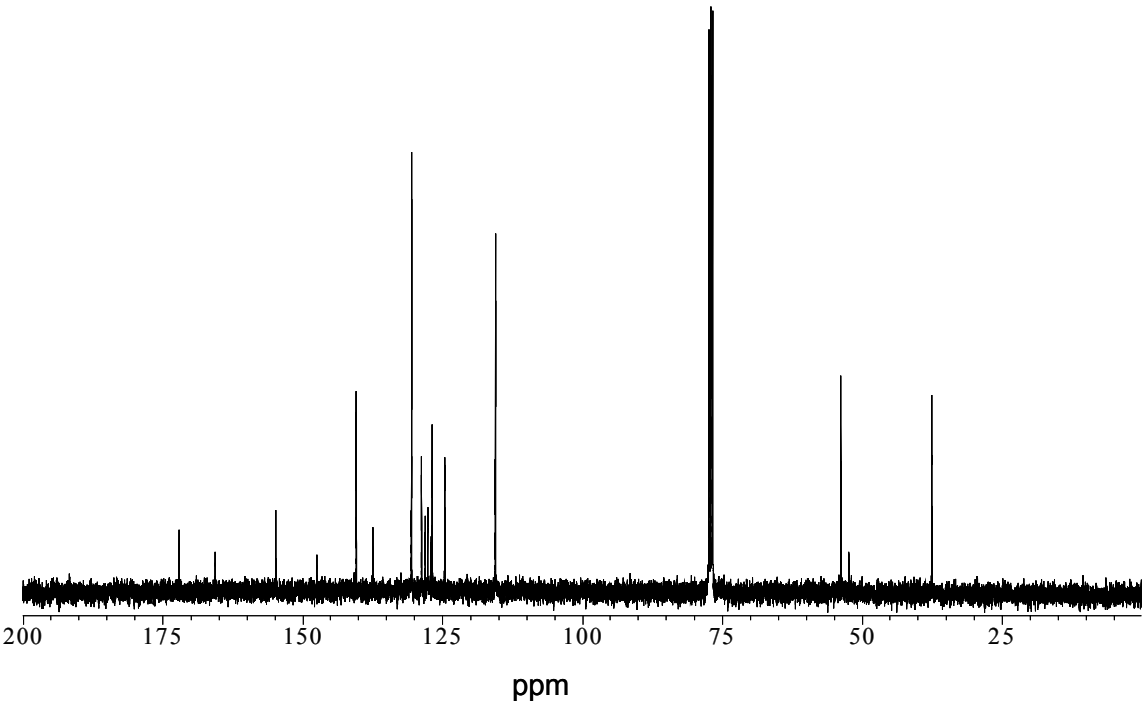

^{1}H-NMR and ^{13}C-NMR in $CDCl_3$ of **(55)**

SPICUM
servicio de publicaciones

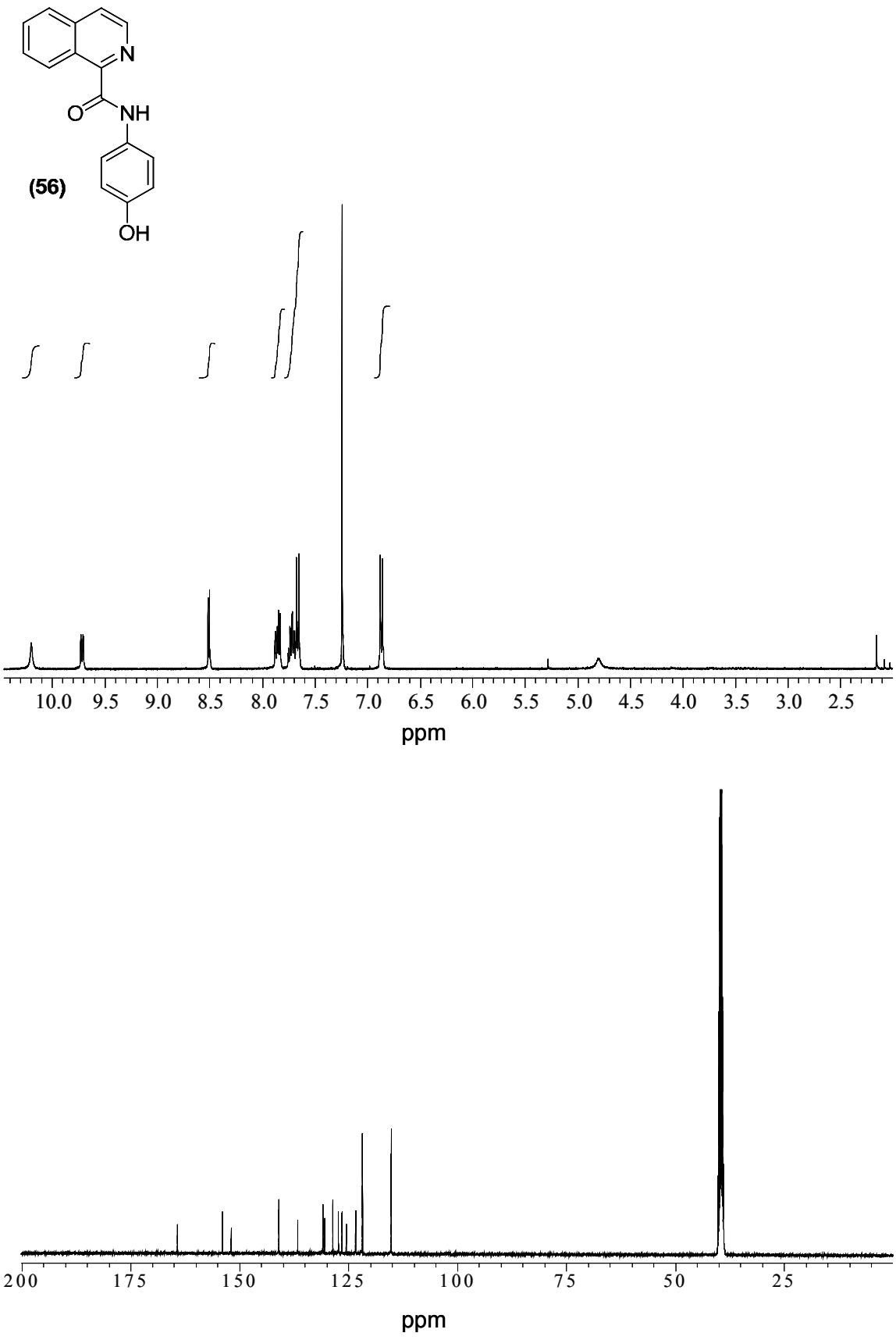

^{1}H-NMR in $CDCl_3$ and ^{13}C-NMR in DMSO-d_6 of **(56)**

SPICUM servicio de publicaciones

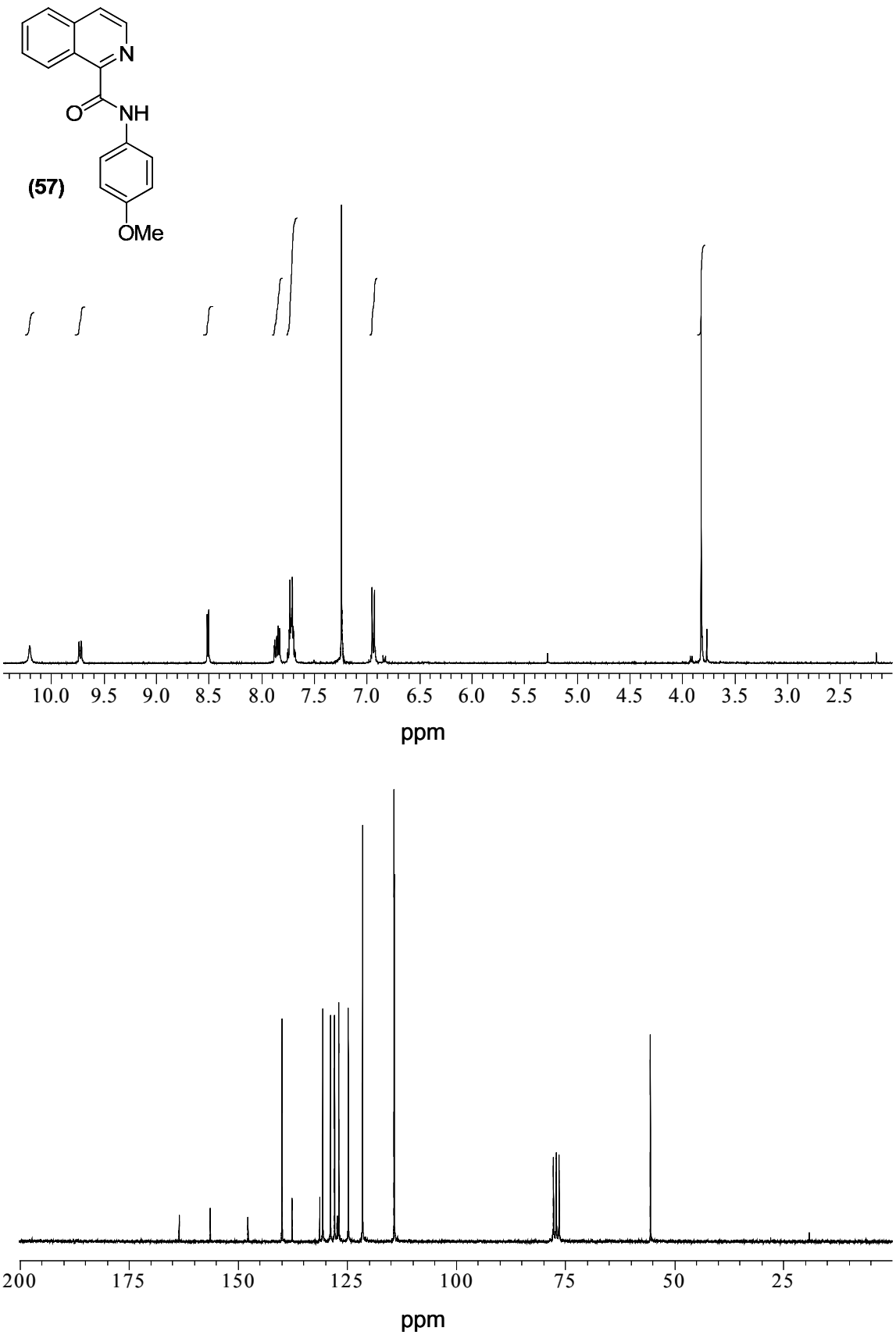

^{1}H-NMR and ^{13}C-NMR in $CDCl_3$ of **(57)**

SPICUM servicio de publicaciones

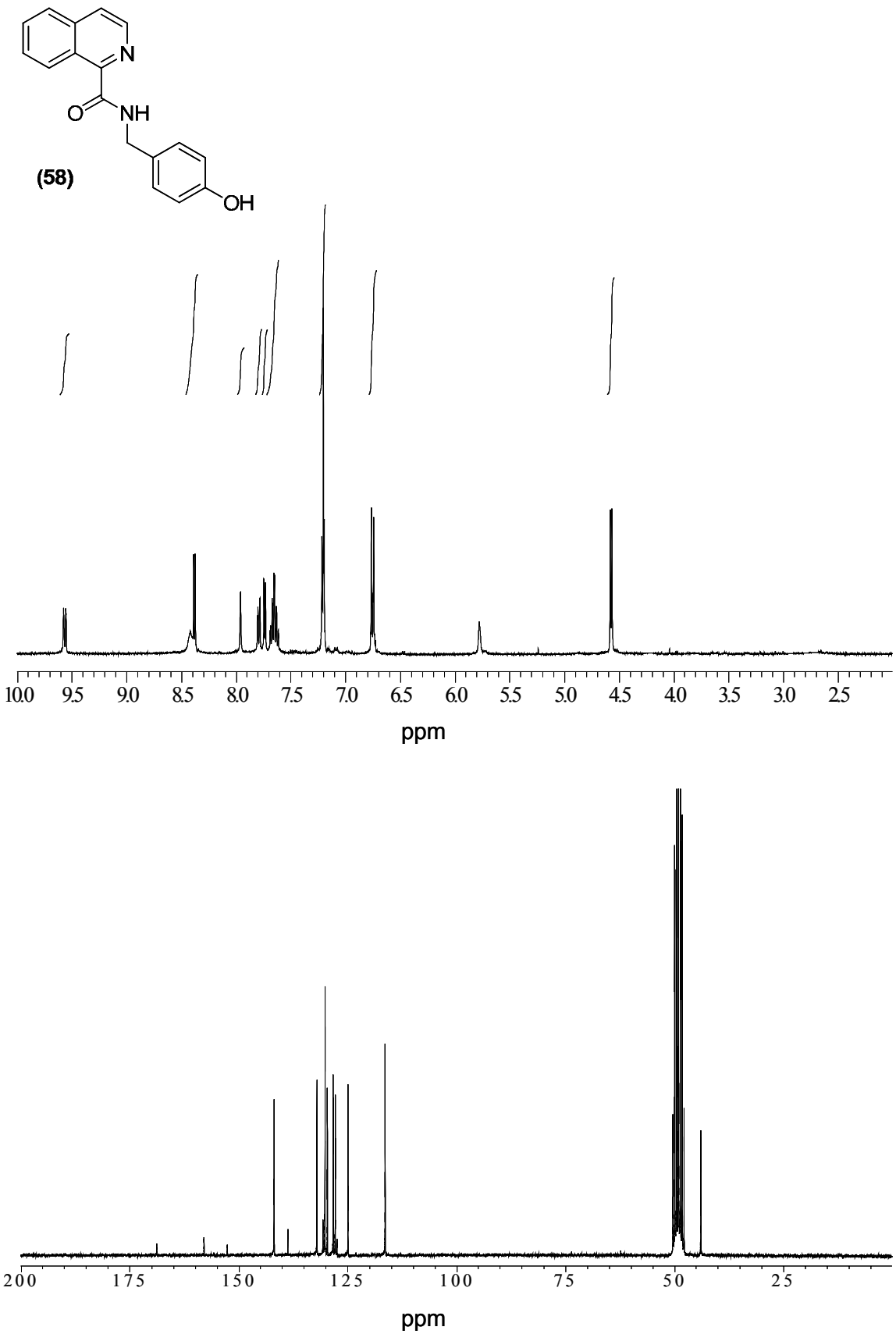

^{1}H-NMR in $CDCl_3$ and ^{13}C-NMR in CD_3OD of **(58)**

SPICUM servicio de publicaciones

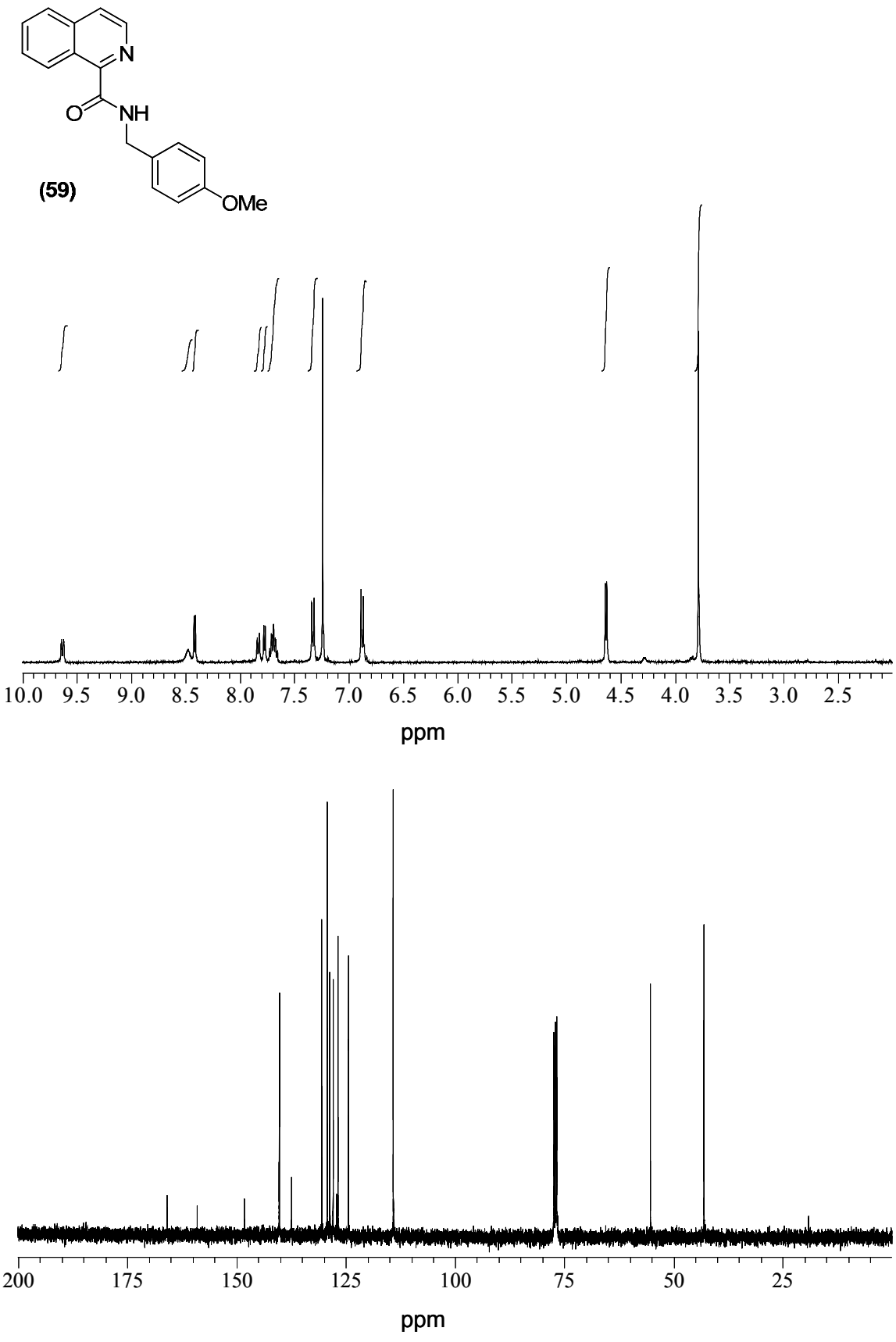

^{1}H-NMR and ^{13}C-NMR in $CDCl_3$ of **(59)**

SPICUM servicio de publicaciones

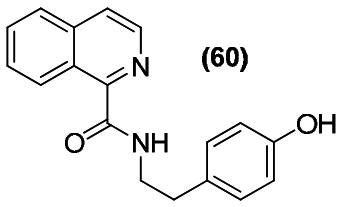

(60)

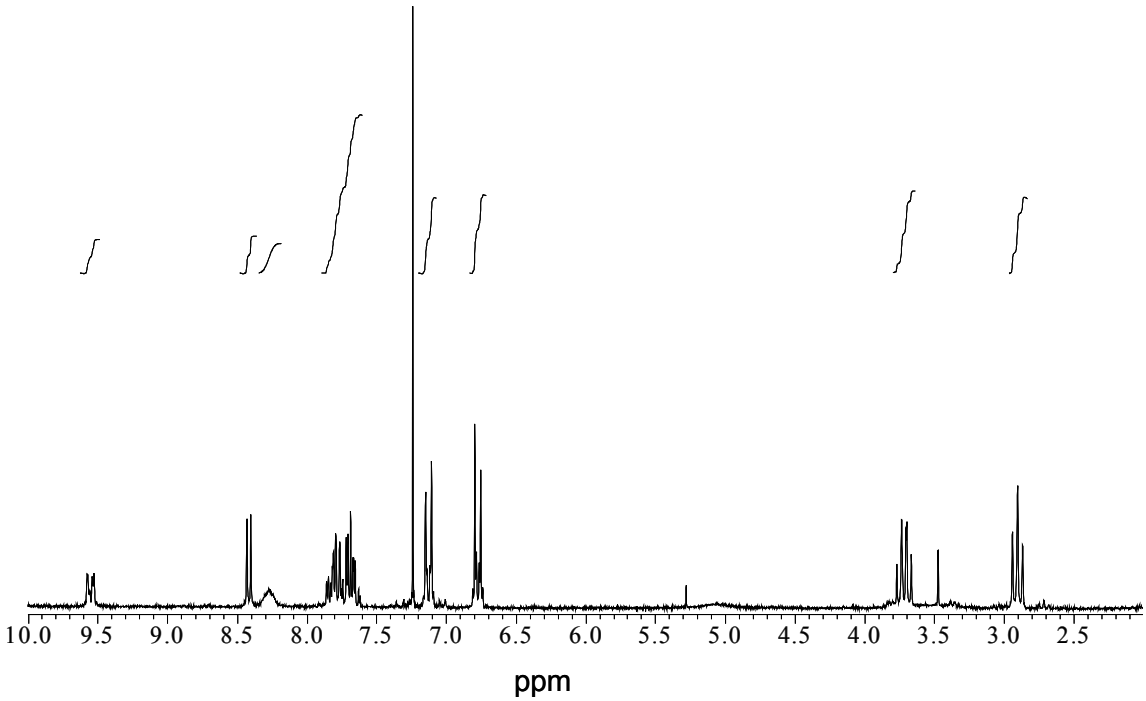

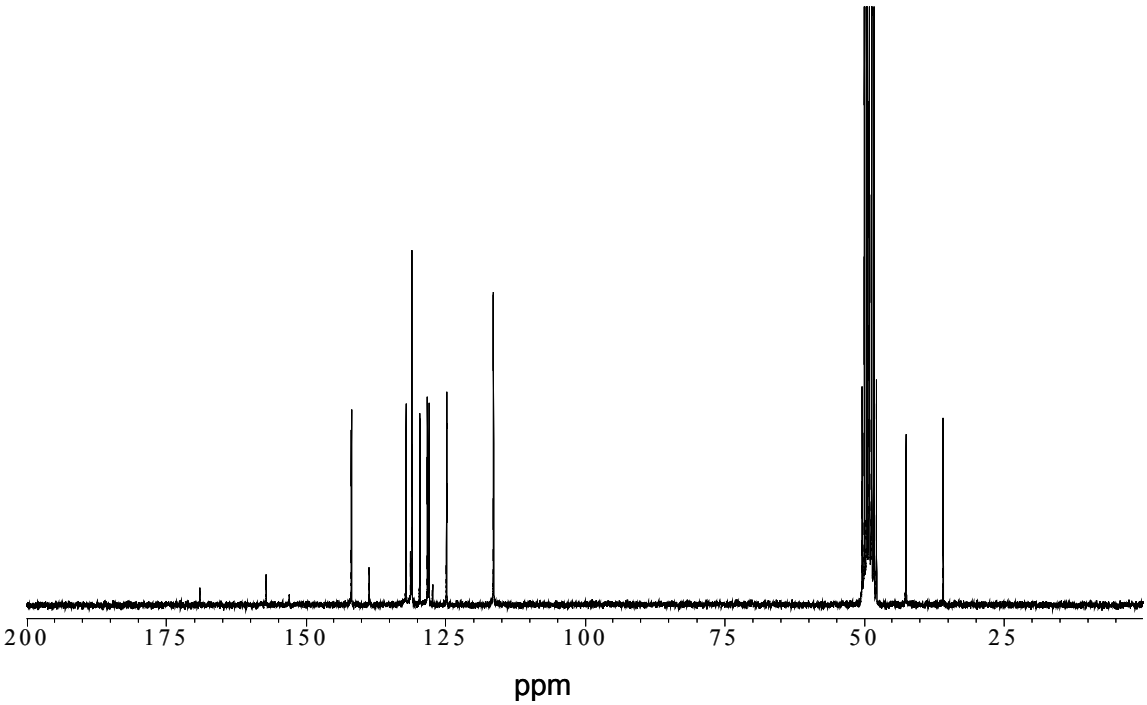

^{1}H-NMR in $CDCl_3$ and ^{13}C-NMR in CD_3OD of **(60)**

SPICUM servicio de publicaciones

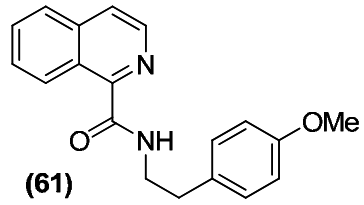

(61)

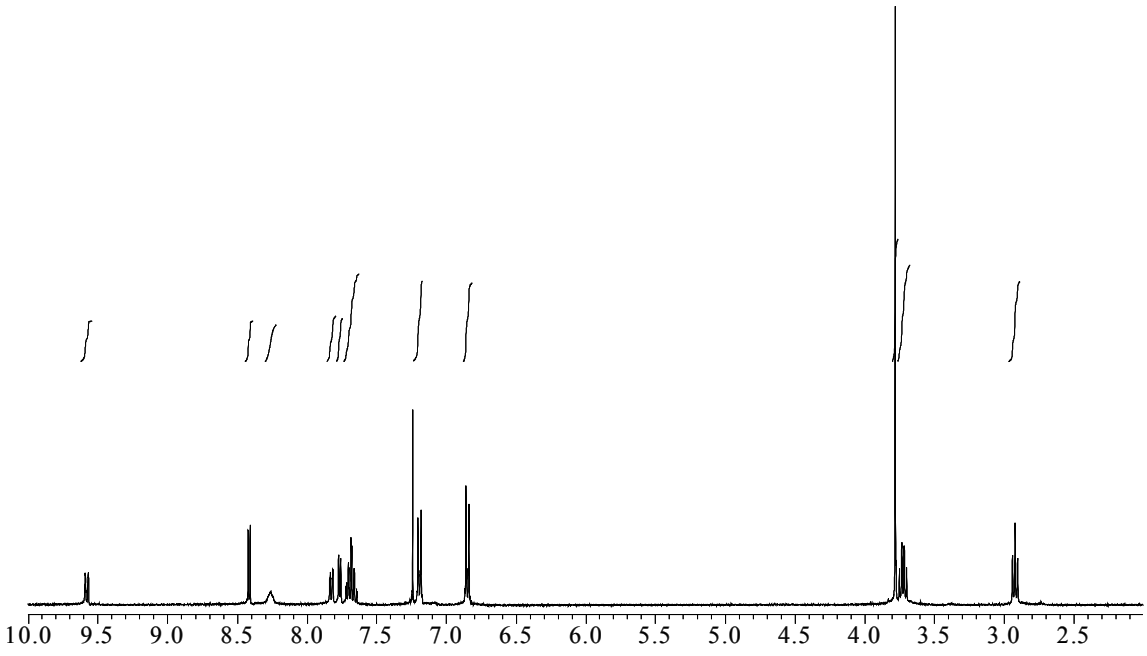

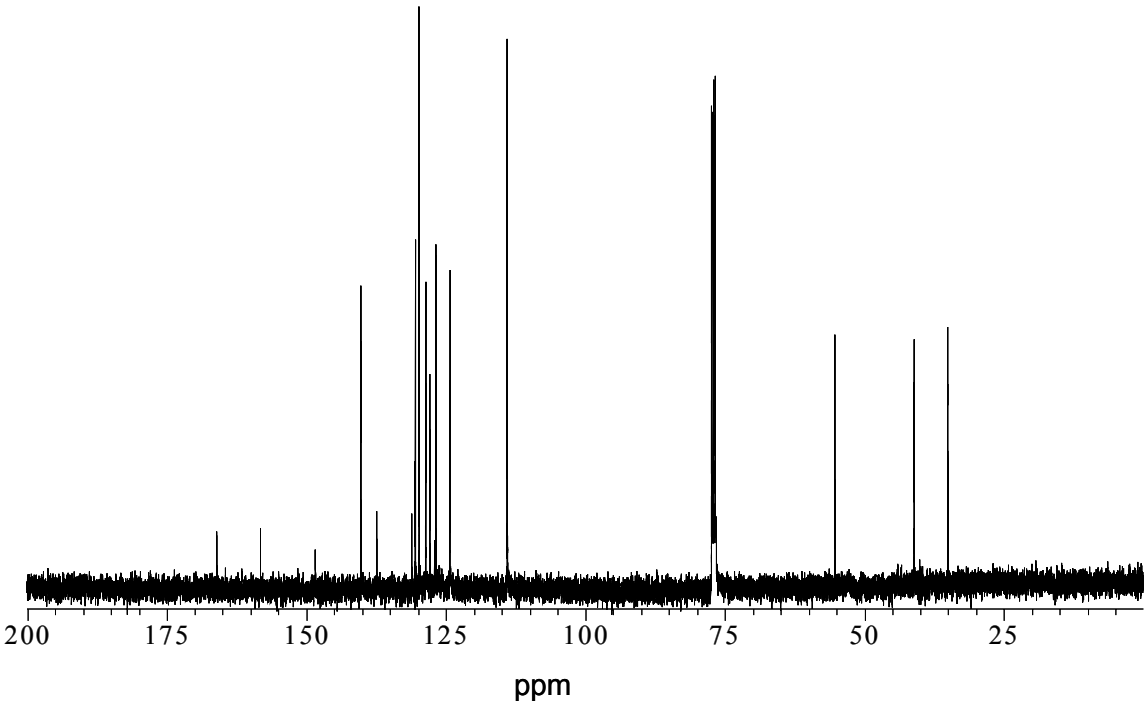

^{1}H-NMR and ^{13}C-NMR in $CDCl_3$ of **(61)**

SPICUM servicio de publicaciones

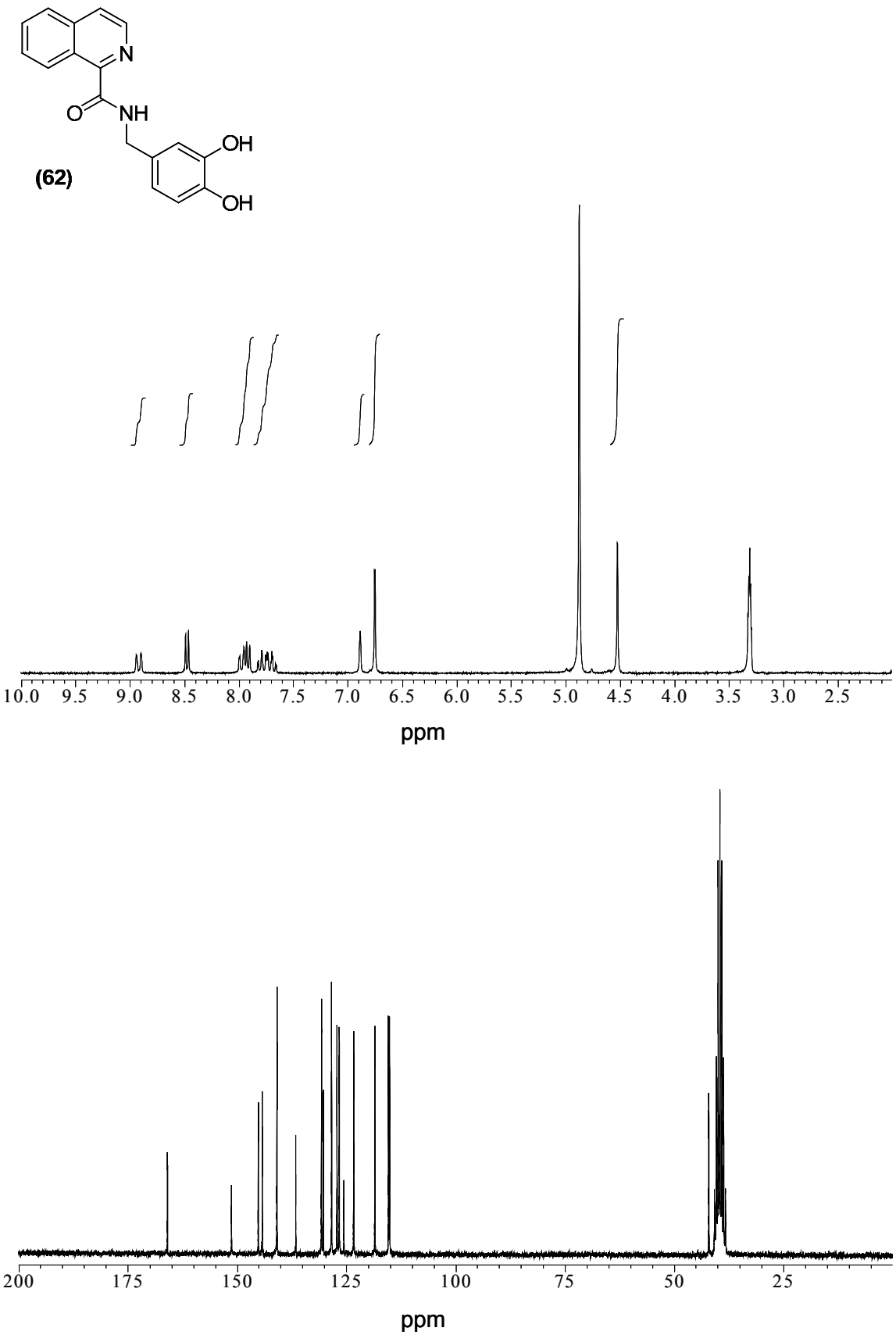

^{1}H-NMR in CD_3OD and ^{13}C-NMR in DMSO-d_6 of **(62)**

SPICUM servicio de publicaciones

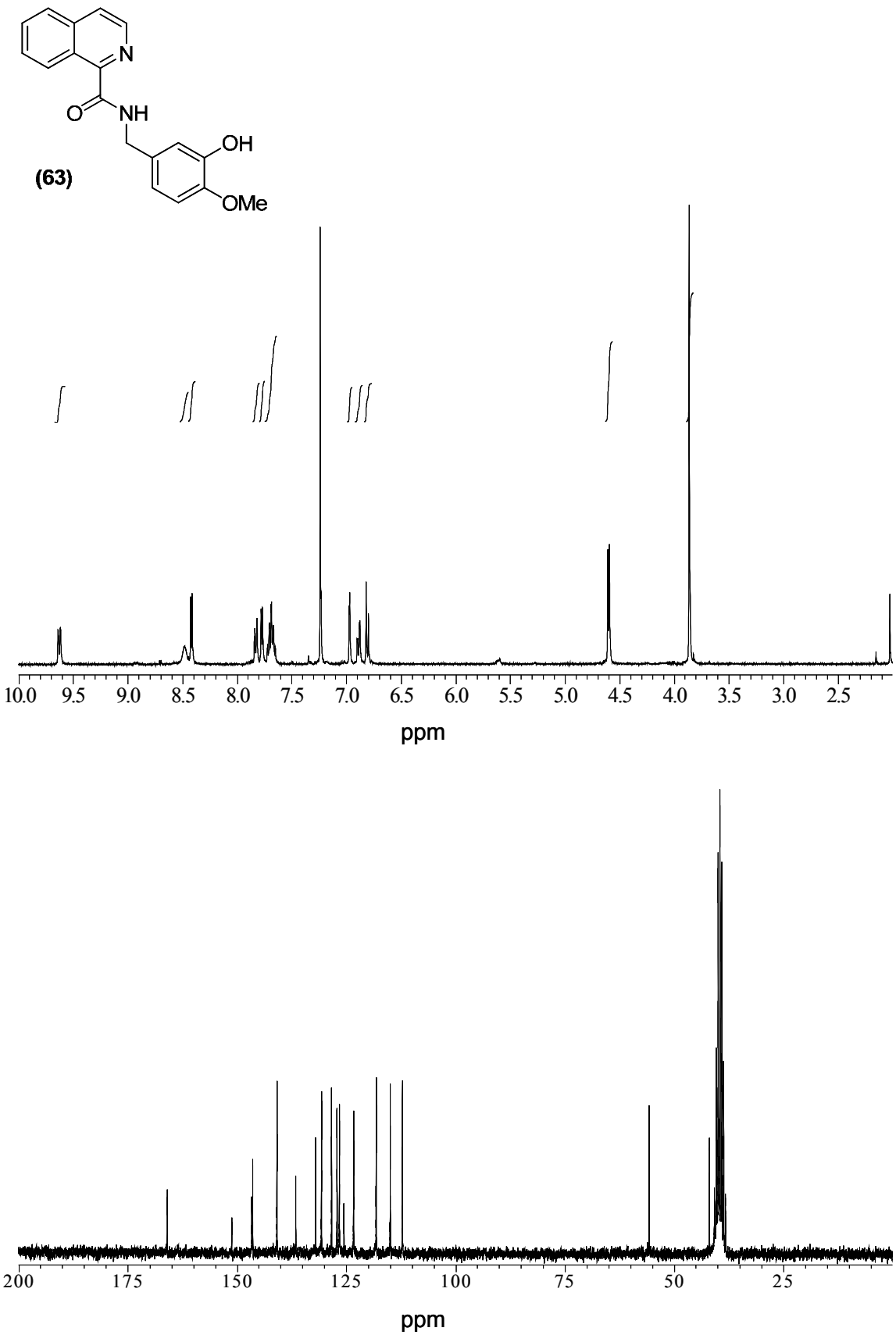

^{1}H-NMR in $CDCl_3$ and ^{13}C-NMR in DMSO-d_6 of **(63)**

SPICUM servicio de publicaciones

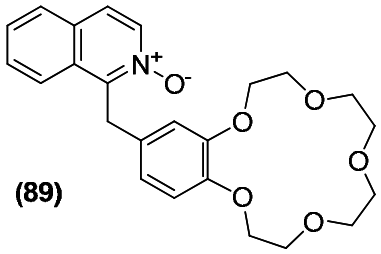

(89)

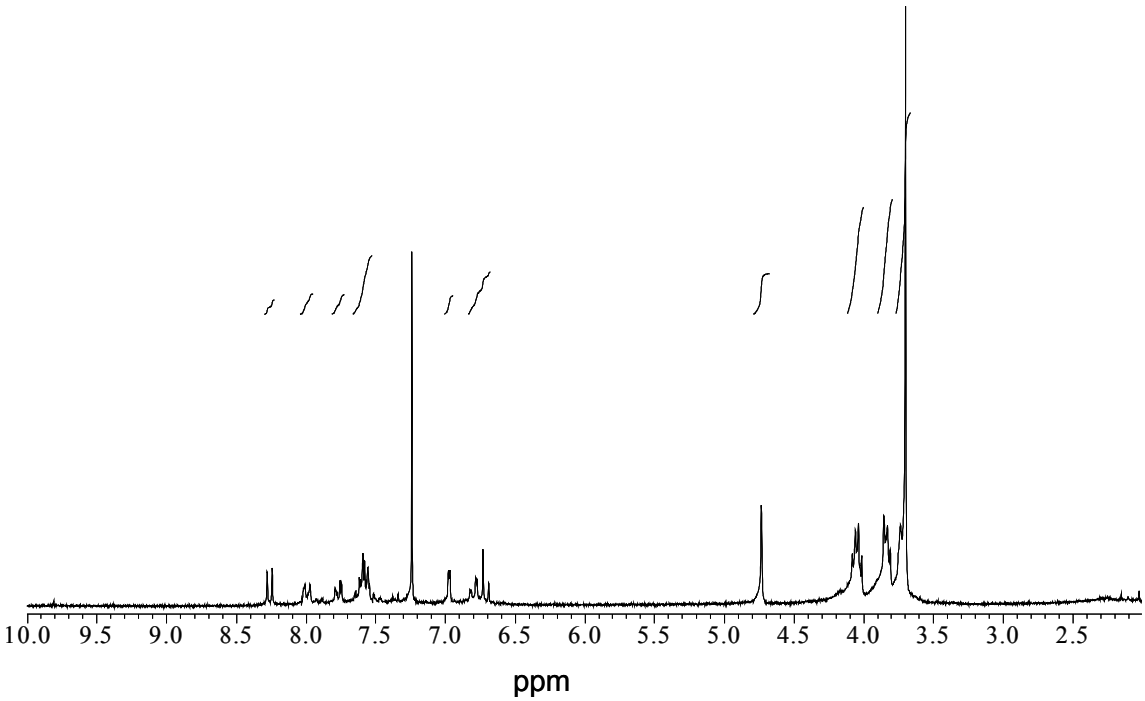

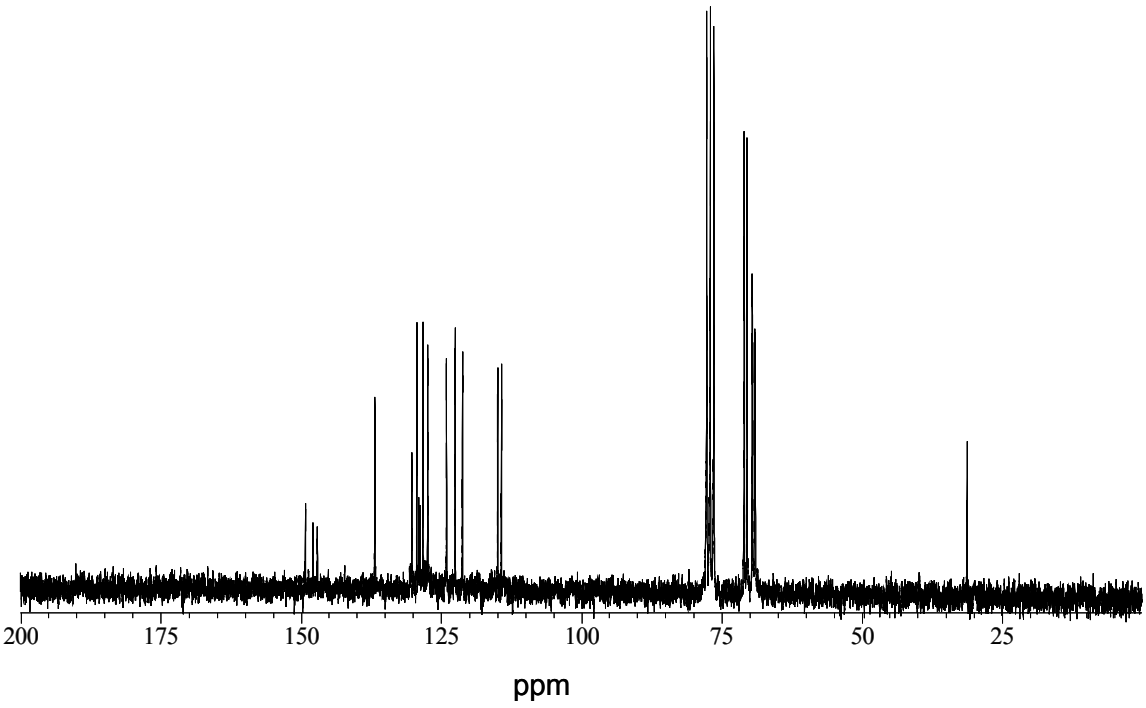

^{1}H-NMR and ^{13}C-NMR in $CDCl_3$ of **(89)**

SPICUM servicio de publicaciones

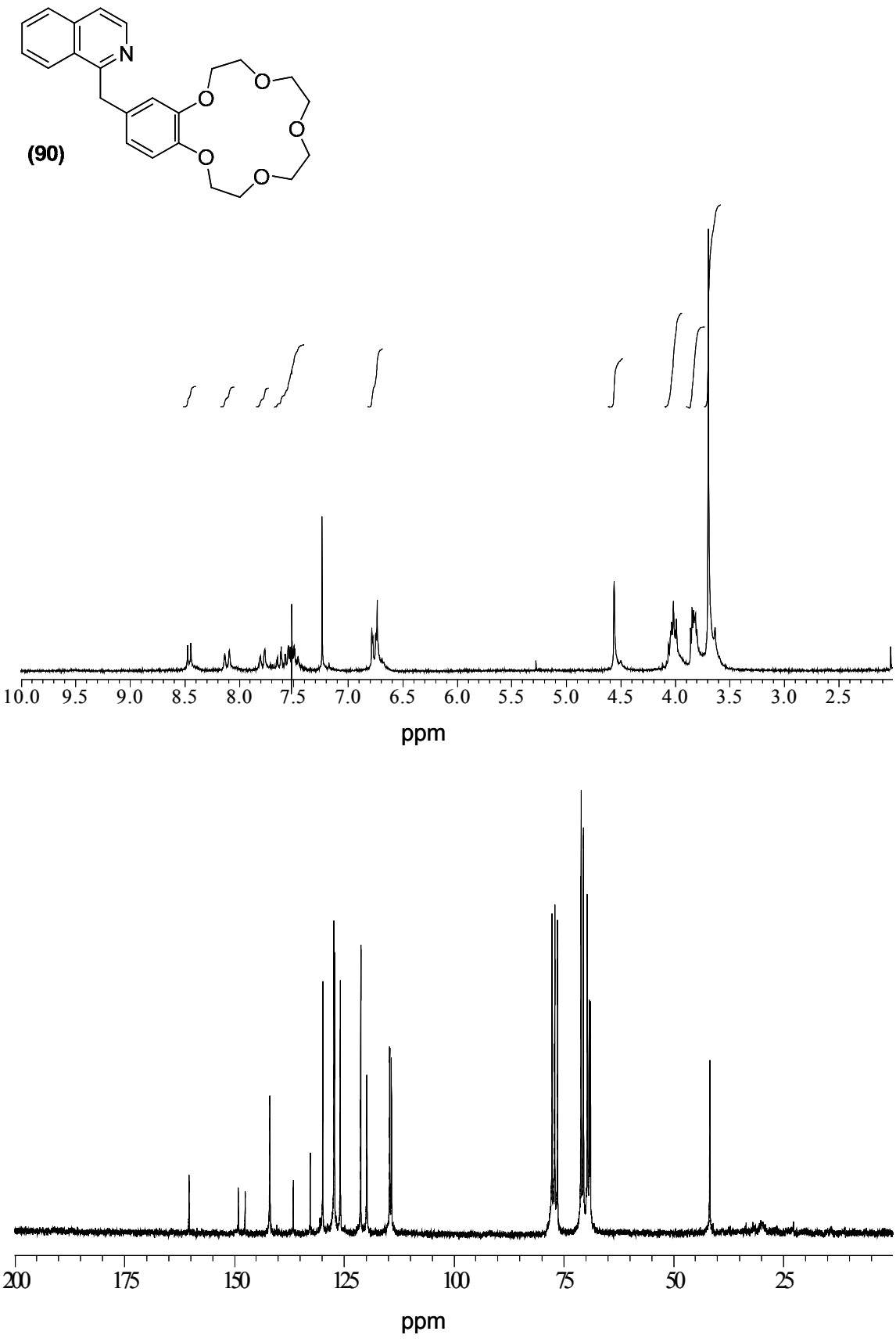

^{1}H-NMR and ^{13}C-NMR in $CDCl_3$ of **(90)**

SPICUM servicio de publicaciones

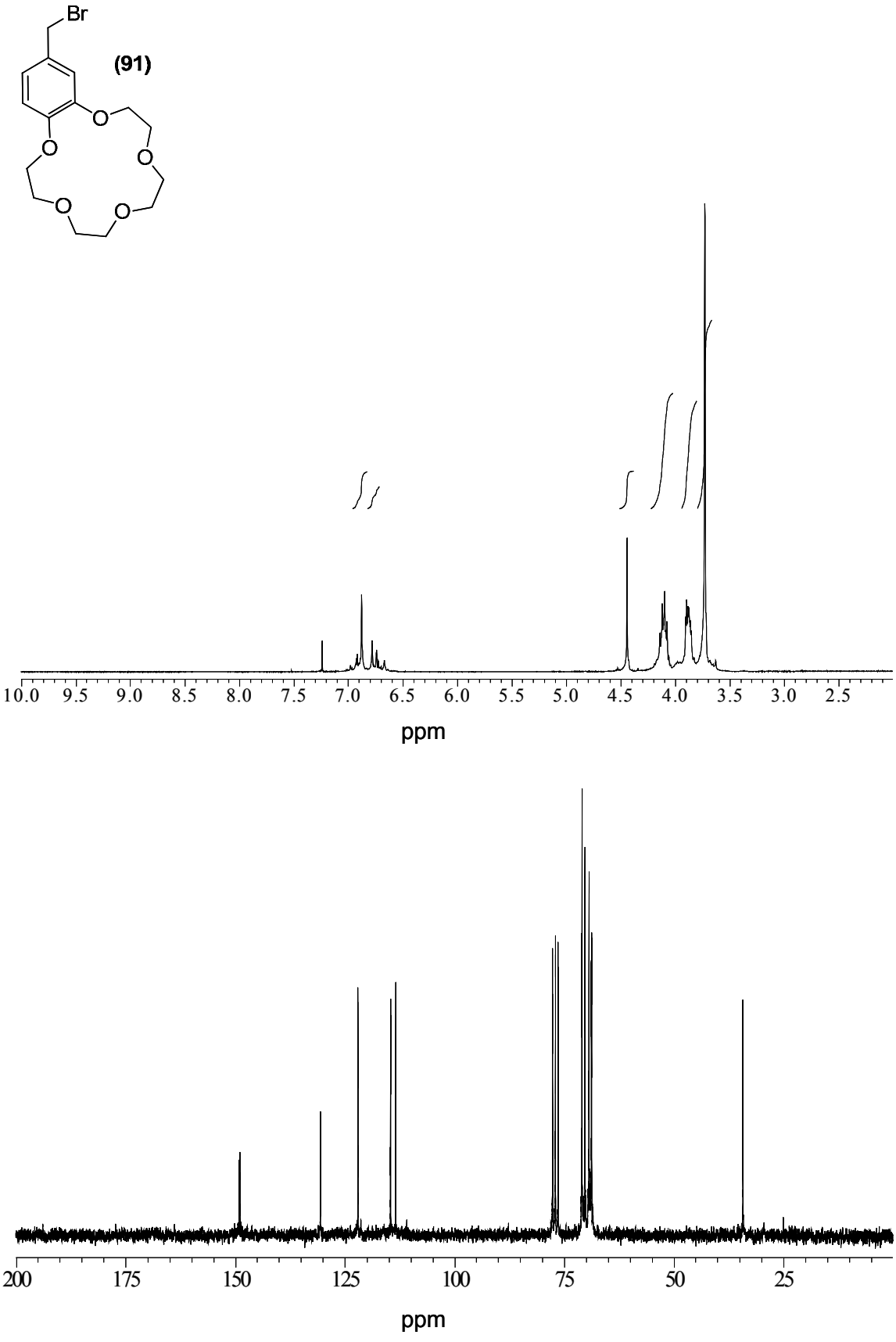

^{1}H-NMR and ^{13}C-NMR in $CDCl_3$ of **(91)**

SPICUM servicio de publicaciones

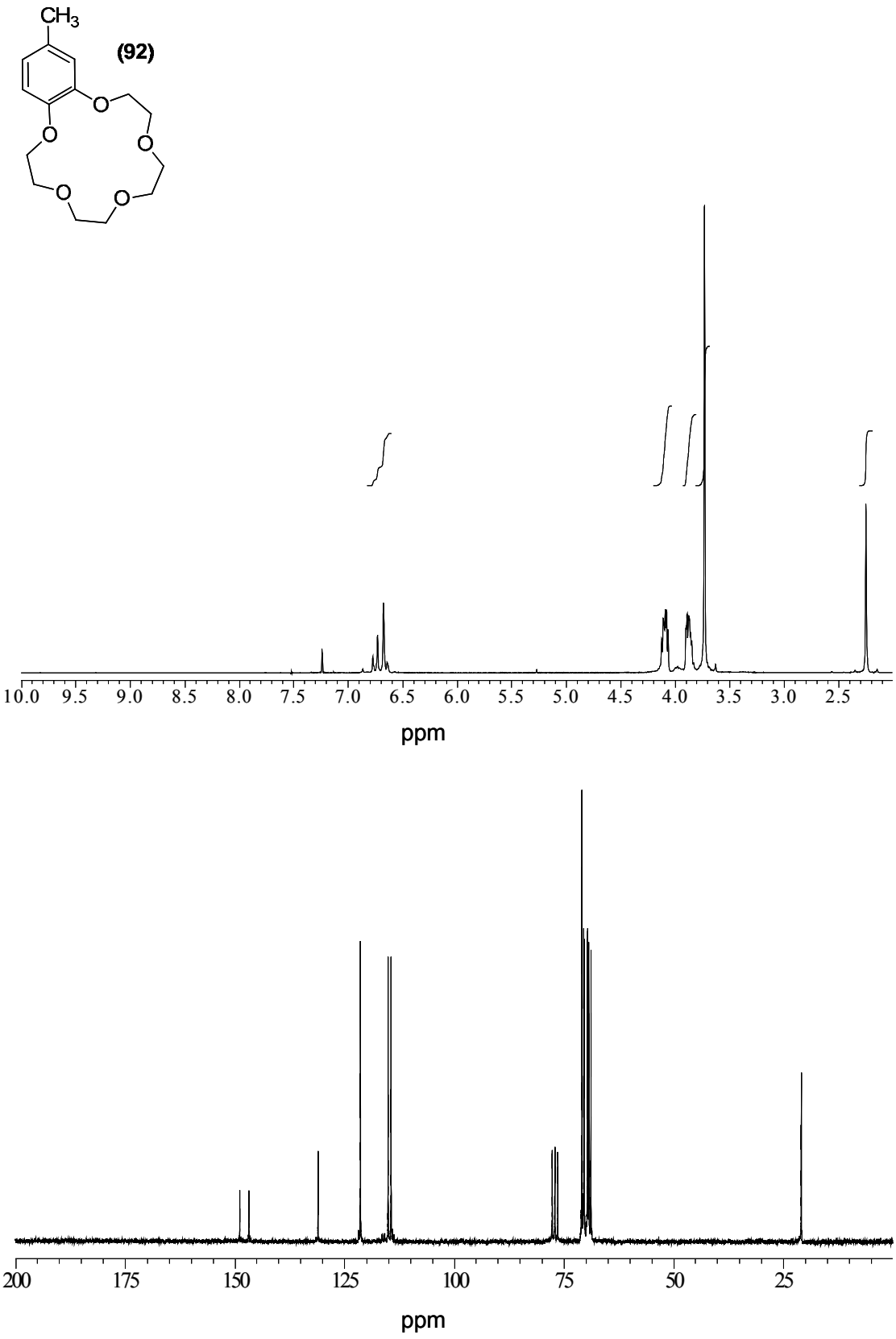

^{1}H-NMR and ^{13}C-NMR in $CDCl_3$ of **(92)**

SPICUM servicio de publicaciones